Characterization of dynamic molecular networks in control ischemic-reperfused mouse heart

Sally Badawi

N°d'ordre NNT : **2019LYSE1158**

THESE de DOCTORAT DE L'UNIVERSITE DE LYON
opérée au sein de
l'Université Claude Bernard Lyon 1 en cotutelle avec
L'Université Libanaise-LIBAN

Ecole Doctorale ED 205
Ecole Doctorale interdisciplinaire Sciences-Santé (EDISS)

Spécialité de doctorat : Biologie
Discipline : (Physiologie, Biologie des Systèmes, Bioinformatique)

Soutenue publiquement le 17/09/2019, par :
Sally Badawi

Characterization of dynamic molecular networks in control ischemic-reperfused mouse heart

Devant le jury composé de :

Abdel-Razzak, Ziad, PhD,	Université Libanaise	President
Perrin, Laurent, PhD,	Aix-Marseille Université	Rapporteur
Habib Abdel Karim, Aida,	PhD, American University of Beirut	Rapporteure
Tokajian, Sima, PhD,	Lebanese American University	Rapporteure
Abdel-Razzak, Ziad, PhD,	Université Libanaise	Examinateur
Baetz, Delphine, PhD,	Université Claude Bernard	Examinatrice
Borjac-Natour, Jamilah, PhD,	Beirut Arab University	Examinatrice
Bidaux, Gabriel,	PhD, Université Claude Bernard	Directeur de thèse
Kurdi, Mazen,	PhD, Université Libanaise	Co-directeur de thèse

Acknowledgements:

I have always thought that home is where we were born, grown up and had our families. In a three-years journey away from my real home, I was reborn, grown up scientifically and mentally, had a bigger family and a new place I call ***HOME***. Throughout this journey, the people I met were life-changing. For those people I owe the success of this work…

Michel Ovize, thank you for accepting me in your team to do this PhD work and help us always grow bigger with your experience. It was an honor I will always cherish.

Gabriel, my "*spiritual father"* and "*daddy"* as Alex says, it was a pleasure to work with you all this time. You have always impressed me with your complex brain. You were my best reference for all the things I didn't know and the problems I didn't know how to solve. I appreciate your challenges and high expectations; they've got me do things I never thought myself capable of doing. Thank you for the joyful times we went like "*Tom and Jerry*". Thank you for your patience and motivation in the times I needed them. Research would not have seemed as interesting as it had been if it wasn't shared with you… Thank you.

Dr Mazen, you were there from the very beginning of my research journey. You pushed me to my limits, and today, I am here because you were the first to believe in me. You will always have that special place. Thank you for all what you have done. Thank you for the beautiful times we have shared in the LU. Such memories are kept in my heart forever.

Fabien, thank you for accepting to co-supervise me with Gabriel. Thank you for your all-time kindness…

Joel and Laurent, thank you for all the kind of advices and supports you have provided me through this thesis. I owe its success as well…

My jury members, thank you for dedicating time to evaluate my thesis work. I deeply appreciate all your comments and advices.

Zeina, no words can be enough to describe how thankful I am for having you by side throughout this time… Thank you for making me smile a bit bigger, laugh a bit louder and live way better.

You have always been there no matter what. You were, are and will forever be the best partner I want to share anything with.

Maya, thank you for always coloring our days with your gorgeous smile, adding life to our Saturdays and being always there for us as well. You will always have a special place in my heart. I wish you nothing but all the beautiful things of the world…

Nolwenn, "Ma femme", "Our fara" … tfou 3laiki…I will miss all the beautiful moments we have shared together. I will miss bothering you, playing dobble and making you lose :p, eating Shawarma, Manakish and Doritos and simply being crazy with you. Thank you for being this special 💔.

Mallory, we may not have spent a lot of time together, but it was always good to have you around. I enjoyed bothering you from time to time, thank you for giving me this pleasure 😁.

Alex, "*My spiritual brother*" … Thank you for being really "chiant" as you say, my days would have not been the same if you hadn't been there bothering me with your "munitions". I will miss these times and I will miss you. Thank you for being my best ELISA teacher 😉

Claire, you have been the one who always ask how things go, the one who cares the most and the one with the kindest heart. You have been one of a kind. The lab is a safer place when you are present. Thank you for all the help you have offered and all the time you have always dedicated to listen to our problems.

Ribal, "thank you" is not enough for you… Since day 1 in Lyon, you were there helping us in every single detail. Thank you for making Lyon a better place, for being a real brother and for all the beautiful times we have shared together. I just deeply wish you all the beautiful things of the world with ***Camille*** because you deserve it. بحبكن كتير

Bruno, Bonsoirrrr!!! It has always been a pleasure to work with you. Thank you for your kindness. Thank you for always making time for all the urgent experiments we had to do, knowing that you always had a busy schedule. Thank you for always being in a happy mood, always singing and always reminding me that: "this is the first mouse, the first mouse, the first mouse" 😁.

Lionel, it was a pleasure working with you all this time. I had much fun during the sampling time, you make a great team together with Bruno. Thank you for your time and kindness…

Melanie and Ludo, thank you for all the advices you have provided me and the good vibes you always had...

Mumu, Noelle, Sylvie, Joe, Christophe, Rene, Yves, Fabrice, Maxime, Christelle, Andrea, Megan and Jenny, we might not have spent a lot of time working together, but the presence of each and every one of you in this team made it the best ever.

My dearest family, thank you for the unconditional love and the support you have provided throughout this journey.

Hadi, "*my one and only*", thank you for having the biggest heart I had ever imagined of. I dedicate this work to you with every piece of my heart ❤️.

Abstract:

English abstract:

Cardiovascular diseases represent a major health burden worldwide. According to the World Health Organization, 17 million people are dying each year by heart diseases which account to 31% of total deaths globally. Among these diseases is myocardial infarction (MI). Several efforts have been made to decrease the associated mortality rates but unfortunately, only few has succeeded to date. This failure is contributed to several factors, among them is the misunderstanding of the mechanism responsible for the progression of the disease.

Our understanding of the MI pathology has been greatly improved by the approaches that have been widely used in the previous decades, relying mainly on studying molecules/pathways separately. However, this knowledge was not enough to make a difference clinically. Therefore, deciphering the interconnections between molecules has become an urge for better understanding of the diseases' progression.

In this regard, the work in this doctoral thesis involves different aspects of the MI pathology. The general aim of this work is to improve the dynamic analytical approach using systems biology tools, where new mechanistic information is decoded. Firstly, in a 3D heart model, we propose a chain of methods using clarified mouse heart and fluorescence microscopy to molecularly characterize the area at risk in the myocardium of ischemia reperfusion (IR) and cardioprotected mice based on its redox state. In addition, we aim to develop a new analytical approach using dynamical large-scale transcriptomic data for characterizing the dynamic transcripts expression. Applying this approach on a control mouse model (mice subjected to anesthesia and surgical interventions), we show that Il-6 is a major mediator of the activated inflammatory reaction. In conclusion, this analytical approach highlights the necessity of the sapatio-temporal analysis to characterize the molecular events occurring in response to MI.

French abstract :

Les maladies cardiovasculaires représentent un important problème de santé publique à travers le monde. Parmi ces pathologies, l'infarctus du myocarde (IM) a fait l'objet de nombreux essais visant à diminuer sa sévérité. Néanmoins peu ont remporté leur pari. Cet échec peut avoir plusieurs composantes parmi lesquelles la méconnaissance de la complexité des mécanismes moléculaires impliqués.

Notre compréhension de l'IM a cependant été nettement améliorée grâce à des méthodes utilisées pendant les dernières décennies et qui consistaient à étudier séparément un nombre limité d'acteurs moléculaires impliqués dans un mécanisme simple et linéaire. Cependant, l'échec des essais cliniques basés sur ces approches réductionnistes ont montré leurs limites. L'émergence de la biologie des systèmes, ces dernières années, a stimulé les recherches visant à mieux intégrer et comprendre la nature complexe et stochastique des réseaux moléculaires et leur dynamique dans la progression des pathologies.

L'objectif général de cette thèse a consisté en le développement et l'amélioration de méthode d'analyses et de combinaison des données spatio-temporelles issus d'expériences réalisées sur un modèle d'infarctus du myocarde chez la souris. L'objectif scientifique visait à caractériser les principaux signaux dynamiques au cours de la séquence d'ischémie-reperfusion. A cet effet, nous avons tout d'abord développé une chaîne de méthode utilisant la clarification d'organe et la microscopie de fluorescence permettant de quantifier, en 3 s, la zone du myocarde soumise au choc oxydant lors de la reperfusion. Dans une seconde partie, nous avons développé une nouvelle chaîne analytique pour caractériser la dynamique d'expression des transcrits. Appliquée aux animaux contrôles (soumis à la chirurgie et l'anesthésie), nous mettrons, grâce à cette chaîne de méthode, le rôle majeur de la voie de l'interleukine 6 dans le développement de la réponse immunitaire et nous concluons ainsi sur la nécessité de réaliser une analyse dynamique du modèle expérimental pour caractériser sa réponse à l'échelle moléculaire et éviter toute surinterprétation de la réponse à l'IM.

Résume :

Les maladies cardiovasculaires représentent un important problème de santé publique à travers le monde. Selon l'organisation mondiale de la santé, 17 millions de personnes meurent chaque année de maladies cardiaques soit environ 31% de la mortalité globale. Parmi ces pathologies, l'infarctus du myocarde (IM) a fait l'objet de nombreux essais visant à diminuer sa sévérité. Néanmoins peu ont remporté leur pari. Ces échecs peuvent avoir plusieurs composantes parmi lesquelles la méconnaissance de la complexité des mécanismes moléculaires impliqués.

Notre compréhension de l'IM a été nettement améliorée grâce à des méthodes utilisées pendant les dernières décennies et qui consistaient à étudier séparément un nombre limité d'acteurs moléculaires impliqués dans un mécanisme simple et linéaire. Cependant, l'échec des essais cliniques basés sur ces approches réductionnistes ont montré leurs limites. Ces échecs pourraient être dûs en partie à la dispersion des connaissances ou l'absence de connexion à leur environnement moléculaire. De plus, la faible caractérisation des modèles expérimentaux animaux pourraient aussi avoir biaisée les interprétations de certaines études antérieures. L'émergence de la biologie des systèmes, ces dernières années, a stimulé les recherches visant à mieux intégrer et comprendre la nature complexe et stochastique des réseaux moléculaires et leur dynamique dans la progression des pathologies.

A cet égard, l'objectif général de ce travail de thèse a consisté en le développement de chaîne de méthodes visant à améliorer la caractérisation spatio-temporelle des évènements moléculaires induit par l'ischémie-reperfusion cardiaque. Grâce à un modèle d'ischémie-reperfusion cardiaque sur des souris C57Bl/6, avec ou sans post-conditionnement ischémique ou hypothermie thérapeutique, nous avons développé une chaîne de méthode utilisant la clarification d'organe et la microscopie de fluorescence permettant de quantifier, en 3 dimensions, la zone du myocarde soumise au choc oxydant lors de la reperfusion. Dans une seconde partie, nous avons développé une nouvelle chaîne analytique visant à caractériser la dynamique d'expression des transcrits lors de la thoracotomie d'animaux anesthésiés. Enfin, dans un troisième volet, nous avons étudié la dynamique de cytokines à l'état protéique dans le plasma et à l'état d'ARNm dans les cellules

cardiaques. Nous avons ensuite comparé la réponse chez le modèle murin avec celle du patient humain.

L'hétérogénéité des lésions de reperfusion entre chaque animal, rend la caractérisation spatiale des réponses cellulaires et moléculaires compliquées a étudier. Dans ce but, nous avons développé une méthode d'imagerie du niveau d'oxydoréduction de la myoglobine cardiaque sur des cœurs clarifiés et non-marqués et qui nous permet de détecter le volume soumis au choc oxydant survenant à la reperfusion. Nous démontrons aussi que cette méthode peut être couplée à l'immuno-marquage pour caractériser des signaux cellulaires/moléculaires d'intérêt. En parallèle de l'organisation spatial du signal, nous avons étudié son organisation dynamique au cours de la séquence d'ischémie-reperfusion. Nous avons pour cela réalisé une étude cinétique de l'ischémie-reperfusion par analyse transcriptomique. Dans les animaux sham (thoracotomie, anesthésie et analgésie), nous montrons une variation significative du transcriptome à 24h après chirurgie avec une forte réponse inflammatoire caractérisée par l'infiltration de neutrophiles et la différenciation de macrophages dans le myocarde. Ces modifications sont vraisemblablement induites par la réponse à l'interleukine 6 (IL-6) dont nous montrons une forte augmentation dans le plasma des animaux dès 45min post-chirurgie. Nous avons identifié l'Il-6 par une analyse de retro-ingénierie dans laquelle l'Il-6 apparaissait comme inducteur potentiel des facteurs de transcription ayant modulés les transcrits dont l'expression varie significativement au cours de la séquence d'ischémie-reperfusion. Dans une troisième étude de nature translationnelle, nous avons caractérisé les cytokines (dont l'Il-6) dont l'expression fluctue au cours du temps chez les patients sujets à un infarctus du myocarde aigu ainsi que dans notre modèle de transcriptomique de l'IM chez la souris. L'analyse de corrélation montrent d'une part que la souris peut être considérée comme un modèle expérimental pertinent pour la réponse inflammatoire induite par l'Il-6 mais aussi que l'origine de la réponse soutenue de certaines cytokines circulantes requière une production par les cellules du tissu endommagé.

En conclusion, grâce à des méthodes de biologie des systèmes et de photonique, notre travail offre un nouvel éclairage sur l'organisation spatial et la dynamique de la réponse inflammatoire dans l'ischémie-reperfusion cardiaque.

Table of Content:

List of Publications and Scientific Communications:

Publications:

A dynamic transcriptional analysis reveals IL-6 axis as a prominent mediator of surgical acute response in non-ischemic mouse heart.
Sally Badawi, Alexandre Paccalet, Zeina Harhous, Bruno Pillot, Lionel Augeul, Fabien Van Coppenolle, Joel Lachuer, Mazen Kurdi, Claire Crola da Silva, Michel Ovize and Gabriel Bidaux*. (Under revision)

Critical appraisal of STAT3 pattern in adult cardiomyocytes.
Zeina Harhous, ***Sally Badawi***, Noelle Gallo Bona, Bruno Pillot, Lionel Augeul, Melanie Paillard, George W. Booz, Emmanuelle Canet-Soulas, Michel Ovize, Mazen Kurdi**, Gabriel Bidaux*.
Journal of Molecular and Cellular Cardiology 131 (2019) 91–100
https://doi.org/10.1016/j.yjmcc.2019.04.021.

Redox-imaging of myoglobin reveals the injured area of infarcted and cleared mouse hearts.
Sally Badawi#, Yves Gouriou#, Alexandre Paccalet, Chris Berd, Bruno Pillot, Lionel Augeul, Emmanuelle Canet-Soula, Radu Bolbos, Tardivel Meryem, Antonino Bongiovani, Clémence Leboullenger, Michel Ovize, Claire Crola Da Silva and Gabriel Bidaux. (In preparation)

Deciphering the crosslink between STAT3 and MAPKs in ischemia-reperfusion and postconditioning.
Zeina Harhous, ***Sally Badaw***i, Bruno Pillot, Lionel Augeul, Michel Ovize, Mazen Kurdi, Gabriel Bidaux. (In preparation)

TRPV1 inhibition supports cell survival during hypoxia/reoxygenation in the rat cardiomyoblast H9C2 cell line
Nolwenn Tessier, ***Sally Badawi***, Mallory Ducrozet, Christophe Chouabe, Claire Crola Da Silva, Gabriel Bidaux, Michel Ovize, Fabien Van Coppenolle*, Sylvie Ducreux*. (In preparation).

Loss of MFN2 induces metabolic reprogramming and confers resistance to hypoxia.
Gouriou Y, Alam MR, Harhous Z, Crola C, Baetz D, ***Badawi S***, Lefai E, Rieusset J, Durand A, Harisseh R, Gharib A, Bidaux G§ & Ovize M§. (Submitted).

Multiparametric analysis by flow cytometry of mouse adult cardiomyocytes in suspension exposed to hypoxia-reoxygenation.

Alexandre Paccalet[#], Nolwenn Tessier[#], Lucille Païta, Melanie Paillard, Ludovic Gomez, Noëlle Gallo Bona, Christophe Chouabe, Christelle Léon, ***Sally Badawi***, Zeina Harhous, Michel Ovize and Claire Crola Da Silva. (Submitted).

Scientific Communications:

Printemps de la Cardiologie (GRRC) 2019, *Lille*: National session oral presentation.+ poster

Les 29es Journées Européennes de la Société Française de Cardiologie 2019, *Paris*: Poster presentation

International Society of Heart Research (ISHR-EU) 2018, *Amsterdam*: Poster presentation

Printemps de la Cardiologie 2018, *Montpellier*: International session oral presentation + poster

Sante Fédération de Recherche (SFR) 2018, *Lyon*: Oral presentation

Systems Biology at University of Lyon (BioSyl) 2018: Lyon: Poster presentation

EDISS and EDST Scientific days (2016-2019), *Lyon and Beyrouth*: Oral presentations and posters.

List of Tables:

List of Figures:

List of abbreviations:

3D	Three-dimensional
CLARITY	Clear Lipid-exchanged Acrylamide-hybridized Rigid Imaging/Immunostaining/ in situ-hybridization compatible Tissue hYdrogel
CRP	C-Reactive Protein
CVD	Cardiovascular Disease
DAMPs	Danger-associated molecular patterns
DET	Differentially Expressed Transcripts
FDR	False Discovery Rate
FPKM	Fragments per Kilobase of Exon Model per Million Reads Mapped
GO	Gene Ontology
IHD	Ischemic Heart Disease
IPost	Ischemic Postconditioning
IR	Ischemia Reperfusion
IRI	Ischemia Reperfusion Injury
LRT	Likelihood Ratio Test
MI	Myocardial Infarction
mPTP	Mitochondrial Permeability Transition Pore
PC	Principal Component
PCA	Principal Component Analysis
PPI	Protein-Protein Interaction
RIMS	Refractive index matching solution

RISK	Reperfusion Injury Salvage Kinase Pathway
ROS	Reactive oxygen species
RQN	RNA Quality Number
SAFE	Survivor activating factor enhancement
STAT3	Single Transducer and Activator of Transcription 3
STEM	Short Time-series Expression Miner
TF	Transcription Factor
TFBS	Transcription Factor Binding Site
TF-PPI	Transcription Factor-Protein-Protein Interaction
TH	Therapeutic Hypothermia
WGCNA	Weighted Gene Co-expression Network Analysis

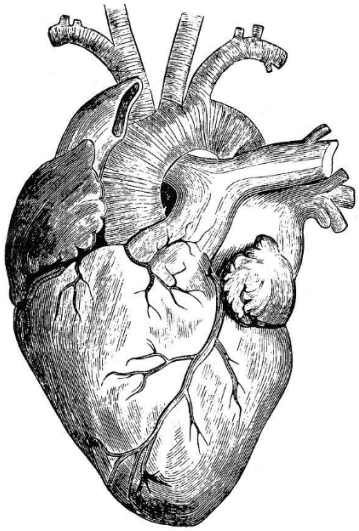

"*No man-made structure is designed like a heart. Considering the highly sophisticated engineering evidenced in the heart, it is not surprising that our understanding of it comes so slowly…*"

D.D. Streeter, 1979

Introduction:

As our first cells start to divide, their need for nutrients supply and wastes removal grows swiftly. Therefore, the heart along with blood and the circulatory system form to be the first functional organ system, the "***cardiovascular system***", responsible for keeping our cells alive. Our hearts beat 100,000 beats and pump continuously around 7600 liters of blood a day without any rest throughout our lives. This dynamical role played by the cardiovascular system and its linear and non-linear crosslinks along with other organs responsible for these regulatory mechanisms are not fully elucidated to date (Porta et al. 2009).

As a consequence of its importance, diseases associated with the cardiovascular system represent a major health burden worldwide. According to the World Health Organization (WHO) latest statistics, cardiovascular diseases (CVD) are responsible for 31% of the total deaths globally. They take the life of over 17 million people each year which is double that of the deaths caused by all forms of cancers (estimated ~ 8 million). Over the years, a considerable amount of publications has described different strategies and efforts in this field to enhance the understanding of these diseases and reduce the severity of clinical outcomes, but to date, only few have succeeded in improving the associated mortality and morbidity rates.

Decoding the non-linear molecular mechanisms behind these pathologies has failed in the last decades due to the straight-forward reductionist approaches that have been used. In the current era of large datasets generation, this task remains to be a challenging and a slowly-evolving one, especially when generated data are not integrated and compared to decode mechanistic information (Louridas, Kanonidis, and Lourida 2010). However, with the evolution of the systems biology tools and network modeling approaches, understanding diseases' progression and the associated molecular and cellular alterations was greatly improved. Integrating mathematics, statistics and computational biology approaches is nowadays revolutionizing biological sciences and is also improving the deciphering of the complex relationships in many fields including the cardiovascular field (Hunter 2012).

In order to preclinically mimic cardiovascular pathologies and find out therapeutic targets, several models including pharmacological and genetically modified ones have been introduced. As an

example, cyclophilin-D (CypD) which is known to be a key regulator of the mitochondrial permeability transition pore (mPTP) opening in response to myocardial infarction. CypD has been of great interest and was inhibited pharmacologically by cyclosporin A or genetically ablated (Lim et al. 2011; Nakagawa et al. 2005; Baines et al. 2005). However, no improvement in the clinical outcomes have been observed to date (Rahman et al. 2018). This failure is contributed to several factors, among them is the absence of a characterized control model of the pathology to compare to, which highlights the importance of retrieving as much as possible data in a control model in space and time dimensions to enhance the outcomes. In addition, the genetic or pharmacological used approach might not be mimicking what is occurring clinically and sorting out unbiased conclusions about the role of the protein of interest will be a challenging task, considering the specificity, interaction and bioavailability in the pharmacological studies which represent a source of bias in the interpretations as well.

In this regard, the work presented throughout this thesis entitled by "*Characterization of dynamic moelcular networks in control and cardioprotected ischemia-reperfused mouse heart*" addresses new integrative analytical approaches and characterizes a control IR model in a spatio-temporal dimension. This doctoral work involves the analysis of dynamic transcriptomics and three dimensional (3D) images of control and cardioprotective ischemia-reperfused mouse heart using integrative systems biology tools to better understand our cardiovascular system response to stress.

Thesis organization:

This thesis is divided into 10 chapters. Following this brief introduction of our work, a literature overview about the mechanistic insights of myocardial infarction (MI) and the associated activated inflammatory response are provided in Chapters 1 and 2, respectively. Chapter 3 displays some cardioprotective strategies used to protect the heart against MI associated damage. Afterwards, Chapter 4 introduces systems biology and transcriptomics and their contribution in cardiovascular system. Later on, in Chapter 5, a different aspect concerned with tissue clarification and imaging concepts is detailed. Moreover, after stating the aims in Chapter 6, methodologies, results, discussion and conclusions are displayed in the following chapters.

Chapter 1: Myocardial Infarction

Among the major CVDs is the ischemic heart disease (IHD), also known as myocardial infraction, which represents the most common cause of death and disability globally, despite all medical advances achieved in the past few years. The effects of IHD are attributed to the injury caused by myocardial ischemia-reperfusion (IR) (Hausenloy and Yellon 2013). The heart is considered a non-regenerative organ. If injured, its muscle cells will die and a scar will be formed which consequently will weaken its functioning and lead to heart failure (Yang 2018).

In order to understand how cardiomyocytes respond to injuries, it is important to have a prior knowledge about their structure and function under physiological conditions. Cardiomyocytes make up to ~ 70-85% of the mammalian heart's volume (Zhou and Pu 2016). The heart acts as a blood pump where cardiomyocytes' major function is to contract homogenously so that sufficient blood perfusion is provided to organs to meet their different nutrients and oxygen demands. This rhythmic procedure is regulated by controlled calcium (Ca^{2+}) ion entry and exit into and out of the cell achieved via ion channels and exchangers (Woodcock and Matkovich 2005).

Heart contraction demands high-energy consumption. In adult cardiomyocytes, mitochondria, occupying 30% of the cell's volume, provide 90% of the total energy in the form of ATP via aerobic respiration (Piquereau et al. 2013). Thus, efficient cardiac function is highly dependent on the adequate amount of oxygen and nutrients received. However, what happens if less or no oxygen and nutrients reach the heart, how would cardiomyocytes respond, and will they manage to survive?

1. Myocardial Ischemia:

Partial or complete coronary arterial occlusion in the heart leads to the obstruction of oxygen and nutrients supply, a process known by "myocardial ischemia". Few seconds post-ischemia, heart's oxygen demands exceed the amount supplied by the arterial flow. The heart's response to this imbalance is not homogenous and thus it is separated into two major areas as displayed in **Fig. 1**, the ischemic area at risk and the non-ischemic area. In the area at risk, some cells are more

damaged than others, generating a heterogeneous zone divided into necrotic and ischemic zones (Fernández-Friera et al. 2017). The size of these zones is the major determinant of the infarct size and its clinical outcomes.

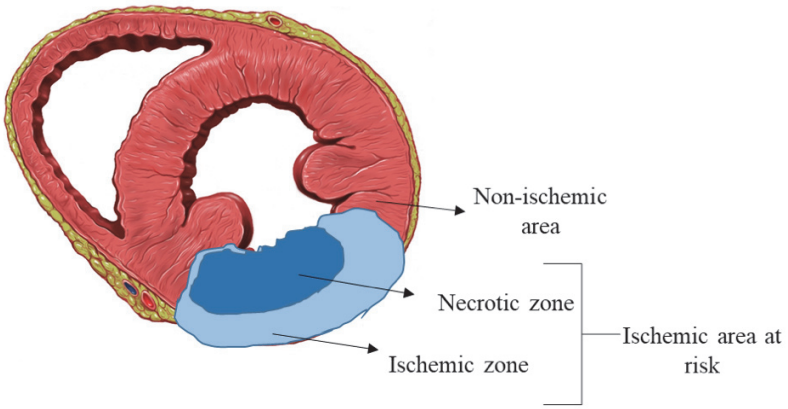

Figure 1: **Myocardial heterogenous areas in response to ischemia.**

A scheme representing the different myocardial areas in response to oxygen deprivation to a specific area in the heart. Red area corresponds to the non-ischemic myocardium and blue area corresponds to the ischemic area at risk which is divided into necrotic and ischemic zone as well.

The consequent ischemic injury is greatly affected by the severity and the duration of ischemia. Within 15-20 minutes of the blood blockage, cells are not dead yet and injury is considered reversible; if blood flow is restored, cells might resume their normal contractile activity. However, if the duration of ischemia is prolonged, cardiac cells enter a phase of irreversible injury (Hausenloy and Yellon 2013; Jennings and Reimer 1981). Necrosis of cardiomyocytes in response to ischemia occurs in a form of wave starting in the endocardium and progressing towards the epicardium through the myocardial wall (Reimer et al. 1977). Once dead, due to their poor regenerative activity, cells will be replaced by a fibrous matrix and eventually they will impair the contractile activity of the heart.

The contractile activity is regulated by calcium homeostasis in the cardiomyocytes. However, under ischemic conditions, cells possess alterations in their calcium level caused by a chain of events summarized in **Fig. 2** by the following. The decreased amounts of oxygen reaching the

heart eventually disrupts the mitochondrial respiration process and leads to the anaerobic metabolic shift that is triggered by the consequent decrease of ATP production (Wu et al. 2018). This shift results in lactate accumulation, consequently leading to decreased pH (< 7) inside the cell. As a compensatory action, Na^+ ions are exchanged with the protons. However, increased Na^+ in the cell activates the $2Na^+$-Ca^{2+} ion exchanger leading to calcium overload which thus disrupts the contractile activity and alters cardiomyocytes homeostasis (X. Li et al. 2016).

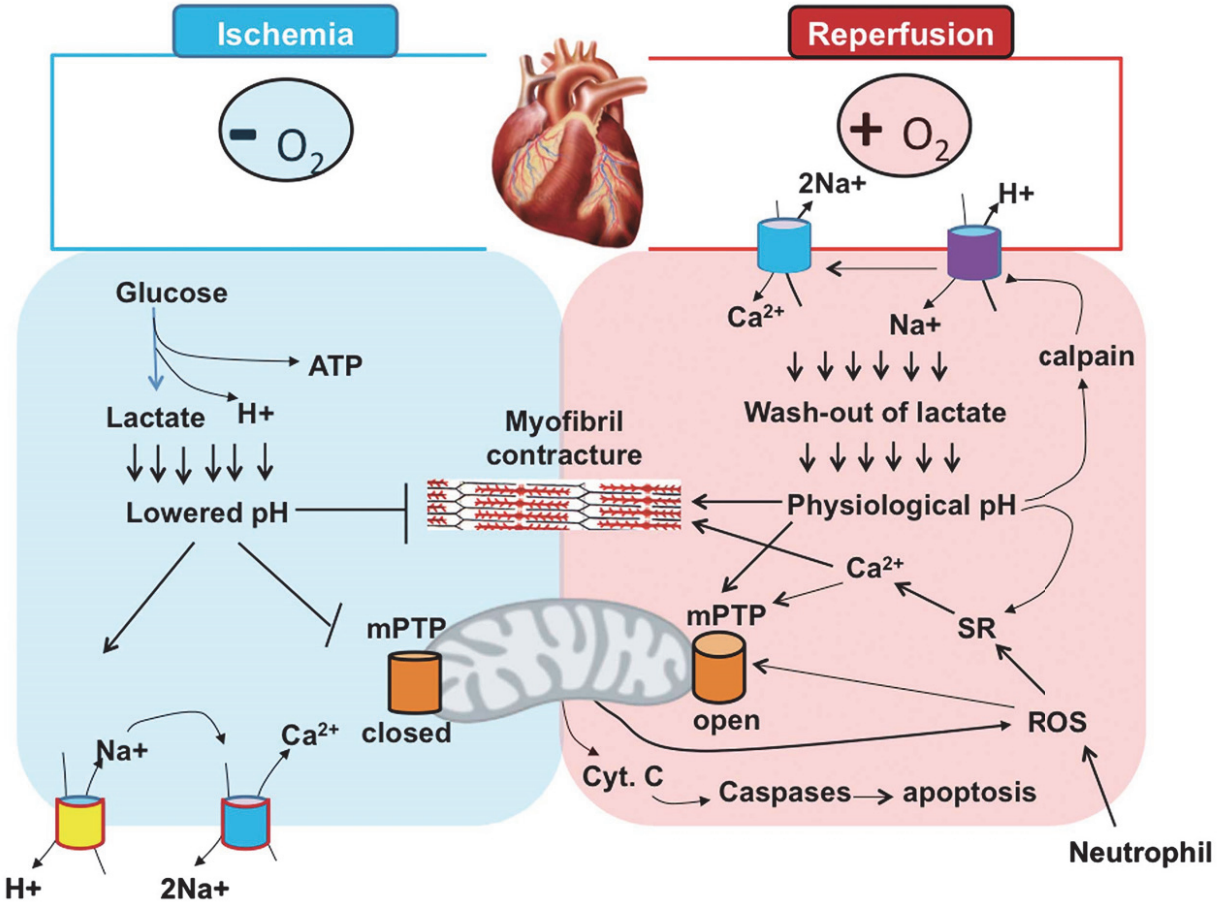

Figure 2: Molecular events in response to myocardial ischemia and reperfusion.

A scheme representing the major events taking place in the myocardium in response to blood blockage (ischemia) and its reflow (reperfusion). mPTP: mitochondrial permeability transition pore, SR: sarcoplasmic reticulum, ROS: Reactive oxygen species (Li et al. 2016).

2. *Myocardial Reperfusion:*

Previously, it was thought that myocardial salvage by blood reflow, known as reperfusion, was the promising tool to reduce ischemia deleterious consequences. However, reperfusion was found to act as "*a double-edged sword*" accelerating cardiac cell death and worsening clinical outcomes (Hausenloy and Yellon 2013; Braunwald and Kloner 1985; Bell and Yellon 2011). As shown in **Fig. 3** cell death caused by the ischemic injury progresses in a time dependent manner, blood reflow induces increased cell death in the heart but to a lesser extent than that induced when no reperfusion is applied (Ovize et al. 2010; Garcia-Dorado and Piper 2006).

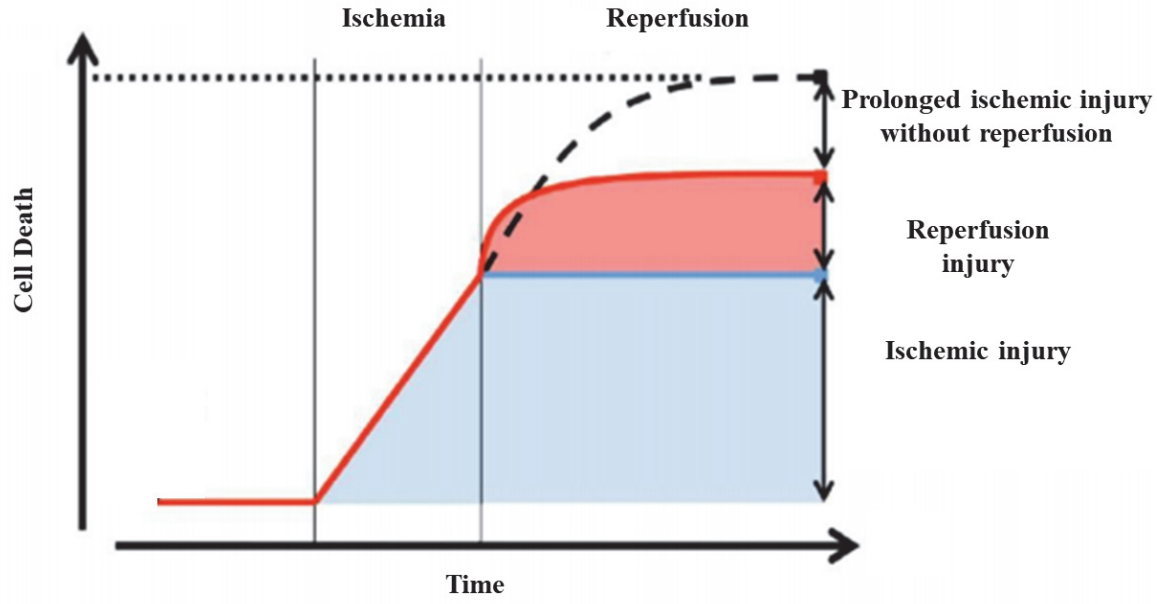

Figure 3:The evolvement of cell death in response to myocardial ischemia and reperfusion.

A scheme representing the consequent cell death caused by ischemia which is further increased in response to reperfusion (curved red line). If the myocardium is not reperfused, it is subjected to further cell death (dashed black line). Figure is adapted from Garcia-Dorado and Piper 2006.

Although blood reperfusion carries back oxygen and nutrients to the injured cells, it possesses an exacerbated response characterized finally by cell swelling via the following structural alterations reviewed in **Fig. 2**:

- ***Correction of the pH***: Acidosis in the cell is increased during ischemia due to the accumulation of H^+, Na^+, Ca^{2+} ions and lactate in the cell. The rapid correction of pH, also known as the pH paradox, induced by the blood reflow triggers mitochondrial membrane permeability transition pore opening (mPTP) and leads to cell death (Yang 2018; D. M. Yellon and Hausenloy 2007).

- ***Oxidative stress***: Reactive oxygen species (ROS) are considered major mediators of the reperfusion injury. At the onset of reperfusion, ROS are massively released in the cell from different sources (like mitochondria, uncoupled nitric oxide synthase and xanthine oxidase). These species are highly reactive and affect several axes in the cardiac cell death such as calcium release from the sarcoplasmic reticulum (SR), neutrophils trafficking and mPTP opening (Hausenloy and Yellon 2013; Yang 2018; D. M. Yellon and Hausenloy 2007).

- ***Calcium overload*:** Increased cytosolic calcium present during the ischemic phase enhances the accumulation of Ca^{2+} in the mitochondria as a compensatory action. During reperfusion, the re-availability of ATP over-activates the ATP-dependent calcium channels which act inversely due to their exceeded capacity (Garcia-Dorado et al. 2014). Additionally, the disruption of the sarcolemmal-membranes will lead to a further increase of the intracellular calcium which consequently leads to a hyper-contractile activity and enhances mPTP opening (D. M. Yellon and Hausenloy 2007).

- ***Mitochondrial dysfunction and mPTP opening****:* Mitochondrial function in the cells is also affected by their calcium homeostasis. Under physiological conditions, calcium is a major activator of ATP production. However, during ischemia-reperfusion, calcium accumulation in the mitochondrial matrix causes its dysfunction (Yang 2018). The inner mitochondrial membrane, acting as a barrier against ions and metabolites and is responsible for maintaining mitochondrial potential, can be subjected to transient permeability by a

non-selective channel known by the mPTP. During ischemia, mPTP is kept closed. However, as shown previously, during reperfusion all the activated events trigger its opening, as considered the driving wheel of death. Consequently, once opened, a massive amount of protons enter the mitochondrial matrix leading to uncoupled oxidative phosphorylation associated with ATP depletion and impairment in the mitochondrial polarization. At the same time any molecule smaller than 1.5 kDa leaks from the matrix, which includes many metabolites required for bioenergetics. Finally, mitochondrial swelling develops what can induce the permeabilization of the outer mitochondrial membrane leading to activation of pro-apoptotic pathways via the release of cytochrome c which eventually drives cell death (Yang 2018; Halestrap 2009).

3. Cell death mechanisms during myocardial ischemia-reperfusion:

As previously discussed, myocardial ischemia consequent injury has been mainly attributed to energetic stress, whereas reperfusion was linked to ionic shifts and mitochondrial dysfunction resulting in cell death. Cardiomyocytes die in response to ischemia-reperfusion injury (IRI) mainly by apoptotic and necrotic pathways. However, other mechanisms of death like autophagy do still occur and are overviewed below:

- ***Necrosis****:* Necrosis has been long viewed as an uncontrolled passive mechanism of cell death in response to stresses. It is morphologically characterized by cell swelling and lack of nuclear fragmentation and is activated via different cellular processes (Tavernarakis 2007). During ischemia-reperfusion, the major contributor of necrotic cell death is thought to be the loss of ATP caused by impaired oxidative phosphorylation. Additionally, the H^+, Na^+ and Ca^{2+} ions shift and accumulation and the mPTP opening leads to the disruption of the cardiomyocytes membrane's integrity contribute to the necrotic activated pathways (Chiong et al. 2011; Orogo and Gustafsson 2013). However, unlike to what was thought for so long, necrosis can be a slightly regulated process during ischemia-reperfusion. Necrotic pathways might cross-link with the apoptotic ones in a process named "*necroptosis*" and induce a new form of cardiac cell death that combines both characteristics of necrosis and apoptosis (Zhe-Wei, Li-Sha, and Yue-Chun 2018).

- ***Apoptosis**:* Necrosis has been regarded as the only cause of cardiomyocytes death for a long time. However, studies have shown that apoptosis contribute to tissue damage during IRI. Apoptosis is defined as an energy-dependent programmed cell death. It occurs as a homeostatic mechanism to maintain healthy cellular populations in tissues. It is morphologically characterized by cell shrinking, DNA and nuclear fragmentation and formation of apoptotic bodies (Konstantinidis, Whelan, and Kitsis 2012; Elmore 2007). In the cells, two apoptotic pathways are present, the extrinsic and intrinsic pathways

    - ***Extrinsic pathway**:* Extrinsic apoptotic pathway, also known as the death receptor pathway, is activated via death ligands (soluble ligands like tumor necrotic factor-α (TNFα) and surface bound ligands like Fas) binding to their receptors. This binding results in the formation of the Death Inducing Signaling Complex (DISC) (Konstantinidis, Whelan, and Kitsis 2012). The latter constitute several proteins like Caspase-8, Fas-associated death domain (FADD) or TNF-receptor associated death domain (TRADD) and receptor-interacting protein 1 (RIP1). Caspase-8 plays a role in activating other caspases (Caspase-3 and Caspase-7) that play a proteolytic role and lead to apoptotic death.

    - ***Intrinsic pathway**:* Unlike the extrinsic pathway, intrinsic apoptotic induced cell death is activated by internal signals such as the hypoxic conditions and the oxidative stress caused during IRI. Mitochondria are the major mediators for intrinsic apoptotic pathway activation. Their permeabilization during ischemia-reperfusion leads to the release of pro-apoptotic proteins (Bcl-2 protein family, cytochrome c, second mitochondria-derived activator of caspases (SMAC)/direct inhibitor of apoptosis binding protein with low pI (DIABLO)) into the cytosol. Cytochrome c binds to apoptotic protease activating factor 1 Apaf1 and procaspase-9 to form the “apoptosome”. The latter activates caspase-9 which in turn activates other caspases that has as well proteolytic cleavage role leading to apoptotic cell death (Orogo and Gustafsson 2013; Elmore 2007; Krijnen et al. 2002; Kalogeris et al. 2012).

- ***Autophagy**:* Autophagy is regarded as the "housekeeping" mechanism in cells disposing their aggregates and damaged proteins and organelles. It is usually considered a degradation survival mechanism rather than a death process. Similar to apoptosis, autophagy is highly regulated. It is achieved in a mammalian target of rapamycin (mTOR) dependent manner induced by ATP depletion during ischemia-reperfusion. ATP depletion is sensed via the AMP-activated protein kinase (AMPK) which inhibits mTOR and activates eukaryotic elongation factor 2 (eEF2) proteins by its phosphorylation activity. Other than AMPK, Bnip3, a protein upregulated under hypoxic conditions, contributes to the activation of autophagy-induced cell death (Kalogeris et al. 2012; Gustafsson and Gottlieb 2009).

4. Myocardial infarction induced models:

In order to get insights into the precedent mechanism that cannot be obtained clinically, several *ex-vivo, in-vitro* and *in-vivo* preclinical models have been historically developed to mimic the myocardial infarction model respectively through the Langendorff's heart isolation (de Leiris, Harding, and Pestre 1984), isolated cardiomyocytes and coronary artery ligation (Lindsey et al. 2018). The latter includes ischemia-reperfusion sequence which was first introduced by Johns and Olson in 1954 (Johns and Olson 1954) and modified in small animals by Ahn et al. (Ahn et al. 2004). Coronary artery ligation in mice is achieved by mechanical pressure obstruction which might cause tissue damage. It is induced via different procedures including the open-chest and closed-chest surgery models. However, surgical interventions have been reported to have adverse effect on the studied system and modifying them would affect the outcomes like the uniformity of the infarct size and the survival rate. In this regard, the open-chest surgical model remains the commonly used one for inducing myocardial infarction in small laboratory animals like the mice and rats, including ours (Kumar et al. 2016). This invasive model is achieved via three major procedures: open-chest sternotomy, thoracotomy by breaking one rib and intercostal surgery. However, this procedure might be associated with activated inflammatory response that might be a confounding factor in characterizing myocardial infarction induced effect.

Chapter 2: Inflammation in Myocardial Infarction

As any other injury, myocardial ischemia-reperfusion injury initiates intense inflammatory response which is prerequisite for wound healing and formation of the scar that replaces damaged cardiac cells and preserves the ventricle's architecture. The resultant decrease in the infarct size by applying anti-inflammatory strategies (like corticosteroids) in infarcted animals was the first experimental clue that inflammation could contribute to extending ischemic-reperfusion injury (Libby et al. 1973).

Repair and healing mechanisms post myocardial injury are highly dependent on the activated cellular events leading to the formation of collagen-based matrix due to the heart's little regenerative characteristic. The fact that inflammation is regarded as a two-edged mechanism, contributing to the exacerbation of the reperfusion injury and the tissue repair as well, complicates the comprehension of the dynamic orchestrated interplay between inflammatory mediators (pro-inflammatory and anti-inflammatory). The inflammatory response in the injured myocardium is described in three phases, the inflammatory phase, the proliferative phase and finally the maturation phase which are mediated by different cells and molecules (N. G. Frangogiannis 2012) briefed below and reviewed in **Fig. 4**.

1. Innate immune response:

In the ischemic area, cardiomyocytes dying by necrosis release their intracellular content and activate the innate immunity via the danger-associated molecular patterns (DAMPs). DAMPs, like mitochondrial DNA, RNA and ATP, are recognized by pattern recognition receptors as the toll-like receptors (TLR). TLRs, a family of transmembrane receptors, are expressed on endothelial cells, cardiomyocytes and inflammatory cells and play a role in activating pro-inflammatory cascades mainly via the TLR2 and TLR4 post infarction (N. G. Frangogiannis 2014). TLRs activation consequently leads the activation of pro-apoptotic signals, leukocytes recruitment to the infarcted area and the formation of NLRP3 (nucleotide-binding oligomerization domain-like receptor family of cytosolic proteins) inflammasomes (**Fig. 5**) (Ong et al. 2018).

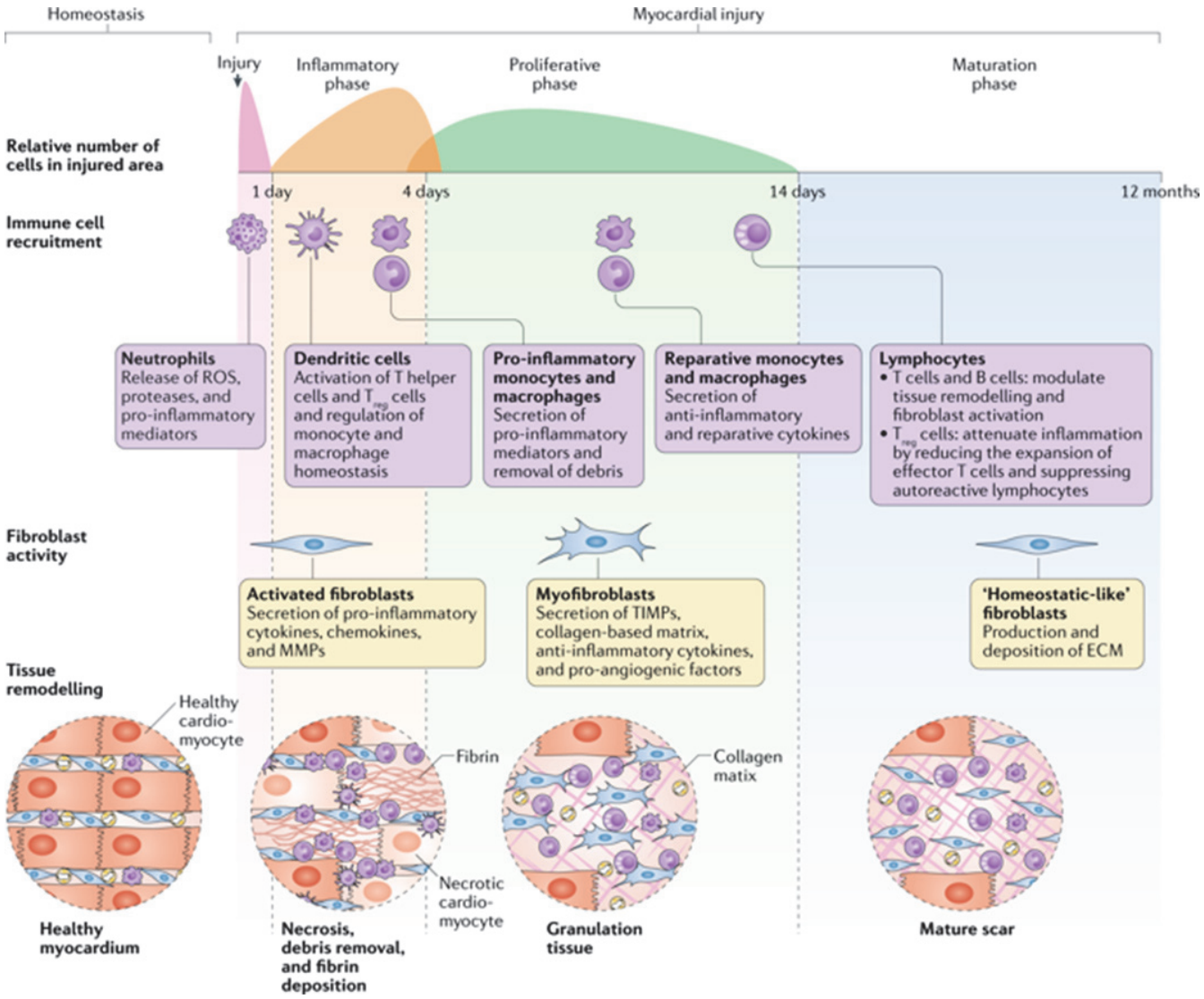

Figure 4: Inflammatory response major components activated by myocardial infarction.

A scheme displaying the different phases of the activated inflammatory response post myocardial infarction (Forte et al. 2018).

Together, the inflammasomes and the activated immune cells release pro-inflammatory cytokines like IL-18 and IL-1β. Additionally, DAMPs also lead to the activation of the early components of the complement cascade contributing to acute inflammatory response (Ong et al. 2018; N. Frangogiannis 2002).

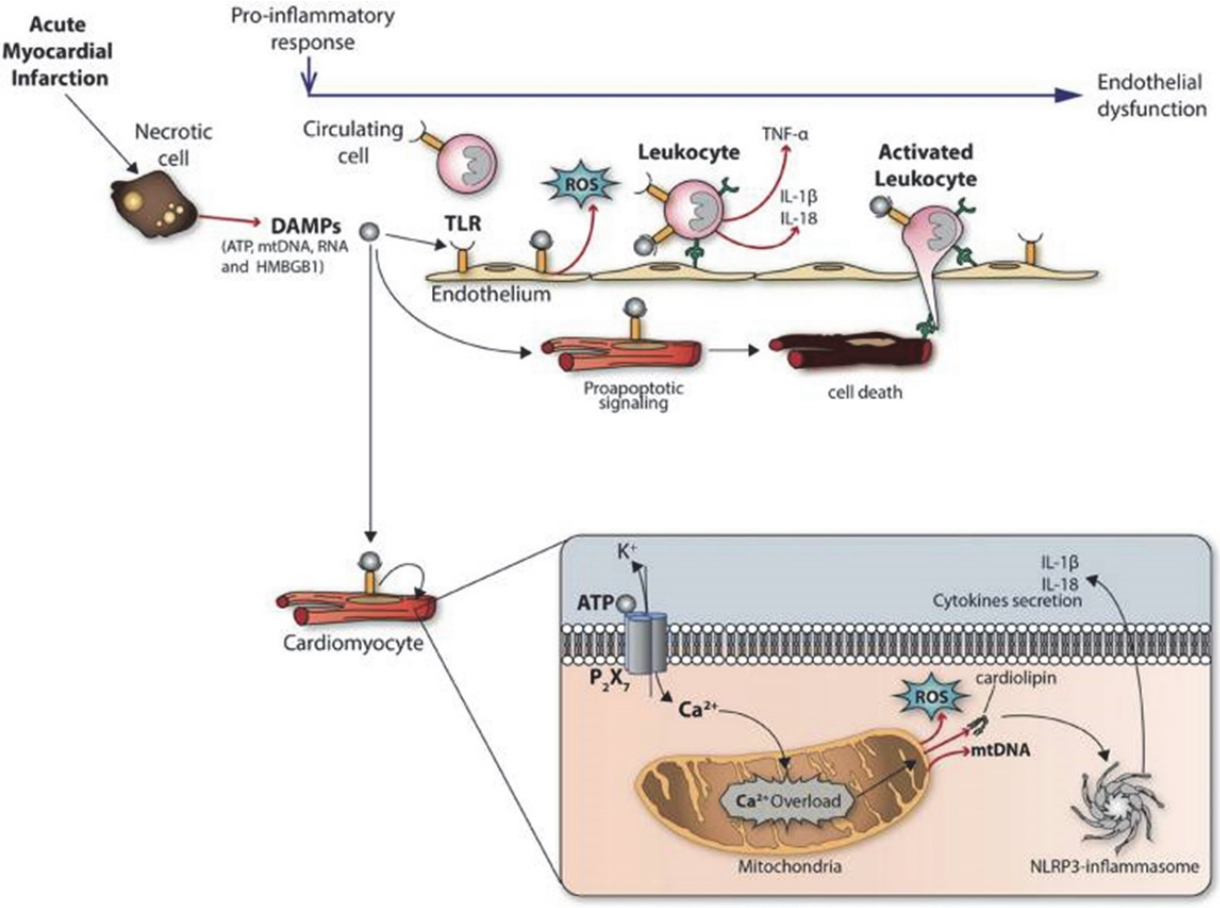

Figure 5: Activation of the innate inflammatory response.

A scheme displaying the activation of the pro-inflammatory response and endothelial dysfunction in response to the activation of the Toll-like receptors by the DAMPs released by necrotic cardiomyocytes, where leukocytes are recruited, cytokines are released and inflammasomes are formed (Ong et al. 2018).

2. Cell-mediated immune response:

The activated inflammatory response involves both cells localized in the heart and newly recruited ones in response to the ischemia-reperfusion injury. As discussed previously, necrotic dead

cardiomyocytes release their DAMPs and trigger the activation of the inflammatory response via several axes. These axes indeed include resident non-cardiomyocytes cell populations (endothelial cells, fibroblasts and cardiac resident macrophages) and recruited inflammatory cells (neutrophils, monocytes/macrophages, dendritic cells and lymphocytes) which play a pivotal role in the progress of the inflammatory response post injury as follows:

2.1. Cardiac resident cells:

2.1.1. ***Endothelial cells***: As displayed in **Fig. 5**, endothelial cells are also activated by the release of DAMPs from necrotic cells via the TLRs. Their activation is associated with increased ROS production and pro-inflammatory cytokines in the infarct area. In addition, the expression of adhesion molecules and surface receptors is increased in order to facilitate immune cells binding and locomotion to the injured area (N. G. Frangogiannis 2012; Ong et al. 2018; Cheng et al. 2017).

2.1.2. ***Fibroblasts*:** Fibroblasts are viewed as the architects of the heart. They are embedded between cardiomyocytes and share tight connections via the abundant connexins they exhibit. Under physiological conditions, fibroblasts secrete extracellular components matrix (ECM) to render the tissue intact. However, under ischemia-reperfusion conditions, fibroblasts play a major inflammatory role where they undergo phenotypic and functional alterations (like trans-differentiation into myofibroblast secreting matrix proteins) during the different inflammatory phases post infarction (**Fig. 4**). Once activated, by DAMPs as well, they are triggered to activate inflammasome formation, produce cytokines, chemokines and proteases that have a matrix-degrading activity which helps in removing cell debris, wound healing and scar formation (Forte, Furtado, and Rosenthal 2018; Shinde and Frangogiannis 2014).

2.1.3. ***Resident macrophages*:** Under normal physiological conditions, cardiac resident macrophages, originating from embryonic precursors, account for 5-10% of the total non-myocyte population in the heart. In steady state, they are spindle-shaped, dispersed between cardiomyocytes and are considered non-inflammatory. Their role is to obtain myocardial homeostatic maintenance via removing damaged cells and protecting against infections (Yonggang Ma, Mouton, and Lindsey 2018). Resident macrophages have different expression profiles than monocytes-derived recruited cells (to be reviewed later) so that they can be distinguished, example the chemokine receptor CCR2 that is less expressed in resident macrophages and F4/80 is highly expressed compared to monocyte-derived macrophages (Mouton et al. 2018). Cells localized in the ischemic area begin to die post infarction and resident macrophages present in the non-ischemic area proliferate locally and replace dead cells days after MI and display an efficient role in removing dead cardiomyocytes (Cheng et al. 2017; Yonggang Ma, Mouton, and Lindsey 2018; Epelman et al. 2014).

2.2. Recruited cells:

2.2.1. ***Neutrophils*:** Post ischemic-reperfusion injury, neutrophils were found the first to be recruited to the inflamed site within the first 24 hours, attracted via the DAMPs and cytokine secretions. Anti-inflammatory strategies reducing the influx of neutrophils to the infarct area has shown to limit the IR injury and reduce infarct size post MI (N. Frangogiannis 2002; Horckmans et al. 2016).

At the onset of reperfusion and upon neutrophil-chemoattractant interaction, neutrophils undergo some rearrangements, change in their shape and polarization to enhance their interaction with the endothelial cells on the vessel's walls through adhesion molecules expressed on cells' surfaces like selectins and integrins, and enabling them to move intravascularly in a concentration gradient manner towards the inflamed site. Neutrophils then extravasate into the extracellular matrix where they are programmed to release high levels of ROS and proteolytic enzymes and finally undergo apoptosis (Petri and Sanz 2018).

2.2.2. ***Monocytes and macrophages*****:** Neutrophils accumulation in the injured myocardium are also associated with increased recruitment of monocytes and macrophages. Monocytes from bone marrow and splenic reservoirs are attracted to heart post infarction in 2 phases. Phase 1 is characterized by the recruitment of the pro-inflammatory circulating $Ly6C^{high}$ monocytes that peak 3-4 days post-infarction and the second phase is however associated with the recruitment of the anti-inflammatory $Ly6C^{low}$ monocytes which peak 7 days post-MI (Ong et al. 2018). $Ly6C^{high}$ and $Ly6C^{low}$ recruited monocytes interact with the endothelial cells via the monocytic CCR2 and CX_3CR1, respectively, and CCL2 endothelial chemokine (C-C motif) ligands along with the cell adhesion molecules to reach the infarct area. After extravasation, recruited monocytes release TNF-α and IL-1β and differentiate into macrophages that release ROS and proteases and phagocyte dead cells and matrix debris (Sager, Kessler, and Schunkert 2017). Monocytes and macrophages are characterized by their phenotypic plasticity due to their ability to shift their functional phenotype continuously. Infiltrating monocytes differentiate into M1 macrophages that are responsible for clearing the infarct area from necrotic cells and the extracellular matrix. These macrophages secrete pro-inflammatory chemokines and cytokines and attract other immune cells. However, their prolonged activation in the myocardium extends the inflammatory response and exacerbates the injury. Days after infarction, a reparative phase is activated governed mainly by $Ly6C^{low}$ monocytes, originating from $Ly6C^{high}$ monocytes or circulation, and the anti-inflammatory M2 macrophages which activate reparative processes like myofibroblasts formation, angiogenesis and promote matrix formation via the secretion of pro-fibrotic and anti-inflammatory factors like IL-10 and TNF-β (Nahrendorf et al. 2007; Gombozhapova et al. 2017; Walter et al. 2018). However, how this phenotypic shift is orchestrated is still not clearly defined where dynamic transcriptional changes was reported in the macrophages' subtypes resulting in heterogenous populations post infarction (Walter et al. 2018).

2.2.3. ***Dendritic cells***: Acting as antigen-presenting cells, dendritic cells play a crucial role in activating the adaptive immune response via capturing and processing targets and consequently activating T cells post infarction. Following ischemia-reperfusion, dendritic cells, coming from bone marrow and splenic reservoirs and monocytes differentiation, were shown to infiltrate to the myocardium and accumulate in the border zone of the infarct area (Ong et al. 2018; Yilmaz et al. 2010). Dendritic cells are activated by DAMPs via the TLR2 and TLR4 and release inflammatory cytokines. Depletion of dendritic cells was shown to extend inflammatory response and prevent cardiac repair (Anzai et al. 2012). Dendritic cells activate both the regulatory T cells (Treg) and the T helper cells which play anti-inflammatory role via preventing cell destructive autoimmunity and help preventing left ventricular remodeling's effects post injury (Forte, Furtado, and Rosenthal 2018).

2.2.4. ***Lymphocytes*****:** adaptive innate immunity is mediated by the T and B cells that originate from bone marrow progenitor cells. Adaptive immune response is activated later during myocardial injury in an antigen specific manner displayed to lymphocytes by different cells, mainly the dendritic cells. T cells and B cells are involved in tissue remodeling and myocardial repair post injury. They were shown to infiltrate to the myocardium and peak 7 days later where their level is increased 5-10 folds. T cells activation in the lymph node is associated with two subtypes, the T helper cells (CD4+ cells) and the Tregs. The latter play an immunosuppressive role by secreting anti-inflammatory cytokines like IL-10, inhibiting the recruitment of inflammatory cells and preventing cardiomyocytes' apoptosis (T.-T. Tang et al. 2012). In addition, Tregs augment the macrophages' phenotypic shift toward the anti-inflammatory M2 phenotype associated with myofibroblast activation prompting wound healing (Weirather Johannes et al. 2014). However, little is known about B cells in the myocardial injury, it was shown that their infiltration enhances proinflammatory response via the secretion of CCL7 chemokine which consequently induces $Ly6C^{high}$ monocytes recruitment to the inflamed area post injury (Hofmann Ulrich and Frantz Stefan 2015; Zouggari et al. 2013).

Post-infarction activated inflammatory response characterized by the inflammatory cells' infiltration, innate immunity and adaptive immune response activation is a prerequisite step in resolving myocardial injury and tissue repair. The complex interconnections and involved mediators orchestrating the pro and anti-inflammatory phases represent promising therapeutic targets to reduce the deleterious effects associated with the ischemic reperfusion injury and thus improving clinical outcomes. Several anti-inflammatory treatments have shown encouraging pre-clinical results like the glucocorticoids (example, hydrocortisone and dexamethasone) and nonsteroidal anti-inflammatory drugs (NSAIDs) and other drugs targeting cytokines (example, humanized monoclonal antibody Tocilizumab), complement cascades, metalloproteinases (example, doxycycline) and integrins. However, no significant effect was detected in clinical studies, where further research is required to find out the good strategies to enhance healing and maintain inflammatory balance post injury (Seropian et al. 2014).

Chapter 3: Cardioprotection against Myocardial Infarction

Aside from the failing therapeutic inflammatory targets, earlier efforts have been made to salvage the ischemic myocardium from the resultant ischemia-reperfusion injury via cardioprotective strategies. Cardioprotection is defined as all the mechanisms that aim to preserve heart function and reduce or prevent myocardial damage (Kübler and Haass 1996). In this regard, small episodes of ischemia/reperfusion cycles have been applied to the heart in order to render it resistant and adaptable against stress. These strategies were referred to the ischemic conditioning phenomena. As displayed in **Fig. 6**, conditioning strategies can be classified in a temporal and a spatial manner. It can be applied before (preconditioning), during (preconditioning) and after (postconditioning) the ischemic stress where, it can be performed directly to the heart (classical conditioning) or from a distance to the ischemic site (remote conditioning). In addition, ischemic conditioning can also refer to the use of pharmacological agents that have succeeded in mimicking the effect induced by the previously described mechanical strategies (Hausenloy and Yellon 2016; R. L. Yellon and Yellon 2018).

In this work, the focus will be on the ischemic postconditioning strategy which is applied in our model as will be described in the methods section.

1. What is ischemic postconditioning?

Initially, the term “ischemic postconditioning (IPost)” was firstly introduced as anti-arrhythmic strategy applied in a cat model via intermittent reperfusion to reduce ventricular fibrillation (Na et al. 1996). Later in 2003, IPost was reported to induce a cardioprotective effect similar to that achieved by the previously applied preconditioning interventions, which usually needed to occur before the ischemic events that are not always feasible to detect (Zhao et al. 2003). As discussed earlier in this manuscript, because reperfusion activates a chain of lethal events within a short time after blood restoration, it was sought that the first few minutes of reperfusion might act as a therapeutic window where myocardial salvage can still be achievable. Thus, IPost is applied to the heart directly at the onset of reperfusion. Models and algorithms of the ischemia-reperfusion cycles applied differ considerably between the different species depending on several factors like the infarction evolution that is mainly determined by the duration of ischemia (Ovize et al. 2010).

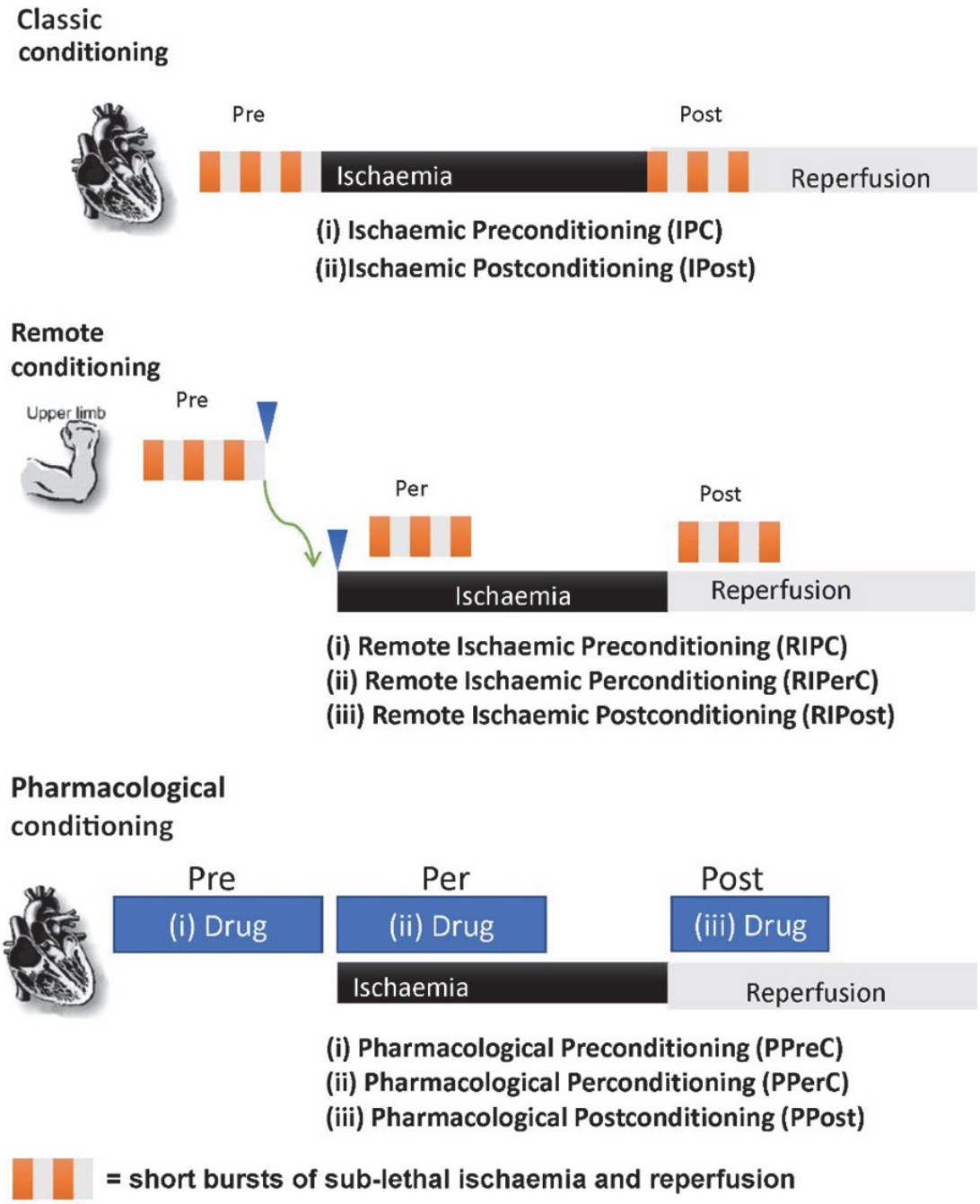

Figure 6: Various forms of the conditioning strategies.

A scheme displaying the different conditioning strategies via short cycles of ischemia-reperfusion or pharmacologically that are applied directly or at a distance from the heart, before, during or after myocardial ischemia (R. L. Yellon and Yellon 2018).

2. *Ischemic postconditioning mechanism of action and the consequent protective effects*

IPost has been reported to reduce the infarct size, cardiomyocytes' associated death and endothelial dysfunction and improve the hearts' contractile activity. It has shown great efficiency against the reperfusion injury in different species and organs like brain, kidney and intestines (Ovize et al. 2010). Cardioprotective effect was achieved via signaling mechanisms involving two major pathways, the reperfusion injury salvage kinase pathway (RISK) and the survivor activating factor enhancement (SAFE) pathways. The IPost stimulus (ischemia/reperfusion cycles) initiates the production of mediators, termed autacoids (adenosine, bradykinin and opioids), which bind to their subsequent receptors on the cardiac cells' plasma membrane and activate cardioprotective signals conveyed to different cellular compartments, mainly the mitochondria (**Fig. 7**). These signals were found to restore cellular pH and reduce calcium overload and ROS production which consequently inhibits mPTP opening (Hausenloy and Yellon 2016).

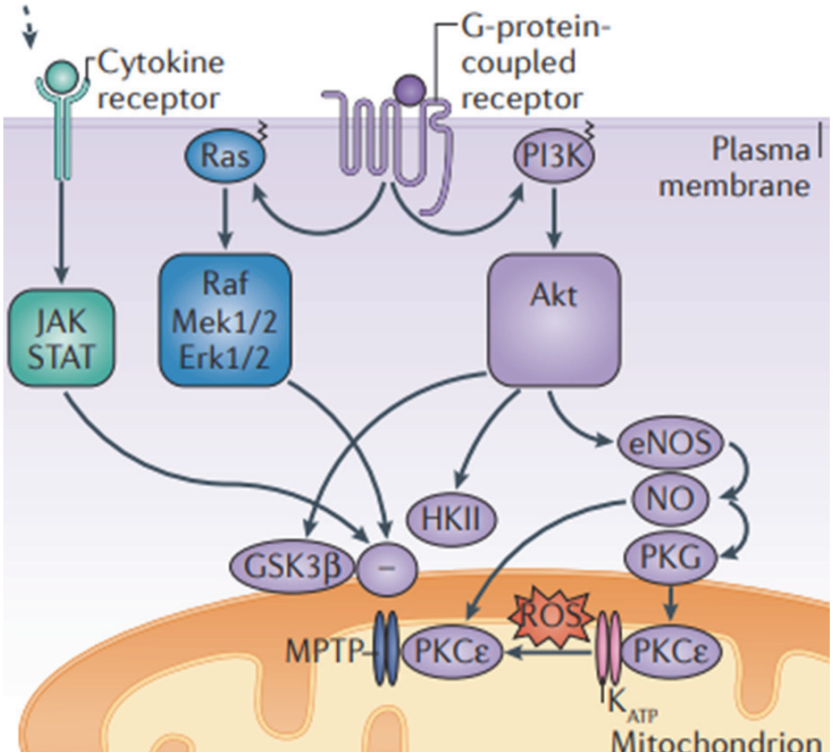

Figure 7: Ischemic postconditioning signaling pathways.

A scheme displaying the activated signaling pathways starting at the plasma membrane of cardiomyocytes and conveyed to the mitochondrion via the SAFE (JAK/STAT3) and RISK (PI3K–Akt and Mek1/2–Erk1/2) pathways.

Among the major mediators that play an important role in achieving the postconditioning cardioprotective effect is the signal transducer and activator of transcription (STAT3) studied by our team. STAT3 is a transcription factor that belongs to the family of the 7 mammalian STATs. Upon activation by different stimuli (like cytokines and growth factors), STAT3 plays a protective role in the myocardium in response to stress other than its canonical role in cellular growth, differentiation and survival. It has been reported that STAT3 protective activity is realized via the traditional transcriptional function as a transcription factor stimulating protective and anti-apoptotic genes expression (like the Bcl-xl and Bcl2) and the mitochondrial function that is still under investigations (Zgheib et al. 2012; Zouein, Kurdi, and Booz 2013; Wagner and Siddiqui 2009). Mitochondrial and transcriptional functions of STAT3 are being extensively studied in our lab, where I will be later displaying how STAT3 target genes are affected in response to ischemia-reperfusion in our studied model.

3. Therapeutic hypothermia:

In addition to the ischemic conditioning strategies that have been long used to protect the myocardium against the lethal reperfusion injury, therapeutic hypothermia (TH) has been an alternative approach. When body temperature usually drops below 35℃, a phenomenon called hypothermia, the case is considered life-threatening; however, when therapeutically applied in certain medical cases like myocardial infarction, it was found to be a protective strategy decreasing the infarct size (Kang, Fumiaki, and Pyun 2016). TH can be classified into profound (<20 ℃), severe (20-28 ℃), moderate (28-32℃) and mild (32-35 ℃) and can be applied by skin cooling or endovascular cooling (Kang, Fumiaki, and Pyun 2016; Song and Lyden 2012). TH was shown to decrease infarct size in different species including swine, rabbits and mice (Duncker et al. 1996; Simkhovich, Hale, and Kloner 2004; Tissier et al. 2009; Knoop et al. 2019), however the mechanism to achieve this cardioprotective effect is still not well elucidated and requires further investigations.

4. *Therapeutic hypothermia induced mechanism:*

Few are the studies that characterize the major mediators and targets of TH. Mild cooling of the heart during ischemia has been a potent strategy that showed beneficial effects in the myocardium, preserving its contractile activity (Dixon et al. 2002; Miki et al. 1998). The suggested mechanism behind this protective effect is contributed to the preservation of the mitochondrial function and inhibition of the mPTP opening via conserving ATP, reducing myocardial metabolic demands, maintaining normal pH and reducing calcium and sodium overload (Kang, Fumiaki, and Pyun 2016). Although TH shares some signaling mediators with the ischemic conditioning strategies, they have different approaches. Unlike conditioning, TH was sought to protect the cells against the initially occurring ischemic injury and not the consequent reperfusion injury (Tissier et al. 2012).

5. *Improving clinical outcomes: where do we stand?*

To date, preclinical studies show encouraging results, however, none of the attempts made for protecting the heart against myocardial infarction damage has succeeded in ameliorating the clinical outcomes. It has been challenging and disappointing, where novel strategies and more efforts are needed to be made in order to decrease mortality rates. Several multi-targeted approaches have also been tried, like combining different conditioning strategies together, and have also failed to mediate a protective effect in myocardial infarction patients (Hausenloy et al. 2017). Several factors likely contribute to this failure, among them are the biased results that originate from the experimental design and the widely used reductionist approaches which will be detailed in the following chapters.

Chapter 4: Systems Biology: A new-revolutionary approach in the heart

"A cell of a higher organism contains a thousand different substances, arranged in a complex system. This great organized system was not discovered by chemical or physical methods; they are inadequate to its refinement and delicacy and complexity." In his saying, Professor Herbert Spencer Jennings addresses the complexity of living organisms that is much more complicated than being studied via the reductionist biological approaches. Decades ago, scientists were concerned in studying entities separately not taking into account integrated-systems as a whole. Such approaches have succeeded in providing knowledge about single compartments, genes, proteins and metabolites, but unfortunately, they have failed in providing perception about the dynamic interactions between such entities which are pivotal to life (Diaz-Beltran et al. 2013).

The rapid progress in genetics and molecular biology tools along with the availability of massive biological data - especially the Human Genome Project data announced complete in 2003 (Collins and Mansoura 2001) - had been the accelerating engine in the revolution of new biological fields such as systems biology that aims to provide insights into our complex bodies and their associated diseases. Are not biological systems complicated? Indeed, they are. Systems biology aims to simplify these systems and clarifies that dimensionality reduction does not succeed in providing a conclusion about the whole system because the latter cannot be the sum of the parts (Breitling 2010).

Systems biology involves integrative holistic approaches which comprise the study of the non-linear behaviors of systems that cannot be simply inferred by adding up the parts' behaviors. It comprises dynamic networks construction that constitute nodes representing molecules (genes, proteins or transcripts) and edges defining the interactive relationship between them (gene-gene, gene-protein or protein-protein interactions). As displayed in **Fig. 8**, systems biology involves the integration and iteration of different fields of knowledge, like computational biology, bioinformatics, physics and mathematics to mine and analyze experimental biological information extracted at bench (Diaz-Beltran et al. 2013).

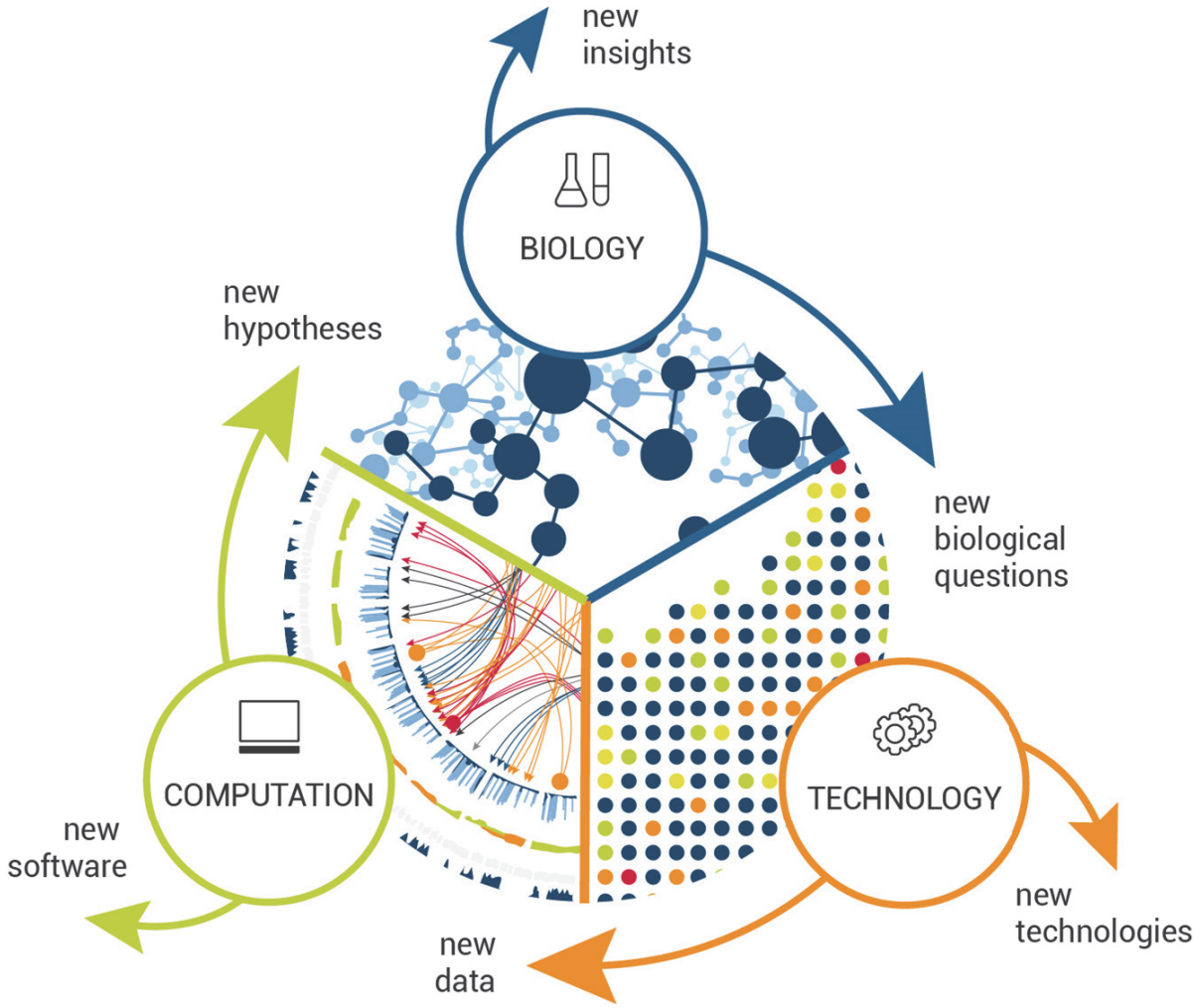

Figure 8: Systems biology engine.

A scheme displaying the major components of systems biology where biology drives technology and technology drives computational sciences leading to the generation of new data, software and biological insights (reference: The systems biology institute platform portal).

1. "Omics" in systems biology:

In 1985, Francis Crick was the first to introduce the "*central dogma of molecular biology*". He has described the framework of life in a cell characterized by the flow of information from DNA nucleotide sequences to proteins that make up the unique individuals we are (Cobb 2017). However, understanding the molecular and functional details of cells and tissues has been revolutionized by the -omics technologies (genomic, transcriptomic, proteomic and metabolomics) that have been extensively used in basic research in the recent years and resulted in a bulk of -

omics data. “Omics”, a suffix added to molecular terms, refers to the study of understanding molecules of interest like genes, proteins and transcripts. The generated large-scale datasets require statistical and mathematical tools to be correctly analyzed and interpreted based on the premise that some information cannot be unveiled by molecular biology approaches alone (Boogerd et al. 2007). However, due to the limited shared knowledge in the other fields, applying mathematical laws to biological data can be challenging for biologists and mathematicians as well.

Single -omics studies have rarely generated well comprehensible informational flow. These single approaches have failed to provide deep insights into the therapeutic strategies required for the treatment of complex multifactorial diseases, among them myocardial infarction. However, improving studies’ designs and involving systems biology approaches are the promising tools for deciphering the complex etiology of several disorders like cancers, neurological and importantly cardiovascular diseases (Hasin, Seldin, and Lusis 2017; R.-S. Wang, Maron, and Loscalzo 2015).

2. Systems biology in the heart:

In the recent decades, systems biology have greatly enhanced the understanding of the development, the unique characteristics and the pathologies associated with the cardiovascular system (Louridas, Kanonidis, and Lourida 2010; Sperling 2011). Cardiovascular diseases are complex and multi-factorial. As discussed in earlier chapters, ischemia reperfusion injury progression is mediated by the interconnections between the various involved mediators. Therefore, understanding this interplay between genes, proteins and other molecules with their surrounding environment and the reconstruction of functional networks via the systems biology approach will help unravel the unlinear spatio-temporal interactions responsible for diseases’ deleterious consequences and help in improving the associated pathology.

In myocardial infarction studied models, researchers have studied the progression of the disease in different animal models (mice, rats, rabbits and pigs) and at different levels (like proteins, metabolites, genes and transcripts…). However, because of the dynamic characteristic of the proteins and their inability to fully describe the historical story of the cell, many researchers and we as well were interested in studying the transcriptome which represent the key mediator between the genome and the proteome. In this regard, many studies were concerned with the changes

occurring in the different regions of the myocardium (ischemic and non-ischemic) during early or late reperfusion phase (Harpster et al., n.d.; Zimmermann et al. 2017; Prat-Vidal et al. 2013; Roy et al. 2006). The analytical strategy applied in these studies varied considerably from the experimental design (static vs kinetical sampling) to the statistical considerations (number of subjects and statistical strategy) and the data integration and validation if considered. These factors might act as a confounding factor in deciphering the real mechanism behind the pathology due to the biased conclusions made as a result of the reduced non-integrative approaches.

3. Confounding factors in cardiovascular transcriptomic studies analysis:

3.1. Experimental design of the transcriptomic studies:

A successful transcriptomic study relies on the ability of its generated data to answer the biological question of interest. In addition to the RNA extraction procedure, which is critical in fibrous tissues like the myocardium, and the RNA sequencing considerations (library type, randomization, and sequencing length), the experimental design of transcriptomic studies is largely affected by several factors like the experimental cost, the statistical power and the precision of measures. The more complex the transcriptome and the deeper the sequencing is, the greater the cost will be (Conesa et al. 2016). The fact which will make scientists compensate between a greater number of subjects and a deeper sequencing for greater transcripts coverage, which makes the results prone to bias caused by the consequent statistical power. Some studies have estimated a minimum of five and six replicates per condition are required to obtain stable significant results in microarray and RNA sequencing experiments, respectively (Lamarre et al. 2018; Pavlidis, Li, and Noble 2003; Schurch et al. 2016; Lin et al. 2018). However, unfortunately, these statistical requirements have not been met in several transcriptomic myocardial infarction induced models (Prat-Vidal et al. 2013; Roy et al. 2006).

In addition, the precision of measures is highly dependent on the biological variability of the studied system (which is greater in animals than in cellular models) and the introduced experimental error. The latter might originate from different factors like the RNA-seq protocol, mainly during cDNA libraries construction (Conesa et al. 2016) and the animal surgical-induced effect. As described earlier in this manuscript, several surgical models have been developed to

mimic myocardial infarction including the open-chest surgical model which remains the mostly used one (Kumar et al. 2016). This model was found to activate the inflammatory response (Hoffmann et al. 2014; Nossuli et al. 2000) and thus is artifact prone and might challenge the author's interpretation of the results if not quantified.

Other errors in such studies might originate from the static comparisons between the "pretreatment" and "post-treatment" groups of samples which, unlike kinetical comparisons, do not permit to cover the dynamic changes in expression profiles. With the exception of blood, kinetical analysis in the myocardium relies on sacrificing different animals at the studied time points and consequently contributing to higher biological variability.

3.2. Analysis of the transcriptomic data:

With the accumulation of massive large-scale data, the need of integrative analytical approaches and tools to construct biochemical networks is extensively growing. These integrative approaches have shown efficiency in incorporating quantitative experimental information and providing experimental predictions that are validated functionally. The large-scale datasets resulting from the high-throughput sequencing technologies, including the RNA-seq data used in our study, are immense in volume and are referred to big data that cannot be processed via the traditional applications therefore, their analysis requires computational algorithms to draw up conclusions and derive new insights.

Several pipelines and software packages have been developed to aid in the management and analysis of RNA-seq data, where their storage, processing and retrieval are major challenges faced in these studies. These pipelines differ considerably in their transcript quantification method, quality checks, statistical model (negative binomial and non-parametric models…) and normalization tool (Total counts, Upper Quartile, Fragments per kilobase per million (FPKMs), Trimmed mean of M values and DESeq normalization tools implemented in R Bioconductor packages EdgeR and DESeq respectively…) (Conesa et al. 2016; Zhong Wang, Gerstein, and Snyder 2009a). The choice between these normalization tools strongly influences the differential expression analysis (Burden, Qureshi, and Wilson 2014), where Cuffdiff, and DESeq2 remain the most frequently used ones (Lamarre et al. 2018). However, retrieving lists of differentially

expressed genes based on statistical comparisons is not enough for understanding disease's progression mechanism, where functional enrichment studies of these gene lists are required. Several curated databases are available for classifying functional categories (Gene ontology consortium, STRING, DAVID and Ingenuity Pathway Analysis IPA as examples) associated with statistical test to asses that the overrepresented enriched term did not occur by chance (The Gene Ontology Consortium 2019; Franceschini et al. 2013; Jr et al. 2003; Krämer et al. 2014). However, no optimum pipeline that can be used as a gold standard is present for kinetical analysis to date.

Complexity of the studied system is a major quality of the systems biology. Indeed, cardiovascular system is a complex one. Defining the concept of complexity is itself a complicated task where it is best described by the interconnections of a variety of components which are responsible for the behavior of the system that cannot be predicted when studied in subsystems or isolated components (Breitling 2010). However, these latter approaches have greatly improved our knowledge in understanding the behavior of various isolated single entities, but unfortunately, to date it didn't help in predicting the dynamic alterations taking place at the system's level and thus further efforts are needed to be made.

Chapter 5: Tissue Clearing

Aside from studying specific components in an isolated system, understanding the 3D perspective of tissues provides important insights into the structure-function relationship and thus new opportunities to manage the associated pathologies, including myocardial infarction. However, biological specimens have been long restricted to thin two-dimensional sections which researchers have used to construct volumetric images. Although volumetric construction was advantageous and had greatly improved mainly brain research, it had several drawbacks summarized by tissue distortion, some major structural information loss and importantly light scattering that had decreased images resolution and quality (Epp et al. 2015; Richardson and Lichtman 2015).

1. What is light scattering?

Any energy wave (light or sound for example) cannot travel in a straight path, except in vacuum, due to the diopter created at the interface between media (whether water, air, glass or any other) of different refractive index which refracts the energy wave in several directions. This phenomenon is also known by "light scattering". Cells are composed of 2 main solvents: water and lipids whose interface create a diopter. In tissues and organs, the light path of propagating photons is full of lipid/water interfaces, each one diffracting a part of the energy. Consequently, this makes it impossible to examine intact volumetric tissues/organs under microscopes (Richardson and Lichtman 2015).

In this regard, several advancements have been made in the imaging field to improve biological specimen's penetration. Light microscopic tools were revolutionized by the confocal methods where sectioning thickness was increased to tens of micrometers. Later, two-photon microscopy has improved imaging depth to hundreds of micrometers (Tomer et al. 2014). However, results were not satisfying enough and hence, the microscopy progress was accompanied by the emergence of new techniques that involved increasing tissues transparency chemically (like SCALE (Hama et al. 2011) and benzyl alcohol/benzyl benzoate clearing (Dodt et al. 2007)…). These methods, although effective in decreasing light scattering, had several molecular limitations regarding proteins and nucleic acids labeling (Sylwestrak et al. 2016) which resulted in the

formation of unstable fluorophores during the clearing procedure (Tomer et al. 2014). Such limitations lead to the development of CLARITY which renders tissues transparent and easily accessible by macromolecules, like labelled antibodies and oligonucleotides, with preserved structure and conformation (Tomer et al. 2014; Chung et al. 2013).

2. Principle of tissue clearing by CLARITY:

CLARITY, an abbreviation of Clear Lipid-exchanged Acrylamide-hybridized Rigid Imaging / Immunostaining / in situ-hybridization compatible Tissue hydrogel, is a tissue-clearing tool that preserves the tissue/organ structure and its capability of probing via the formation of hydrogel matrix through crosslinking hydrogel monomers and formaldehyde to proteins and nucleic acids. CLARITY involves removal of lipids in a hydrophilic environment using SDS (sodium dodecyl sulfate) detergent actively via an electrophoretic force or passively as displayed in **Fig. 9**. Cleared tissues might be subjected to molecular examination and then optically cleared in a refractive index mounting solution to render intact tissues transparent to light and ready for imaging (Tomer et al. 2014; Liu et al. 2016).

3. Tissue clarification applications:

Tissue clarification was made in an attempt to enable three-dimensional examination of intact and immunostained organs/tissues which improves the study of their fine structures like the vasculature, neurons and cilia... and helps in understanding their complex function. Other than the traditional protein labelling, RNA targeting has emerged as a new tool to enhance molecular phenotyping (Sylwestrak et al. 2016). To date, tissue clarification has been successfully applied to different tissue biopsies and organs like brain, kidneys, spleen, intestine, pancreas and lungs (Epp et al. 2015; Sindhwani et al. 2016) and has greatly improved basic and research specially in the neuropathological field like Alzheimer and Parkinson diseases (Liu et al. 2016).

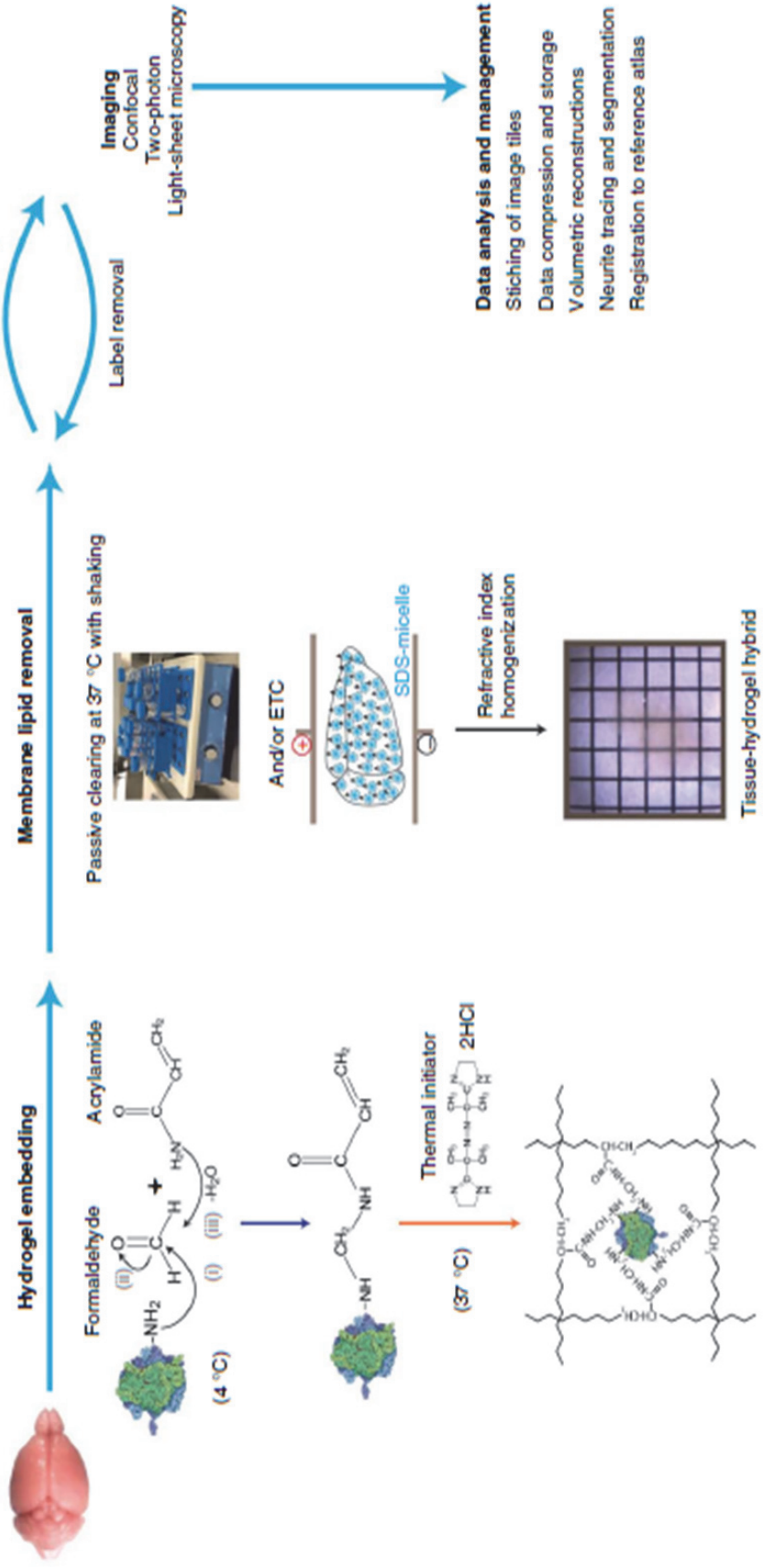

Figure 9: Principles and pipeline of tissue clearing by CLARITY.

A scheme representing the major steps of tissue clearing by the CLARITY approach starting with hydrogel matrix formation, lipid removal passively or actively by electrophoresis, molecular labeling then imaging and analysis (Tomer et al. 2014).

In the heart, researchers have used clarification methods to understand the 3D multi-layered helical structure of cardiomyocytes in the ventricles and examine the microstructure that has been rarely visualized due to its architectural complexity (S.-E. Lee et al. 2018; Perbellini et al. 2017). Clarified cardiac cells architecture has been studied under ischemic conditions and their orientation in ischemic area was found to be significantly disorganized compared to control hearts (S.-E. Lee et al. 2018). In this regard, fibroblasts were also targeted in ischemic clarified hearts and results showed that they increased one day post-infarction and they peaked three days later (Zhiwei Wang et al. 2018). Interestingly, these clarification techniques have been mainly used as a qualitative tool to decipher structural changes from a different newly developed approach.

4. Microscopy and imaging tools:

4.1. Imaging tools used in cleared volumes:

Acquiring high-resolution images of clarified large tissue volumes remains challenging and is highly dependent on the imaging tool used. Aside from the detection objective that determines major parameters in the imaging system (image's maximum resolution and sample's size), the microscopic system used is an important factor to be considered (Tomer et al. 2014). Among the widely used imaging techniques are the confocal, two-photon and light sheet microscopy. In non-cleared tissues, scattering had limited penetration depths to 200 µm and 1 mm in confocal and two-photon microscopes, respectively, which was greatly improved upon clarification. As shown in **Fig. 10**, cleared transparent tissues can be imaged by the standard confocal microscopy which uses a pinhole in front of the detection plane (photomultiplier tube, PMT) for achieving optical sectioning. Furthermore, the imaging speed of confocal microscopy is slow specially when working with large volumes which consequently leads to photobleaching due to increased illumination during prolonged imaging periods. Likewise, two-photon microscopy is a point-by-point scanning tool but leads to a lower sample photobleaching due to its emission fluorescence property, which is achieved by the two-photon simultaneous absorption. Because of these major drawbacks, the limiting speed and photobleaching, light sheet microscopy has been used. In opposition to confocal and two-photon microscopy, the optical sectioning achieved by light sheet microscope is confined to the plane of interest only via orthogonal illumination where signals are detected by a fast-scientific complementary metal-oxide semiconductor camera (sCMOS).

Altogether, these properties make light-sheet microscopy a good tool to be used with an increased imaging speed and therefore lower photobleaching (Richardson and Lichtman 2015; Tomer et al. 2014; Jensen and Berg 2017).

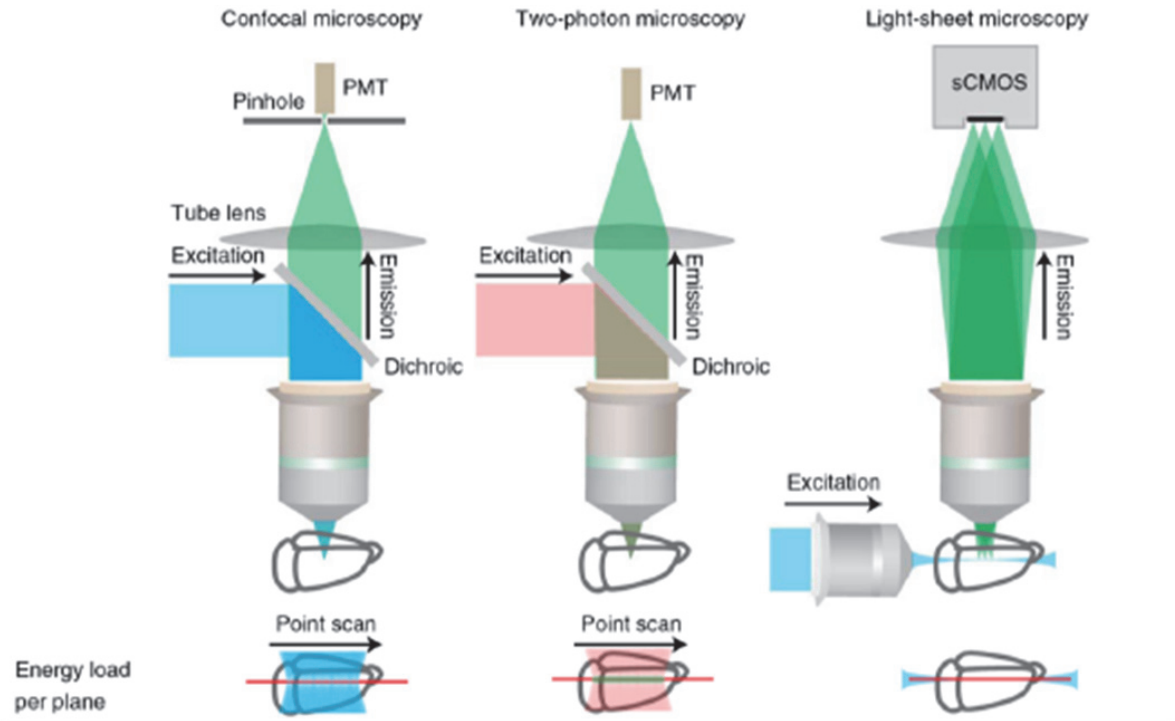

Figure 10: Imaging tools of clarified tissues.

A scheme displaying the comparison between the confocal, two-photon and light sheet microscopy. Light sheet is fast with low photobleaching properties unlike the confocal and two-photon microscopy which are point scanning and consequently slow (Tomer et al, 2015).

4.2. Endogenous fluorescence property:

When molecules absorb light (photon), electrons are excited and are moved from a state to another. On their way back to their initial (ground) state, the molecule emits light known by the "fluorescence". During this process, a part of the energy is lost as heat. As a result, emitted and absorbed lights possess different wavelengths what is known as stoke shift as explained in **Fig. 11**.

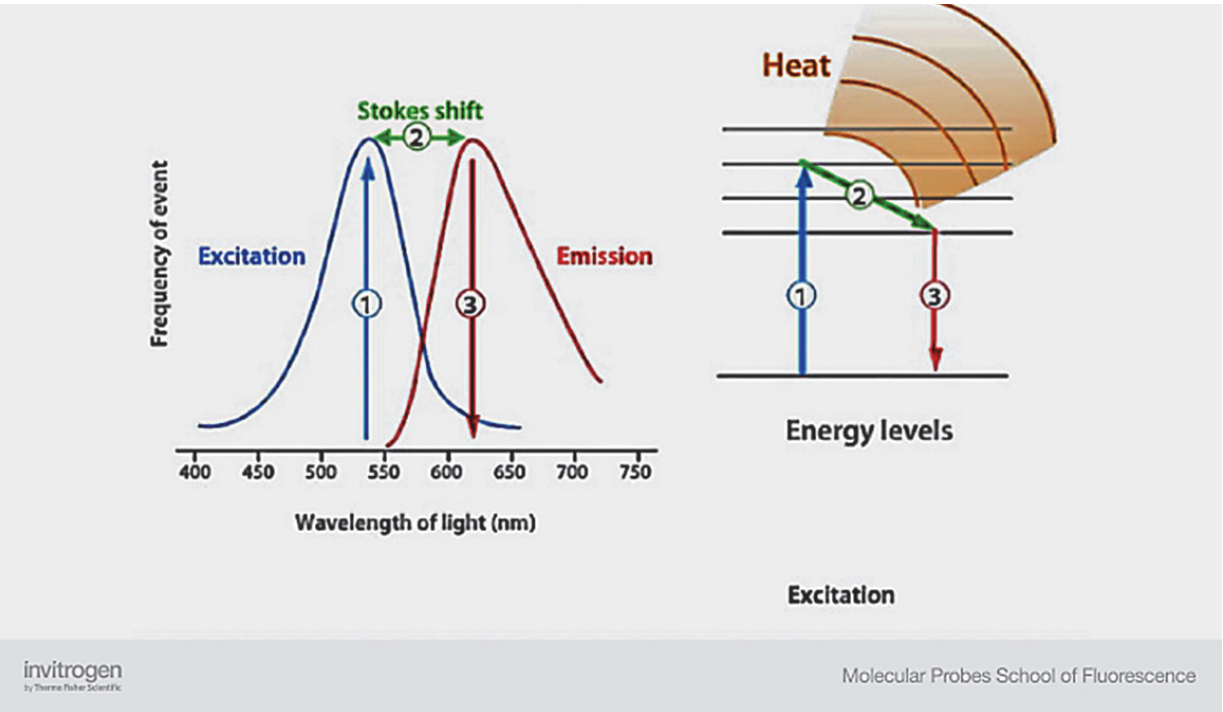

Figure 11: Stoke shift representation.

A scheme representing the stoke shift generated by the energy lost in the form of heat during light fluorescence's excitation and emission.

Imaged biological specimens usually contain endogenous molecules acting as fluorophores (Monici 2005). In the body, several endogenous molecules were known to be fluorescent and their emission spectrum has been well characterized like NAD(P)H, collagen and vitamin A displayed in **Fig. 12** (Croce and Bottiroli 2014). With the progress of the microscopy fields, scientists have given great attention on the importance of endogenous fluorescence in clinical and diagnostic research (Sepah et al. 2014; Pavlova et al. 2008).

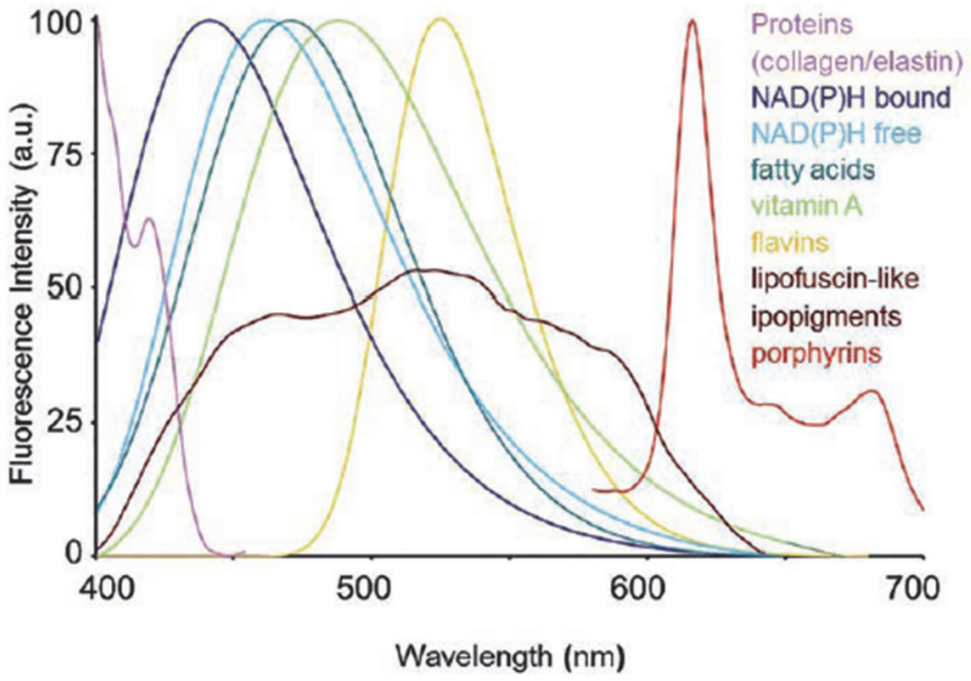

Figure 12: Emission spectral profiles of endogenous fluorophores.

A scheme displaying the emission spectrum of certain endogenous fluorophores present in the tissues. For presentation, data were normalized to the maximum emission peak (Croce and Bottiroli 2014).

In the heart, little is known about the fluorescence properties of myoglobin. The latter is an oxygen and iron binding protein, present in muscle cells including cardiomyocytes and has a major role in storing oxygen which is released under hypoxic or anoxic conditions (Sykes et al. 1999; Ordway 2004). Myoglobin is considered a marker for myocardial ischemia which is usually detected in serum 2 hours post infarction (Sabatasso et al. 2016). It exists in different forms similar to hemoglobin, oxymyoglobin (oxygenated, MbO2), carbmyoglobin (reduced, MbCO) and metmyoglobin (oxidized, met-Mb). However, to date, only their absorbance spectra are known in literature and their emission spectral profiles are not fully elucidated yet and it is not well clarified to which extent they contribute to the heart's autofluorescence signal unlike mitochondrial FADs and NADHs that have attracted great concern due to their hypothesized role in the heart oxidation and are studied by spectral imaging under ischemic and normoxic conditions (Papayan, Petrishchev, and Galagudza 2014; Monici 2005).

5. *Spectral imaging and spectral unmixing:*

Because of these endogenous fluorescent signals and the possibility of having fluorophores with overlapping excitation and emission spectra (bleed-through phenomenon), spectral imaging along with linear unmixing technique have emerged. Imaging tools have been successfully merged with spectroscopic technology to produce spectral images which represent three-dimensional data in the form of a lambda stack characterized by the lateral dimensions of each pixel (x,y) and a wavelength λ as displayed in **Fig. 13** (Garini, Young, and McNamara 2006). This technique has been long used in examining how sun light is reflected and scattered and has been already applied in satellite imaging.

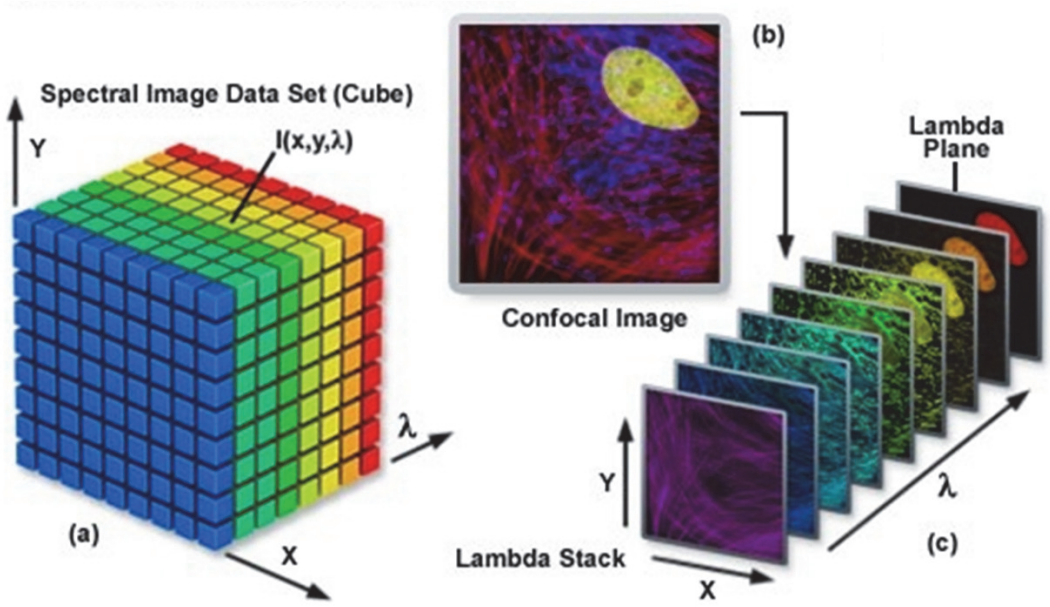

Figure 13: Spectral imaging lambda stack.

A scheme representing the spectral confocal image forming finally a lambda stack image acquired at different wavelengths λ and lateral dimensions (x,y) (www.zeiss.com).

Data associated with spectral imaging are quite large compared to single lambda ones and are hard to analyze visually, therefore, mathematical analytical tools was needed to be used. Among these approaches was the supervised linear unmixing analysis. For instance, in a specific region of interest in this set of images, fluorescent signals can be found separate or spatially distributed. In

this regard, linear unmixing is used to define the contribution of each fluorophore in each pixel of the image and fitting it to a reference spectrum obtained in control samples under similar conditions. Spectral unmixing is a linear decomposition based algorithm that is used to separate fluorescent signal through assuming that the measured signal of each fluorophore is linearly proportional to its concentration in the acquired object at each pixel (Garini, Young, and McNamara 2006). Once spectra contribution is done, the end-result will be individual images originally converted from a lambda-stack without any modifications in their raw data.

Chapter 6: Aims of this work

The work presented throughout this thesis involves three different aspects of the myocardial infarction pathology. The general aim behind working on these topics is to develop an analytical approach based on systems biology tools so that complex, non-linear and multi-scale mechanistic information is decoded in space and time dimensions. However, the specific aims of each topic are detailed below:

1. To develop an approach to quantify the oxidative injury in the area at risk in mouse heart subjected to ischemia-reperfusion sequence using fluorescence imaging of non-labelled myoglobin.

2. To improve and standardize the analytical pipeline used in dynamic transcriptomic studies via integrating systems biology tools.

3. To validate the analytical pipeline studying the effect of the surgical interventions, used in inducing MI model in mice, on the change of gene expression profiles in the myocardium and characterize major mediators behind these alterations.

4. To characterize gene regulatory networks and molecular pathways activated in a control and cardioprotective model of ischemia-reperfused mouse heart.

5. To study the mechanisms ruling the dynamics of circulating inflammatory markers during myocardial infarction in mouse and human patients as well.

Chapter 7: Materials and Methods

1. Biological Model

1.1. Animal model used:

This study was approved by the Ethics Committee of the Université Claude Bernard Lyon 1 (Approval number DR2017-48) in compliance with NIH Guide on the Use of Laboratory Animals (NIH Publication No. 85-23, revised 1996).

Throughout this project**,** male C57BL/6J mice aging 8-12 weeks and weighing 20-30g were obtained from Charles River Laboratories (L'arbresle, France). Some studies have shown that the activated mechanisms within the cardiomyocytes and the response of the myocardium to ischemia-reperfusion is affected by aging (Boyle et al. 2013; Lehrke Stephanie et al. 2006). In addition, ischemic postconditioning cardioprotective effect was shown to be attenuated in MI-induced model in old mice (Boengler Kerstin et al. 2008). Therefore, in this context, we have chosen to work with 8-12 weeks old mice so that we characterize the molecular changes in response to IR and cardioprotective strategies, including ischemic postconditioning, in a good representative MI-induced mouse model. Having a young control model, the mechanism leading to the resistance of ischemic postconditioning can be later unraveled in old mice heart.

Mice were housed in the animal facility of the laboratory, ISO 9001 certified, in a controlled environment with standard cycle of 12 hr light/12 hr dark and had free access to water and standard diet that are regularly monitored. Animals were kept in a temperature 20-21 °C and placed in an enriched environment (not too small cages, minimum 2 mice per cage, cotton balls to play with…).

1.2. Ischemia-reperfusion in vivo mouse model:

Mice (n=8 per time point) were anesthetized with pentobarbital (73 mg/kg) intraperitoneally. Analgesia was provided by the mean of buprenorphine (0.075 mg/kg) intraperitoneal injection as well. Mice were then intubated orally and ventilated via a rodent ventilator. Rectal thermometer

was used to monitor body temperature which is maintained within normal range by the mean of a heating pad. Left thoracotomy was performed. A small curved needle with an 8-0 polypropylene suture was passed, under a Euromex microscope, around the left anterior descending coronary artery to mimic exactly the procedure of myocardial ischemia. After 45 minutes occlusion, the suture was released, mice hearts were reperfused, chest was closed and animals were kept alive until sacrifice. Animals were divided into 3 groups:

- **Control mice**: Anesthesia only
- **Sham-operated mice**: Anesthesia and thoracotomy for different time intervals indicated in **Fig. 14**.
- **Ischemia/reperfused mice**: Anesthesia, thoracotomy and ischemia/reperfusion sequence for different time intervals indicated in **Fig. 14** as well.

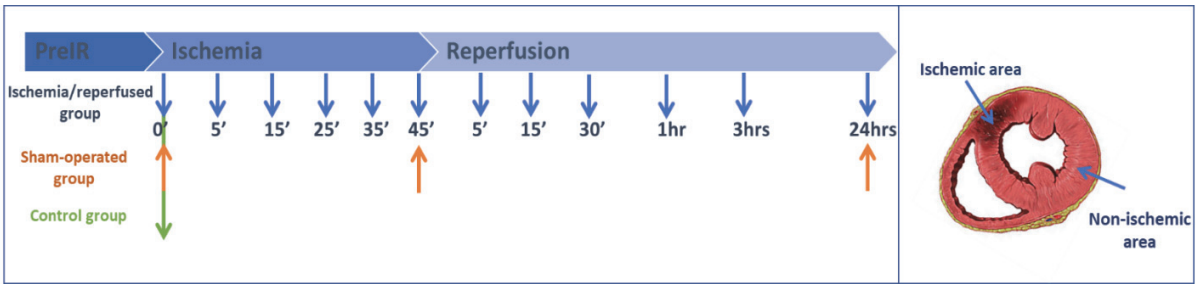

Figure 14: Experimental design.

Scheme displaying the different groups and times in which mice were sacrificed and an illustration of the ischemic and non-ischemic myocardium dissected upon mice sacrifice.

1.3. Cardioprotection mouse model:

Mice (n=8 per group) were randomly allocated to groups. Animals were intraperitoneally anesthetized with (80 mg/kg) alfaxan and (0.3 mg/kg) medetomidine accompanied with (0.075 mg/kg) buprenorphine and (2mg/kg) lidocaine as analgesics, and were divided into 4 different groups and all were sacrificed at 3 hours after the following protocol which is also displayed in **Fig. 15**:

- **Ischemic postconditioning (IPost) mice**: 45 minutes of ischemia was applied as described previously. At the onset of reperfusion, three cycles of 1-minute ischemia followed by 1-minute reperfusion were mechanically performed.

- **IPost sham-operated mice**: 45 minutes post anesthesia and thoracotomy (no suture ligature); three cycles of 1-minute ischemia followed by 1-minute reperfusion were mechanically performed.

- **Therapeutic hypothermia (TH) mice**: Ischemia was applied for 45 minutes as mentioned previously. At 15 minutes of ischemia, temperature of the heating pad was decreased to 33 °C. This drop in temperature was maintained for the following 30 minutes of ischemia and the first 30 minutes of reperfusion where temperature was returned back to its normal degree (37 °C).

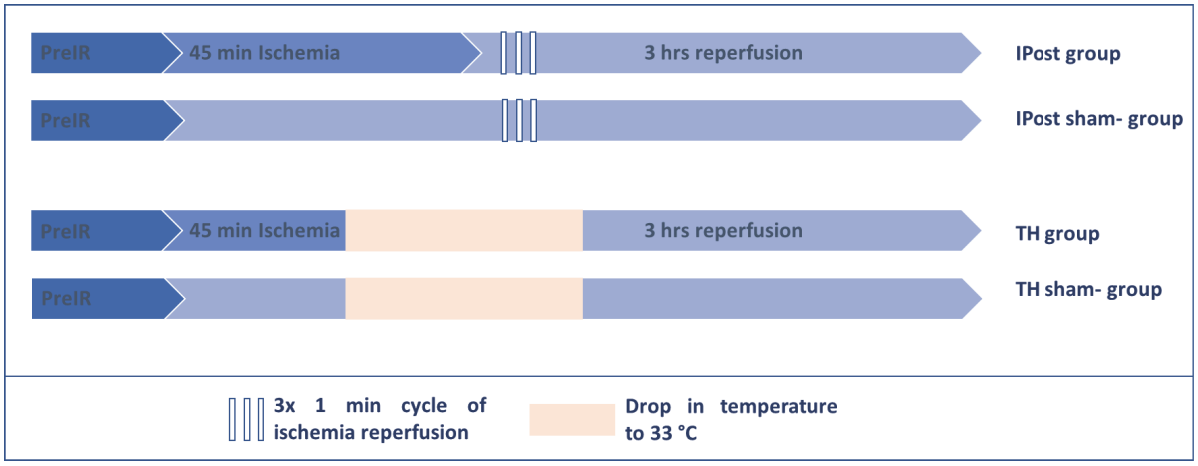

Figure 15: Cardioprotective strategies experimental design.

Ischemic postconditioning (IPost) protocol applied to IR and sham-operated mice via mechanically applying three cycles of 1-minute ischemia-reperfusion. On another group of animals, therapeutic hypothermia (TH) protocol is applied to IR and sham-operated mice as well via decreasing temperature to 33 °C.

1.4. Isolation of Heart Cells:

Animals (n=4 per time point) were injected intraperitoneally with 50UI/kg heparin sodium for 10 min. Mice were euthanized and heart was harvested and cannulated through the aorta. Afterward, a small clip was attached to the aorta's end and a thread beneath it was tied to prevent the heart from falling (O'Connell, Rodrigo, and Simpson 2007). The heart was firstly perfused for three minutes with the perfusion buffer (NaCl 120.4 mM, KCl 14.7 mM, KH_2PO_4 0.6 mM, Na_2HPO_4 0.6 mM, $MgSO_4$-$7H_2O$ 1.5 mL, Na-HEPES 10 mM, $NaHCO_3$ 4.6 mM, Taurine 30 mM, 2,3-butanedione monoxime (BDM) 10 mM, and Glucose 5.5 mM, pH 7.0). The latter was replaced by digestion buffer (50 mL of perfusion buffer and Collagenase II 2.4 mg/mL) for 2 minutes and 30 seconds. 100 mM $CaCl_2$ (final concentration 40 µM) were then added. Perfusion was continued for 6 minutes and 30 seconds. During the entire procedure, the heart was perfused at 4mL/min rate and the solutions were maintained at 37°C to mimic physiological conditions. After 12 minutes, the heart was removed and placed in a 100-mm dish. It was then cut into small pieces that were placed in a tube containing myocyte digestion buffer. Small pieces were gently pipetted several times to ensure the complete myocardium digestion. Digestion stop buffer (45 mL of perfusion buffer, 5 mL of fetal bovine serum (10 %), and 6.25 µM of 100 mM $CaCl_2$ (12.5 µM)) was then added up to a final volume of 100 ml. The tube was then centrifuged for 3 mins at 20g at room temperature (Eppendorf 5810R). Supernatant, containing non-cardiac cells, was collected and centrifuged for 5 min at 500g. Cells pellet was used for labelling protocol prior flow cytometry analysis.

2. Samples preparation

2.1. Blood and Tissue Collection:

Prior to euthanasia, blood samples (500µl) were taken from the inferior vena cava, and hearts were harvested where the left ventricle was dissected regionally to maximally provide the myocardium known to be at risk in ischemic hearts (ischemic myocardium) and the non-ischemic myocardium displayed in **Fig. 14**. Myocardium samples were placed in RNA*later* stabilizing solution (Ambion, Thermo Fisher Scientific) and stored at -80 °C until use.

2.2. Plasma separation and peripheral blood mononuclear cells (PBMC) extraction:

Blood samples were firstly centrifuged at 300g for 5 minutes at room temperature in order to isolate plasma. The latter samples were stored at -80 °C for later use. Remaining blood samples contained granulocytes, erythrocytes and mononuclear cells. These cells vary in their densities, which enables us to separate them based on a density gradient method. Blood samples were diluted with equal volume of PBS + 2% fetal bovine serum and added to a density gradient medium (Lymphoprep™) for mononuclear cells separation in SepMate™-15 (IVD) tubes supplied by Stem Cell Technologies. Granulocytes and erythrocytes have a higher density at the osmotic pressure of Lymphoprep™, and they sediment through the Lymphoprep™ layer during centrifugation. The polysaccharide in Lymphoprep™ enhances erythrocyte aggregation, thereby increasing erythrocyte sedimentation. Mononuclear cells, with lower densities, remain at the interface Lymphoprep:PBS. These cells were finally washed with PBS +2% fetal bovine serum and stored at -80 °C for later use.

2.3. Human plasma samples:

The study design is composed of consecutive patients hospitalized at our institution (Hopital Cardiologique-Lyon). These patients were at risk of acute STEMI from 2016 to 2019. The study was approved by our institution Review Board and Ethics Committee. All patients gave written informed consent. STEMI was defined according to the European Society of Cardiology guidelines by the presence of clinical symptoms (chest pain) associated with an ST elevation of more than 2 mm in two contiguous leads on a standard 12-lead electrocardiogram, and significant troponin-I elevation. All patients underwent coronary angiography at admission with subsequent reperfusion by primary percutaneous intervention (PCI). All patients had a complete myocardial enzyme release assessment and underwent contrast enhanced Cardiac Magnetic Resonance (CMR) one-month post AMI.

Individuals' clinical, treatment and outcome data have been stored prospectively in the database of the Centre for Clinical Investigation of Hospices Civils de Lyon. Adverse clinical events have been registered at follow-up visits scheduled at 1 month, 1 year and 2 years after the index hospitalization.

Blood samples from all patients were collected at 5 time-points post admission, 4 hours (H4), 24 hours (H24), 48 hours (H48), and 1 month (M1) after PCI revascularization. Serum has been collected from blood and samples were frozen at -80°C and stored at the local hospital biobank until assay (NeuroBioTec Biological Resource Center). All serum from the study were thawed only once to avoid biomarkers alteration.

3. Molecular Assays:

3.1. RNA Extraction:

Myocardial samples were removed from RNA*later* solution and homogenized by Tripure reagent solution (Roche) in a Precellys homogenizer associated with a Cryolys cooling system to ensure homogenization at 4 C°. Total RNA was extracted by the mean of a phase separation procedure based on the manufacturer protocol. Obtained RNA was then purified by RNeasy Mini kit (Qiagen) with Proteinase k (Qiagen) and DNase I (Qiagen) treatment on column as shown in **Fig. 16** for an enhanced quality of RNA to be used in sequencing. RNA purity, quantity and were assessed by spectrophotometry. Mini kit (Qiagen) with Proteinase k (Qiagen) and DNase I (Qiagen) treatment on column as shown in **Fig. 16** for an enhanced quality of RNA to be used in sequencing. RNA purity, quantity and were assessed by spectrophotometry.

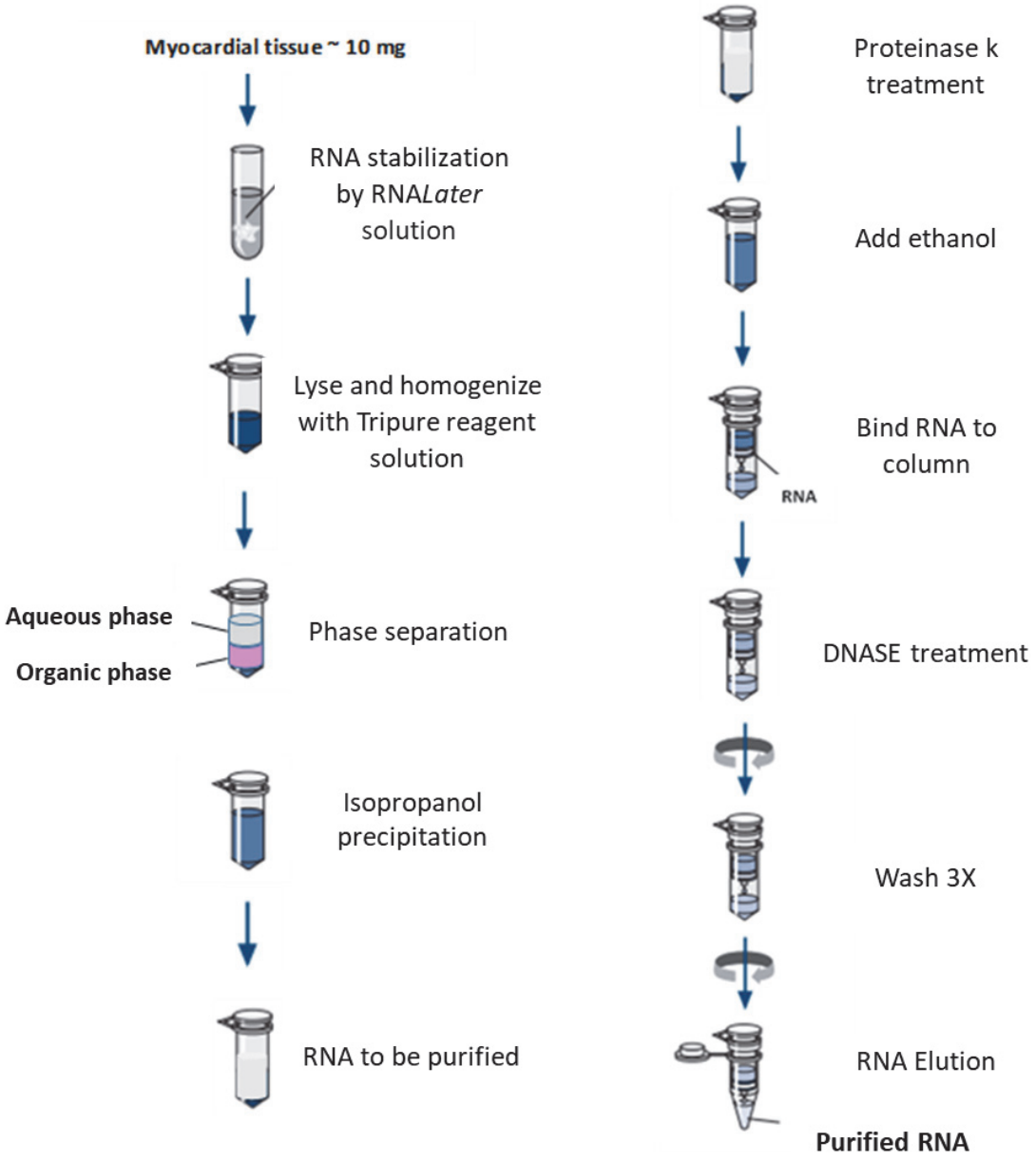

Figure 16: Optimized RNA extraction protocol.

Total RNA was extracted by Tripure reagent via a phase separation process. Isolated RNA was later purified by RNeasy minikit column using proteinase K to remove RNAases if present and DNase I to remove any contaminating DNA.

3.2. RNA sequencing:

Purified RNA samples were provided to ProfileXpert Inc for cDNA library construction and sequencing. Integrity, quantity and quality checks were performed by the means of QuantiFluor RNA dye (Promega) and Bioanalyzer 2100 (Agilent Technologies), respectively. RNA was considered pure if they have $A_{260/280} \sim 1.8$ and $A_{260/230} \sim 2$ ratios. RNA samples were checked in capillary electrophoresis and samples were proceeded to sequencing only if they had an RNA quality number (RQN), calculated based on the ratios of the 18S and 28S ribosomal subunits, between 8 and 10. **Fig. 17** presents an example of one of our samples.

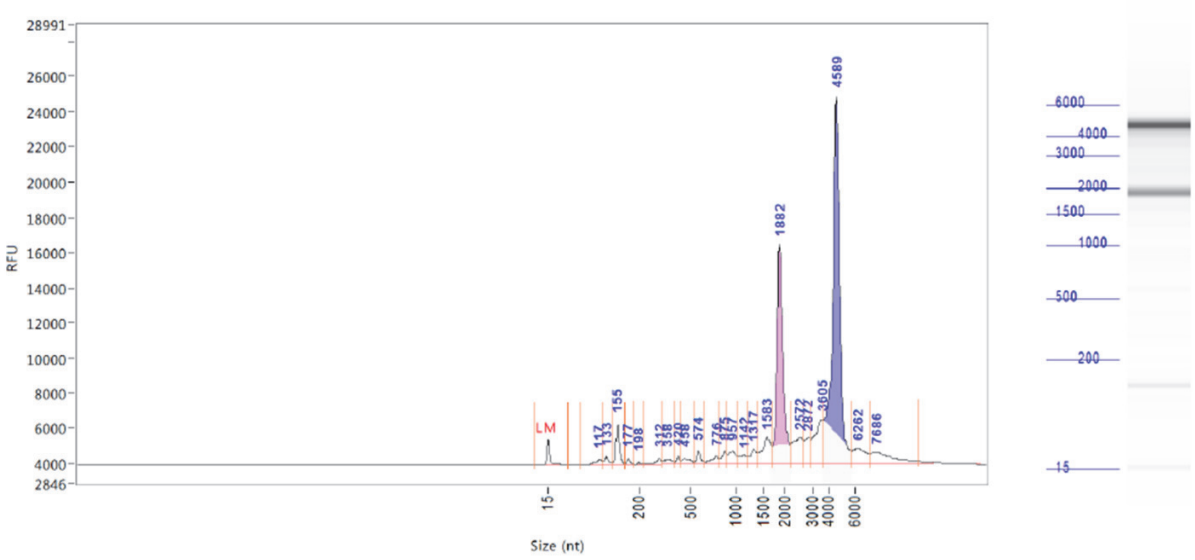

Figure 17: RNA samples quality checks.

Capillary electrophoresis of RNA sample ran in a Fragment Analyzer machine. The purple and pink peaks represent the large and small ribosomal RNA peaks, respectively. RQN of this sample is 9,5 based on the ratio of the 28S and 18S subunits of the ribosomal RNA.

Library construction was carried out using NextFlex Rapid Directional mRNA-Seq (Bio-Scientific, PerkinElmer Company) following the manufacturer protocol. Libraries were applied to an Illumina flow cell and run on the Illumina Nextseq 500 as a single end read for 76 bp. On average, 12 samples were loaded to each flow cell. Sequencing was performed in to three major steps, demultiplexing, trimming (known also as primary analysis) and mapping on host genome

(secondary analysis). Image analysis and base calling was carried out using the NCS 2.0.2 and RTA 2.4.11 Illumina software suite implemented on the Illumina sequencing machine. Final file formatting, demultiplexing, and fastq generation were carried out using Bcl2fastq v2.17.1.14. Trimming of reads was performed using cutadapt v1.9.1 software (Martin 2011). Then the reads were mapped to the mm10 genome using TopHat v2.1.0 (Kim et al. 2013) software with default parameters (bowtie 2.2.9) (Langmead and Salzberg 2012). Reads were counted and quantified by different methods including htseq-count software, kallisto and cufflinks to generate raw counts, with stranded and un-stranded parameters, and normalized data as fragments per kilobase of exon model per million reads mapped (FPKM).

4. Biochemical assays

4.1. Inflammatory markers measurement by ELISA Assay:

IL-6, VCAM-1, CCL2 and CRP concentrations were measured by the mouse IL-6, VCAM1, CCL2 and CRP Quantikine ELISA Kit (R&D Systems, Minneapolis MN, USA). Based on the manufacturer protocol, sandwich ELISAs were carried out. Plates were firstly incubated with the specific capture antibody and then they were blocked with Reagent diluents. Standard and testing plasma samples were added to the plate with the appropriate dilution which were later detected via the Streptavidine horseradish peroxidase and read optical density by the spectrophotometer at the specific wavelength with the correction of the optical imperfections of the plate at 450nm.

4.2. Inflammatory cells recruitment test by Flow cytometry:

4.2.1. Labeling protocol:

Isolated non-cardiomyocyte cardiac cell pellets were re-suspended in PBS and divided in two tubes: Labeling and isotypic control. PBS was added in each tube and tubes were centrifuged 5 min at 500g and the supernatant was discarded. FCR (Fc receptor) blocking solution (diluted FCR: 1:10 in PBS; 100 µl/tube of dilute FCR solution; FCR blocking mouse reagent, Miltenyi biotec, 130-092-575) was then added for 10 min at 4°C. Following incubation, PBS+ 0.5% BSA (Bovine

Serum Albumin) was added and tubes were centrifuged 5min at 500g. The two tubes were incubated for 30 min at 4°C in dark with the isotypic or the labeling solution. Incubation was stopped with the addition of PBS + 5% BSA followed by a 5 min centrifugation at 500g. Supernatants were discarded and pellets re suspended in PBS before flow cytometry analysis.

4.3. Samples' processing and data analysis:

Flow cytometry experiments were conducted using Fortessa X-20 equipped with 4 lasers and 16 fluorescent detectors. Markers of macrophages (CD11B, F4/80, CD206 and CD86) and neutrophils (Ly6g) were analyzed after immunostaining (antibodies are listed in **Table 1**) in order to estimate the proportion of each population. 100,000 events were acquired for each fluorescent marker. Data were analyzed by DIVA Software (BD Biosciences). The percentage of each cell subtype was calculated after the multiple gating of the different fluorescent markers. The sorting of macrophage subtypes was performed as followed: CD11b+ and/or F4/80+ positive cells were gated and represented the total macrophage population. Within this cell population, the percentages of type 1 macrophages (M1) (CD206+/CD86-), type 2 macrophages (M2) (CD206-/CD86+), M1+M2 (CD206+/CD86+) and negative M1+M2 (CD206-/CD86-) macrophages population were figured out. Percentage of M1, M2 and double M1+M2 phenotypes were normalized by the sum of these three population to assess the shift in differentiation.

Table 1: List of antibodies used in the flow cytometry analysis.

Antibodies	Supplier	References	Isotypic control	Supplier	References
PE-F4/80	Miltenyi biotec	130-102-422	REA control-PE	Miltenyi biotec	130-104-628
VIOBLUE - CD11B	Miltenyi biotec	130-097-336	Rat IgG2b-Vioblue	Miltenyi biotec	130-102-661
APC-CD86-	Miltenyi biotec	130-102-558	Rat IgG2b-APC	Miltenyi biotec	130-102-664
AF488-CD206	Biolegend	BLE141710	AF488 Rat IgG2a	Biolegend	BLE400525
Anti Ly6g-FiTC	Miltenyi biotec	130-107-913	Rat control-PE	Miltenyi biotec	130-104-628

5. *Statistical analysis*

5.1. Unsupervised vs Supervised analysis:

The RNA-seq data includes the expression values of thousands of genes for different conditions and how these data are analyzed is highly dependent over the biological question of interest. The analysis presented in this thesis is divided into two categories: supervised and unsupervised analysis. These two types of analyses are classified based on the available data input and the desired output. Supervised analysis is considered when a prior knowledge is applied to the large-scale RNA-seq data and genes are previously classified based on a specific criterion like function, regulation or cell type origin as an example **Fig**. **18A**. This pre-existing information drives the results' interpretation. In addition, reducing the features in the supervised analysis helps classifying the desired information correctly. However, unlike supervised analysis, unsupervised one doesn't require any additional information of the genes/transcripts except their expression values, example **Fig. 18B** (Raychaudhuri et al. 2001; GREENE et al. 2016; Yan Ma et al. 2018). These analyses are performed by certain algorithms that aim to decode new information in our data via mainly two approaches, clustering and dimension reduction. These two approaches are applied in both analyses to facilitate data handling and easily visualize them. Data grouping, also known as clustering, and reduction of the data dimensions are usually performed to remove unessential features and classify objects within a dataset based on certain similar criteria in order to reach a fathomable scale for the human brain. Among the tools used to achieve this, weighted gene co-expression network analysis (WGCNA) and the principal component analysis (PCA) explained later in this section.

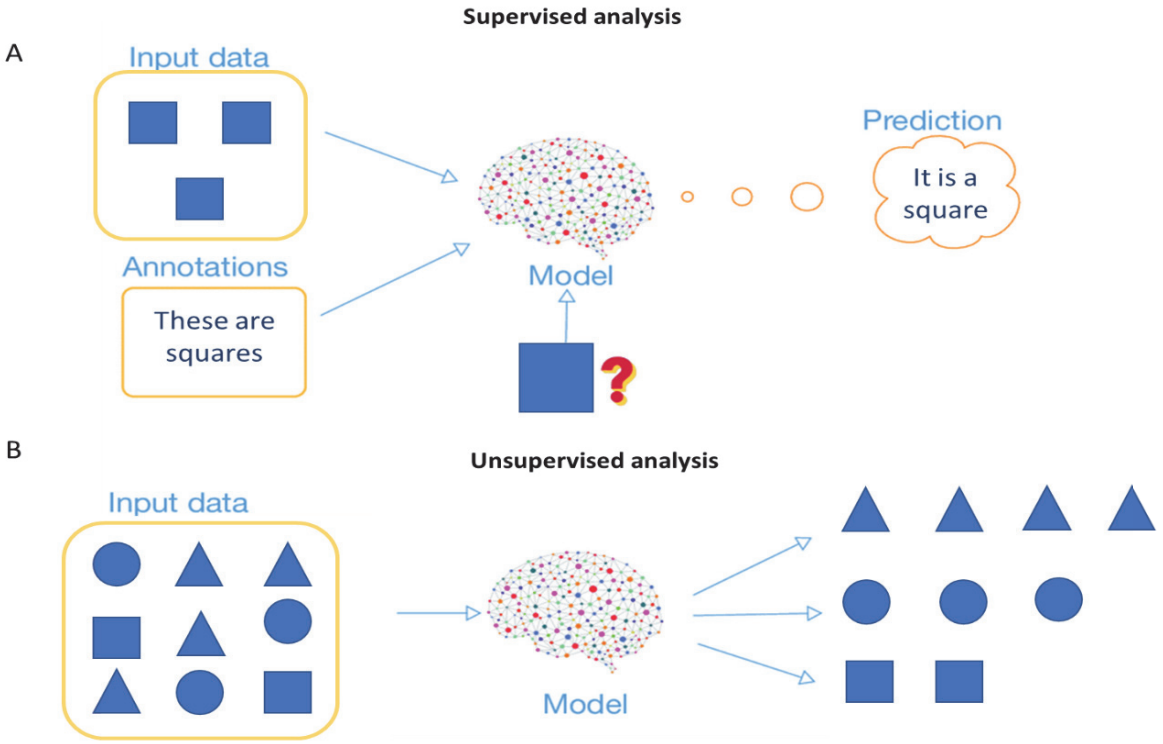

Figure 18: Supervised analysis versus unsupervised analysis.

(A) Supervised analysis uses pre-existing annotations to draw out results. (B) Unsupervised analysis doesn't need any prior knowledge and conclusions are drawn based on available features only. Adapted from Ma et al., 2018.

5.2. Differential Gene Expression analysis:

Data were organized by condition prior analysis and the resulting count matrix was modeled based on the assumption that RNA sequencing data follow a negative binomial distribution. Data normalization was performed via the median-of-ratios method implemented in DESeq2 R package version 1.20.0 supplied by R software (version 3.4.4) which accounts for sequencing depth differences between samples (Love, Huber, and Anders 2014). Differentially expressed transcripts (DETs) were computed with "Wald" or "Likelihood ratio" test (LRT) implemented in *DESeq* function. For all the analysis, we kept the adjusted *P* values below 0.05 corrected via the Benjamini and Hochberg method (Benjamini and Hochberg 1995).

Normalized data were subjected to a multivariate statistical method of principal component analysis (PCA) implemented in R language version 3.4.4. PCA is an unsupervised linear learning method that aims to sort/cluster data that consists of interrelated variables through reducing its dimensionality with preserving as much variability as possible with minimized loss of information if any. PCA identifies smaller number (generally 1 to 3) of uncorrelated variables known by principal components (PC). PC1 axis represents efficiently the dataset and accounts for the highest variation in the original data. However, the second PC, perpendicular to PC1, accounts to most of the remaining variances (Abdi and Williams, 2010; Lever et al., 2017). As an example, **Fig. 19** displays the distribution of certain data on a two-dimensional coordinate corresponding to the variables of interest. PCA finds out the directions in which the data is mostly spread on and having the highest variation along PC1 and PC2.

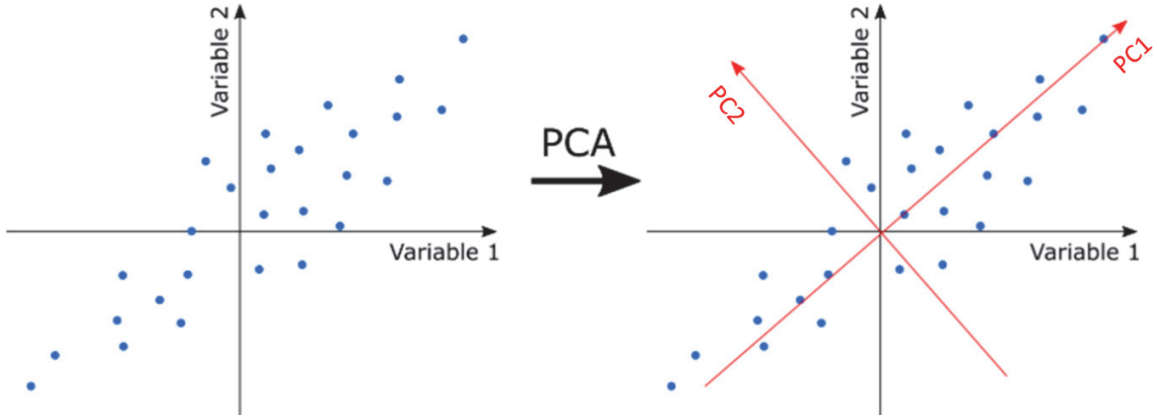

Figure 19: Principal component analysis representation.

A scheme displaying the reduction of data's dimensions by PCA via projecting them on new coordinates where the data is mostly spread.

5.3. Weighted gene co-expression network analysis:

In order to cluster highly correlated transcripts and construct transcript co-expression network, we ran the *cutreeDynamic* function of the weighted gene co-expression network analysis (WGCNA) R package (version 1.63) (Langfelder and Horvath 2008) on the matrix of normalized counts for the DETs identified with DESeq2. The matrix of the normalized counts was computed with the *varianceStabilizingTransformation* function of the DESeq2 package. WGCNA applies principal

component analysis where the first PCs of each formed module are called eigengenes instead. Soft threshold (beta) that represents the exponential parameter for power law distribution was chosen based on a scale free topology criterion. Adjacency matrix was constructed and then transformed into a topological overlap matrix. Transcripts were hierarchically clustered using the *flashClust* function and clusters of transcripts having similar profiles, referred to as modules, were formed.

5.4. Gene Ontology Analysis:

Gene ontology is a bioinformatic approach that aims to develop a controlled vocabulary and attribute genes and gene products into three major biological domains: biological processes, molecular functions and cellular component (The Gene Ontology Consortium 2019). Functional interpretation of a certain list of genes obtained from experimental data is made easier through enrichment analysis via the different available tools. Differentially expressed transcripts obtained in our analysis were subjected to functional enrichment analysis by STRING software version 10.5 (Franceschini et al. 2013). Hypergeometric statistical tests are used to identify enriched terms that are sorted by their FDR. GO terms with FDR < 10^{-4} were kept for further analysis. In order to measure the enrichment of the GO terms in WGCNA assigned modules, we have calculated a z-score (z) as follows:

Eq.1 $$z = \frac{\left(x - 0.5 - \frac{B \times n}{N}\right)}{\sqrt[2]{n \times \frac{B}{N} \times \left(1 - \left(\frac{B}{N}\right)\right)}}$$

x: count of observed transcripts in each GO term of WGCNA module

B: count of observed transcripts in each GO term of DETs

n: total count of observed transcripts in module

N: count of DETs

This z-score estimates whether a given GO term is enriched in a transcript module compared to all DETs and is thus assessing whether this small group of transcripts is involved in a common biological process. We assumed that a GO term is enriched in a certain module if z-score >2.

5.5. Short Time-series Expression Miner (STEM) analysis:

STEM version 1.3.11. (Ernst and Bar-Joseph 2006), a Java clustering algorithm was used to visualize expression profiles from short time series experiments (fewer than 8 time points). It is primarily designed for microarray experiments. STEM algorithm defines a set of model temporal profiles, independent of the input data, which correspond to possible profiles of the genes' behavior over time. All these model profiles start at 0 and between time points they are either increased, decreased or remained steady. Input data are transformed so that expression profiles can start at 0. Gene are assigned to profiles based on a correlation coefficient.

5.6. Transcription factor analysis:

oPOSSUM 3.0 (Kwon et al. 2012), a freely available web accessible software was used to identify enriched transcription factors binding sites (TFBSs) in the 5000bp upstream and downstream sequence of the differentially expressed transcripts. Default search parameters of the single site analysis were kept as they are originally set in the software. oPOSSUM performs an exact Fisher test which measures the probability of a non-random association between the co-expressed gene set and the TFBS of interest and calculate a F-score as equal to -ln(p-value). F-score is thus assessing the probability that at least 1 TFBS would be significantly associated with the observed transcript list. Besides, a z-score is calculated using the normal approximation to the binomial distribution to compare the rate of occurrence of a TFBS in the target set of genes to the expected rate estimated from the pre-computed background set. Thus, the z-score is estimating the specific enrichment of given TFBS in the gene set compared to background gene set. TFs were ranked by F-score and z-score, respectively and were clustered into 5 groups.

5.7. Functional network inference

Protein-protein interaction (PPI) networks were generated using the freely available STRING database version 10.5 (Franceschini et al. 2013). Clustered TFs were inputted separately in STRING to generate background networks based on the predicted associations between these TFs

(curated or experimentally determined interactions). Resulting TF-PPI networks were expanded into several layers (shells) via sequentially adding predicted associated proteins (nodes) until networks of 5 layers were generated as detailed in the results section. During each step, GO terms with FDR < 10^{-4} were assigned to major biological processes. The major biological processes were then normalized to the total number of identified GO terms in each network. To quantify the specificity and sensitivity of STRING's predictions, shared biological processes between TF-PPI network and DET were sorted out and then were normalized by the total number of shared GO terms. TF-PPI networks that recapitulated the greatest number of biological processes obtained from the DETs were selected as being the best putative TFs-regulated networks.

5.8. Statistics:

In order to determine the number of mice per group, a power analysis was performed with G*Power (version 3.1.9.2) (Faul et al. 2007) with the following conditions: One-way ANOVA parameters with alpha = 0.05, beta = 0.2 and effect size = 0.7 with 3 groups (0 minutes, 45minutes, 24 hours).

Statistical analysis were performed with One-way Anova, (Tukey's multicomparison test and Kruskal-Wallis non-parametric test), student t-test, two-way anova tests and spearman correlation analysis were performed with Graphpad Prism (version 7.0a), GraphPad Software, La Jolla California USA, "www.graphpad.com".

6. Heart Clarification

6.1. Animal model and heart preparation:

In this protocol, mice have undergone the same procedure for inducing ischemia-reperfusion injury as discussed previously. Mice were classified into 3 groups, sham operated mice (anesthesia and thoracotomy), ischemia/reperfused mice (anesthesia, thoracotomy and ischemia/reperfusion) and post-conditioned mice (anesthesia, thoracotomy, ischemia/reperfusion and postconditioning sequence). Animals were euthanized at different time points of the experiments shown in **Fig. 20**.

Unisperse blue was injected in mice undergone ischemia-reperfusion in order to label the area at risk. 10 ml of cold PBS were injected to the mice in order to wash blood in a 2ml / minute rate via the carotid. Once blood was washed, 5ml 4% PFA was injected in a rate of 1 ml / minute to fix protein and avoid their conformational changes.

Once done, hearts were removed and placed in 4% PFA overnight at 4 °C for fixation. Hearts were then washed with PBS, injected with a hydrogel solution (Acrylamide 4%, VA-044 0.25%, PBS 1X and H2O) and incubated overnight at 4 °C. In order to polymerize the hydrogel, hearts were placed in warm water bath of 37 °C under agitation for 3 hours.

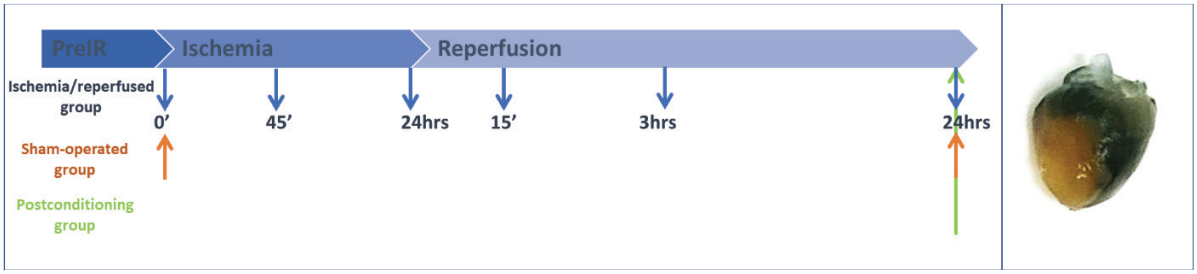

Figure 20: Area at risk quantification experimental design.

The time points at which mice were sacrificed for heart clarification protocol and the heart injected labeled with unisperse blue. Non-blue area corresponds to the ischemic area at risk.

6.2. Heart Active Clarification:

After the formation of the gel-like structure, hearts are placed in a small tissue container and put in an electrophoretic tissue clarity (ETC) machine (X-Clarity^{TM} machine) chamber containing a ready to use Logos Biosystem electrophoretic tissues clearing solution. The ETC machine consists of four major parts, the ETC chamber where the samples are placed, the ETC controller to control for the temperature, current/voltage, the pump and the reservoir shown in **Fig. 21**. The clearing solution consists mainly of SDS that enables lipid extraction through active electrophoresis yielding a transparent and stable tissue-hydrogel heart. Throughout this process, current was set to 1.3 A, the pump was set to 30 rpm and temperature was kept at 37 °C.

Figure 21: X-ClarityTM machine compartments.

A scheme displaying the X-Clarity machine components. From left to the right, the pump, the reservoir, the ETC chamber and the ETC controller.

6.3. Confocal Imaging:

Prior to imaging, clarified hearts are incubated in a refractive index matching solution (RIMS), X-Clarity™ Mounting solution (Logos Biosystems), for 30 minutes to 1 hour. This process reduces light scatter through homogenizing the environment between the tissue and the solution and therefore, increases the heart's transparency which consequently improves image's resolution and depth.

Confocal microscope is equipped with a motorized platform on which the sample is placed. This platform moves in the three directions of space (x, y and z) in order to make produce volumetric images that covers the area at risk to be analyzed. In this regard, transparent heart samples were placed in a container and were kept in the RIMS to prevent its drying during the acquisition. Objective 10X of the Nikon Eclipse Ti, A1R confocal microscope was used for all the acquired images. Mosaic Z-stack spectral images of 100 µm thickness were taken via the excitation of all the lasers (diode 405 nm (blue), argon ion 488-514 nm (blue-green), diode 561 nm (orange-red) and diode 642 nm (deep red)). Images were acquired by averaging 4-scanning lines for better resolution. A lambda-stack of 2mm depth was obtained for the clarified hearts. Z-stacks were stored and analyzed by the NIS-Element AR4 Nikon software.

Chapter 8: Results

Section I: Spatial organization of oxidation in the area-at-risk

As previewed earlier in the manuscript, several factors contribute to the myocardial injury following ischemia-reperfusion. Among these factors is the elevated oxidation which is not fully characterized to date. Therefore, throughout this section of the results, a new approach is proposed to characterize MI-induced oxidation and quantify the myocardial area at risk, which represent major determinants of MI severity, in mouse heart subjected to ischemia-reperfusion and ischemic postconditioning based on the heart endogenous myoglobin emission signals.

1. Experimental design:

For more stringent results, a minimum of four animals were considered for this analysis. To be able to compare among the different confocal images, clarification and imaging parameters have been optimized and set the same for all the studied hearts. Regarding clarification, all hearts have been cleared under the same conditions: 1.3A, 30 rpm at 37 °C for 20 hours, resulting in a well cleared hearts that can be used to image at least 2mm in depth (**Fig. 22**). In addition, the lasers intensity, pinhole size and resolution were optimized to prevent saturation of the images and be able to compare generated signals between hearts.

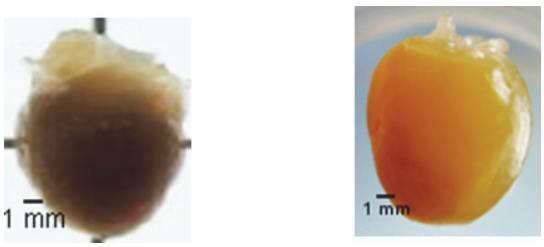

Figure 22: Heart transparency before and after clearing.

A scheme representing a non-clarified heart (left) and clarified one (right) for 20 hours, where enhanced transparency is obtained for imaging.

2. Endogenous tissue fluorescence of clarified hearts:

Acquiring spectral images (420-740nm) of the heart, via excitation with the four available lasers (Method section), a strong endogenous tissue fluorescent signal, also defined as autofluorescent signal, was observed in the visible bandwidth. This finding was advantageous regarding the possibility of imaging the heart without previous labeling.

However, on the other hand this autofluorescence strongly increases the background noise signaled in labeled hearts. Interestingly, as **Fig. 23** displays, the autofluorescent signals obtained by spectral imaging revealed clearly the myocardial structure. In this regard, we have questioned where is this autofluorescence originating from.

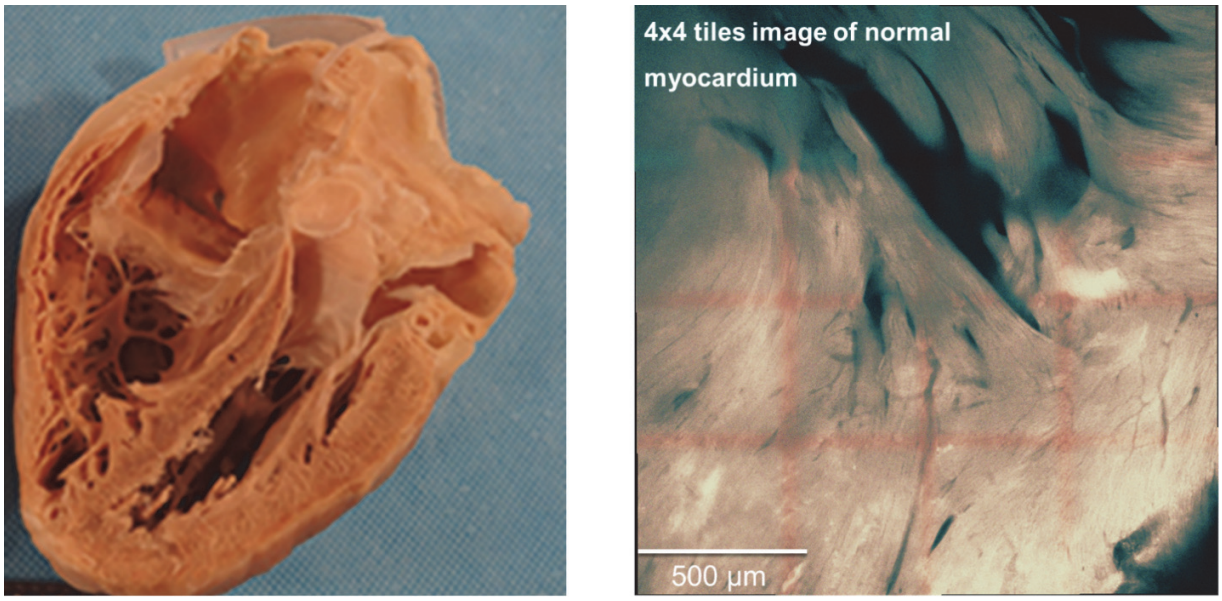

Figure 23: Myocardial spectral imaging

An inside structure image of the myocardium to the left and a confocal spectral image to the right displaying the ability of spectral imaging to reveal myocardial tiny structures.

To answer this, we have used the spectral unmixing algorithm tool available in the NIS Element software. As discussed previously, a fitting spectrum for a specific molecule is used for the aim of detecting if this molecule is recognized and distributed in the image of interest. Therefore, the software extracts for each pixel its spectral content and fits it to the input spectrum which

reconstitutes the detected signal. Finally, the obtained signal will be the sum of all the fitted input spectra as shown in **Fig. 24**. In this figure, we were able to differentiate the different constituents in the imaged myocardial region like the cardiomyocyte and the endothelial cells (vessel).

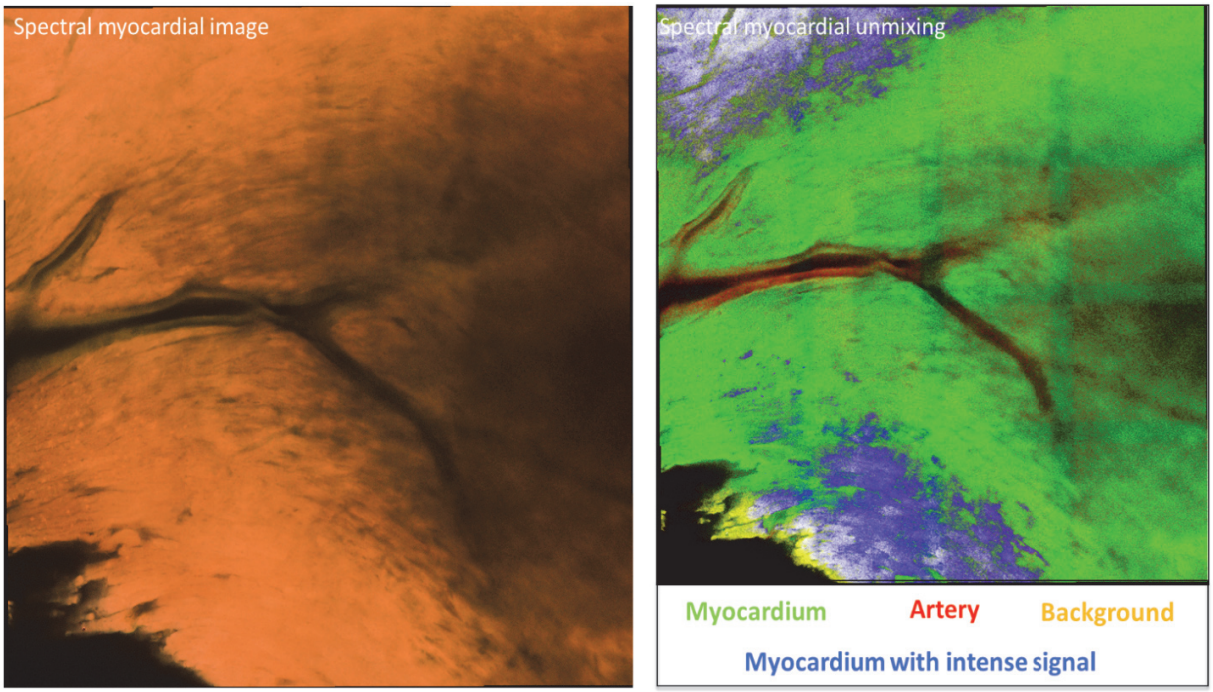

Figure 24: Clarified heart spectral imaging and unmixing.

To the left, a spectral image of a control clarified heart which is spectrally unmixed to the right. Myocardial spectral unmixing reveals the various structures present in the heart, like the endothelial cells in the arteries (red color) and the cardiomyocytes (green color).

Among the various endogenous fluorescent molecules, we were interested in identifying the ones that are most likely to be responsible for cardiomyocytes autofluorescent signals. In this regard, we have studied myoglobin's emission. Myoglobin is present in the cardiomyocytes and is present in three different forms, oxymyoglobin (MbO2), carbmyoglobin ($MbFe^{2+}$) and metmyoglobin ($MbFe^{3+}$). Myoglobin was previously shown to absorb light (Anderson and Robertson 1995; Bowen 1949; Millar, Moss, and Stevenson 1996; Barham et al. 2010). The excitation spectra of its different forms (**Fig. 25**) show that indeed the 3 signals can be discriminated. However, no characterized emission spectra were published to date. Therefore, we had to reproduce ours.

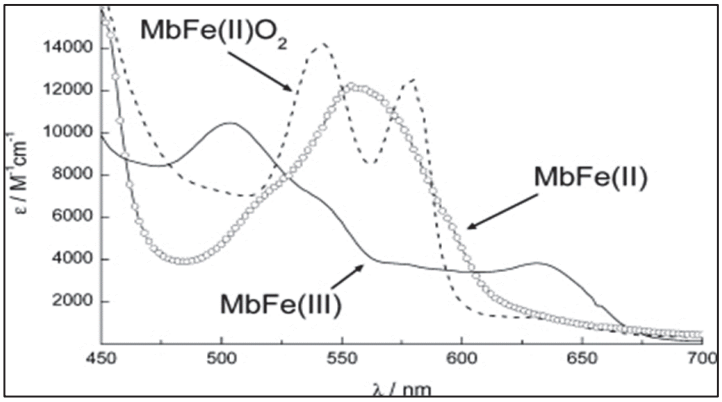

Figure 25: Excitation spectrum of the different myoglobin forms.

The excitation spectral profile of myoglobin in its three different forms, oxygenated, reduced and oxidized (Barham et al. 2010).

3. Myoglobin spectrum optimization:

To start, we have used fresh horse myoglobin to characterize its spectra. Myoglobin was treated with hydrogen peroxide (H2O2) and sodium dithionite (Na2S2O4) to induce its oxidation (metMb) and reduction (carbMb), respectively. Interestingly, a shift in the emission spectrum was observed depending on myoglobin's redox state. However, increasing H2O2 concentration exerted a photobleaching effect destroying the myoglobin autofluorescence as displayed in **Fig. 26**.

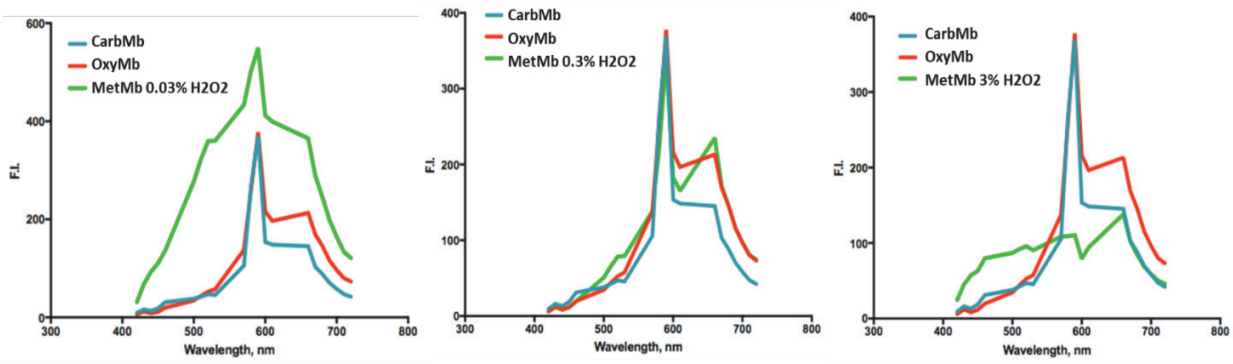

Figure 26: Emission spectra of the various myoglobin forms.

A scheme displaying the various emission spectral profiles of the oxygenated (oxy), reduced (carb) and oxidized (met) myoglobin under different H2O2 concentrations.

In this regard, we wanted to check if we can reproduce these spectral variations in the heart. First, we have used mouse fresh myocardial tissues and treated them with H2O2 and Na2S2O4 as well for different incubation times. As a control, we have incubated the heart in PBS to be able to compare to. **Fig. 27** displays the different obtained emission spectrum under the different incubation conditions.

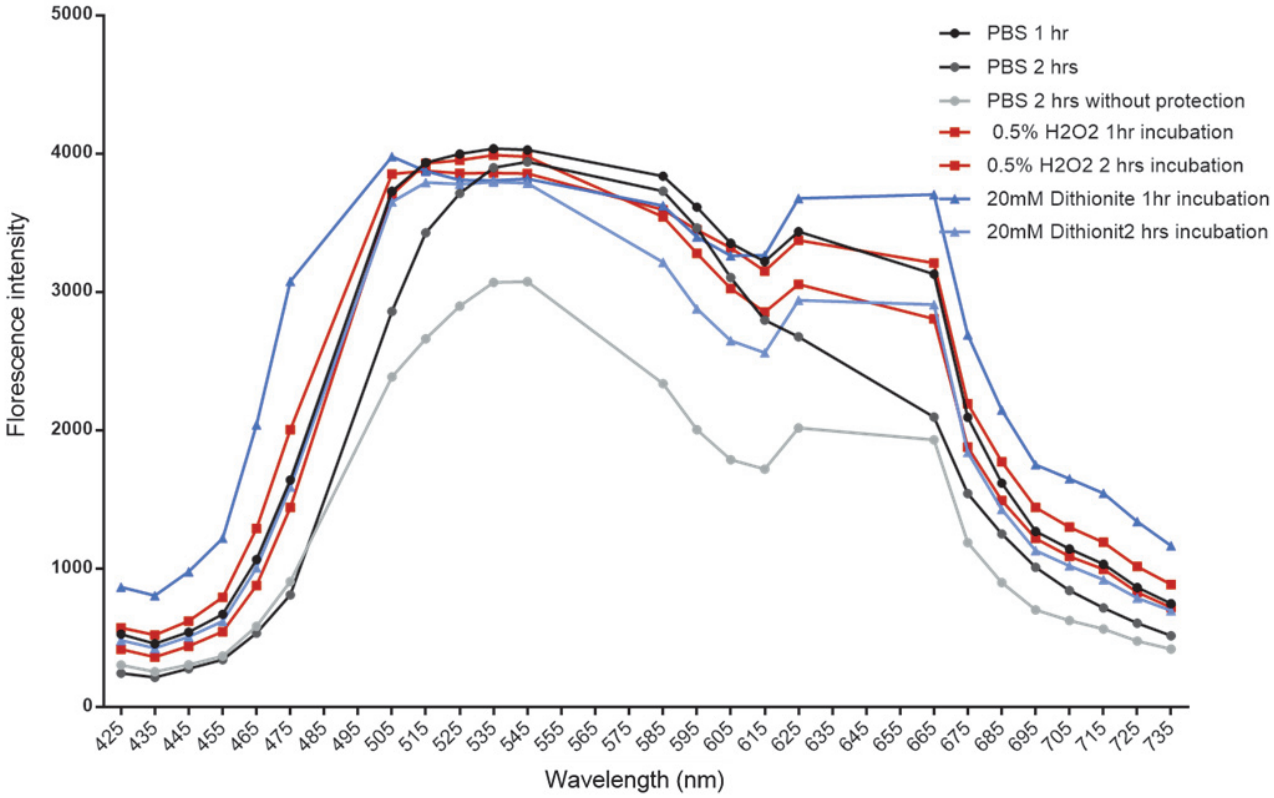

Figure 27: Myoglobin emission spectrum in fresh myocardium.

A scheme displaying myoglobin's emission spectra optimization in non-clarified fresh myocardium under various treatments and different times. Myocardium was treated with 0,5% H2O2 and 20nM sodium dithionite to induce its oxidation and reduction, respectively.

These data indeed show that there is a difference between the different forms of myoglobin. Therefore, next we wanted to assess if this variation is also preserved after heart clarification. In this regard, mouse clarified hearts were pretreated with PBS, H2O2 and Na2S2O4 for different concentrations and different incubation times as well (data not shown). This variation was also

detected in clarified myocardium (**Fig. 28**). However, increasing H2O2 concentration had also induced a photobleaching effect. Therefore finally, a lower concentration (0.3%) compared to the ones used in fresh myocardium (0.5%) was used for the upcoming experiments with clarified myocardium.

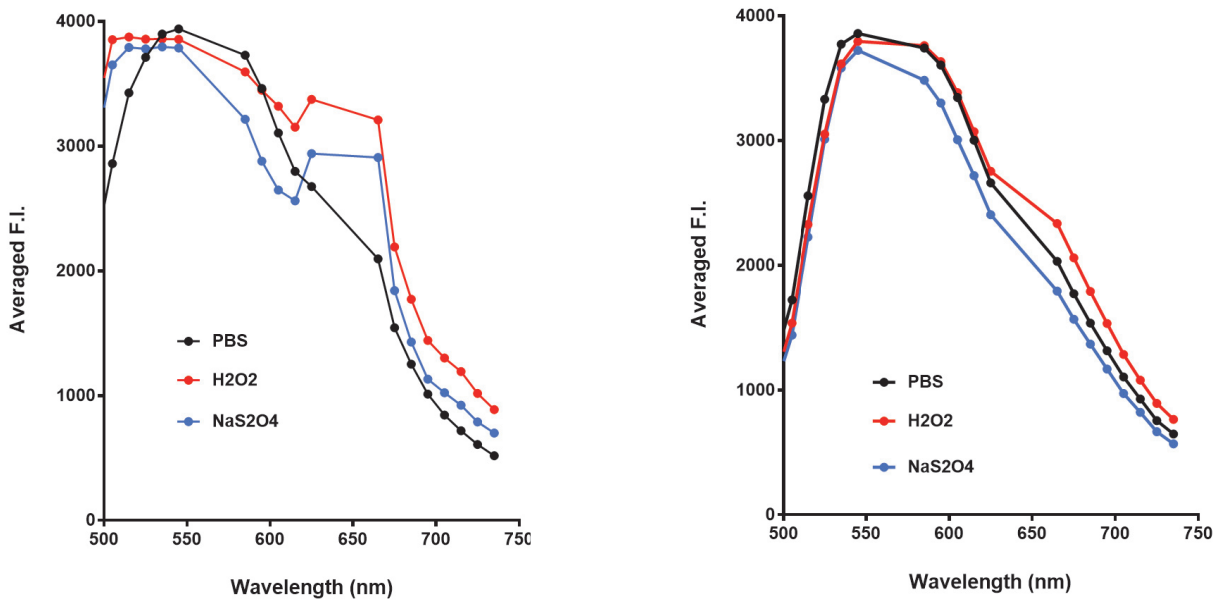

Figure 28: Myoglobin's optimized emission spectrum in fresh and clarified myocardium.

A scheme displaying myoglobin's emission spectral profiles in fresh (left) and clarified (right) myocardium, where 20nM NaS2SO4 and 0.5% and 0.3% H2O2 for 1 hr incubation is used, respectively.

Myoglobin spectra obtained from both fresh and clarified myocardium have shown that the variation in the spectra is occurring in the orange-red range of the spectrum (**Fig. 28**). Therefore, having optimized the oxidized and reduced myoglobin spectrum and having obtained similar results between the non-clarified and clarified myocardium, we next aimed to use these spectra for spectral unmixing in ischemia-reperfused and postconditioned hearts assuming that the oxidized signal is increased in the area at risk during the reperfusion phase.

4. Oxidation-reduction measurement in the area at risk by spectral unmixing:

As mentioned in the method section, hearts were labeled with unisperse blue which absorbs the orange-red light and thus acts as a contrasting compound. This enables us to discriminate the signal obtained from the ischemic versus non-ischemic area as shown in **Fig. 29**.

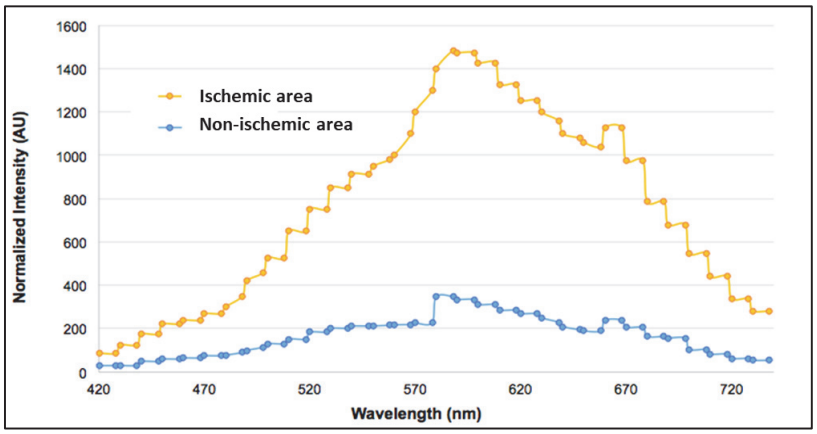

Figure 29: Unisperse blue effect on the spectrum.

A scheme displaying the shift in the spectral profile of the ischemic and no-ischemic area caused by the absorbance of unisperse blue in the non-ischemic area in the ischemia-reperfused hearts.

Z-stack images of the ischemia-reperfused mice hearts were spectrally unmixed with the different myoglobin spectra at the different time points. Interestingly, a heterogeneity in the obtained signals was obtained. As an example, **Fig. 30** displays a clarified heart after 24 hours of reperfusion. The highest signal was for metMb (violet-blue color) which indicates high oxidation level that is expected in IR hearts after 24 hours of reperfusion.

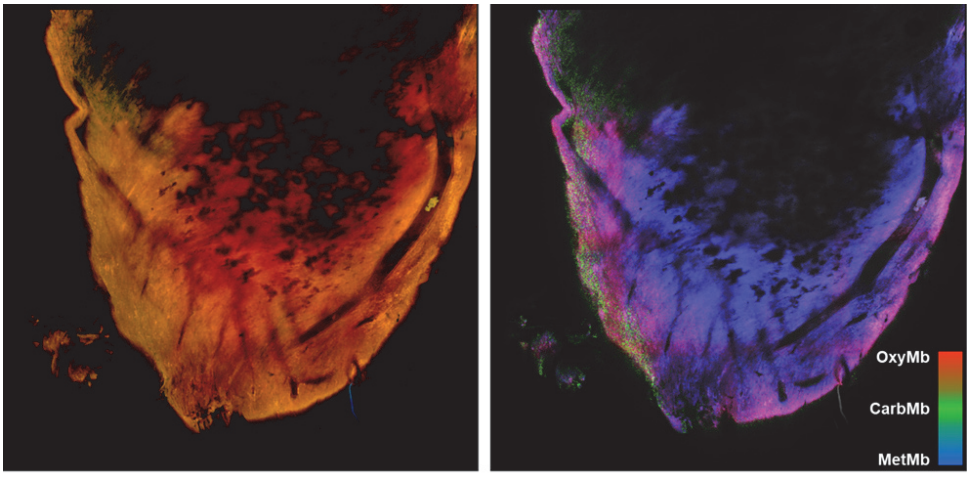

Figure 31: Spectral imaging and unmixing analysis of IR heart.

Spectral image to the left of an ischemic-reperfused mouse heart for 24 hrs showing heterogenous signals after spectral unmixing (right). The major signal was for the oxidized myoglobin form (MetMb, colored in violet-blue).

However, to easily visualize if there is a difference in the signals, we have tested the ratiometric approach in order to discriminate the metmyoglobin signal from the oxy and carbmyoglobin ones. As displayed in **Fig. 31**, indeed this ratio imaging tool was able to characterize the oxidized signal when present in IR 24 hrs hearts but not in sham ones.

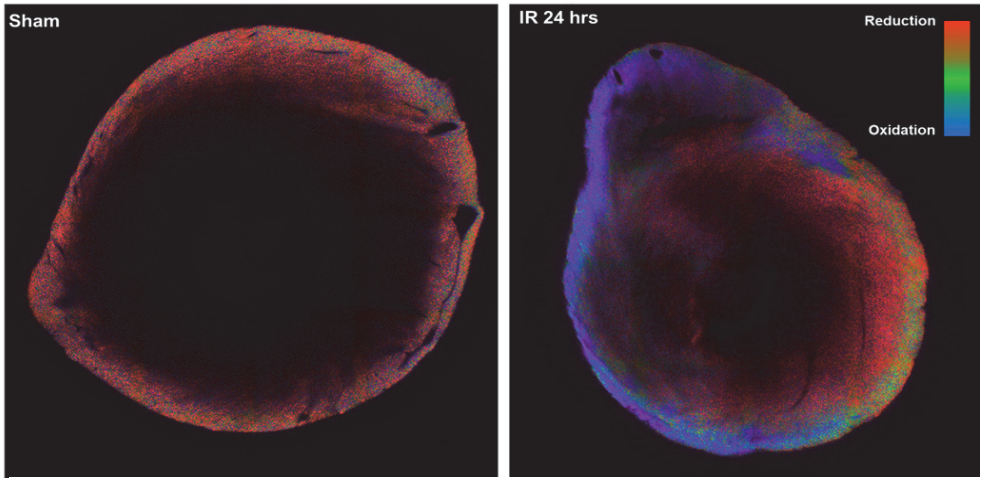

Figure 30: Ratiometric images of clarified hearts.

Ratio imaging of sham and IR mouse heart after 24 hours. [510-550]/[650-750nm] was used to obtain the ratiometric images.

On the other hand, this method has shown an artifact signal in the right ventricle of the IR heart of **Fig. 31**, making it difficult to rely on the whole image for quantifying the oxidation-reduction signals in the area at risk and thus we needed an automated method which can statistically identify different heterogenous signals. In this regard, for the advantages discussed earlier in this manuscript, we sought to image these samples by light sheet microscopy performed in different platform by specialized people.

5. Light-sheet imaging of the IR and postconditioned hearts:

The different heart samples at different time points (Ischemia 45 minutes, Ischemia-reperfusion 3 hrs and 24 hrs and Ischemia-reperfusion + postconditioning at 24 hrs) were imaged by light-sheet microscope (Ultramicroscope, Miltenyi Biotec). 3D volumetric images were acquired and interestingly, visually, we have observed major differences in the profiles. As shown in **Fig. 32**, 15 minutes after reperfusion, an intense oxidation signal is observed which increases gradually after 3 hrs and 24 hrs of reperfusion. Whereas, this signal greatly decreases after applying the ischemic post conditioning strategy compared to IR 24 hrs.

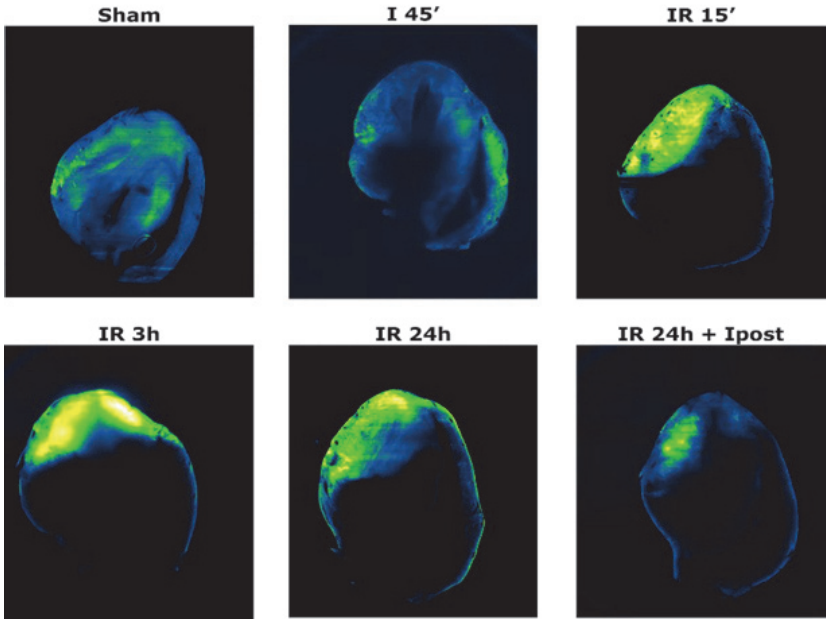

Figure 32: Light sheet imaging of clarified hearts.

Light-sheet images of IR and IPost hearts at different time points during the IR sequence. Increased yellow signal corresponds to increased oxidation, which increases during reperfusion and decreases after applying the cardioprotective ischemic postconditioning protocol (n=4/condition).

As a primary approach, a half-automated algorithm was developed under ImageJ that aims to quantify the percentage of the area at risk out of the total left ventricle volume. This tool is mainly based on three major steps. First, selection of the left ventricle area, second, specify the intensity threshold of pixel distribution and finally calculate the volume of the area at risk as a percentage of the left ventricle volume. An example of IR 24 hrs heart is displayed in **Fig. 33**, it shows different signals where the green+red ones correspond to the area at risk and the red one to the highly oxidized area in the area at risk.

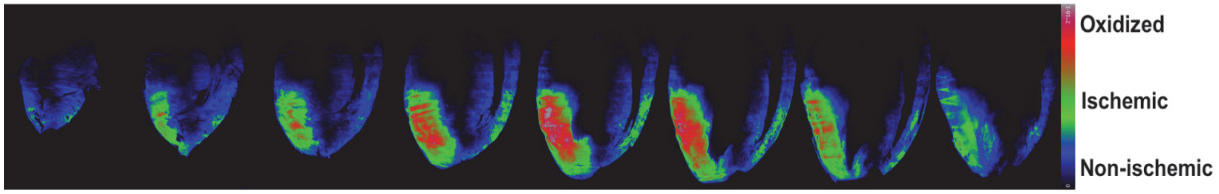

Figure 33: ImageJ half-automated algorithm for quantifying the area at risk.

Quantification of the area at risk as a percentage of the left ventricle volume. Blue area corresponds to the non-ischemic vascularized myocardium, green area corresponds to the ischemic area and red corresponds to the maximally oxidized zone of the ischemic area.

However, the artefacts introduced in the fluorescence intensity due to heterogeneity of the clarification and heterogeneity of the depth of the light path (longer light path when illuminating the tissue at the side opposed to the collection objective) acted as a limiting factor in this approach, which disabled the use of a single intensity threshold prior performing image segmentation and pixel clusterization.

Therefore, we developed a statistical approach via fitting a Gaussian distribution to the pixel distribution of fluorescence intensity taken from 100 images per heart. Interestingly, using this tool, we were able to identify several classes of intensity-based pixels. This analysis has shown that sham and 45 minutes ischemic hearts were fitted to a 1st order gaussian distribution (1 peak in the data histogram distribution in **Fig. 34**) which means a homogenous distribution of the autofluorescence. However, IR 15 minutes hearts didn't fit a Gaussian distribution which suggests a further increased number of hearts to figure out the issue. Whereas, a 2nd order and 3rd order

Gaussian distributions have fitted IR 3hrs and 24 hrs hearts corresponding to 2 and 3 peaks in the histograms, respectively. These 2^{nd} order and 3^{rd} order Gaussian distributions revealed the detection of 2 states of increased oxidation in the area at risk. Interestingly, ischemic

postconditioning has generated data that fits a 1st order Gaussian distribution similar to sham and 45 minutes ischemia group, validating the efficacy of the protective strategy (**Fig. 34**).

6. Macrophages' immunostaining in the myocardium:

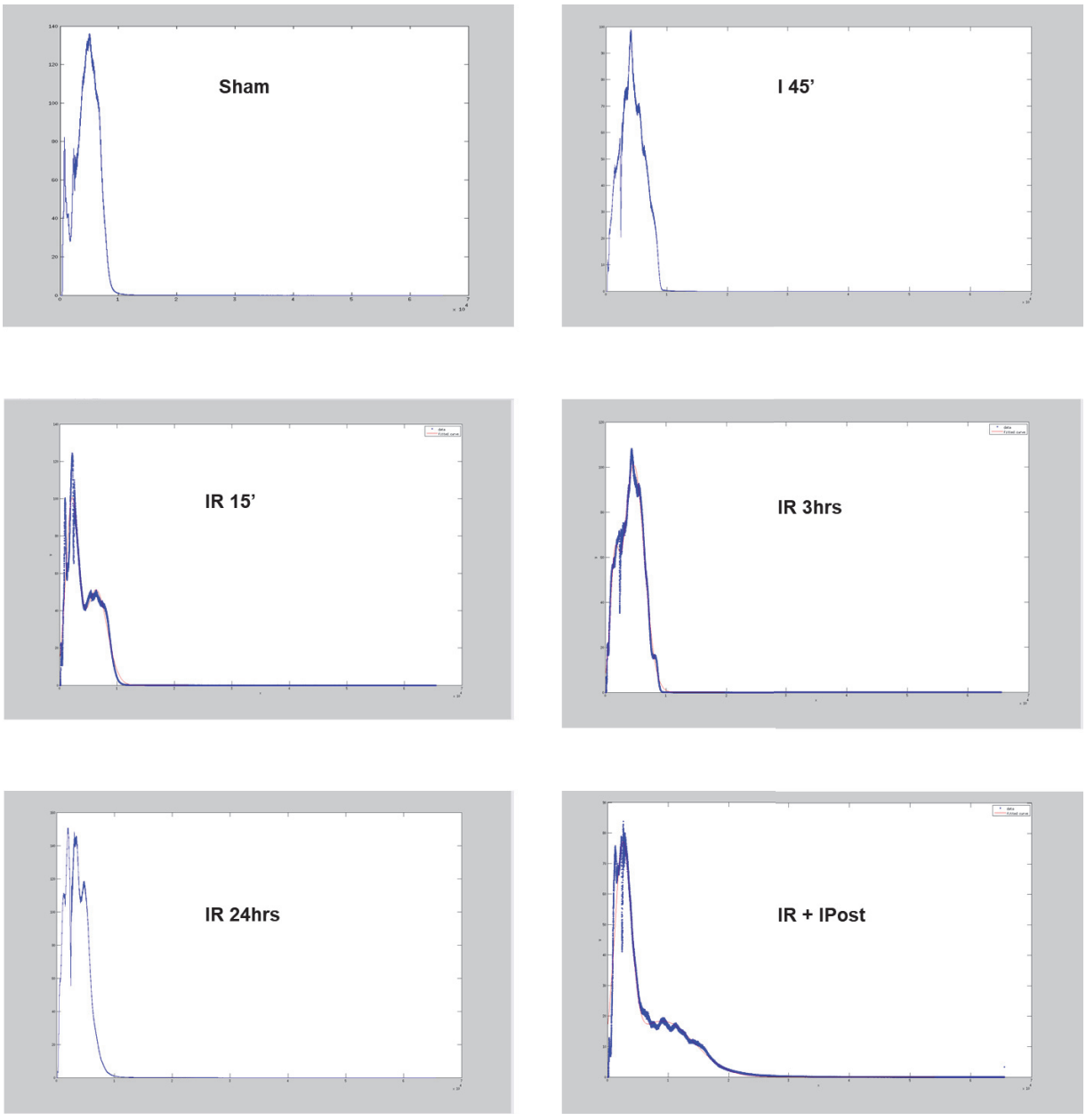

Figure 34: Gaussian distribution fitting of the intensities generated by light-sheet imaging.

Averaged intensities profiles of the hearts imaged by light-sheet microscope fitted to gaussian distribution to identify different signals in the myocardium.

In a collaborative work that aims to study the dynamics of immune cells infiltration to the myocardium, clarified hearts have been immunostained for different target molecules. Among these targets were first the vasculature, the cardiomyocytes and the cardiac fibroblasts. As displayed in **Fig. 35**, immunostaining of the vasculature via the α smooth muscle actin has clearly revealed its structure. Similarly, for the cardiac resident cells, vimentin and troponin staining of the fibroblasts and cardiac cells, respectively has resulted in a clear image of the distribution of the cells in the myocardium.

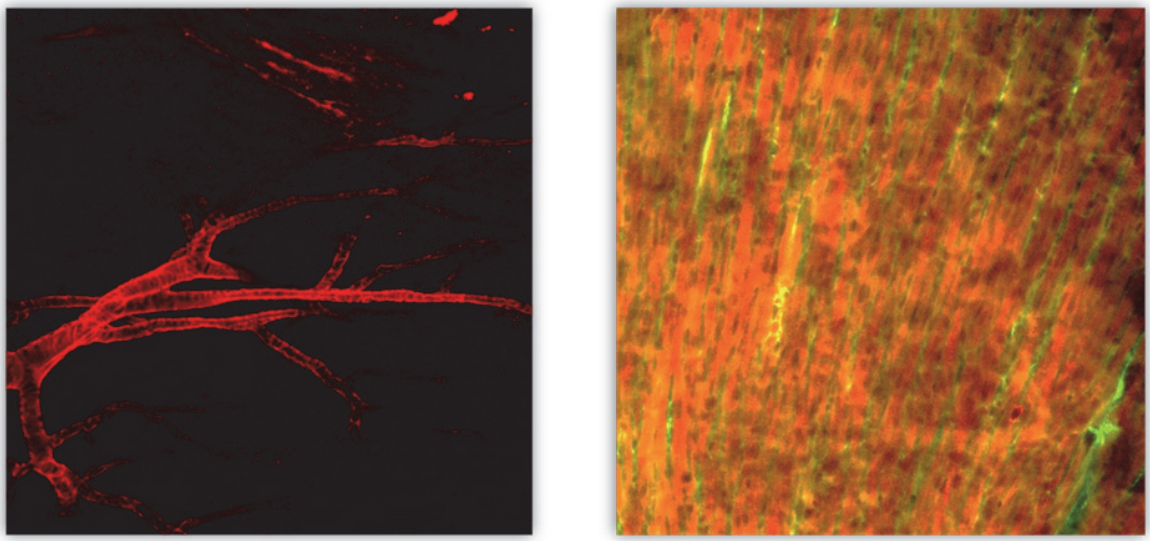

Figure 35: Cardiac structures immunostaining.

Confocal images displaying vasculature staining by α smooth muscle actin (red color) to the left and cardiac myocytes and fibroblasts cells staining by troponin (orange color) and vimentin (green color) to the right, respectively.

In this regard, having controls for this work, we have sought to measure the infiltration of the macrophage population to the myocardium post MI, by immunostaining with CD206 antibody. 24 hours post MI, we show that there is an increased infiltration of macrophages in the ischemic area (**Fig. 36**). However, this protocol as shown in the figure requires further optimization to decrease the unspecific signal present on the borders which might include decreasing the antibody's concentration, validating with a new antibody and imaging with light sheet microscope.

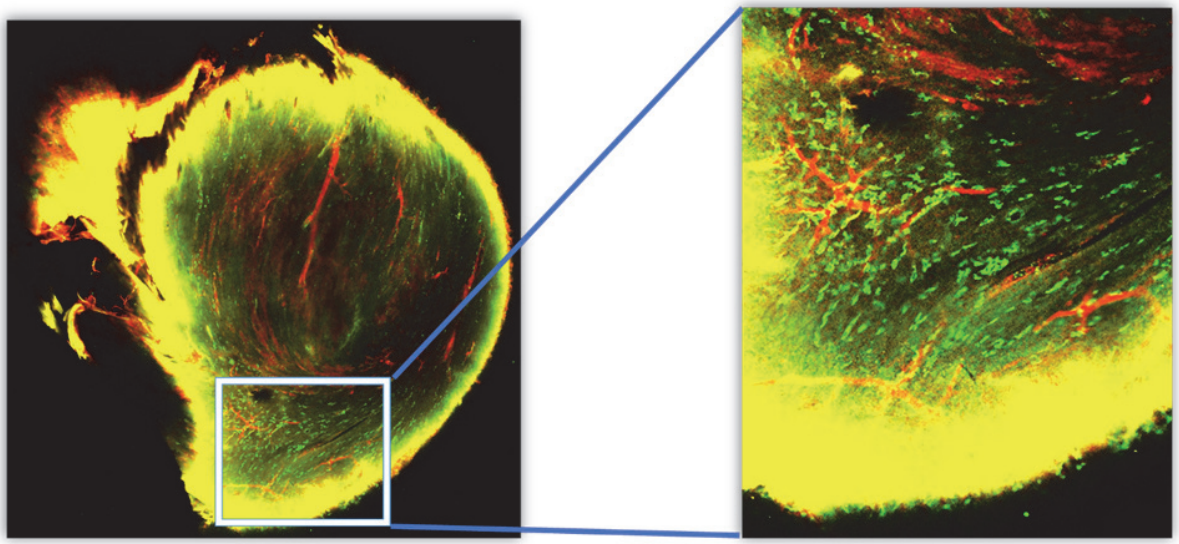

Figure 36: Macrophages' immunostaining in the myocardium.

Confocal image of an immunostained 24 hours MI heart displaying the increased population of macrophages in the ischemic area. Green and red colors correspond to CD206 macrophages and α smooth muscle actin antibodies, respectively.

In this section of the results, we have presented a novel approach for quantifying the oxidation-reduction state of the myocardium in the area at risk in MI-induced mouse model. Our approach integrates different aspects like heart clarification, different imaging and statistical tools in order to be able to quantify the oxidation signals during IR and understand the dynamics of signal propagation in the myocardium which is known by the "wavefront phenomenon" starting centrally and propagating towards the periphery of the area at risk. In addition, we have shown that immunostaining of clarified hearts post MI has succeeded in displaying the infiltration status of inflammatory cells in the myocardium which we to aim to quantify over time and integrate with the upcoming approaches. In this context, a paper of the presented work is under writing and planned to be submitted soon.

Section II: Dynamic Transcriptomic Analysis

In the previous result section, we have displayed an approach of characterizing heterogenous signals in the ischemic area at risk based on the myocardial redox state at different time points during ischemia-reperfusion. Oxidation state was shown to be shifted few hours post reperfusion. However, in order to further understand the transcriptional changes and the activated molecular processes ruling this oxidative shift and consequently leading to myocardial damage, we sought to study the dynamic transcriptional response of the myocardium to ischemia-reperfusion and cardioprotection in a temporal dimension.

Throughout this section, we present an analytical pipeline of large-scale transcriptomic data via unsupervised and supervised approaches that unravels the changes in expression profiles in the heart in response to surgery, ischemia-reperfusion and cardioprotective strategies.

Part 1: Unsupervised Analysis

1. Effect of the surgical interventions on the change of gene expression profiles in the myocardium:

As discussed earlier in the manuscript, surgical interventions applied to mice for mimicking MI is known to induce the activation of the inflammatory response, but to our knowledge, this response is rarely quantified. In this context, throughout the proceeding part, we characterize the surgery-induced effect on the change of gene expression profiles via an analytical approach of big transcriptomic data that integrates different freely available tools to be detailed later.

Throughout this part, only sham-operated animals are considered and raw counts RNA-seq data of 0 minutes, 45 minutes and 24 hours post-surgery myocardial samples are analyzed according to the workflow presented in **Fig. 37.**

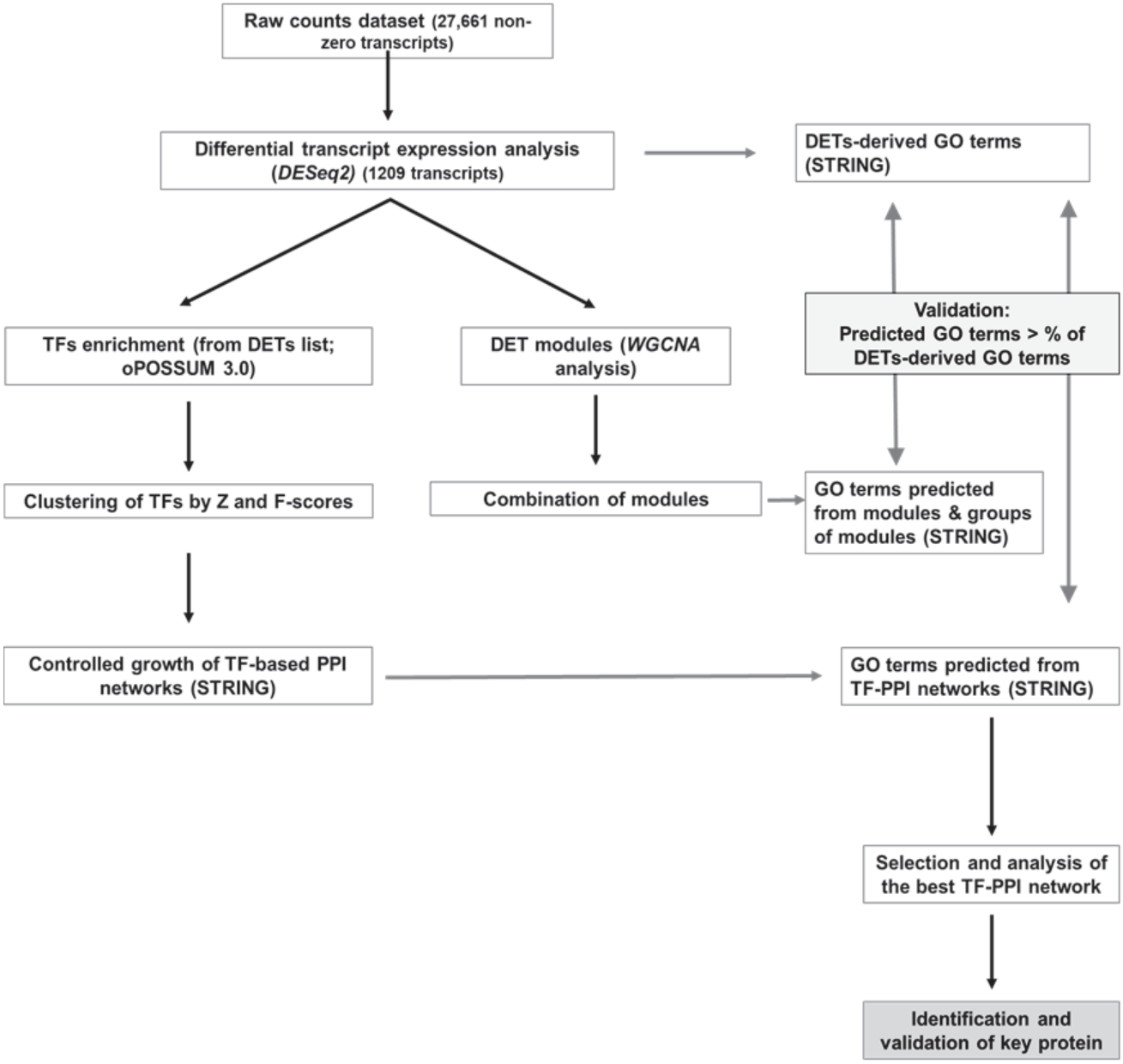

Figure 37: Dynamic transcriptomic analysis pipeline.

A scheme representing the workflow of the Sham-operated mice RNA-seq data at 0 minutes, 45 minutes and 24 hours post-surgery using various R packages and freely available softwares.

1.1. Experimental design:

As discussed earlier, there are several factors that might influence the end results of the transcriptomic analysis. Among these factors are the number of subjects considered and the normalization and analysis method used for detecting the differentially expressed transcripts (DETs). In this regard, the number of mice considered for each time point in our analysis is calculated to meet the statistical power of 80% (detailed in the methods section), where a total of **24** animals (**n=8** per time point) is considered. In addition, seeking a normalization and analysis method that is suitable for kinetical analysis and has high sensitivity to control the false discovery rate (FDR), we have chosen to work with DESeq2 method for detecting differentially expressed transcripts at any time point in our analysis.

1.2. Data quality checks and visualization by principal component analysis:

Prior to proceeding with the data analysis, it is important to visualize it and assess the different sources of variation if present. Several factors might account for these variations and might act as a confounding factor in the analysis if not considered. Among them are the experimental errors introduced, in our case, by the different surgeons performing the surgery on the mice and the different cDNA libraries introduced during RNA sequencing protocol, what is known by the "batch effect". In this regard, we have applied principal component analysis (PCA) to visualize the distribution of our data in reduced two dimensions. As shown in **Fig. 38**, our samples were not clustered neither by the surgeons nor by the batch. However, they were actually clustered by their temporal variation, where 24-hour samples post-surgery accounted for the highest variation in the data. In addition, samples were scattered along two principal components PC1 and PC2 what proposes at least two sources of variation among them is time. Noteworthy, these PCA plots did not display any outlier sample that might affect the analysis and shall be removed, although a great within-group variability, originating from biological or technical sources that we cannot control, was shown by the spreading of the samples along the first principal component PC1.

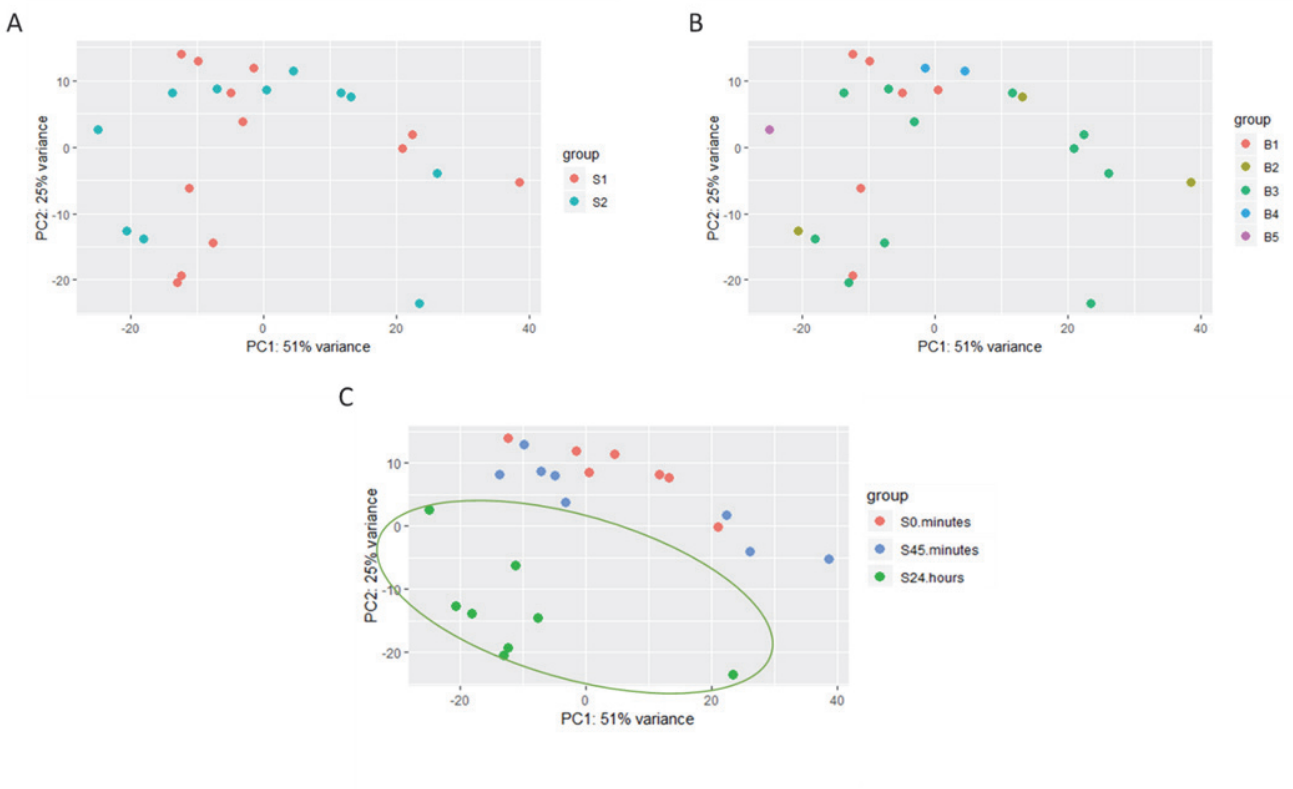

Figure 38: Quality checks by principal component analysis.

A scheme displaying the quality checks of the data by principal component analysis of the 0 minutes, 45 minutes and 24 hours sham samples by (A) surgeons (S1 and S2) (B) batch (B1-5) and (C) time (S0.minutes, S45.minutes and S24.hours). These figures show that data is mainly clustered by time (C) neither by batch nor by surgeon.

1.3. Differential expression analysis by DESeq2:

In order to sort out the differentially expressed transcripts. RNA-seq raw counts data were normalized by DESeq2 via estimating a size factor, where all the genes are multiplied with. Independent filtering of all zero-counts was applied and a total of 27,661 transcripts were kept for analysis. Likelihood ratio test (LRT) was applied including the batch, surgeon and time in the design of the *DESeq* function, so that the sensitivity to detect differentially expressed transcripts affected only by time is increased. Totally, **1209** transcripts were differentially expressed with adjusted *P* value less than 0.05 at any time point included in this analysis (0 minutes, 45 minutes and 24 hours).

1.4. Functional enrichment analysis of the differentially expressed transcripts:

To identify the major biological process that have been modified by the surgical interventions (anesthesia, thoracotomy and rib breaking), functional enrichment analysis of the differentially expressed transcripts have been performed. More than 700 enriched GO terms with the default parameters (FDR < 0.05) of the used database were obtained. Therefore, to minimize their dimensionality, we have arbitrarily selected a cut-off of FDR < 10^{-04} and finally 228 GO terms were kept for further analysis. These GO terms were classified into bigger biological processes so that a better understanding is provided for the surgical consequences. As shown in **Fig. 39**, major processes like signalization (24% of GO terms), regeneration (24%), inflammation (11%), cell death (11%) and cell migration (9%) have been identified, where some like the activation of the inflammatory response is expected based on previous literature.

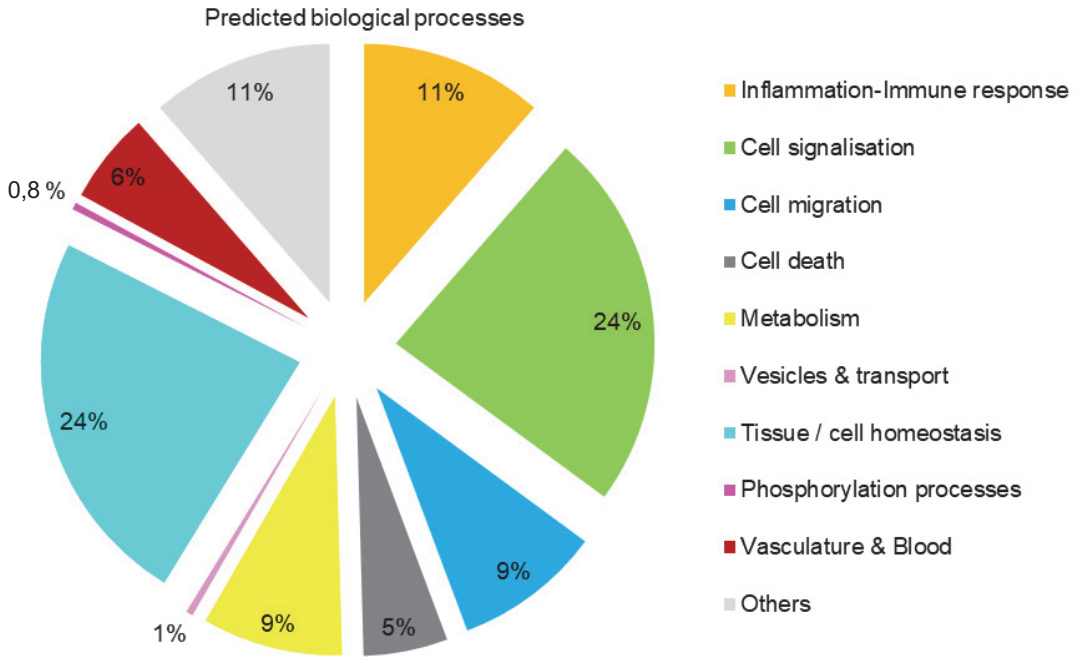

Figure 39: Major biological processes predicted for the differential expressed transcripts.

Pie chart displaying the major biological processes modified by the surgical interventions, where the list of DETs was subjected to enrichment analysis by STRING software. Enriched GO terms were classified into bigger processes presented here and annotated by different colors.

Although this strategy of exploring gene networks in response to stimuli, like the sham effect in our study, is widely used, it lacks the understanding of the organization and modification of genes and proteins over taking place over time. Therefore, we next wanted to identify waves of gene networks by temporally clustering the DETs.

1.5. Differentially expressed transcripts temporal clustering by weighted gene co-expression network analysis (WGCNA).

Normalized DETs obtained by DESeq2 were analyzed by weighted gene co-expression network analysis in order to investigate the temporal alterations of these transcripts and cluster them by their similarity of expression profile. Prior to proceeding with the analysis, quality checks of the samples have been performed in order to ensure the absence of any outlier sample that might affect the analysis. As shown in **Fig. 40**, no outlier samples were present and thus all samples were considered for further transcript clustering approach.

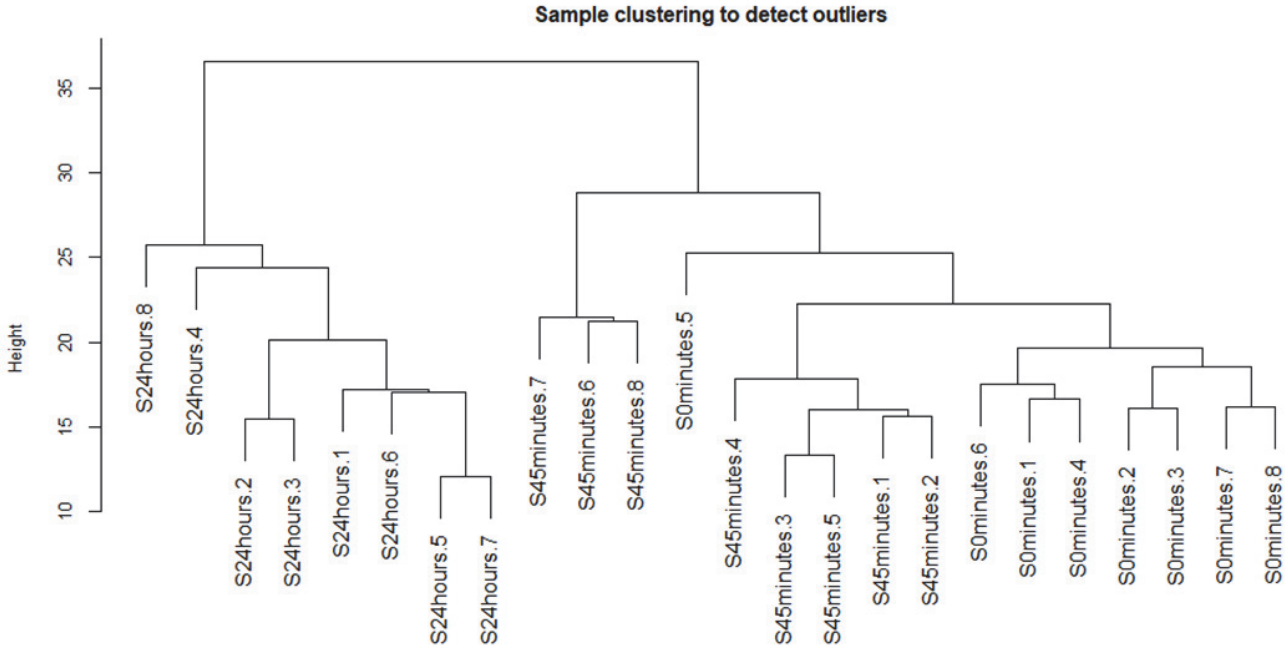

Figure 40: Samples' clustering to detect outliers.

A scheme representing the hierarchal clustering of the 24 samples included in the analysis, to detect outlier samples that might influence the results so that they should excluded from the analysis. 24 hrs samples were mainly clustered together aside from the 45min and 0min samples that formed a big cluster.

Based on a scale free topology criterion, a weighted co-expression network was constructed Interestingly, 9 different co-expression modules/clusters (**Fig. 41**) had been identified using the dynamic tree cutting algorithm, where a color code was assigned to each module. Out of the 1209 total analyzed transcripts, 300 (approximately 25 % of the DETs) had not been assigned to any module (the grey color module). These modules have ranged in size between 27 and 210 transcripts.

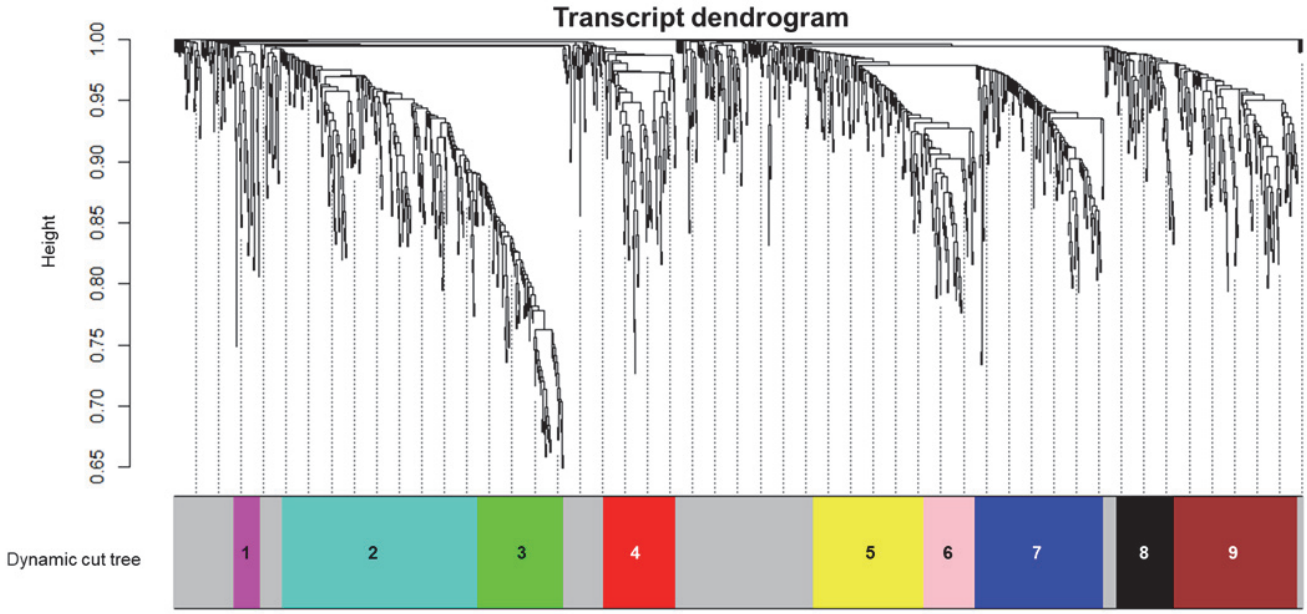

Figure 41: WGCNA co-regulated differentially expressed transcripts clustering.

Transcript dendrogram representing the hierarchical clustering of DETs based on their similarity in the expression profiles. Nine different modules have been identified; each is represented by a color. Tree branches correspond to transcripts and colors underneath the tree corresponds to the modules assignment by Dynamic Tree Cut of the WGCNA R package.

As explained in the method section, WGCNA also uses PCA to summarize the distribution of the transcripts' expression, where the first principal component is called "eigengene". These eigengenes were calculated for each module and their means in plotted in **Fig. 42** to provide the

average variation of the transcript's expression. Three major profiles have been classified throughout this strategy. The First profile includes the transcripts varying at 45 minutes (the magenta color, M[1]). The other profiles include the transcripts displaying an increased and decreased expression at 24 hours, M[2-4] and M[5-9], respectively. The heatmaps of some of these profiles are provided in **Fig. 43** as an example.

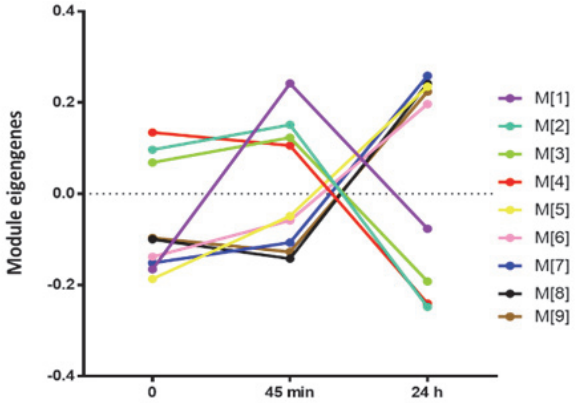

Figure 42: Temporal profiles of WGCNA modules.

Line graph representing the variation of the expression profiles in the different WGCNA modules over time.

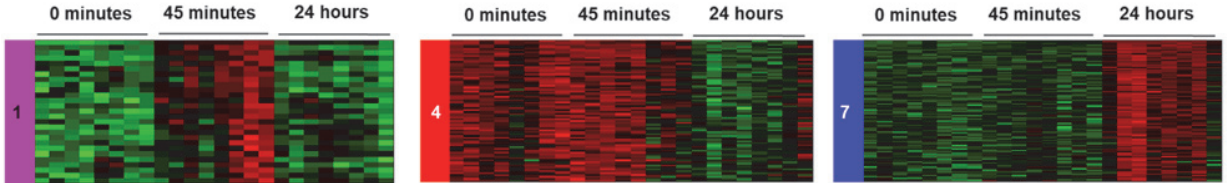

Figure 43: Heatmaps of WGCNA modules.

Heatmaps representing expression levels of transcripts assigned to the three main WGCNA modules displaying variation in profile over time: the magenta (M[1]), red (M[4]) and blue (M[7]) modules. Red color corresponds to higher expression and green color corresponds to lower expression.

1.6. Gene ontology analysis of WGCNA modules and combination of modules:

In order to assess whether the co-variance clustering had gathered transcripts involved in common biological functions as well, we next identified the biological processes that were altered by the transcripts in each module and assessed the strength of these predictions compared to the DETs altered processes. To achieve this, modules were subjected to functional enrichment analysis separately. Only 4 modules out of the 9 had few significant biological processes. However, through this approach, it is assumed that only co-varying genes belong to common biological processes.

Therefore, to enhance these predictions, we also tested different combinations of the modules and looked for the greatest number of the predicted biological processes.

Firstly, we assessed the distribution of the transcript counts as a function of the GO term counts. As displayed in **Fig. 44**, no correlation was observed for the studied modules. As an example, M[2] constitutes 210 transcripts but had no significant GO terms, however, M[1;6] which constitutes only 83 transcripts had 240 significant terms. This has suggested that greater transcript count doesn't mean greater GO term counts and thus no transcript count artifact is introduced when different modules are combined.

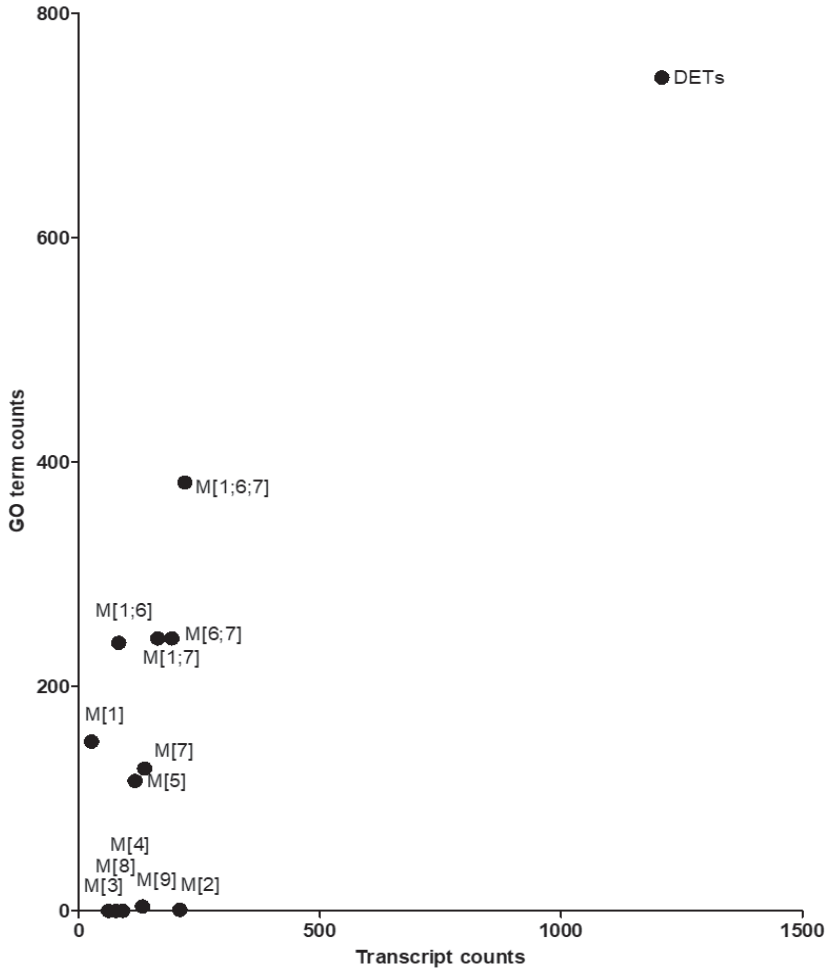

Figure 44: GO terms versus transcript counts relationship.

Dot plot of the GO terms counts predicted for each transcript's modules or all DETs as a function of the count of transcripts.

Next, we assessed whether modules or their combinations can be strong predictors of GO terms derived from the list of all DETs via a feature we have named GO terms enrichment (described in the methods section). As done previously, GO terms predicted for each module or combination of modules have been firstly sorted for FDR $<10^{-4}$ then GO terms having an enrichment score (z-score) > 2 was kept for further analysis (**Fig. 45A**). GO terms counts for modules and the different combinations are displayed in **Fig. 45B**.

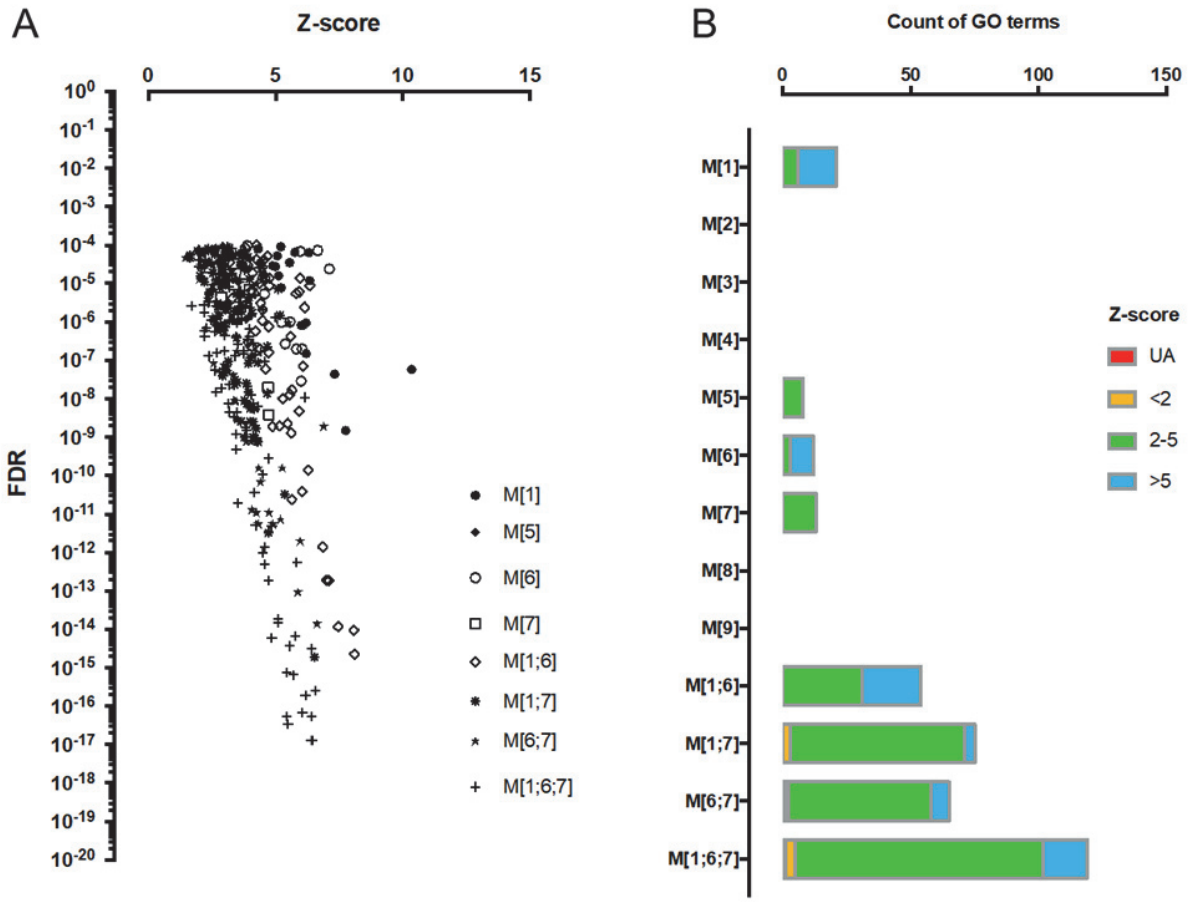

Figure 45: Gene ontology enrichment analysis of the WGCNA modules/combination of modules.

(A) Scatter plot of the enrichment z-score and FDR of GO terms predicted for each module and combination of modules. (B) Bar graph displaying the count of enriched GO terms shared with DETs GO terms. A color code has been assigned to the GO terms based on their enrichment z-score.

Next, modules and combination of modules were sorted by the highest enrichment for each GO term. As **Fig. 46** displays, among the 6 sorted group of modules that were best predictors of the shared GO terms with the DETs, the combination of modules M[1;6;7] had the highest count of the highest enriched terms. Therefore, we concluded that M[1;6;7] was the best predictor of the DETs shared GO terms which also meant that the clustering of 3 groups of co-varying genes gave the best results to predict biological functions.

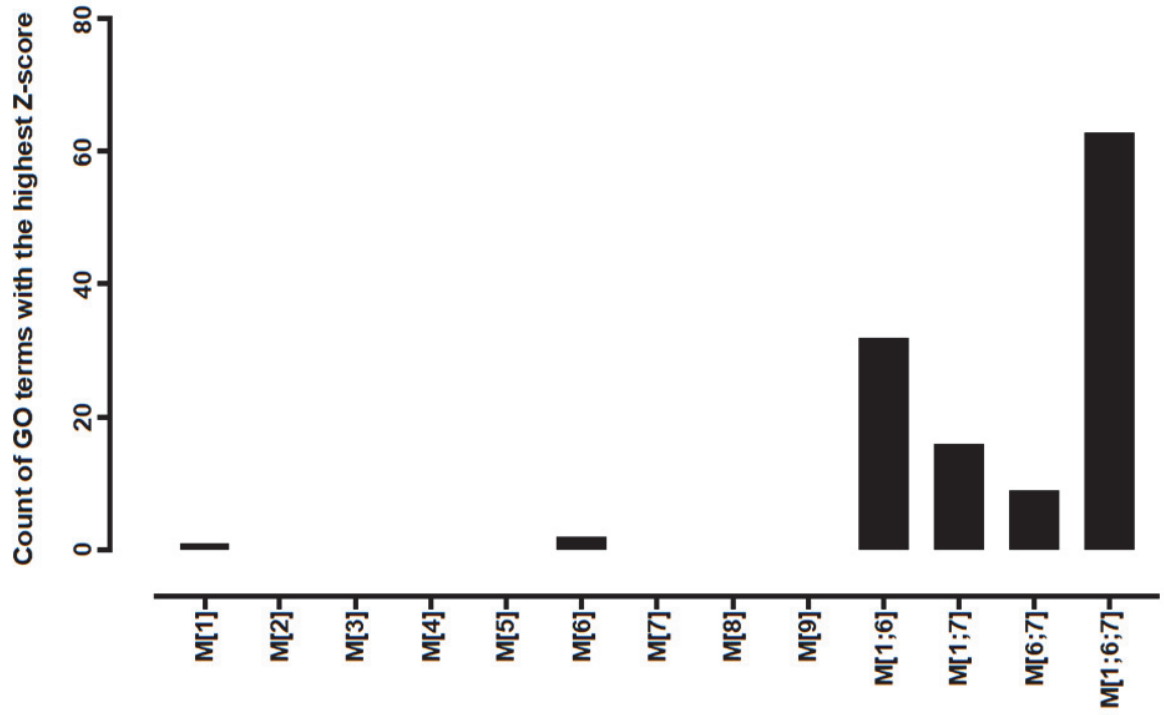

Figure 46: WGCNA modules' enriched GO terms shared with DETs.

Bar graph displaying the count of GO terms shared with the DETs of modules and combination of modules having an FDR less than 10^{-4}.

In order to identify what processes were enriched in each module/combination of modules, we classified the enriched GO terms into bigger biological processes (**Fig. 47**). Transcripts that were significantly increased at 45 minutes (M[1]) were mainly involved in signalization processes which we justified as a homeostatic response following surgery via transcriptional activation.

M[1;6], M[6;7] and M[1;7] were involved mainly in inflammation, signalization and cell migration processes. Being the best putative predictor of the shared DETs GO terms, M[1;6;7] was mainly involved in inflammation, signalization, cell migration, and cell death. Other processes like tissue regeneration was poorly recapitulated in M[1;6;7] GO terms (11 vs. 54 GO terms in DETs), while neither vasculature nor metabolism were detected. These results suggested that the method used was efficient in classifying some of the enriched DETs features but not all.

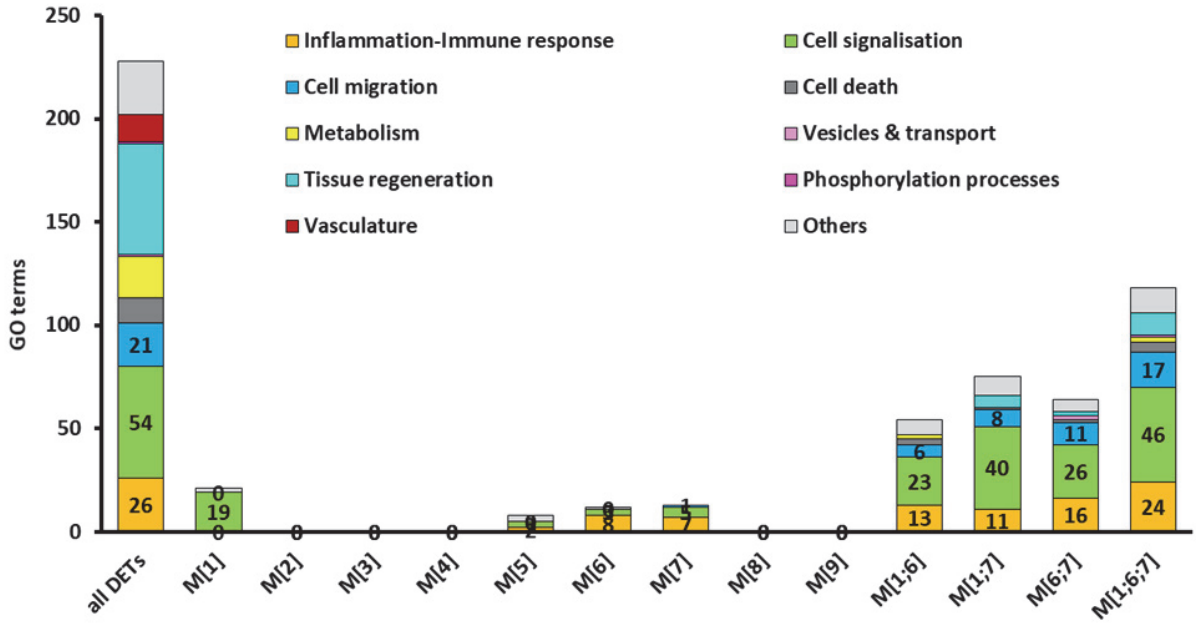

Figure 47: Enriched biological processes in DETs and WGCNA modules.

Histogram displaying the count of GO terms classified into bigger biological processes in DETs in each module and combination of modules. A color code has been assigned to the different biological processes.

Interested in M[1;6;7] combination, we took a closer look on its transcripts, we found many inflammatory markers including neutrophil and macrophage markers (LCN2 and ARG-1, respectively), chemokines (CCL6, CCL9, CCL12, CXCL1 and CXCL3), chemokine receptors (CCR2 and CXCR2), in addition to adhesion markers (ICAM-1 and Sele). We therefore checked for the occurrence of these transcripts in the GO terms of the three major enriched processes, signalization, inflammation and cell migration, and interestingly we found that they are actively

involved in these processes (**Fig. 48**). We thus hypothesized that these transcripts have fingerprinted the recruitment of inflammatory cells to the myocardium post-surgery.

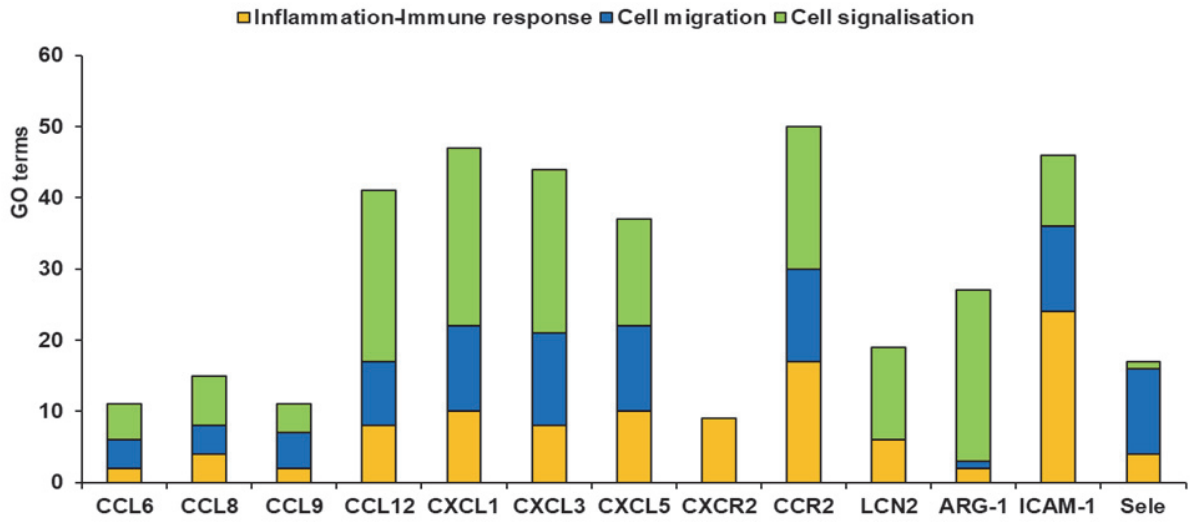

Figure 48: M[1;6;7] inflammatory markers involved processes.

Histogram displaying the occurrence of inflammatory transcripts of module M[1;6;7] in the GO terms of the major enriched biological processes.

1.7. Assessment of inflammatory cells recruitment by FACS analysis:

In order to validate this hypothesis, we quantified the neutrophils and macrophages population in the hearts subjected to surgery via FACS analysis of isolated non-cardiac cells from the myocardium. Ly6g-positive cells showed a 9.3-fold significant increase 24 hours post-surgery (**Fig. 49**), what suggested an increase in the neutrophil population recruitment to the myocardium.

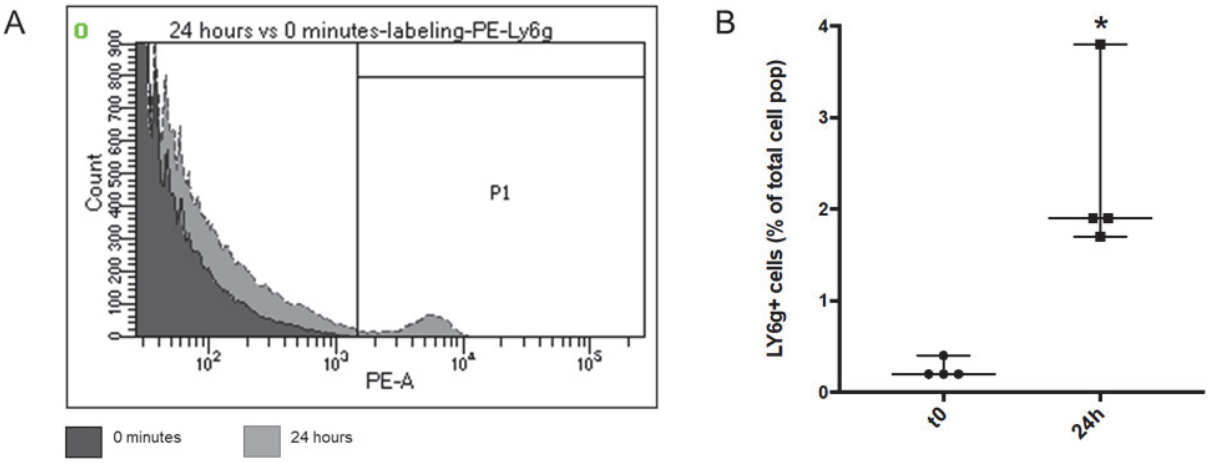

Figure 49: Neutrophils recruitment to the myocardium by FACS analysis.

(A) Distribution plot of Ly6g positive cells in 0 minutes versus 24 hours post-surgery gated in P1. (B) Dot plot displaying the percentage of ly6g-positive cells. (n=4/ time point) and * P < 0.05.

In addition, regarding the macrophage population, we used four different markers, F4/80, CD11b, CD206 (for M2 macrophages) and CD86 (for M1 macrophages). Firstly, as shown in **Fig. 50A** we observed an increase in the $CD206^{-}/CD86^{-}$ cells (from 41.2±2.9 to 59.3±6.3% of F4/80+/CD11b+ macrophages; adjusted p-value <0.0001) which is justified by the recruitment of monocytes to the myocardium 24 hours post-surgery. However, a significant decrease was observed in the double positive population CD206+/CD86+ (70.6±4.0 to 48.8±9.5%; adjusted p-value: 0.0013). Interested in this population alone which has been already been reported to be present in the heart (Walter et al. 2018), we observed what looked like a transition to either the M1 subtype phenotype which wasn't significant (10.0±1.8 to 17.4±3.6%; adjusted p-value: 0.2778) or to the M2 subtype phenotype (CD206+/CD86-) significantly (19.4±2.9 to 33.9±7.0%; adjusted p-value: 0.0181) **(Fig. 50B**).

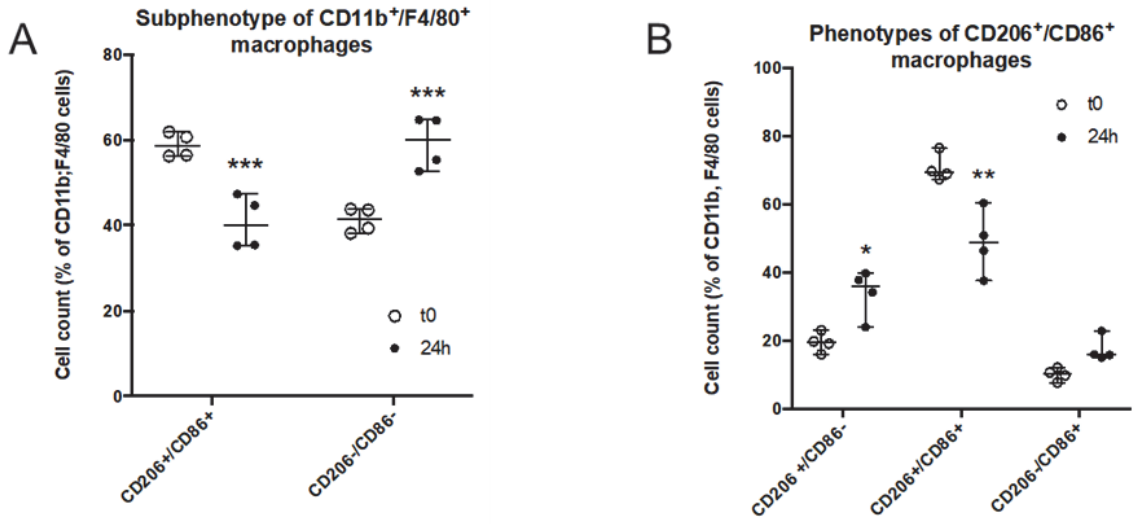

Figure 50: Macrophages population in the myocardium.

Dot plot displaying the percentage of (A) subphenotype of CD11b+/F4/80+ macrophages population and (B) CD206+/CD86+ macrophages by FACS analysis 0 minutes and 24 hours post-surgery, respectively. (n=4/time point) and ** $P < 0.01$ and *** $P < 0.001$.

Therefore, in this regard we concluded that 24 hours post-surgery, neutrophils and monocytes infiltrate to the myocardium and macrophages undergo possible phenotypic changes favoring the M2 subtype and thus have fingerprinted the signalization and inflammatory predictions. However, metabolism and tissue regeneration which were major processes in the DETs derived GO terms were poorly recapitulated by this analysis based the co-variance of transcript expression. Therefore, we thought of a complementary strategy that involves transcription factor enrichment analysis to predict the major mediators activating these pathways.

1.8. Gene network inference via transcription factor enrichment analysis:

In response to stimulus, cells respond via the activation of molecular pathways that lead to the activation of transcription factors (TF) which consequently creates a transcriptomic signature as an outcome. However, in order to understand this signature, we sought to perform a retro-analysis. We have the DETs, enriched transcription factors can be obtained and thus delving into the molecular history might be achievable. In this regard, transcription factor enrichment analysis of the DETs was performed. Over-represented transcription factor binding site (TFBS) in the

promotor sets of the DETs was identified by z-scores and fisher exact test scores (F-score) performed by oPOSSUM software. For stringent results, TFs were first filtered by their F-score (below 20 were discarded) and then they were classified by their z-score into five groups as follows: group were: group 1 (z-score >|35|), group 2 (z-score >|25|), group 3 (z-score >|15|), group 4 (z-score >|10|) and group 5 (z-score >|2|) (**Fig. 51**).

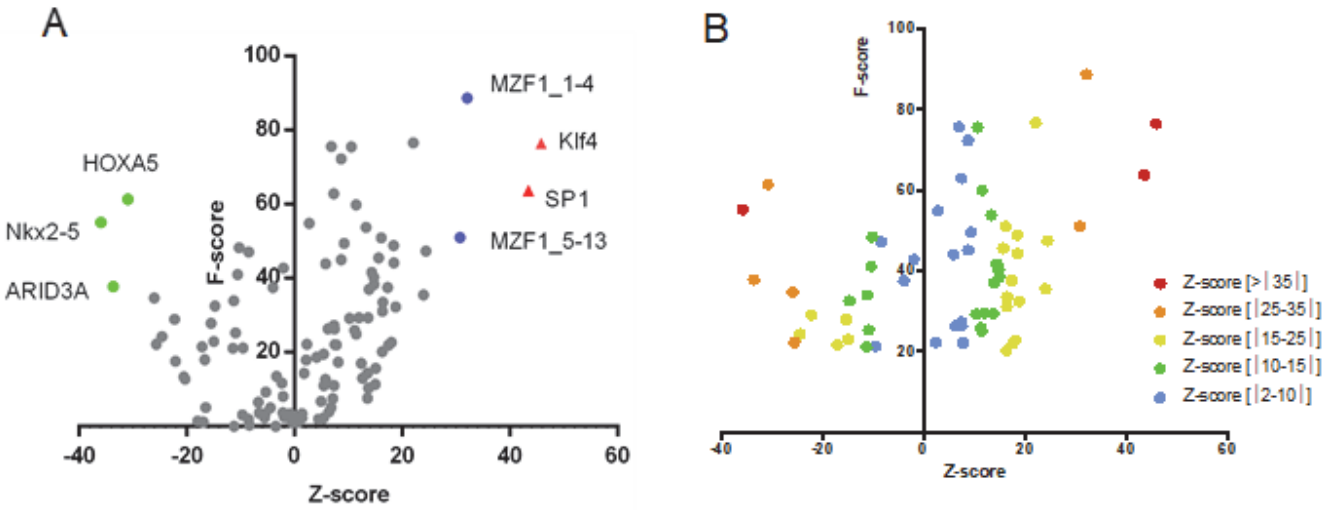

Figure 51: Transcription factor enrichment analysis of differentially expressed transcripts.

Scatter plot of F-scores and Z-scores displaying (A) enriched TFBS in the list of DETs based on Opossium software enrichment analysis and (B) the enriched TFs sorted and classified into 5 groups based on their F-score and Z-score.

Considering that these TFs are activated via signalization pathways in response to a stimulus, we have taken advantage of protein-protein interaction (PPI) networks simulation tool in the STRING database. The different TFs groups were used as an input for this software and the first obtained network, named initial network, relied only on the interplay between these TFs.

STRING networks can be expanded/grown exactly the same way as LinkdIn platform increases the network connections of its members. For a first layer network, neighboring proteins (+ 10N) which are the most likely interactors are added to the initial network where it is named the 1st layer of growth. This step was done consecutively five times (**Fig. 52**).

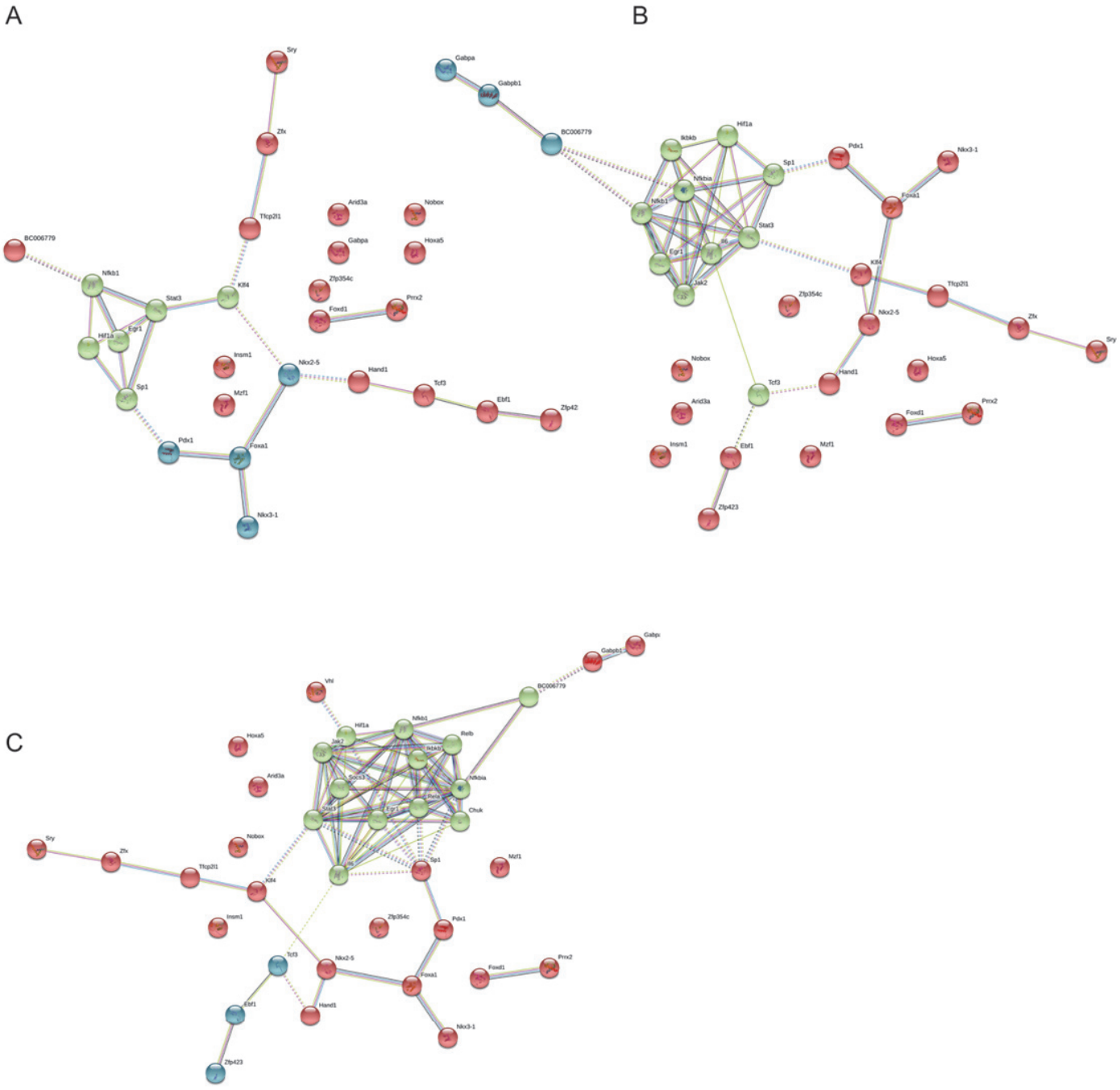

Figure 52: Protein-protein interaction predicted networks of enriched transcription factors.

Scheme displaying the growth of the group 3 TF-PPI network (A) initial network (B) 1st growth network and (C) 2nd growth network, where +5N and +10N are added respectively.

Each network built had a different growth depending on the initial count of TFs used as an input (**Fig. 53**).

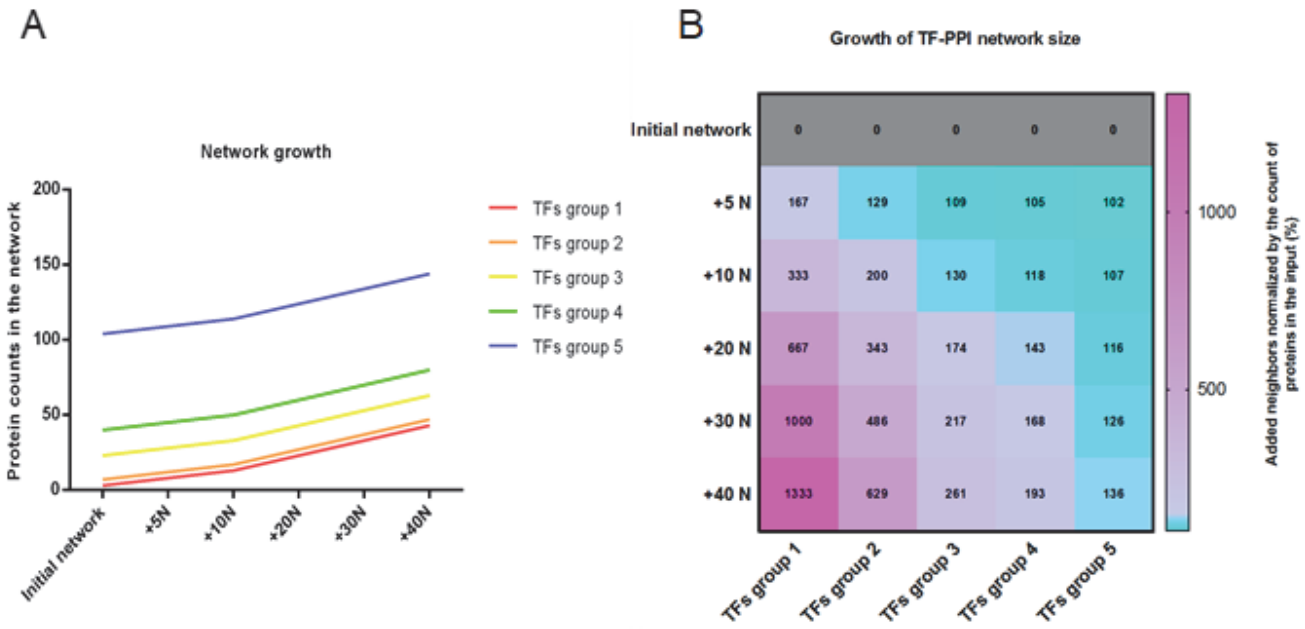

Figure 53: Growth of TF-PPI networks.

(A) Line graph displaying the growth of the TF-PPI network based on the input TFs. (B) Heatmap showing the growth of the TF-PPI as a percentage calculated by percentage of increase in the protein count after each growth layer.

In this context, to select the most informative network that predicts the mechanism upstream the TFs, we have sought to retrieve the biological processes predicted for each TF-PPI after each growth. The obtained GO terms, as described previously for the WGCNA modules, were filtered by their FDR ($< 10^{-4}$) and then they were compared to the GO terms derived from the DETs to determine the shared ones (simulated vs experimental GO terms, respectively).

As a first step, we have assessed the sensitivity of the built TF-PPI network by calculating the proportion of the DETs derived GO terms in the TF-PPI networks. As **Fig. 54A** displays, TF-PPI with too big count of TFs input (group 5) led to the saturation (49-61%) of the DETs-derived GO terms regardless the added neighboring proteins. Being unable to predict upstream mechanisms of TFs activation, we excluded these networks from being good predictors. Unlikely, networks with

low input count (group 1 and 2) shared only 16% of the GO terms, thus they were also not considered as good predictors. Whereas, TFs group 3 and 4 had 8-58% shared GO terms, meaning that a good balance between the TFs input count and the growth of the PPI networks was required to the simulated GO terms to be shared with the experimental ones.

Next, to assess the specificity of the TF-PPI networks, we have calculated the proportion of the simulated GO terms that are shared with the experimental DETs derived GO terms. **Fig. 54B** shows that as the growth of the network increases, its specificity decreases. TFs group 5 had low specificity for any growth, TFs groups 3 and 4 specificity was almost stable from the initial network to the third growth and groups 1 and 2 had an optimal specificity for the 1st growth layer. Therefore, the most specific networks were assigned to TFs group 3 and 4 from initial to 3rd growth layer network. However, combining the three assessed parameters with shared GO terms above 40% (sensitivity, **Fig. 54A**) and growth greater than 150% (**Fig. 53B**), we found that the network of TFs group 3 with the 3rd growth layer was the most dynamic network to be kept for further analysis.

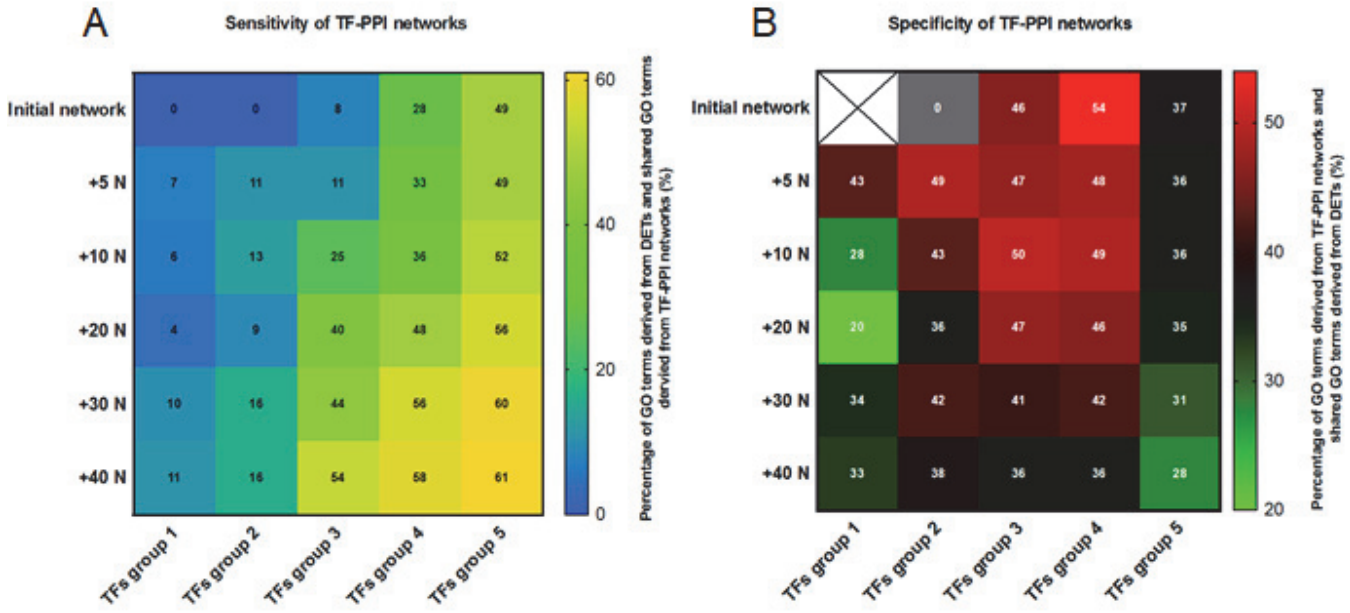

Figure 54: Sensitivity and specificity of TF-PPI networks.

(A) Heatmap showing the sensitivity of the built networks based on the growth and input of the TF-PPI. (B) Correlation matrix between the growth and input displaying the specificity of the TF-PPI network based on the percentage of GO terms derived from the TF-PPI networks and are shared with the GO terms derived from the DETs.

The TF-PPI network of TF group 3 of 3rd layer growth as viewed in **Fig. 55** highlighted 3 distinct clusters obtained via the K-mean clustering method implemented in STRING platform. A major network in green sharing the greatest number of connections, a blue secondary network and a third peripheral red network.

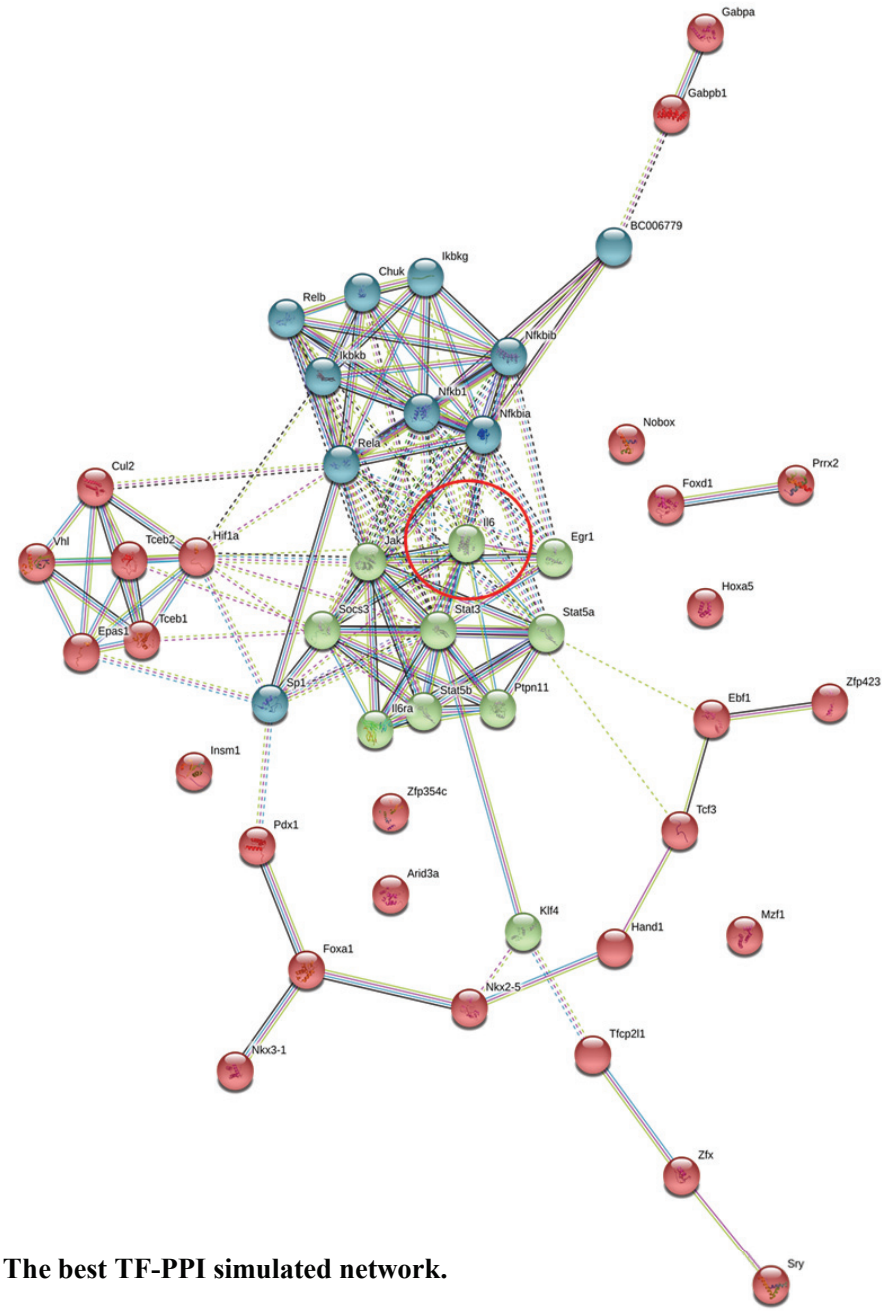

Figure 55: The best TF-PPI simulated network.

TF group 3 PPI network built after 3 layers of growth. Colors of the nodes correspond to different clusters of proteins generated by K-means clustering method

Retrieving the GO terms predicted for this network based on the same criteria mentioned previously (keeping GO terms with FDR < 10-4 and classifying them into bigger biological processes), we have interestingly found that the major processes predicted were cell signalization (36%), tissue regeneration (27%), metabolism (19%), inflammation (7%), cell death and vasculature as well (**Fig. 56**).

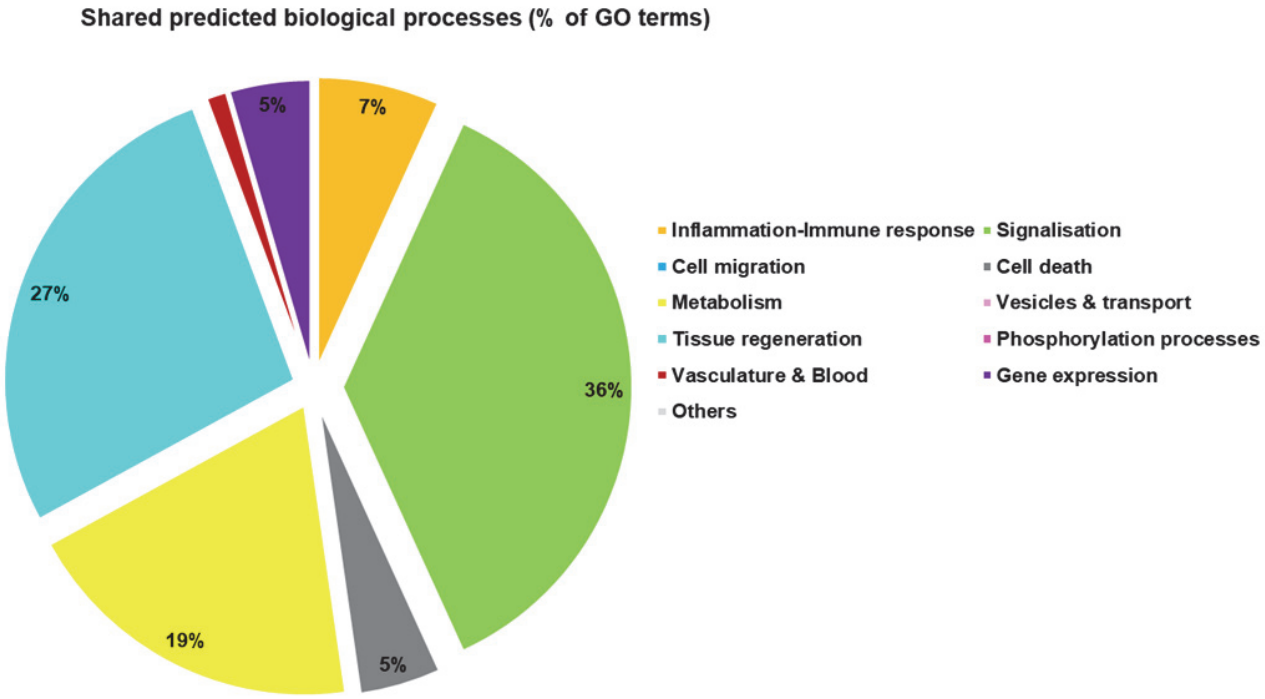

Figure 56: Enriched biological processes of the best TF-PPI simulate network.

Pie chart displaying the shared biological processes of the TF-PPI network of TF group 3 with a 3rd layer of growth. GO terms were identified by the STRING software, they were checked for shared terms with the DETs derived ones.

The overall predicted processes had a very similar pattern to what was detected from the experimental DETs. Interestingly, metabolism and tissue regeneration were richly represented in these simulated predictions. As a control step, we have compared these processes with the ones obtained from less sensitive networks, their predictions have failed to cover all the ones predicted for DETs. These results have supported tissue homeostasis and wound healing in response to the surgical interventions which could involve the cardiac resident cells conversely to what we obtained in the co-variance analysis.

1.9. Il-6 levels assessment in the plasma of sham animals by ELISA:

When taking a deeper look on the chosen network (**Fig. 55**) we found that the central network has mainly relied on STAT signalization pathways with high dependency on interleukin 6 (Il-6) stimulation. In addition, among the major TFs that have been enriched in the analysis of the DETs are STAT3, STAT5a, STAT5b, KLF4, SP1 and SOCS3 which are also linked to the Il-6 axis. Altogether these data, with literature overview where Il-6 is known to activate inflammatory cells recruitment to the injured site via the activation of signaling pathways like JAK/STAT pathway. We thus wanted to assess if Il-6 stores were released in the plasma of the sham animals, which had undergone the transcriptomic analysis. Interestingly, a transient significant increase in blood Il-6 was observed 45 minutes post-surgery (**Fig. 57**) which suggests Il-6 as a major early stimulus in response to the stress caused by the surgical interventions responsible for activating signaling pathways leading to the imprinted gene response.

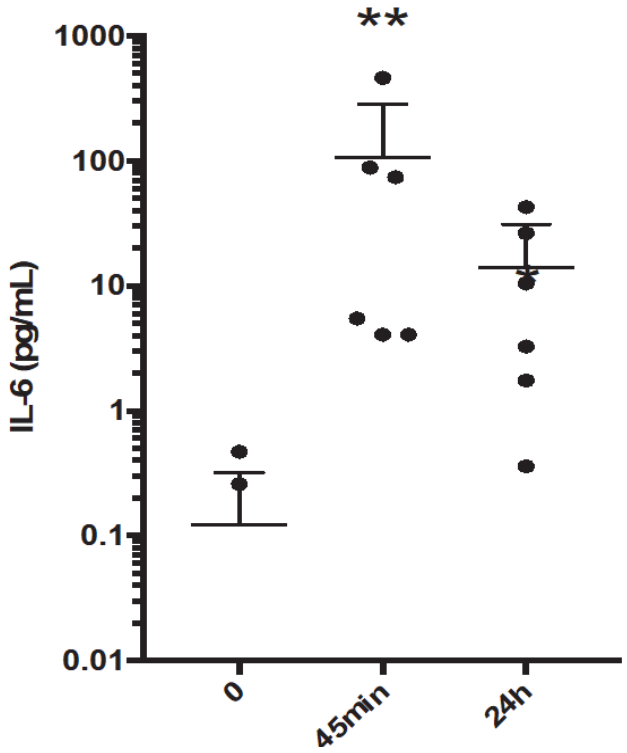

Figure 57: Il-6 quantification in plasma of sham animals.

Dot plot representing Il-6 quantification in the plasma of sham mice 0 minutes, 45 minutes and 24 hours pos-surgery. (n=6/time point) and ** $P < 0.01$.

In conclusion, throughout this section, we propose a new approach for analyzing dynamic transcriptomic large-scale datasets. Our pipeline involved two different axes, the co-variance analysis and the retro-analysis. Co-variance analysis which clustering transcripts into modules/combination of modules enabled us to discriminate the modifications caused by infiltrated and differentiated inflammatory cells in the myocardium. Whereas, the simulated TF-PPI networks enabled the prediction of the processes upstream TFs which might have been caused by the cardiac resident cells and lead to the associated transcriptional response.

Biological validation of these statistical results by the means of FACS and ELISA analysis showed that 45 minutes post-surgery, Il-6 is significantly increased in the plasma of sham animals and it is likely to be involved in the activation of the inflammatory response which had led to the neutrophil infiltration to the myocardium and the differentiation of the hybrid M1/M2 macrophage phenotype.

The work presented in this part of the results is already submitted to Frontiers in physiology journal under the systems biology theme and it is under revision.

2. *Characterization of dynamic gene networks in control and cardioprotective ischemic-reperfused mouse heart model.*

The previously described workflow was applied for time series transcriptomic data in sham-operated animals to study the effect of surgical interventions on the change of transcript expression profiles in the myocardium at 3 time points only. Having an optimized workflow, we next have planned to apply the same pipeline on ischemia-reperfused hearts at different time points during ischemia and reperfusion.

2.1. Experimental design:

As discussed previously in the method section, upon the sacrifice of the mice, ischemic and non-ischemic myocardium are dissected and used in this study. To limit the variation in the data analysis, the non-ischemic myocardium served as control at each studied time point. However, because we have considered 8 animals per time point for optimum statistical power, we had to decrease the number of the sequenced samples due to money constraints. Therefore, a total of 6 time points, displayed in **Fig. 58** labeled in yellow, with 8 animals per time point will be considered for this analysis. In addition to their role as controls, the non-ischemic myocardium data were analyzed separately in order to study the remote effect of IR over time.

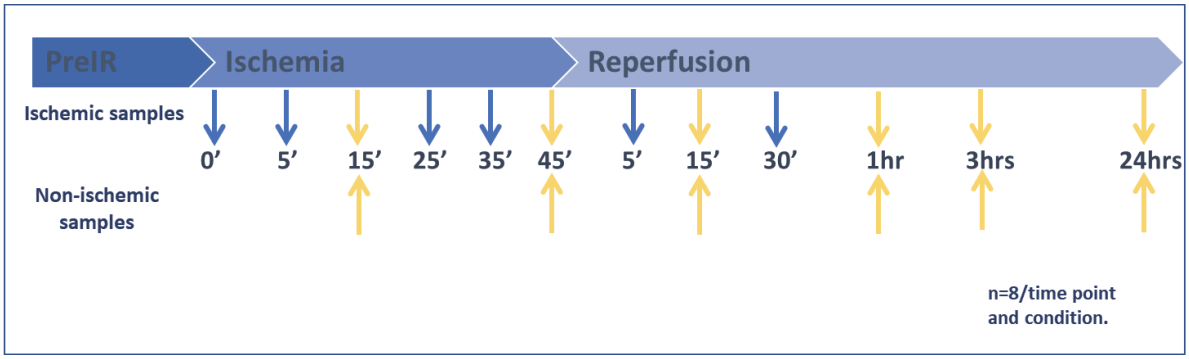

Figure 58: Ischemia-reperfusion analysis experimental design.

A scheme representing the different time points during ischemia-reperfusion that are considered for this analysis.

In addition, having a control ischemia-reperfusion model, we sought to apply cardioprotective strategies to the heart (refer to the method section for details) including ischemic postconditioning (IPost) and therapeutic hypothermia (TH), where mice were sacrificed 3 hours after reperfusion. The RNA-seq data will be analyzed as well to detect key cardioprotective markers that can be targeted to improve clinical outcomes.

However, due to time limitation and some technical issues we have encountered during this work, the analysis of these data has not been completed yet, and only preliminary results are available to date. In this context, for more stringent results, we have questioned which RNA-seq quantification method is more accurate to use. Therefore now, we are in process of testing different quantification methods like the alignment-dependent HTseq count method (Anders, Pyl, and Huber 2015), already used for the previous analysis, and the alignment-independent methods like Kallisto (Bray et al. 2016) to find out the one with the highest accuracy and best fit the aim of our analysis. This work will be continued within the coming few months.

Part 2: Supervised Analysis

The assessment of STAT3 transcriptional activity during ischemic postconditioning.

As mentioned earlier in the manuscript, the signal transducer and activator of transcription (STAT3) is a key cardioprotective player activated during ischemia-reperfusion and postconditioning. In a collaborative proteomic work that aims to determine the kinetics of STAT3 phosphorylation in response to ischemia-reperfusion and post conditioning during the early and late phase of reperfusion, we have taken advantage of the transcriptomic temporal large-scale data to study the kinetical alterations in the expression profiles of STAT3-induced genes.

1. Study's background and experimental design:

In this study, our team had shown that during IR, STAT3 phosphorylation at serine 727 and tyrosine 705 residues was significantly increased 15 minutes post reperfusion (**Fig. 59**) and interestingly, only tyrosine phosphorylated STAT3 was significantly stimulated during postconditioning. As a transcription factor, we were thus interested in studying STAT3 transcriptional activity in a time dependent manner during reperfusion.

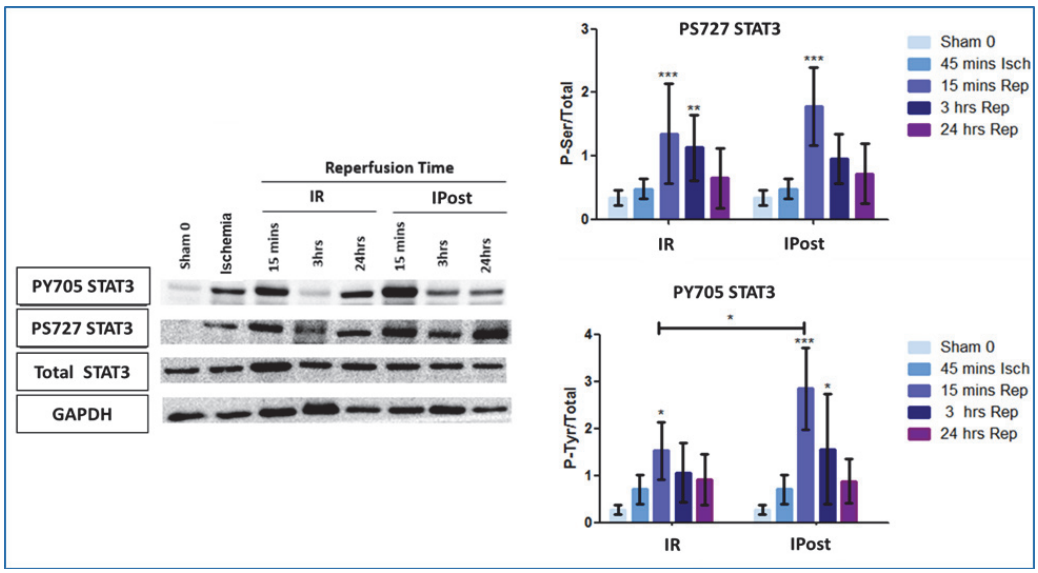

Figure 59: STAT3 phosphorylation in the early and late phase of reperfusion during ischemia reperfusion (IR) and postconditioning (IPost).

A scheme displaying western blot and its analysis of the serine (up) and tyrosine (down) phosphorylated forms of STAT3 during ischemia-reperfusion and postconditioning.

In this regard, literature screening was done to sort out STAT3-induced genes. A total of 480 genes have been selected and used for the supervised approach in our analysis. In an integrative approach, we have selected the same time points in which the proteomic study had been performed with. These time points correspond to 4 out of the 12 studied ones in our transcriptomic project, labeled in green in **Fig. 60**, ischemia 45 minutes, reperfusion 15 minutes, 3 hours and 24 hours.

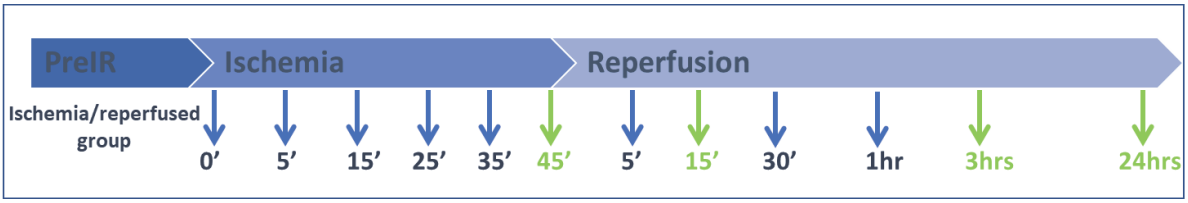

Figure 60: STAT3 analysis experimental design.

A scheme representing the time points considered for studying STAT3 induced genes temporal changes in expression profiles.

2. Differential expression analysis of STAT3-induced genes:

STAT3 screened genes were analyzed by DESeq2 as well. LRT test was performed including batch and surgeon into the design of *DESeq* function. **142** genes were significantly varying at any time point in this analysis.

PCA plot (**Fig. 61**) had shown that samples were clustered by their temporal variation (neither by batch nor by the different surgeons), where the temporal variation is spread along the first PC with 3 hours of reperfusion corresponding to the highest variation in the data.

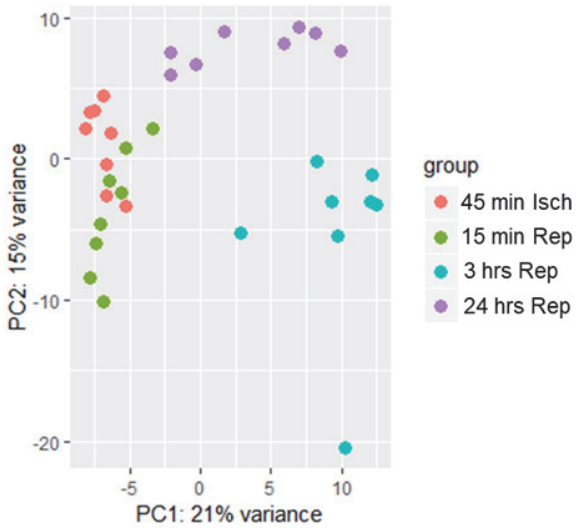

Figure 61: Principal component analysis of STAT3-regulated genes.

PCA plot of the STAT3-induced genes over time.

3. Temporal clustering of the differential expression genes with STEM analysis:

Because the number of genes screened is too small to be analyzed by the WGCNA approach used in the unsupervised analysis, we have sought to use a different algorithm that enable us to cluster and visualize these genes based on their behavior over time (in other words, based on the similarity of their expression profiles). STEM analysis yielded different profiles ordered in **Fig. 62** from the left to the right based on the number of genes assigned to each profile.

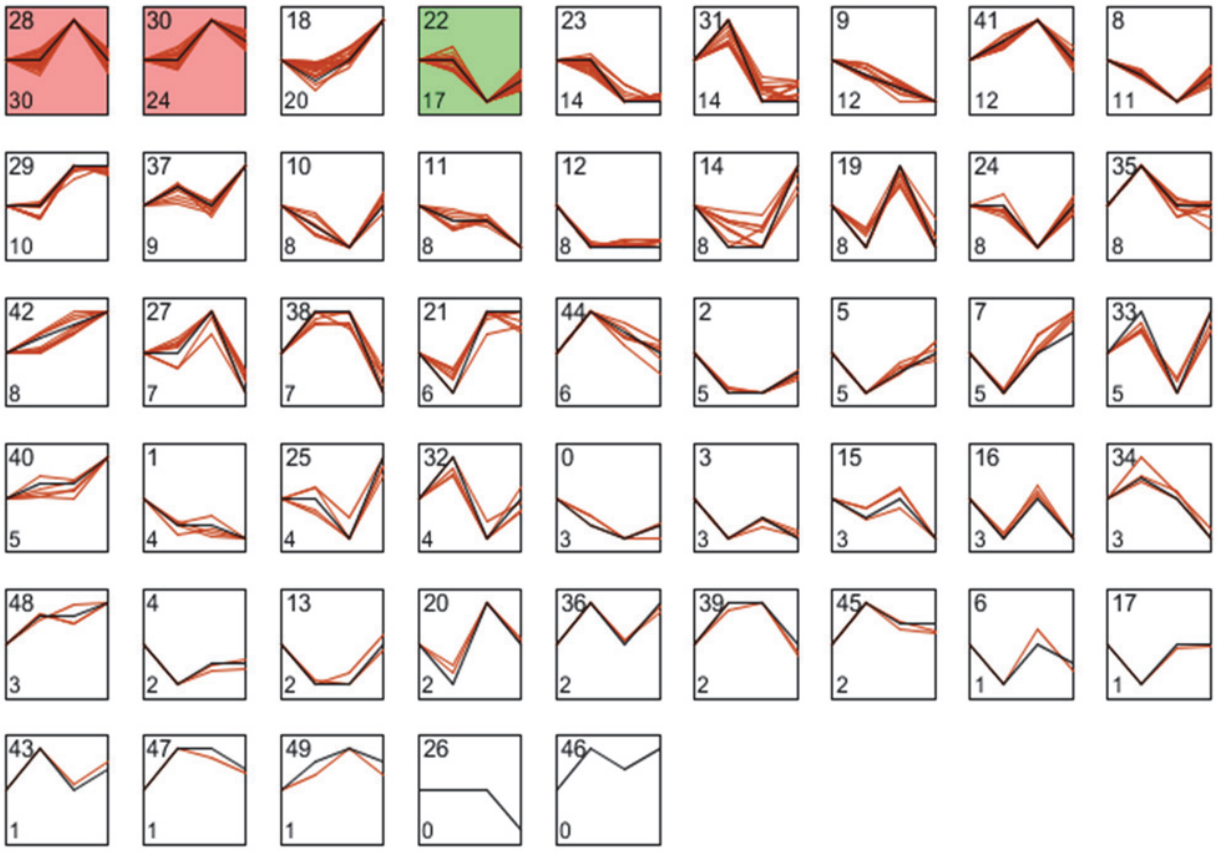

Figure 62: Temporal profiles of STAT3-regulated genes.

A scheme representing STEM analysis clustering profiles at the four time points analyzed (45 min Isch, 15 min Rep, 3 hrs Rep and 24 hrs Rep). The numbers on the top and bottom left of the clusters correspond to the clusters name/ID and number of genes assigned to each cluster, respectively.

Interestingly, a great number of these genes showed variation in the expression profiles at 3 hours after reperfusion (as example clusters 28, 30, 22, 41, 29, 10, 19, 24, 38, 25…). In this regard, we

were then interested in studying the effect of *in-vivo* inhibition of STAT3 at 3 hours after reperfusion under IR and postconditioning, to find out the genes that are significantly regulated by STAT3 during ischemic post conditioning. The latter genes are assessed by polymerase chain reaction and regulatory networks were generated for a better understanding of the involvement of STAT3 transcriptional activity in ischemic postconditioning and its role along the Il-6 signaling axis.

This described work is still under writing and is expected to be submitted soon.

Section III: Inflammation from bench to bedside

Based on the validated transcriptomic analytical pipeline we have explained in the previous section; we have identified Il-6 as a major regulator of the changes occurring in response to the surgical interventions, peaking at 45 minutes in the mouse plasma from non-myocardial origin. In this context, we were interested to know if Il-6 along with other inflammatory markers were also activated in response to IR and whether they originate from the injured myocardium or from different sources. Therefore, throughout this section, we aim to study the origin and the dynamics of circulating inflammatory markers during acute myocardial infarction in mouse and human plasma and test for temporal correlation with mice IR transcriptomics.

1. Experimental design:

Because we were interested only in inflammatory related genes, a supervised analysis of the transcriptomic data has been performed. Unlike the explained previous work, throughout this analysis, normalized data in the form of fragments per kilobase of exon model per million reads mapped (FPKM) were used to assess the variation in the expression profile at 12 time points (method section, **Fig. 14**) during ischemia and reperfusion. In addition, secreted levels of the studied inflammatory markers were quantified by ELISA in the plasma of the same IR mice that were used for the transcriptomic analysis.

Regarding MI human patients, in another study performed by colleagues in our team, blood of 21 patients was sampled at 7 time points after myocardial infarction (0 mins, 4 hrs, 12 hrs, 24 hrs, 48 hrs, 7 days and 1 month). Secreted levels of inflammatory markers (including different cytokines and chemokines) were quantified in their plasma by ELISA as well.

2. Supervised analysis of mRNA expression profiles of inflammatory markers in the ischemic myocardium:

35 inflammatory genes were sorted out from the transcriptomic dataset we have. Anova analysis was performed and only 2 genes were not detected to be significantly varying. Interestingly, most of these genes have shown a significant variation starting 1 hr of reperfusion and none has shown a variation during the ischemic time in the myocardium (points before the dashed black line in **Fig. 63**). Among these genes are some displayed in **Fig. 63**. However, next we wanted to assess the

secreted level of inflammatory markers in the plasma of the same mice during ischemia reperfusion.

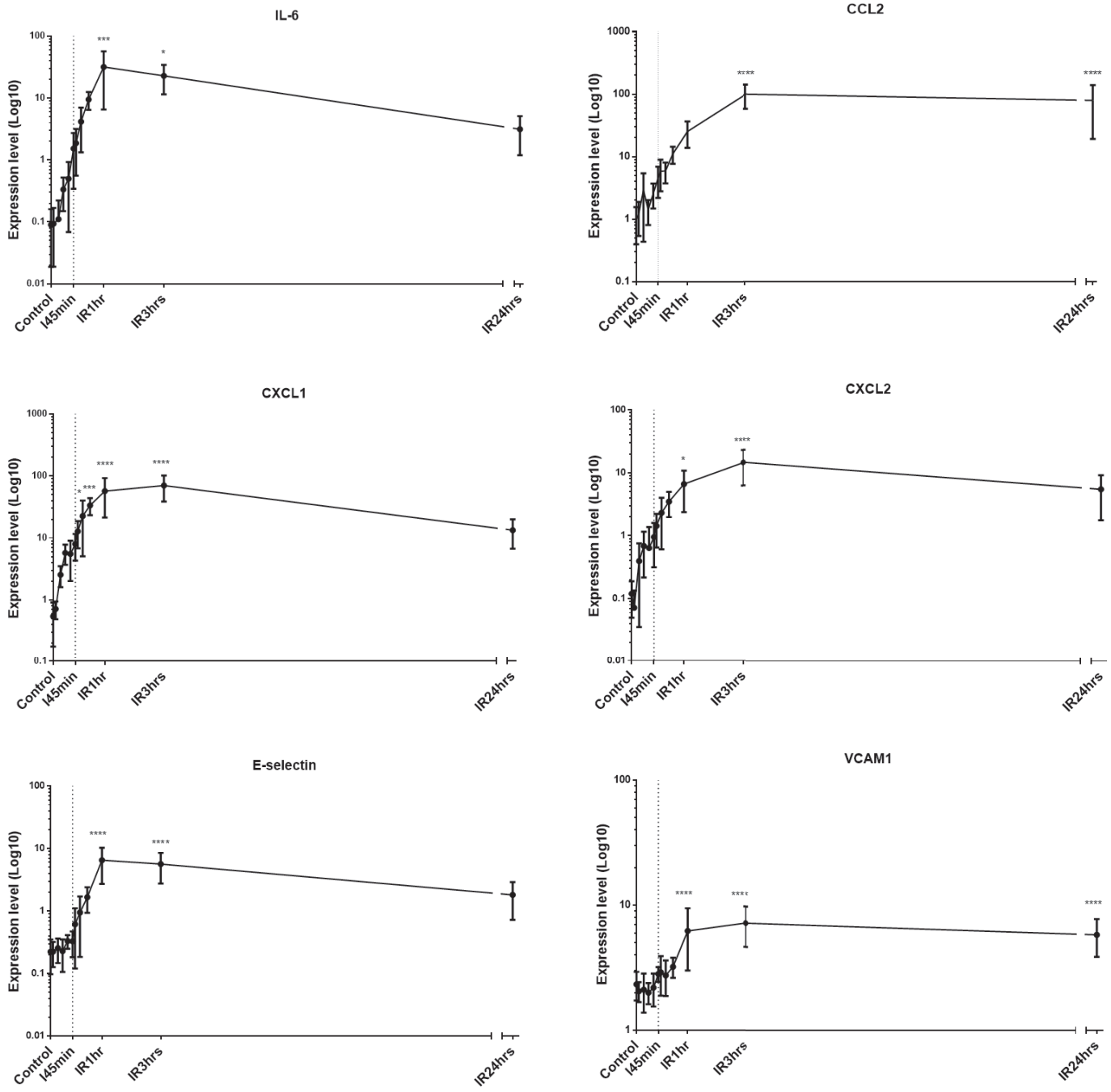

Figure 63: Expression profile of inflammatory markers.

A scheme representing the mRNA expression profile of different inflammatory markers, Il-6, CCL2, CXCL1, CXCL2, E-Selectin and VCAM1, in the ischemic area at different time points during ischemia-reperfusion (n=8/time point). * P <0.05, ** P <0.01, *** P <0.001 and **** P <0.0001 compared to control. Dashed black line correspond to the end of ischemic times and start of reperfusion.

As displayed in **Fig. 64**, the variety of these cytokines share similar kinetics, in which there is no significant variation in their expression during the ischemic time and they were significantly varying mainly during the early phase of reperfusion where 24 hours later, no significant variation was observed for the majority.

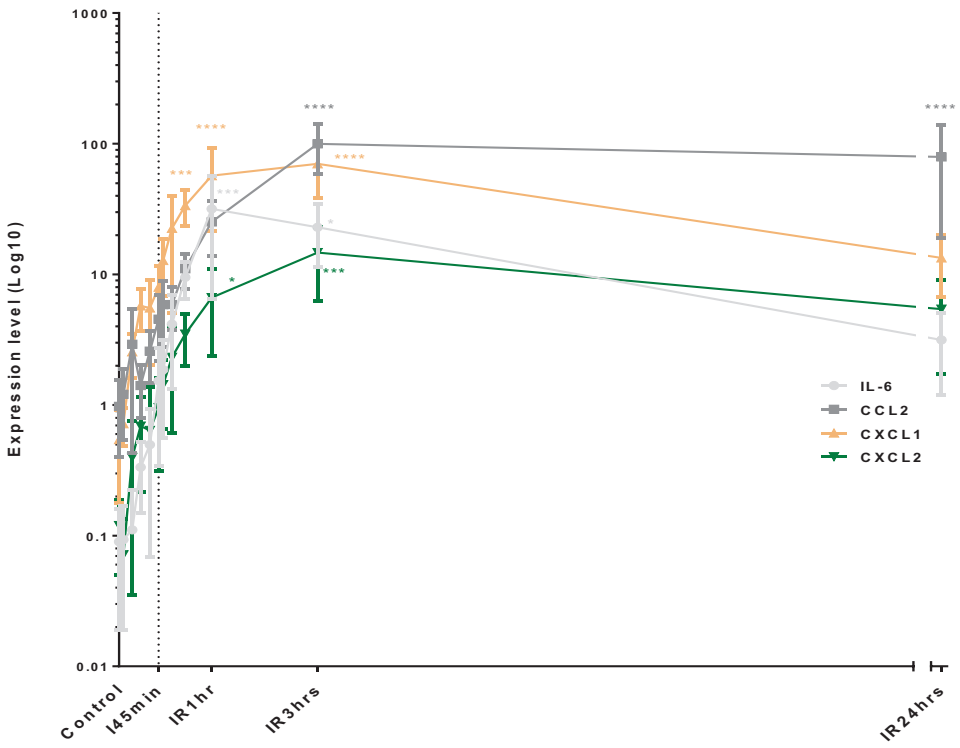

Figure 64: Temporal correlation of inflammatory markers.

A scheme displaying the temporal correlation present in the expression profiles between different inflammatory markers during ischemia-reperfusion in the ischemic myocardium. (n=8/time point).

3. Inflammatory markers measurement in the plasma of ischemia-reperfused mice:

Because a small volume of blood can be obtained from the mouse, the amount of plasma we had was limited, and thus we had to choose only few markers to test. Among these markers were

VCAM1, CCL2, CRP and importantly Il-6. CRP is a major inflammatory marker that is tested in MI patients however, it was not detected in the mouse transcriptomic dataset which served as a negative control in this study. As displayed in **Fig.65**, plasma levels of all the markers, except VCAM1, have shown an increase during mainly the reperfusion phase. However, because there was a great variability in the data, firstly, we have increased the confidence interval in the analysis test used for 10% to have an intuition about their significance, and next we sought to increase the number of animals to increase the statistical power of the analysis (experiment to be completed soon).

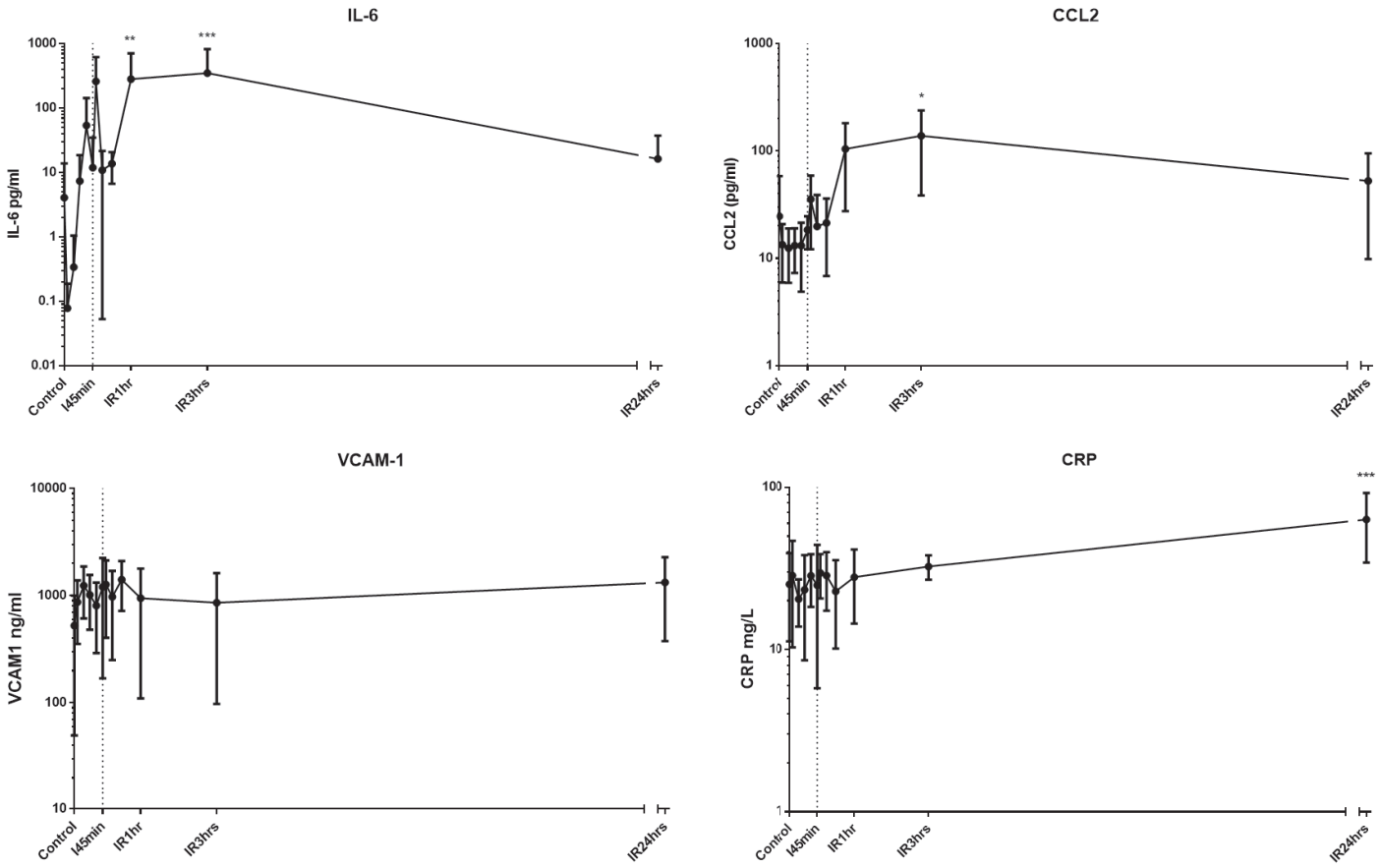

Figure 65: Inflammatory markers plasma levels in ischemia-reperfused mice.

Il-6, CCL2, VCAM1 and CRP plasma levels were quantified by ELISA in mice at different time points during ischemia reperfusion (n=6/time point). Ischemic times were labeled in red and reperfusion times in blue. * P <0.1, ** P <0.05 and *** P<0.01 compared to control.

Next, we wanted to assess if an ischemia-reperfused mouse model can be indeed a good one for recapitulating the inflammatory events taking place in human patients during myocardial infarction. To validate this, we needed to compare with clinical data.

4. Inflammatory markers measurement in the plasma of MI human patients:

Among the different markers our colleagues have tested, are the Il-6 and CRP (**Fig. 66**). These two markers were significantly varying throughout the temporal analysis. Il-6 and CRP were significantly increasing starting 12 hrs and 24 hrs post MI despite the increased variation, respectively.

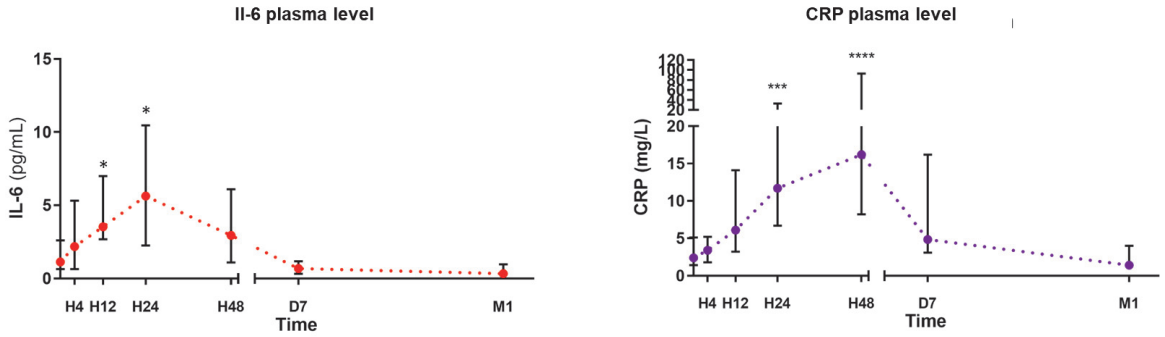

Figure 66: Inflammatory markers plasma levels in MI human patients.

Il-6 and CRP plasma levels were quantified by ELISA in MI human patients at different time points during their hospitalization. * P <0.1, *** P <0.01 and **** P < 0.001 compared to control (H0).

As displayed in **Fig. 67**, comparing the mouse secretome and transcriptomic data to clinical ones, we have found that some markers like Il-6 and VCAM-1 and CRP were correlated for the studied time points. Il-6 mRNA expression was significantly increased 1 hr after reperfusion. Its plasma secretion in the mouse although was not significant but showed the same pattern of variation as that of the human's that was significantly increased 12 hrs pot MI, peaked at 24 hrs and decreased after. Similarly, VCAM1's mRNA expression level was significantly increased 1 hr after reperfusion until 24 hrs. Its plasma level in human patients was also increased in a similar manner which correlates with mouse plasma except at 24 hrs which shows high inter-variability.

Additionally, CRP mouse and human plasma levels were correlated for the studied time points as well, however, CRP's mRNA expression was not detected in our transcriptomic data in the ischemic myocardium which suggests that, unlike Il-6 and VCAM1, CRP in the plasma is not originating from the injured myocardium.

In addition, other factors like TGF-β, although not tested in the plasma of the mouse due to limited plasma amount, shows significant variation mRNA and plasma secretion in the mouse and human 24 hrs and 1 month after MI, respectively. However, the lag in the time is big in this case and thus, no conclusion about the correlation can be made, which suggests further experiments during the late reperfusion phase (more than 24 hrs) in mouse to conclude.

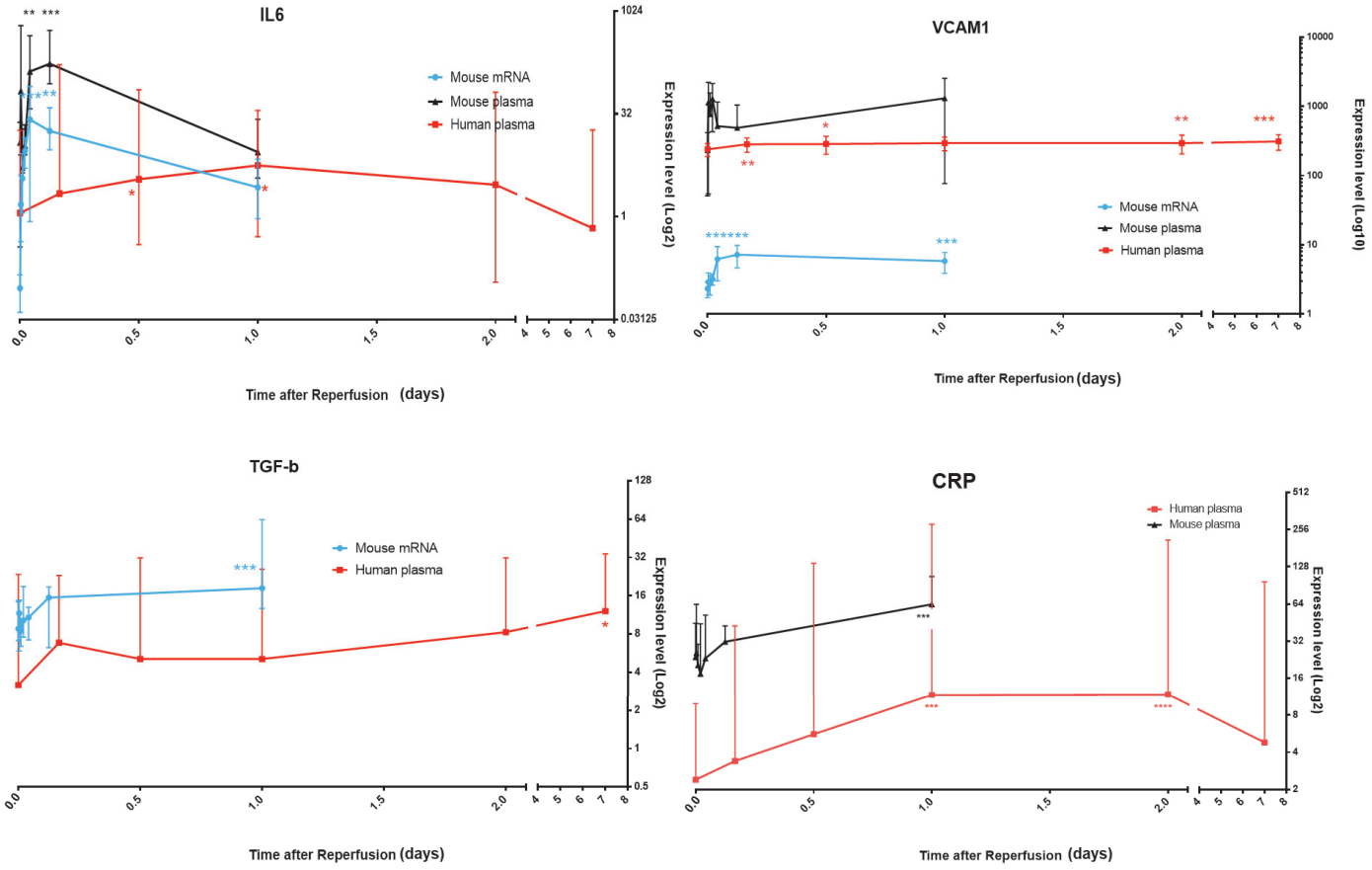

Figure 67: Correlation of inflammatory markers' mRNA and protein levels in ischemic myocardium and plasma, respectively.

A Scheme displaying the correlation between mRNA and protein levels of Il-6, VCAM1 and TGF-β in mouse ischemic myocardium and MI human patients' plasma. Il-6 and VCAM1 show similar variation patterns unlike TGF-β. * P <0.1, *** P <0.01 and **** P < 0.001.

In this context, we also aim to measure troponin in the plasma of both MI-induced mouse model and MI human patients being directly correlated to the infarct size which will enable us to figure out the correlation the temporal cytokine expression and release into the circulation. In conclusion, through this collaborative work, we have profited from the large-scale transcriptomic data we have, where some inflammatory related genes were studied and used to correlate with plasma secretions of these markers in mice and MI human patients over time. Indeed, with the preliminary results we have, we show that correlation for major inflammatory markers exists. However, further markers are needed to be studied to conclude that MI-induced mouse model can serve as a good one for predicting inflammatory changes over time during myocardial infarction.

Chapter 9: Discussion

Throughout the work presented in this thesis, myocardial infarction pathology has been studied in a different spatio-temporal approach. Knowing that MI progression is dynamic in nature, time variable was introduced as an important factor in our analysis. In order to improve our understanding of this pathology, a "*zoom-in*" perspective in the myocardial space was established. In this context, we have studied the oxidation of the ischemic area in a 3D heart intact structure and assessed the macrophage population in the myocardium post MI in a clarified 3D model. Next, we have isolated the ischemic area and studied its modified transcriptional activity and later, a further zoom was applied where specific inflammatory markers were analyzed. As for the results, the discussion of these aspects is divided into three major sections and detailed below.

Molecular characterization of the Area at risk:

With the development of several protective strategies, tools were required to validate their efficacy. Infarct size measurement has been a major end point that was used in this regard. The latter has several advantages, in which it enables the evaluation of the different cardioprotective strategies compared to pre-existing ones and it helps in the optimization of new-drug dosage when used as a target therapy. In the past decades, several approaches have been developed to measure the infarct size post MI. Among these approaches was the biochemical assays where serum markers like the creatine kinase (CK) were measured (Maroko Peter R. et al. 1971). Few years later histochemical assays have been introduced. Tetrazolium dyes like triphenyl tetrazolium chloride (TTC) were used to quantify the necrotic area where it precipitates in the intact myocardium due to dehydrogenase activity and leaves necrotic area unstained (Fishbein et al. 1981). Later in time, echocardiography, which measures the heart function and elasticity based on the ventricular wall motion abnormalities, and imaging approaches have been developed like the 3D late gadolinium enhancement MRI technique (3D-LGE) and the ^{99m}Tc-sestamibi single photon emission computed tomographic (SPECT) imaging technique for extracellular edema measurements (Bohl et al. 2009; Gibbons Raymond J., Miller Todd D., and Christian Timothy F. 2000). However, these tools were

either inaccurate enough or less feasible to apply on small animals like mice and thus to date, TTC quantification method remains the most frequently used one.

In a comparative study of TTC staining with propidium iodide (PI) fluorescent stain, it was shown that infarct size measurement reproducibility of the two methods were dependent on the reperfusion time and suggested that PI fluorescent stain might be more reliable (Ito et al. 1997). In addition, the accuracy of TTC quantification is dependent on several factors. Among these factors, the accuracy in calculating the unstained area in each slice and adding them up, the loss of some information caused by slicing the heart and importantly the dehydrogenases that might still be present in the necrotic area depending on the reperfusion efficacy and time (Redfors, Shao, and Omerovic 2012). In this context, comes the importance of our work which involves the quantification and characterization of the molecular events, mainly oxidation, of the area at risk in a non-distorted 3D heart without any labeling and depending only on the autofluorescent endogenous molecules' signals. Nevertheless, this approach as any other also has several limitations. Among these limitations are: 1) the quality of the clarified heart: although the same parameters are being used, the biological variation between animals might introduce an artifact in this regard leading to variability in the clarified tissue and consequently different absorption and light scattering which alters the ability to compare the generated signals between hearts, 2) the variability in the efficiency of the blue stain used which as well alters the obtained signals across stack images in certain pixels, 3) the coordinates (x,y,z) at which images are acquired, knowing that tissue absorbance increases as we go deeper in the z plane makes results comparison and interpretation a challenging task and 4) the big size of the z-stack images acquired which requires large available spaces for storage and handling. However, the work in this field is still in its early optimization phase and correction of these artefacts might be possible with the correction of image intensity for photon absorption, in the green wavelength for example, which will consequently correct for the depth and clarification artefacts. In addition, imaging only the ischemic are at risk decreases imaging time and the size of the generated files.

In our approach, we have shown that oxidation levels have increased in a time dependent manner caused by the increased oxidation in the ischemic area at risk and was decreased after applying the ischemic postconditioning cardioprotective strategy. This approach was achieved via spectral unmixing and statistical distribution fitting of the images' pixels intensity. However, in order to

understand the molecular events and transcriptional regulation behind this increased oxidation, we have studied the dynamics of transcriptomic data in the ischemic and cardioprotective myocardium.

Dynamic transcriptomic analysis section:

The transcriptome represents the whole set of transcripts in a cell and its quantification and understanding is an essential step for interpreting the physiological and pathophysiological state of cells and tissues (Zhong Wang, Gerstein, and Snyder 2009b). Transcriptome quantification has been performed via microarrays then by RNA-seq. Several comparison studies between the two techniques have been made and RNA-seq was found to better estimate the transcript levels and shows higher accuracy and precision in quantification (Fu et al. 2009; Marioni et al. 2008). Thanks to the decrease in its costs, transcriptomic is not only studied in a static manner but can probe dynamics during developmental stages and diseases' progression. However, due to the lack in literature of clear analytical integrative approaches that can be used for analyzing time series transcriptomics, in the dynamic transcriptomic result section of this doctoral work, we have proposed a new RNA-seq analytical pipeline based on the combination of several freely available R packages and softwares for systems biology.

Throughout this work, we made sure to be working with a good statistical power (>80%) to ensure that the differentially expressed transcripts obtained were indeed temporally varying and not significant by chance, a criterion not achieved by many studies involved in myocardial infarction, even recent ones (Y. Li et al. 2019; Prat-Vidal et al. 2013; Roy et al. 2006). In addition, many of the kinetical studies, had a similar pattern of analyzing time series data which usually constitutes of analyzing each time point alone comparing it to a control (Prat-Vidal et al. 2013; Roy et al. 2006; Andreeva et al. 2014). Applying this strategy might lead to the loss of important information due to uncovering all the changes that might take place between the considered time points. However, finding the tools to analyze kinetical data is also a challenging task. Among the available tools that might be compatible with our data (considering the input data and the number of time points considered for the analysis for example), we have chosen to work with DESeq2 (Love, Huber, and Anders 2014). DESeq2 in this analysis only tells if a gene is significantly varying at any time point of the study. Thus, analyzing the biological processes of the obtained list will result in a bulk of processes that is big enough and will not enable the identification of specific processes

or pathways of interest. Therefore, we have characterized the temporal variation of the differentially expressed transcripts and identified their dysregulated processes so that a signature of the activated molecular pathways is generated. However, this analysis provided an idea about the processes activated by the coregulated transcripts which has identified an inflammatory fingerprint in the myocardium of sham animals and was validated biologically by the recruitment of macrophages and monocytes and differentiation of the heterogenous phenotype towards the M2 subtype macrophages 24 hours after surgery. A recent study performed on MI and sham-operated animals have shown a similar inflammatory cells circulation pattern over time (Hoffmann et al. 2014). In this regard, it was expected and already known in literature that surgical interventions activate inflammatory response, however, this response has not been fully elucidated to date. Open-chest surgery was shown to induce the release of creatine kinase and glycogen phosphorylase enzymes in the lymph of dogs (Michael et al. 1985) and induces the significant variation of inflammatory cytokines like TGF-β and Il-6 in the myocardium (Nossuli et al. 2000). In addition profiling of the genome of mouse blood has shown a significant variation in the expression profiles of many genes 6 hours after the surgery (Coon et al. 2010). Our study thus confirms the activation of inflammatory response and characterizes the changes in the transcripts' profiles in the myocardium 45 minutes and 24 hours post-surgery.

In the heart, macrophages are present in different populations where they differ morphologically and functionally. They are characterized by their plasticity and continuous shift in their phenotypes based on the surrounding environment. In a recent study, the dynamic transcriptional regulation of macrophages in the heart post MI has been studied and interestingly, a heterogenous M1/M2 population, a hybrid cell subtype expressing both M1 and M2 markers, is observed (Walter et al. 2018) which is also presented in our analysis where 24 hours post-surgery a shift towards M2 markers has been detected. In order to further understand this transcriptional activity, we have checked for enriched transcription factor binding sites in the list of the differentially expressed transcripts. In this regard, among the mostly enriched TFs were the kuppler like factor (Klf4) and the specificity protein 1 (SP1). Aside from their role in development, cell differentiation and cell growth, these two TFs were shown to play an inflammatory role. More specifically, several studies have reported the involvement of these TFs in macrophages' activation and polarization (Kapoor et al. 2015; Feinberg et al. 2005; Karpurapu et al. 2014; K.-W. Lee et al. 2005; Liao et al. 2011), which could have justified the transcriptional modifications occurring in the inflammatory cells

phenotypes and not in the cardiac resident cells. In this context, we wanted to identify a major mediator that might be linked to these modifications. After simulating biological data similar to our experimental ones via transcription factor enrichment analysis and protein-protein interaction networks, Il-6 was detected as a major hub in the best predictive network. Biologically, Il-6 was also increased in the plasma 45 minutes post-surgery. Noteworthy, Il-6 transcript level was not even detected in the myocardium post-surgery. The plasma level was more likely exerted by the release of stores of Il-6 into the blood as a response of the stress caused by the surgery.

Il-6 is an inflammatory cytokine that is known since a long time to be elevated in the plasma of myocardial infarction patients (Miyao et al. 1993). Our data also confirms these findings where Il-6 was elevated in the IR mouse plasma and MI human patients 1 hr after reperfusion and 12 hrs post MI (as shown in the inflammatory section as well), respectively. When bound to its receptor, which is present on the surface of various cell types including inflammatory and cardiac resident cells, Il-6 activates Il-6/gp30 signaling pathway and consequently leading to downstream propagation of this signal (Heinrich et al. 2003). Among these downstream activated pathways are the PI3K and the JAK/STAT pathway which were found to be directly related to neutrophils trafficking to the injured site and recruitment of monocytes to the myocardium (Hartman et al. 2016; P. Tang et al. 2018; Fielding et al. 2008; Kaplanski 2003), which could suggest that Il-6 acts as an early activator induced by surgical interventions that activates signaling pathways and leads to transcriptional response.

Among these proposed pathways is the JAK2/STAT3 one which is shown to be stimulated in ischemic postconditioning and is validated in our collaborative data during the early phase of reperfusion (displayed as well in the results section). However, how STAT3 plays a role in the cardioprotective strategy is not fully elucidated to date. In this line of evidence, some studies have reported that this action is mediated via the mitochondrial role of STAT3, where it inhibits the activity of mitochondrial electron transport chain complexes I and decreased ROS production (Heusch et al. 2011). Herein, we have shown that mitochondrial STAT3 itself is likely a myth since we could not detected it in the mitochondria in our studied model (Harhous et al. 2019). Thus, we have shifted towards studying its transcriptional role within the first 24 hours of reperfusion. In the best predictive network generated in our analysis, IL-6 was connected to several signaling molecules, among them is STAT3. Il-6 is considered a direct activator of STAT3 and

thus studying how Il-6 mRNA expression is affected in response to STAT3 inhibition by Stattic (tyrosine phosphorylation STAT3 inhibitor), we found that Il-6 is significantly affected, which strongly comes in evidence with our results and tested hypothesis.

In this regard, having an optimized pipeline for analyzing time series transcriptomic data, we are in process of using it with IR and cardioprotective data with increased time points. However, in the IR and cardioprotective exposed mouse heart we were interested in studying their effect on the ischemic and non-ischemic adjacent myocardium. Little attention is given in literature for the changes occurring as an effect of IR in the non-ischemic myocardium. A recent study has shown that this area is significantly affected and was slightly remodeled after MI, where affected genes in this area were mostly downregulated 24 hours post MI (Zimmermann et al. 2017). In addition, in a temporal study that involved studying the effect of MI on expression profiles weeks after reperfusion, the non-ischemic myocardium had several deregulated transcripts over time (Prat-Vidal et al. 2013). In this regard, having the data, we aim to characterize these changes and assess whether the propagation of the IR signal has reached the non-ischemic myocardium 24 hours post-surgery. In addition, not a lot of data is available regarding the transcriptional changes that occur in the myocardium during the ischemic phase and prior to reperfusion. In the results, we have shown that 45 minutes post-surgery, representing a control for 45 minutes of ischemia samples in our MI-induced model, induces the activation of signalization pathways and significant release of Il-6 stores into the blood. In this context, we have questioned how Il-6 responded to the IR stress over time, as mRNA expression and plasma level, and tried to find out if it is correlated with the MI human patient plasma levels, which might also have a remote effect in the non-ischemic myocardium to be explored soon with the STAT3 regulated genes, being direct a direct activator of STAT3 activation.

Therefore, throughout this pipeline, not only we provide an analytical approach that can be applied in any kinetical study, but we also highlight the importance of considering surgical controls (sham-operated animals) at each time point during such studies. Sham animals were shown to display an inflammatory background regulated mainly by the Il-6 signaling axis which, if not quantified, will be a challenging task to discriminate the IR induced effect from the surgery induced one. Therefore, in this context we were interested in studying the origin and dynamics of Il-6 during MI, along with other inflammatory markers in the plasma of IR mice and MI human patients.

Inflammation from bench to bedside section:

Establishing clinically relevant models of cardiovascular diseases has been a major challenge throughout the years. The choice of the animal model mimicking the human cardiovascular physiology shall be considered carefully so that experimental findings can be translated to humans. Due to ethical requirements, the use of large-animals has been limited due to the restricted acceptable number of animals to be used, where the mouse model remains the most commonly used one in the MI context. Nevertheless, few are the studies that evaluate whether the mouse model can be a good one to mimic what is happening in humans. Today, 99% of the known human genes have direct orthologs in mice, however, it is still questioned if the genomic response correlates in the two species (Camacho et al. 2016).

As discussed previously in this manuscript, inflammation is a major axis in orchestrating the progress and healing during MI. Several anti-inflammatory candidates have been tested in clinical trials but all have failed to improve clinical outcomes. In this regard, a comparative study of the genomic response between humans and mice was performed by Seok et al (Seok et al. 2013). The results published have captured researchers' and media's attention, mouse model was found to poorly mimic human inflammatory diseases, where poor correlation was detected between the mouse and human differentially expressed genes. However, a re-evaluating study was performed by Takao et al on the same datasets using different and more conventional statistical tools have shown contradicting results in which mice genomic response was greatly correlating with humans' (Takao and Miyakawa 2015). Our preliminary results show that few markers like Il-6 and VCAM-1 and CRP have shown correlation between the expression level and the secreted plasma levels. Interestingly, Il-6 mRNA and plasma level display high variation in the data which is introduced in mice and human patients as well. In addition, CRP plasma levels have shown high correlation between the two tested species, noting that its mRNA expression was below the detection level in our sequencing experiment, which suggests that CRP in the plasma is not of myocardial origin and thus acting as a control of our analysis. CRP is usually highly increased in infections and inflammation. It is known as an acute phase marker of inflammation and is secreted by mainly in the liver and by different cells like macrophages and lymphocytes (Sproston and Ashworth 2018). However, CRP is not a cardiokine, protein secreted from the heart to the circulation (Dewey et al. 2016). It is not reported to be secreted by myocytes, which comes along the line of evidence of our results. Unlikely, TGF-β mRNA expression and plasma levels correlation was hard to guess,

although TGF-β stimulation has shown similar dynamical response in mice and humans in different cell types and tissues (Abnaof et al. 2014), which could show encouraging results if its secretion was studied during later time. However, these preliminary results are not enough to make a firm conclusion if the mouse model can recapitulate the inflammatory changes occurring during MI and thus further research is required.

Altogether, in this study, a new analytical approach concerned with myocardial infarction pathology in a holistic manner is provided, where we have tried to gather the maximum possible data from different perspectives and integrate them together to gain better insights into the myocardial infarction induced mechanism in a spatio-temporal dimension. Throughout this work, we have combined imaging tools with transcriptomic and secretomic and applied different multivariate statistical methods to generate the most possibly informative data. In this regard, in order to better understand the spatial mechanism behind IR, we aim to localize some target transcripts in the ischemic myocardium by insitu-hybridization in cleared IR hearts, where we can figure out the spatio-temporal dynamics of the abundance of the target of interest post-injury.

Chapter 10: Concluding Remarks and Perspectives

The work presented in this thesis provides important insights into the myocardial infarction's pathology in a mouse model. Our study has provided a chain of methods in different aspects of the pathology via the use of systems biology approaches which represent a promising tool for improving the clinical outcomes. The specific conclusions and future work of the different studied aspects are listed below:

- In the context of area at risk characterization and quantification, we have provided a new approach to molecularly characterize the ischemic area at risk based on the myoglobin autofluorescence in clarified heart by imaging techniques. Next, we aim to find out to which extent the applied redox imaging we developed, correlates with the measurements of extracellular edema using the 3D-LGE MRI. In addition, heart clarification enables immunolabeling, therefore we sought of labeling other inflammatory cells (neutrophils and macrophages subtypes) and identify their dynamic recruitment into the myocardium in the early phase post MI. Moreover, we also aim to do in situ hybridization of significantly varying RNAs in response to MI to specifically locate their abundance in the myocardium over time.

- Regarding the dynamic transcriptomic analysis, our results have proposed a new analytical pipeline that has combined several existing R packages and freely available platforms for systems biology that can be applied in time series transcriptomic experiments. This dynamic pipeline has revealed Il-6 as a major activator of the acute phase inflammatory response in sham-operated animals where 24 hours post-surgery, infiltration of neutrophils and monocytes and differentiation of macrophages has been detected. In this regard, we aim to use this pipeline on our IR and cardioprotective data, so that Il-6 signaling axis is better understood and new pathways/mediators can be detected and targeted to improve clinical outcomes.

- In an inflammatory perspective, our preliminary results show correlated dynamics of transcriptomic and plasma levels of certain inflammatory markers between mice and human patients. This suggests that IR-induced mouse model can be a good model for recapitulating the inflammatory response activated post MI. Thus, next we aim to assess if activated signals by these markers, like the Il-6/STAT3 pathway for example, share similar activation pattern and correlate in both species as well.

References

Abnaof, Khalid, Nikhil Mallela, Gudrun Walenda, Steffen K Meurer, Kristin Seré, Qiong Lin, Bert Smeets, et al. 2014. "TGF-β Stimulation in Human and Murine Cells Reveals Commonly Affected Biological Processes and Pathways at Transcription Level." *BMC Systems Biology* 8 (May): 55. https://doi.org/10.1186/1752-0509-8-55.

Ahn, Dongchoon, Linda Cheng, Chanil Moon, Harold Spurgeon, Edward G. Lakatta, and Mark I. Talan. 2004. "Induction of Myocardial Infarcts of a Predictable Size and Location by Branch Pattern Probability-Assisted Coronary Ligation in C57BL/6 Mice." *American Journal of Physiology-Heart and Circulatory Physiology* 286 (3): H1201–7. https://doi.org/10.1152/ajpheart.00862.2003.

Anders, S., P. T. Pyl, and W. Huber. 2015. "HTSeq--a Python Framework to Work with High-Throughput Sequencing Data." *Bioinformatics* 31 (2): 166–69. https://doi.org/10.1093/bioinformatics/btu638.

Anderson, A B, and C R Robertson. 1995. "Absorption Spectra Indicate Conformational Alteration of Myoglobin Adsorbed on Polydimethylsiloxane." *Biophysical Journal* 68 (5): 2091–97.

Andreeva, Kalina, Meixia Zhang, Wei Fan, Xiaohong Li, Yinlu Chen, Jovan D Rebolledo-Mendez, and Nigel G Cooper. 2014. "Time-Dependent Gene Profiling Indicates the Presence of Different Phases for Ischemia/Reperfusion Injury in Retina." *Ophthalmology and Eye Diseases* 6 (August): 43–54. https://doi.org/10.4137/OED.S17671.

Anzai, Atsushi, Toshihisa Anzai, Shigenori Nagai, Yuichiro Maekawa, Kotaro Naito, Hidehiro Kaneko, Yasuo Sugano, et al. 2012. "Regulatory Role of Dendritic Cells in Postinfarction Healing and Left Ventricular Remodeling." *Circulation* 125 (10): 1234–45. https://doi.org/10.1161/CIRCULATIONAHA.111.052126.

Baines, Christopher P., Robert A. Kaiser, Nicole H. Purcell, N. Scott Blair, Hanna Osinska, Michael A. Hambleton, Eric W. Brunskill, et al. 2005. "Loss of Cyclophilin D Reveals a

Critical Role for Mitochondrial Permeability Transition in Cell Death." *Nature* 434 (7033): 658–62. https://doi.org/10.1038/nature03434.

Barham, Peter, Leif H. Skibsted, Wender L. P. Bredie, Michael Bom Frøst, Per Møller, Jens Risbo, Pia Snitkjær, and Louise Mørch Mortensen. 2010. "Molecular Gastronomy: A New Emerging Scientific Discipline." *Chemical Reviews* 110 (4): 2313–65. https://doi.org/10.1021/cr900105w.

Bell, Robert M., and Derek M. Yellon. 2011. "There Is More to Life than Revascularization: Therapeutic Targeting of Myocardial Ischemia/Reperfusion Injury." *Cardiovascular Therapeutics* 29 (6): e67–79. https://doi.org/10.1111/j.1755-5922.2010.00190.x.

Benjamini, Yoav, and Yosef Hochberg. 1995. "Controlling the False Discovery Rate: A Practical and Powerful Approach to Multiple Testing." *Journal of the Royal Statistical Society. Series B (Methodological)* 57 (1): 289–300.

Boengler Kerstin, Buechert Astrid, Heinen Yvonne, Roeskes Christin, Hilfiker-Kleiner Denise, Heusch Gerd, and Schulz Rainer. 2008. "Cardioprotection by Ischemic Postconditioning Is Lost in Aged and STAT3-Deficient Mice." *Circulation Research* 102 (1): 131–35. https://doi.org/10.1161/CIRCRESAHA.107.164699.

Bohl, Steffen, Craig A. Lygate, Hannah Barnes, Debra Medway, Lee-Anne Stork, Jeanette Schulz-Menger, Stefan Neubauer, and Jurgen E. Schneider. 2009. "Advanced Methods for Quantification of Infarct Size in Mice Using Three-Dimensional High-Field Late Gadolinium Enhancement MRI." *American Journal of Physiology - Heart and Circulatory Physiology* 296 (4): H1200–1208. https://doi.org/10.1152/ajpheart.01294.2008.

Boogerd, Fred, Frank J. Bruggeman, Jan-Hendrik S. Hofmeyr, and H. V. Westerhoff. 2007. *Systems Biology: Philosophical Foundations*. Elsevier.

Bowen, William J. 1949. "The Absorption Spectra and Extinction Coefficients of Myoglobin." *The Journal of Biological Chemistry* 179 (1): 235–45.

Boyle, Andrew J, Joy Hwang, Jianqin Ye, Henry Shih, Kristine Jun, Yan Zhang, Qizhi Fang, Richard Sievers, Yerem Yeghiazarians, and Randall J Lee. 2013. "The Effects of Aging on

Apoptosis Following Myocardial Infarction." *Cardiovascular Therapeutics* 31 (6): e102–10. https://doi.org/10.1111/1755-5922.12043.

Braunwald, E, and R A Kloner. 1985. "Myocardial Reperfusion: A Double-Edged Sword?" *Journal of Clinical Investigation* 76 (5): 1713–19.

Bray, Nicolas L, Harold Pimentel, Páll Melsted, and Lior Pachter. 2016. "Near-Optimal Probabilistic RNA-Seq Quantification." *Nature Biotechnology* 34 (5): 525–27. https://doi.org/10.1038/nbt.3519.

Breitling, Rainer. 2010. "What Is Systems Biology?" *Frontiers in Physiology* 1 (May). https://doi.org/10.3389/fphys.2010.00009.

Burden, Conrad J., Sumaira E. Qureshi, and Susan R. Wilson. 2014. "Error Estimates for the Analysis of Differential Expression from RNA-Seq Count Data." *PeerJ* 2 (September): e576. https://doi.org/10.7717/peerj.576.

Camacho, Paula, Huimin Fan, Zhongmin Liu, and Jia-Qiang He. 2016. "Small Mammalian Animal Models of Heart Disease." *American Journal of Cardiovascular Disease* 6 (3): 70–80.

Cheng, Bill, H. C. Chen, I. W. Chou, Tony W. H. Tang, and Patrick C. H. Hsieh. 2017. "Harnessing the Early Post-Injury Inflammatory Responses for Cardiac Regeneration." *Journal of Biomedical Science* 24 (1). https://doi.org/10.1186/s12929-017-0315-2.

Chiong, M, Z V Wang, Z Pedrozo, D J Cao, R Troncoso, M Ibacache, A Criollo, A Nemchenko, J A Hill, and S Lavandero. 2011. "Cardiomyocyte Death: Mechanisms and Translational Implications." *Cell Death & Disease* 2 (12): e244. https://doi.org/10.1038/cddis.2011.130.

Chung, Kwanghun, Jenelle Wallace, Sung-Yon Kim, Sandhiya Kalyanasundaram, Aaron S. Andalman, Thomas J. Davidson, Julie J. Mirzabekov, et al. 2013. "Structural and Molecular Interrogation of Intact Biological Systems." *Nature* 497 (7449): 332–37. https://doi.org/10.1038/nature12107.

Cobb, Matthew. 2017. "60 Years Ago, Francis Crick Changed the Logic of Biology." *PLoS Biology* 15 (9). https://doi.org/10.1371/journal.pbio.2003243.

Collins, F. S., and M. K. Mansoura. 2001. “The Human Genome Project. Revealing the Shared Inheritance of All Humankind.” *Cancer* 91 (1 Suppl): 221–25.

Conesa, Ana, Pedro Madrigal, Sonia Tarazona, David Gomez-Cabrero, Alejandra Cervera, Andrew McPherson, Michał Wojciech Szcześniak, et al. 2016. “A Survey of Best Practices for RNA-Seq Data Analysis.” *Genome Biology* 17. https://doi.org/10.1186/s13059-016-0881-8.

Coon, Keith D., Landon J. Inge, Kristen Swetel, Valerie Felton, Phillip Stafford, and Ross M. Bremner. 2010. “Genomic Characterization of the Inflammatory Response Initiated by Surgical Intervention and the Effect of Perioperative Cyclooxygenase 2 Blockade.” *The Journal of Thoracic and Cardiovascular Surgery* 139 (5): 1253-1260.e2. https://doi.org/10.1016/j.jtcvs.2010.01.022.

Croce, A.C., and G. Bottiroli. 2014. “Autofluorescence Spectroscopy and Imaging: A Tool for Biomedical Research and Diagnosis.” *European Journal of Histochemistry* 58 (4). https://doi.org/10.4081/ejh.2014.2461.

Dewey, Colleen M., Kathryn M. Spitler, Jessica M. Ponce, Duane D. Hall, and Chad E. Grueter. 2016. “Cardiac-Secreted Factors as Peripheral Metabolic Regulators and Potential Disease Biomarkers.” *Journal of the American Heart Association: Cardiovascular and Cerebrovascular Disease* 5 (6). https://doi.org/10.1161/JAHA.115.003101.

Diaz-Beltran, Leticia, Carlos Cano, Dennis P. Wall, and Francisco J. Esteban. 2013. “Systems Biology as a Comparative Approach to Understand Complex Gene Expression in Neurological Diseases.” *Behavioral Sciences* 3 (2): 253–72. https://doi.org/10.3390/bs3020253.

Dixon, Simon R., Robert J. Whitbourn, Michael W. Dae, Eberhard Grube, Warren Sherman, Gary L. Schaer, J. Stephen Jenkins, et al. 2002. “Induction of Mild Systemic Hypothermia with Endovascular Cooling during Primary Percutaneous Coronary Intervention for Acute Myocardial Infarction.” *Journal of the American College of Cardiology* 40 (11): 1928–34.

Dodt, Hans-Ulrich, Ulrich Leischner, Anja Schierloh, Nina Jährling, Christoph Peter Mauch, Katrin Deininger, Jan Michael Deussing, Matthias Eder, Walter Zieglgänsberger, and Klaus Becker. 2007. "Ultramicroscopy: Three-Dimensional Visualization of Neuronal Networks in the Whole Mouse Brain." *Nature Methods* 4 (4): 331–36. https://doi.org/10.1038/nmeth1036.

Duncker, D. J., C. L. Klassen, Y. Ishibashi, S. H. Herrlinger, T. J. Pavek, and R. J. Bache. 1996. "Effect of Temperature on Myocardial Infarction in Swine." *The American Journal of Physiology* 270 (4 Pt 2): H1189-1199. https://doi.org/10.1152/ajpheart.1996.270.4.H1189.

Elmore, Susan. 2007. "Apoptosis: A Review of Programmed Cell Death." *Toxicologic Pathology* 35 (4): 495–516. https://doi.org/10.1080/01926230701320337.

Epelman, Slava, Kory J. Lavine, Anna E. Beaudin, Dorothy K. Sojka, Javier A. Carrero, Boris Calderon, Thaddeus Brija, et al. 2014. "Embryonic and Adult-Derived Resident Cardiac Macrophages Are Maintained through Distinct Mechanisms at Steady State and during Inflammation." *Immunity* 40 (1): 91–104. https://doi.org/10.1016/j.immuni.2013.11.019.

Epp, J. R., Y. Niibori, H.-L. (Liz) Hsiang, V. Mercaldo, K. Deisseroth, S. A. Josselyn, and P. W. Frankland. 2015. "Optimization of CLARITY for Clearing Whole-Brain and Other Intact Organs." *ENeuro* 2 (3). https://doi.org/10.1523/ENEURO.0022-15.2015.

Ernst, Jason, and Ziv Bar-Joseph. 2006. "STEM: A Tool for the Analysis of Short Time Series Gene Expression Data." *BMC Bioinformatics* 7 (1): 191. https://doi.org/10.1186/1471-2105-7-191.

Faul, Franz, Edgar Erdfelder, Albert-Georg Lang, and Axel Buchner. 2007. "G*Power 3: A Flexible Statistical Power Analysis Program for the Social, Behavioral, and Biomedical Sciences." *Behavior Research Methods* 39 (2): 175–91. https://doi.org/10.3758/BF03193146.

Feinberg, Mark W., Zhuoxiao Cao, Akm Khyrul Wara, Maria A. Lebedeva, Sucharita SenBanerjee, and Mukesh K. Jain. 2005. "Kruppel-like Factor 4 Is a Mediator of

Proinflammatory Signaling in Macrophages." *Journal of Biological Chemistry* 280 (46): 38247–58. https://doi.org/10.1074/jbc.M509378200.

Fernández-Friera, Leticia, José Manuel García-Ruiz, Ana García-Álvarez, Rodrigo Fernández-Jiménez, Javier Sánchez-González, Xavier Rossello, Sandra Gómez-Talavera, et al. 2017. "Accuracy of Area at Risk Quantification by Cardiac Magnetic Resonance According to the Myocardial Infarction Territory." *Revista Española de Cardiología* 70 (05): 323–30. https://doi.org/10.1016/j.rec.2016.07.004.

Fielding, C. A., R. M. McLoughlin, L. McLeod, C. S. Colmont, M. Najdovska, D. Grail, M. Ernst, S. A. Jones, N. Topley, and B. J. Jenkins. 2008. "IL-6 Regulates Neutrophil Trafficking during Acute Inflammation via STAT3." *The Journal of Immunology* 181 (3): 2189–95. https://doi.org/10.4049/jimmunol.181.3.2189.

Fishbein, Michael C., Samuel Meerbaum, Jacob Rit, Ulf Lando, Katsuo Kanmatsuse, Jean C. Mercier, Eliot Corday, and William Ganz. 1981. "Early Phase Acute Myocardial Infarct Size Quantification: Validation of the Triphenyl Tetrazolium Chloride Tissue Enzyme Staining Technique." *American Heart Journal* 101 (5): 593–600. https://doi.org/10.1016/0002-8703(81)90226-X.

Forte, Elvira, Milena Bastos Furtado, and Nadia Rosenthal. 2018. "The Interstitium in Cardiac Repair: Role of the Immune–Stromal Cell Interplay." *Nature Reviews Cardiology* 15 (10): 601. https://doi.org/10.1038/s41569-018-0077-x.

Franceschini, Andrea, Damian Szklarczyk, Sune Frankild, Michael Kuhn, Milan Simonovic, Alexander Roth, Jianyi Lin, et al. 2013. "STRING v9.1: Protein-Protein Interaction Networks, with Increased Coverage and Integration." *Nucleic Acids Research* 41 (Database issue): D808–15. https://doi.org/10.1093/nar/gks1094.

Frangogiannis, N. 2002. "The Inflammatory Response in Myocardial Infarction." *Cardiovascular Research* 53 (1): 31–47. https://doi.org/10.1016/S0008-6363(01)00434-5.

Frangogiannis, Nikolaos G. 2012. “Regulation of the Inflammatory Response in Cardiac Repair.” Edited by Anthony Rosenzweig. *Circulation Research* 110 (1): 159–73. https://doi.org/10.1161/CIRCRESAHA.111.243162.

Frangogiannis, Nikolaos G. 2014. “The Inflammatory Response in Myocardial Injury, Repair and Remodeling.” *Nature Reviews. Cardiology* 11 (5): 255–65. https://doi.org/10.1038/nrcardio.2014.28.

Fu, Xing, Ning Fu, Song Guo, Zheng Yan, Ying Xu, Hao Hu, Corinna Menzel, et al. 2009. “Estimating Accuracy of RNA-Seq and Microarrays with Proteomics.” *BMC Genomics* 10 (April): 161. https://doi.org/10.1186/1471-2164-10-161.

Garcia-Dorado, David, and Hans Michael Piper. 2006. “Postconditioning: Reperfusion of ‘Reperfusion Injury’ after Hibernation.” *Cardiovascular Research* 69 (1): 1–3. https://doi.org/10.1016/j.cardiores.2005.11.011.

Garcia-Dorado, David, Antonio Rodríguez-Sinovas, Marisol Ruiz-Meana, Javier Inserte, David Garcia-Dorado, Antonio Rodríguez-Sinovas, Marisol Ruiz-Meana, and Javier Inserte. 2014. “Protection Against Myocardial Ischemia-reperfusion Injury in Clinical Practice.” *Revista Española de Cardiología* 67 (05): 394–404. https://doi.org/10.1016/j.rec.2014.01.010.

Garini, Yuval, Ian T. Young, and George McNamara. 2006. “Spectral Imaging: Principles and Applications.” *Cytometry Part A* 69A (8): 735–47. https://doi.org/10.1002/cyto.a.20311.

Gibbons Raymond J., Miller Todd D., and Christian Timothy F. 2000. “Infarct Size Measured by Single Photon Emission Computed Tomographic Imaging With 99mTc-Sestamibi.” *Circulation* 101 (1): 101–8. https://doi.org/10.1161/01.CIR.101.1.101.

Gombozhapova, Aleksandra, Yuliya Rogovskaya, Vladimir Shurupov, Mariya Rebenkova, Julia Kzhyshkowska, Sergey V. Popov, Rostislav S. Karpov, and Vyacheslav Ryabov. 2017. “Macrophage Activation and Polarization in Post-Infarction Cardiac Remodeling.” *Journal of Biomedical Science* 24 (February). https://doi.org/10.1186/s12929-017-0322-3.

GREENE, CASEY S., JIE TAN, MATTHEW UNG, JASON H. MOORE, and CHAO CHENG. 2016. “Big Data Bioinformatics.” *Methods (San Diego, Calif.)* 111 (December): 1–2. https://doi.org/10.1016/j.ymeth.2016.11.017.

Gustafsson, Åsa B., and Roberta A. Gottlieb. 2009. “Autophagy in Ischemic Heart Disease.” *Circulation Research* 104 (2): 150–58. https://doi.org/10.1161/CIRCRESAHA.108.187427.

Halestrap, Andrew P. 2009. “What Is the Mitochondrial Permeability Transition Pore?” *Journal of Molecular and Cellular Cardiology* 46 (6): 821–31. https://doi.org/10.1016/j.yjmcc.2009.02.021.

Hama, Hiroshi, Hiroshi Kurokawa, Hiroyuki Kawano, Ryoko Ando, Tomomi Shimogori, Hisayori Noda, Kiyoko Fukami, Asako Sakaue-Sawano, and Atsushi Miyawaki. 2011. “Scale: A Chemical Approach for Fluorescence Imaging and Reconstruction of Transparent Mouse Brain.” *Nature Neuroscience* 14 (11): 1481–88. https://doi.org/10.1038/nn.2928.

Harhous, Zeina, Sally Badawi, Noelle Gallo Bona, Bruno Pillot, Lionel Augeul, Melanie Paillard, George W. Booz, et al. 2019. “Critical Appraisal of STAT3 Pattern in Adult Cardiomyocytes.” *Journal of Molecular and Cellular Cardiology* 131 (June): 91–100. https://doi.org/10.1016/j.yjmcc.2019.04.021.

Harpster, Mark H, Somnath Bandyopadhyay, D Paul Thomas, Pavel S Ivanov, Jacque A Keele, Natalia Pineguina, Bifeng Gao, et al. n.d. “Earliest Changes in the Left Ventricular Transcriptome Post-Myocardial Infarction,” 15.

Hartman, Minke H. T., Inge Vreeswijk-Baudoin, Hilde E. Groot, Kees W. A. van de Kolk, Rudolf A. de Boer, Irene Mateo Leach, Rozemarijn Vliegenthart, Herman H. W. Sillje, and Pim van der Harst. 2016. “Inhibition of Interleukin-6 Receptor in a Murine Model of Myocardial Ischemia-Reperfusion.” *PLoS ONE* 11 (12). https://doi.org/10.1371/journal.pone.0167195.

Hasin, Yehudit, Marcus Seldin, and Aldons Lusis. 2017. “Multi-Omics Approaches to Disease.” *Genome Biology* 18 (May). https://doi.org/10.1186/s13059-017-1215-1.

Hausenloy, Derek J., David Garcia-Dorado, Hans Erik Bøtker, Sean M. Davidson, James Downey, Felix B. Engel, Robert Jennings, et al. 2017. "Novel Targets and Future Strategies for Acute Cardioprotection: Position Paper of the European Society of Cardiology Working Group on Cellular Biology of the Heart." *Cardiovascular Research* 113 (6): 564–85. https://doi.org/10.1093/cvr/cvx049.

Hausenloy, Derek J., and Derek M. Yellon. 2013. "Myocardial Ischemia-Reperfusion Injury: A Neglected Therapeutic Target." *The Journal of Clinical Investigation* 123 (1): 92–100. https://doi.org/10.1172/JCI62874.

Hausenloy, Derek J., and Derek M. Yellon 2016. "Ischaemic Conditioning and Reperfusion Injury." *Nature Reviews Cardiology* 13 (4): 193–209. https://doi.org/10.1038/nrcardio.2016.5.

Heinrich, Peter C, Iris Behrmann, Serge Haan, Heike M Hermanns, Gerhard Müller-Newen, and Fred Schaper. 2003. "Principles of Interleukin (IL)-6-Type Cytokine Signalling and Its Regulation." *Biochemical Journal* 374 (Pt 1): 1–20. https://doi.org/10.1042/BJ20030407.

Heusch, Gerd, Judith Musiolik, Nilguen Gedik, and Andreas Skyschally. 2011. "Mitochondrial STAT3 Activation and Cardioprotection by Ischemic Postconditioning in Pigs with Regional Myocardial Ischemia/Reperfusion." *Circulation Research* 109 (11): 1302–8. https://doi.org/10.1161/CIRCRESAHA.111.255604.

Hoffmann, Jedrzej, Manuel Ospelt, Christian Troidl, Sandra Voss, Christoph Liebetrau, Won-Keun Kim, Andreas Rolf, et al. 2014. "Sham Surgery and Inter-Individual Heterogeneity Are Major Determinants of Monocyte Subset Kinetics in a Mouse Model of Myocardial Infarction." *PLoS ONE* 9 (6). https://doi.org/10.1371/journal.pone.0098456.

Hofmann Ulrich, and Frantz Stefan. 2015. "Role of Lymphocytes in Myocardial Injury, Healing, and Remodeling After Myocardial Infarction." *Circulation Research* 116 (2): 354–67. https://doi.org/10.1161/CIRCRESAHA.116.304072.

Horckmans, Michael, Larisa Ring, Johan Duchene, Donato Santovito, Maximilian J. Schloss, Maik Drechsler, Christian Weber, Oliver Soehnlein, and Sabine Steffens. 2016.

"Neutrophils Orchestrate Post-Myocardial Infarction Healing by Polarizing Macrophages towards a Reparative Phenotype." *European Heart Journal*, February, ehw002. https://doi.org/10.1093/eurheartj/ehw002.

Hunter, Philip. 2012. "Back down to Earth." *EMBO Reports* 13 (5): 408–11. https://doi.org/10.1038/embor.2012.49.

Ito, W. D., S. Schaarschmidt, R. Klask, S. Hansen, H. J. Schäfer, D. Mathey, and S. Bhakdi. 1997. "Infarct Size Measurement by Triphenyltetrazolium Chloride StainingVersus In VivoInjection of Propidium Iodide." *Journal of Molecular and Cellular Cardiology* 29 (8): 2169–75. https://doi.org/10.1006/jmcc.1997.0456.

Jennings, Robert B., and Keith A. Reimer. 1981. "Lethal Myocardial Ischemic Injury." *The American Journal of Pathology* 102 (2): 241–55.

Jensen, Kristian H. Reveles, and Rune W. Berg. 2017. "Advances and Perspectives in Tissue Clearing Using CLARITY." *Journal of Chemical Neuroanatomy* 86 (December): 19–34. https://doi.org/10.1016/j.jchemneu.2017.07.005.

Johns, Thomas N. P., and Byron J. Olson. 1954. "Experimental Myocardial Infarction: I. A Method of Coronary Occlusion in Small Animals." *Annals of Surgery* 140 (5): 675–82.

Jr, Glynn Dennis, Brad T Sherman, Douglas A Hosack, Jun Yang, Wei Gao, H Clifford Lane, and Richard A Lempicki. 2003. "DAVID: Database for Annotation, Visualization, and Integrated Discovery." *Genome Biology*, 11.

Kalogeris, Theodore, Christopher P. Baines, Maike Krenz, and Ronald J. Korthuis. 2012. "Cell Biology of Ischemia/Reperfusion Injury." *International Review of Cell and Molecular Biology* 298: 229–317. https://doi.org/10.1016/B978-0-12-394309-5.00006-7.

Kang, In Sook, Ikeno Fumiaki, and Wook Bum Pyun. 2016. "Therapeutic Hypothermia for Cardioprotection in Acute Myocardial Infarction." *Yonsei Medical Journal* 57 (2): 291–97. https://doi.org/10.3349/ymj.2016.57.2.291.

Kaplanski, G. 2003. “IL-6: A Regulator of the Transition from Neutrophil to Monocyte Recruitment during Inflammation.” *Trends in Immunology* 24 (1): 25–29. https://doi.org/10.1016/S1471-4906(02)00013-3.

Kapoor, Nidhi, Jianli Niu, Yasser Saad, Sanjay Kumar, Tatiana Sirakova, Edilu Becerra, Xiaoman Li, and Pappachan E. Kolattukudy. 2015. “Transcription Factors STAT6 and KLF4 Implement Macrophage Polarization via the Dual Catalytic Powers of MCPIP.” *Journal of Immunology (Baltimore, Md. : 1950)* 194 (12): 6011–23. https://doi.org/10.4049/jimmunol.1402797.

Karpurapu, Manjula, Ravi Ranjan, Jing Deng, Sangwoon Chung, Yong Gyu Lee, Lei Xiao, Teja Srinivas Nirujogi, Jeffrey R. Jacobson, Gye Young Park, and John W Christman. 2014. “Krüppel Like Factor 4 Promoter Undergoes Active Demethylation during Monocyte/Macrophage Differentiation.” Edited by Chi Zhang. *PLoS ONE* 9 (4): e93362. https://doi.org/10.1371/journal.pone.0093362.

Kim, Daehwan, Geo Pertea, Cole Trapnell, Harold Pimentel, Ryan Kelley, and Steven L Salzberg. 2013. “TopHat2: Accurate Alignment of Transcriptomes in the Presence of Insertions, Deletions and Gene Fusions.” *Genome Biology* 14 (4): R36. https://doi.org/10.1186/gb-2013-14-4-r36.

Knoop, Betül, David Naguib, Lisa Dannenberg, Carolin Helten, Saif Zako, Christian Jung, Bodo Levkau, et al. 2019. “Cardioprotection by Very Mild Hypothermia in Mice.” *Cardiovascular Diagnosis and Therapy* 9 (1): 64–67. https://doi.org/10.21037/cdt.2018.08.07.

Konstantinidis, Klitos, Russell S. Whelan, and Richard N. Kitsis. 2012. “Mechanisms of Cell Death in Heart Disease.” *Arteriosclerosis, Thrombosis, and Vascular Biology* 32 (7). https://doi.org/10.1161/ATVBAHA.111.224915.

Krämer, Andreas, Jeff Green, Jack Pollard, and Stuart Tugendreich. 2014. “Causal Analysis Approaches in Ingenuity Pathway Analysis.” *Bioinformatics* 30 (4): 523–30. https://doi.org/10.1093/bioinformatics/btt703.

Krijnen, P A J, R Nijmeijer, C J L M Meijer, C A Visser, C E Hack, and H W M Niessen. 2002. "Apoptosis in Myocardial Ischaemia and Infarction." *Journal of Clinical Pathology* 55 (11): 801–11.

Kübler, W., and M. Haass. 1996. "Cardioprotection: Definition, Classification, and Fundamental Principles." *Heart* 75 (4): 330–33.

Kumar, Mukesh, Eshvendar Reddy Kasala, Lakshmi Narendra Bodduluru, Vicky Dahiya, Dinesh Sharma, Vikas Kumar, and Mangala Lahkar. 2016. "Animal Models of Myocardial Infarction: Mainstay in Clinical Translation." *Regulatory Toxicology and Pharmacology* 76 (April): 221–30. https://doi.org/10.1016/j.yrtph.2016.03.005.

Kwon, Andrew T., David J. Arenillas, Rebecca Worsley Hunt, and Wyeth W. Wasserman. 2012. "OPOSSUM-3: Advanced Analysis of Regulatory Motif Over-Representation Across Genes or ChIP-Seq Datasets." *G3: Genes|Genomes|Genetics* 2 (9): 987–1002. https://doi.org/10.1534/g3.112.003202.

Lamarre, Sophie, Pierre Frasse, Mohamed Zouine, Delphine Labourdette, Elise Sainderichin, Guojian Hu, Véronique Le Berre-Anton, Mondher Bouzayen, and Elie Maza. 2018. "Optimization of an RNA-Seq Differential Gene Expression Analysis Depending on Biological Replicate Number and Library Size." *Frontiers in Plant Science* 9 (February). https://doi.org/10.3389/fpls.2018.00108.

Langfelder, Peter, and Steve Horvath. 2008. "WGCNA: An R Package for Weighted Correlation Network Analysis." *BMC Bioinformatics* 9 (1): 559. https://doi.org/10.1186/1471-2105-9-559.

Langmead, Ben, and Steven L Salzberg. 2012. "Fast Gapped-Read Alignment with Bowtie 2." *Nature Methods* 9 (4): 357–59. https://doi.org/10.1038/nmeth.1923.

Lee, K.-W., Y. Lee, H.-J. Kwon, and D.-S. Kim. 2005. "Sp1-Associated Activation of Macrophage Inflammatory Protein-2 Promoter by CpG-Oligodeoxynucleotide and Lipopolysaccharide." *Cellular and Molecular Life Sciences: CMLS* 62 (2): 188–98. https://doi.org/10.1007/s00018-004-4399-y.

Lee, Sang-Eun, Christopher Nguyen, Jongjin Yoon, Hyuk-Jae Chang, Sekeun Kim, Chul Hoon Kim, and Debiao Li. 2018. "Three-Dimensional Cardiomyocytes Structure Revealed By Diffusion Tensor Imaging and Its Validation Using a Tissue-Clearing Technique." *Scientific Reports* 8 (1). https://doi.org/10.1038/s41598-018-24622-6.

Lehrke Stephanie, Mazhari Ramesh, Durand Daniel J., Zheng Meizi, Bedja Djahida, Zimmet Jeffrey M., Schuleri Karl H., Chi Andrew S., Gabrielson Kathleen L., and Hare Joshua M. 2006. "Aging Impairs the Beneficial Effect of Granulocyte Colony-Stimulating Factor and Stem Cell Factor on Post-Myocardial Infarction Remodeling." *Circulation Research* 99 (5): 553–60. https://doi.org/10.1161/01.RES.0000238375.88582.d8.

Leiris, J. de, D. P. Harding, and S. Pestre. 1984. "The Isolated Perfused Rat Heart: A Model for Studying Myocardial Hypoxia or Ischaemia." *Basic Research in Cardiology* 79 (3): 313–21.

Li, Xianchi, Min Liu, Rongrong Sun, Yi Zeng, Shuang Chen, and Peiying Zhang. 2016. "Protective Approaches against Myocardial Ischemia Reperfusion Injury (Review)." *Experimental and Therapeutic Medicine* 12 (6): 3823–29. https://doi.org/10.3892/etm.2016.3877.

Li, Yanfei, Cuiping Wang, Tingting Li, Linlin Ma, Fangzhou Fan, Yueling Jin, and Junwei Shen. 2019. "The Whole Transcriptome and Proteome Changes in the Early Stage of Myocardial Infarction." *Cell Death Discovery* 5 (1): 73. https://doi.org/10.1038/s41420-019-0152-z.

Liao, Xudong, Nikunj Sharma, Fehmida Kapadia, Guangjin Zhou, Yuan Lu, Hong Hong, Kaavya Paruchuri, et al. 2011. "Krüppel-like Factor 4 Regulates Macrophage Polarization." *The Journal of Clinical Investigation* 121 (7): 2736–49. https://doi.org/10.1172/JCI45444.

Libby, Peter, Peter R. Maroko, Colin M. Bloor, Burton E. Sobel, and Eugene Braunwald. 1973. "Reduction of Experimental Myocardial Infarct Size by Corticosteroid Administration." *Journal of Clinical Investigation* 52 (3): 599–607.

Lim, Shiang Y, Derek J Hausenloy, Sapna Arjun, Anthony N Price, Sean M Davidson, Mark F Lythgoe, and Derek M Yellon. 2011. "Mitochondrial Cyclophilin-D as a Potential

Therapeutic Target for Post-Myocardial Infarction Heart Failure." *Journal of Cellular and Molecular Medicine* 15 (11): 2443–51. https://doi.org/10.1111/j.1582-4934.2010.01235.x.

Lin, Lin, Zhengfei Yang, Guanghui Zheng, Yongxun Zhuansun, Yue Wang, Jianguo Li, Rui Chen, and Wanchun Tang. 2018. "Analyses of Changes in Myocardial Long Non-Coding RNA and MRNA Profiles after Severe Hemorrhagic Shock and Resuscitation via RNA Sequencing in a Rat Model." *BMC Molecular Biology* 19 (1): 11. https://doi.org/10.1186/s12867-018-0113-8.

Lindsey, Merry L., Roberto Bolli, John M. Canty, Xiao-Jun Du, Nikolaos G. Frangogiannis, Stefan Frantz, Robert G. Gourdie, et al. 2018. "Guidelines for Experimental Models of Myocardial Ischemia and Infarction." *American Journal of Physiology - Heart and Circulatory Physiology* 314 (4): H812–38. https://doi.org/10.1152/ajpheart.00335.2017.

Liu, A. K. L., M. E. D. Hurry, O.T. W. Ng, J. DeFelice, H. M. Lai, R. K. B. Pearce, G. T-C. Wong, R. C-C. Chang, and S. M. Gentleman. 2016. "Bringing CLARITY to the Human Brain: Visualization of Lewy Pathology in Three Dimensions." *Neuropathology and Applied Neurobiology* 42 (6): 573–87. https://doi.org/10.1111/nan.12293.

Louridas, G E, I E Kanonidis, and K G Lourida. 2010. "Systems Biology in Heart Diseases." *Hippokratia* 14 (1): 10–16.

Love, Michael I, Wolfgang Huber, and Simon Anders. 2014. "Moderated Estimation of Fold Change and Dispersion for RNA-Seq Data with DESeq2." *Genome Biology* 15 (12). https://doi.org/10.1186/s13059-014-0550-8.

Ma, Yan, Kang Liu, Zhibin Guan, Xinkai Xu, Xu Qian, and Hong Bao. 2018. "Background Augmentation Generative Adversarial Networks (BAGANs): Effective Data Generation Based on GAN-Augmented 3D Synthesizing." *Symmetry* 10 (12): 734. https://doi.org/10.3390/sym10120734.

Ma, Yonggang, Alan J. Mouton, and Merry L. Lindsey. 2018. "Cardiac Macrophage Biology in the Steady-State Heart, the Aging Heart, and Following Myocardial Infarction."

Translational Research : The Journal of Laboratory and Clinical Medicine 191 (January): 15–28. https://doi.org/10.1016/j.trsl.2017.10.001.

Marioni, John C., Christopher E. Mason, Shrikant M. Mane, Matthew Stephens, and Yoav Gilad. 2008. "RNA-Seq: An Assessment of Technical Reproducibility and Comparison with Gene Expression Arrays." *Genome Research* 18 (9): 1509–17. https://doi.org/10.1101/gr.079558.108.

Maroko Peter R., Kjekshus John K., Sobel Burton E., Watanabe Tan, Covell James W., Ross John, and Braunwald Eugene. 1971. "Factors Influencing Infarct Size Following Experimental Coronary Artery Occlusions." *Circulation* 43 (1): 67–82. https://doi.org/10.1161/01.CIR.43.1.67.

Martin, Marcel. 2011. "Cutadapt Removes Adapter Sequences from High-Throughput Sequencing Reads." *EMBnet.Journal* 17 (1): 10–12. https://doi.org/10.14806/ej.17.1.200.

Michael, L. H., J. R. Hunt, D. Weilbaecher, M. B. Perryman, R. Roberts, R. M. Lewis, and M. L. Entman. 1985. "Creatine Kinase and Phosphorylase in Cardiac Lymph: Coronary Occlusion and Reperfusion." *American Journal of Physiology-Heart and Circulatory Physiology* 248 (3): H350–59. https://doi.org/10.1152/ajpheart.1985.248.3.H350.

Miki, T., G. S. Liu, M. V. Cohen, and J. M. Downey. 1998. "Mild Hypothermia Reduces Infarct Size in the Beating Rabbit Heart: A Practical Intervention for Acute Myocardial Infarction?" *Basic Research in Cardiology* 93 (5): 372–83.

Millar, S.J., B.W. Moss, and M.H. Stevenson. 1996. "Some Observations on the Absorption Spectra of Various Myoglobin Derivatives Found in Meat." *Meat Science* 42 (3): 277–88. https://doi.org/10.1016/0309-1740(94)00045-X.

Miyao, Y., H. Yasue, H. Ogawa, I. Misumi, T. Masuda, T. Sakamoto, and E. Morita. 1993. "Elevated Plasma Interleukin-6 Levels in Patients with Acute Myocardial Infarction." *American Heart Journal* 126 (6): 1299–1304.

Monici, Monica. 2005. “Cell and Tissue Autofluorescence Research and Diagnostic Applications.” In *Biotechnology Annual Review*, 11:227–56. Elsevier. https://doi.org/10.1016/S1387-2656(05)11007-2.

Mouton, Alan J., Kristine Y. DeLeon-Pennell, Osvaldo J. Rivera Gonzalez, Elizabeth R. Flynn, Tom C. Freeman, Jeffrey J. Saucerman, Michael R. Garrett, Yonggang Ma, Romain Harmancey, and Merry L. Lindsey. 2018. “Mapping Macrophage Polarization over the Myocardial Infarction Time Continuum.” *Basic Research in Cardiology* 113 (4). https://doi.org/10.1007/s00395-018-0686-x.

Na, Heung Sik, Yang In Kim, Young Wook Yoon, Hee Chul Han, Sook Hyun Nahm, and Seung Kil Hong. 1996. “Ventricular Premature Beat—Driven Intermittent Restoration of Coronary Blood Flow Reduces the Incidence of Reperfusion-Induced Ventricular Fibrillation in a Cat Model of Regional Ischemia.” *American Heart Journal* 132 (1, Part 1): 78–83. https://doi.org/10.1016/S0002-8703(96)90393-2.

Nahrendorf, Matthias, Filip K. Swirski, Elena Aikawa, Lars Stangenberg, Thomas Wurdinger, Jose-Luiz Figueiredo, Peter Libby, Ralph Weissleder, and Mikael J. Pittet. 2007. “The Healing Myocardium Sequentially Mobilizes Two Monocyte Subsets with Divergent and Complementary Functions.” *The Journal of Experimental Medicine* 204 (12): 3037–47. https://doi.org/10.1084/jem.20070885.

Nakagawa, Takashi, Shigeomi Shimizu, Tetsuya Watanabe, Osamu Yamaguchi, Kinya Otsu, Hirotaka Yamagata, Hidenori Inohara, Takeshi Kubo, and Yoshihide Tsujimoto. 2005. “Cyclophilin D-Dependent Mitochondrial Permeability Transition Regulates Some Necrotic but Not Apoptotic Cell Death.” *Nature* 434 (7033): 652–58. https://doi.org/10.1038/nature03317.

Nossuli, T. O., V. Lakshminarayanan, G. Baumgarten, G. E. Taffet, C. M. Ballantyne, L. H. Michael, and M. L. Entman. 2000. “A Chronic Mouse Model of Myocardial Ischemia-Reperfusion: Essential in Cytokine Studies.” *American Journal of Physiology-Heart and Circulatory Physiology* 278 (4): H1049–55. https://doi.org/10.1152/ajpheart.2000.278.4.H1049.

O'Connell, Timothy D., Manoj C. Rodrigo, and Paul C. Simpson. 2007. "Isolation and Culture of Adult Mouse Cardiac Myocytes." *Methods in Molecular Biology (Clifton, N.J.)* 357: 271–96. https://doi.org/10.1385/1-59745-214-9:271.

Ong, Sang-Bing, Sauri Hernández-Reséndiz, Gustavo E. Crespo-Avilan, Regina T. Mukhametshina, Xiu-Yi Kwek, Hector A. Cabrera-Fuentes, and Derek J. Hausenloy. 2018. "Inflammation Following Acute Myocardial Infarction: Multiple Players, Dynamic Roles, and Novel Therapeutic Opportunities." *Pharmacology & Therapeutics* 186 (June): 73–87. https://doi.org/10.1016/j.pharmthera.2018.01.001.

Ordway, G. A. 2004. "Myoglobin: An Essential Hemoprotein in Striated Muscle." *Journal of Experimental Biology* 207 (20): 3441–46. https://doi.org/10.1242/jeb.01172.

Orogo, Amabel M., and Åsa B. Gustafsson. 2013. "Cell Death in the Myocardium: My Heart Won't Go On." *IUBMB Life* 65 (8): 651–56. https://doi.org/10.1002/iub.1180.

Ovize, Michel, Gary F. Baxter, Fabio Di Lisa, Péter Ferdinandy, David Garcia-Dorado, Derek J. Hausenloy, Gerd Heusch, Jakob Vinten-Johansen, Derek M. Yellon, and Rainer Schulz. 2010. "Postconditioning and Protection from Reperfusion Injury: Where Do We Stand?Position Paper from the Working Group of Cellular Biology of the Heart of the European Society of Cardiology." *Cardiovascular Research* 87 (3): 406–23. https://doi.org/10.1093/cvr/cvq129.

Papayan, Garry, Nickolay Petrishchev, and Michael Galagudza. 2014. "Autofluorescence Spectroscopy for NADH and Flavoproteins Redox State Monitoring in the Isolated Rat Heart Subjected to Ischemia-Reperfusion." *Photodiagnosis and Photodynamic Therapy* 11 (3): 400–408. https://doi.org/10.1016/j.pdpdt.2014.05.003.

Pavlidis, P., Q. Li, and W. S. Noble. 2003. "The Effect of Replication on Gene Expression Microarray Experiments." *Bioinformatics* 19 (13): 1620–27. https://doi.org/10.1093/bioinformatics/btg227.

Pavlova, I., M. Williams, A. El-Naggar, R. Richards-Kortum, and A. Gillenwater. 2008. "Understanding the Biological Basis of Autofluorescence Imaging for Oral Cancer

Detection: High-Resolution Fluorescence Microscopy in Viable Tissue." *Clinical Cancer Research* 14 (8): 2396–2404. https://doi.org/10.1158/1078-0432.CCR-07-1609.

Perbellini, Filippo, Alan K. L. Liu, Samuel A. Watson, Ifigeneia Bardi, Stephen M. Rothery, and Cesare M. Terracciano. 2017. "Free-of-Acrylamide SDS-Based Tissue Clearing (FASTClear) for Three Dimensional Visualization of Myocardial Tissue." *Scientific Reports* 7 (1). https://doi.org/10.1038/s41598-017-05406-w.

Petri, Björn, and Maria-Jesús Sanz. 2018. "Neutrophil Chemotaxis." *Cell and Tissue Research* 371 (3): 425–36. https://doi.org/10.1007/s00441-017-2776-8.

Piquereau, Jerome, Fanny Caffin, Marta Novotova, Christophe Lemaire, Vladimir Veksler, Anne Garnier, Renee Ventura-Clapier, and Frederic Joubert. 2013. "Mitochondrial Dynamics in the Adult Cardiomyocytes: Which Roles for a Highly Specialized Cell?" *Frontiers in Physiology* 4 (May). https://doi.org/10.3389/fphys.2013.00102.

Porta, Alberto, Marco Di Rienzo, Niels Wessel, and Juergen Kurths. 2009. "Addressing the Complexity of Cardiovascular Regulation." *Philosophical Transactions of the Royal Society A: Mathematical, Physical and Engineering Sciences* 367 (1892): 1215–18. https://doi.org/10.1098/rsta.2008.0292.

Prat-Vidal, Cristina, Carolina Ga, Francesc Sole, and Antoni Bayes-Genis. 2013. "Identification of Temporal and Region-Specific Myocardial Gene Expression Patterns in Response to Infarction in Swine." *PLOS ONE* 8 (1): 13.

Rahman, Firdaus A., Siti S. Abdullah, Wan Zanariah W. A. Manan, Loh Teng-Hern Tan, Chin-Fen Neoh, Long Chiau Ming, Kok-Gan Chan, et al. 2018. "Efficacy and Safety of Cyclosporine in Acute Myocardial Infarction: A Systematic Review and Meta-Analysis." *Frontiers in Pharmacology* 9 (June). https://doi.org/10.3389/fphar.2018.00238.

Raychaudhuri, Soumya, Patrick D. Sutphin, Jeffrey T. Chang, and Russ B. Altman. 2001. "Basic Microarray Analysis: Grouping and Feature Reduction." *Trends in Biotechnology* 19 (5): 189–93. https://doi.org/10.1016/S0167-7799(01)01599-2.

Redfors, Bjorn, Yangzhen Shao, and Elmir Omerovic. 2012. "Myocardial Infarct Size and Area at Risk Assessment in Mice." *Experimental & Clinical Cardiology* 17 (4): 268–72.

Reimer, K A, J E Lowe, M M Rasmussen, and R B Jennings. 1977. "The Wavefront Phenomenon of Ischemic Cell Death. 1. Myocardial Infarct Size vs Duration of Coronary Occlusion in Dogs." *Circulation* 56 (5): 786–94. https://doi.org/10.1161/01.CIR.56.5.786.

Richardson, Douglas S., and Jeff W. Lichtman. 2015. "Clarifying Tissue Clearing." *Cell* 162 (2): 246–57. https://doi.org/10.1016/j.cell.2015.06.067.

Roy, Sashwati, Savita Khanna, Donald E. Kuhn, Cameron Rink, Willis T. Williams, Jay L. Zweier, and Chandan K. Sen. 2006. "Transcriptome Analysis of the Ischemia-Reperfused Remodeling Myocardium: Temporal Changes in Inflammation and Extracellular Matrix." *Physiological Genomics* 25 (3): 364–74. https://doi.org/10.1152/physiolgenomics.00013.2006.

Sabatasso, Sara, Patrice Mangin, Tony Fracasso, Milena Moretti, Mylène Docquier, and Valentin Djonov. 2016. "Early Markers for Myocardial Ischemia and Sudden Cardiac Death." *International Journal of Legal Medicine* 130 (5): 1265–80. https://doi.org/10.1007/s00414-016-1401-9.

Sager, Hendrik B., Thorsten Kessler, and Heribert Schunkert. 2017. "Monocytes and Macrophages in Cardiac Injury and Repair." *Journal of Thoracic Disease* 9 (Suppl 1): S30–35. https://doi.org/10.21037/jtd.2016.11.17.

Schurch, Nicholas J., Pietá Schofield, Marek Gierliński, Christian Cole, Alexander Sherstnev, Vijender Singh, Nicola Wrobel, et al. 2016. "How Many Biological Replicates Are Needed in an RNA-Seq Experiment and Which Differential Expression Tool Should You Use?" *RNA* 22 (6): 839–51. https://doi.org/10.1261/rna.053959.115.

Seok, Junhee, H. Shaw Warren, Alex G. Cuenca, Michael N. Mindrinos, Henry V. Baker, Weihong Xu, Daniel R. Richards, et al. 2013. "Genomic Responses in Mouse Models Poorly Mimic Human Inflammatory Diseases." *Proceedings of the National Academy of Sciences of the United States of America* 110 (9): 3507–12. https://doi.org/10.1073/pnas.1222878110.

Sepah, Yasir J., Abeer Akhtar, Mohammad Ali Sadiq, Yamama Hafeez, Humzah Nasir, Brian Perez, Narissa Mawji, Diana J. Dean, Daniel Ferraz, and Quan Dong Nguyen. 2014. "Fundus Autofluorescence Imaging: Fundamentals and Clinical Relevance." *Saudi Journal of Ophthalmology* 28 (2): 111–16. https://doi.org/10.1016/j.sjopt.2014.03.008.

Seropian, Ignacio M., Stefano Toldo, Benjamin W. Van Tassell, and Antonio Abbate. 2014. "Anti-Inflammatory Strategies for Ventricular Remodeling Following ST-Segment Elevation Acute Myocardial Infarction." *Journal of the American College of Cardiology* 63 (16): 1593–1603. https://doi.org/10.1016/j.jacc.2014.01.014.

Shinde, Arti V., and Nikolaos G. Frangogiannis. 2014. "Fibroblasts in Myocardial Infarction: A Role in Inflammation and Repair." *Journal of Molecular and Cellular Cardiology* 0 (May): 74–82. https://doi.org/10.1016/j.yjmcc.2013.11.015.

Simkhovich, Boris Z., Sharon L. Hale, and Robert A. Kloner. 2004. "Metabolic Mechanism by Which Mild Regional Hypothermia Preserves Ischemic Tissue." *Journal of Cardiovascular Pharmacology and Therapeutics* 9 (2): 83–90. https://doi.org/10.1177/107424840400900203.

Sindhwani, Shrey, Abdullah Muhammad Syed, Stefan Wilhelm, Dylan R. Glancy, Yih Yang Chen, Michael Dobosz, and Warren C. W. Chan. 2016. "Three-Dimensional Optical Mapping of Nanoparticle Distribution in Intact Tissues." *ACS Nano* 10 (5): 5468–78. https://doi.org/10.1021/acsnano.6b01879.

Song, Shlee S., and Patrick D. Lyden. 2012. "Overview of Therapeutic Hypothermia." *Current Treatment Options in Neurology* 14 (6): 541–48. https://doi.org/10.1007/s11940-012-0201-x.

Sperling, Silke R. 2011. "Systems Biology Approaches to Heart Development and Congenital Heart Disease." *Cardiovascular Research* 91 (2): 269–78. https://doi.org/10.1093/cvr/cvr126.

Sproston, Nicola R., and Jason J. Ashworth. 2018. “Role of C-Reactive Protein at Sites of Inflammation and Infection.” *Frontiers in Immunology* 9 (April). https://doi.org/10.3389/fimmu.2018.00754.

Sykes, Paul A., Harn-Cherng Shiue, Jon R. Walker, and Robert C. Bateman. 1999. “Determination of Myoglobin Stability by Visible Spectroscopy.” *Journal of Chemical Education* 76 (9): 1283. https://doi.org/10.1021/ed076p1283.

Sylwestrak, Emily Lauren, Priyamvada Rajasethupathy, Matthew Arnot Wright, Anna Jaffe, and Karl Deisseroth. 2016. “Multiplexed Intact-Tissue Transcriptional Analysis at Cellular Resolution.” *Cell* 164 (4): 792–804. https://doi.org/10.1016/j.cell.2016.01.038.

Takao, Keizo, and Tsuyoshi Miyakawa. 2015. “Genomic Responses in Mouse Models Greatly Mimic Human Inflammatory Diseases.” *Proceedings of the National Academy of Sciences of the United States of America* 112 (4): 1167–72. https://doi.org/10.1073/pnas.1401965111.

Tang, Peizhe, Shengjun Ma, Mingfeng Dong, Jiantang Wang, Shoudong Chai, Tao Liu, and Jindong Li. 2018. “Effect of Interleukin-6 on Myocardial Regeneration in Mice after Cardiac Injury.” *Biomedicine & Pharmacotherapy* 106 (October): 303–8. https://doi.org/10.1016/j.biopha.2018.06.090.

Tang, Ting-Ting, Jing Yuan, Zheng-Feng Zhu, Wen-Cai Zhang, Hong Xiao, Ni Xia, Xin-Xin Yan, et al. 2012. “Regulatory T Cells Ameliorate Cardiac Remodeling after Myocardial Infarction.” *Basic Research in Cardiology* 107 (1). https://doi.org/10.1007/s00395-011-0232-6.

Tavernarakis, Nektarios. 2007. “Cardiomyocyte Necrosis: Alternative Mechanisms, Effective Interventions.” *Biochimica et Biophysica Acta (BBA) - Molecular Cell Research* 1773 (4): 480–82. https://doi.org/10.1016/j.bbamcr.2007.01.011.

The Gene Ontology Consortium. 2019. “The Gene Ontology Resource: 20 Years and Still GOing Strong.” *Nucleic Acids Research* 47 (D1): D330–38. https://doi.org/10.1093/nar/gky1055.

Tissier, Renaud, Nicolas Couvreur, Bijan Ghaleh, Patrick Bruneval, Fanny Lidouren, Didier Morin, Roland Zini, et al. 2009. “Rapid Cooling Preserves the Ischaemic Myocardium against Mitochondrial Damage and Left Ventricular Dysfunction.” *Cardiovascular Research* 83 (2): 345–53. https://doi.org/10.1093/cvr/cvp046.

Tissier, Renaud, Bijan Ghaleh, Michael V. Cohen, James M. Downey, and Alain Berdeaux. 2012. “Myocardial Protection with Mild Hypothermia.” *Cardiovascular Research* 94 (2): 217–25. https://doi.org/10.1093/cvr/cvr315.

Tomer, Raju, Li Ye, Brian Hsueh, and Karl Deisseroth. 2014. “Advanced CLARITY for Rapid and High-Resolution Imaging of Intact Tissues.” *Nature Protocols* 9 (7): 1682–97. https://doi.org/10.1038/nprot.2014.123.

Wagner, Michael, and M. Aq Siddiqui. 2009. “Signaling Networks Regulating Cardiac Myocyte Survival and Death.” *Current Opinion in Investigational Drugs (London, England: 2000)* 10 (9): 928–37.

Walter, Wencke, Laura Alonso-Herranz, Verdiana Trappetti, Isaac Crespo, Mark Ibberson, Marta Cedenilla, Anna Karaszewska, et al. 2018. “Deciphering the Dynamic Transcriptional and Post-Transcriptional Networks of Macrophages in the Healthy Heart and after Myocardial Injury.” *Cell Reports* 23 (2): 622–36. https://doi.org/10.1016/j.celrep.2018.03.029.

Wang, Rui-Sheng, Bradley A. Maron, and Joseph Loscalzo. 2015. “Systems Medicine: Evolution of Systems Biology From Bench To Bedside.” *Wiley Interdisciplinary Reviews. Systems Biology and Medicine* 7 (4): 141–61. https://doi.org/10.1002/wsbm.1297.

Wang, Zhiwei, Jie Zhang, Guangpu Fan, Hui Zhao, Xu Wang, Jing Zhang, Peide Zhang, and Wei Wang. 2018. “Imaging Transparent Intact Cardiac Tissue with Single-Cell Resolution.” *Biomedical Optics Express* 9 (2): 423. https://doi.org/10.1364/BOE.9.000423.

Wang, Zhong, Mark Gerstein, and Michael Snyder. 2009a. “RNA-Seq: A Revolutionary Tool for Transcriptomics.” *Nature Reviews. Genetics* 10 (1): 57–63. https://doi.org/10.1038/nrg2484.

Zhong Wang, Mark Gerstein, and Michael Snyder.. 2009b. “RNA-Seq: A Revolutionary Tool for Transcriptomics.” *Nature Reviews. Genetics* 10 (1): 57–63. https://doi.org/10.1038/nrg2484.

Weirather Johannes, Hofmann Ulrich D.W., Beyersdorf Niklas, Ramos Gustavo C., Vogel Benjamin, Frey Anna, Ertl Georg, Kerkau Thomas, and Frantz Stefan. 2014. “Foxp3+ CD4+ T Cells Improve Healing After Myocardial Infarction by Modulating Monocyte/Macrophage Differentiation.” *Circulation Research* 115 (1): 55–67. https://doi.org/10.1161/CIRCRESAHA.115.303895.

Woodcock, Elizabeth A., and Scot J. Matkovich. 2005. “Cardiomyocytes Structure, Function and Associated Pathologies.” *The International Journal of Biochemistry & Cell Biology* 37 (9): 1746–51. https://doi.org/10.1016/j.biocel.2005.04.011.

Wu, Meng-Yu, Giou-Teng Yiang, Wan-Ting Liao, Andy Po-Yi Tsai, Yeung-Leung Cheng, Pei-Wen Cheng, Chia-Ying Li, and Chia-Jung Li. 2018. “Current Mechanistic Concepts in Ischemia and Reperfusion Injury.” *Cellular Physiology and Biochemistry* 46 (4): 1650–67. https://doi.org/10.1159/000489241.

Yang, Chiu-Fen. 2018. “Clinical Manifestations and Basic Mechanisms of Myocardial Ischemia/Reperfusion Injury.” *Tzu-Chi Medical Journal* 30 (4): 209–15. https://doi.org/10.4103/tcmj.tcmj_33_18.

Yellon, Derek M., and Derek J. Hausenloy. 2007. “Myocardial Reperfusion Injury.” *New England Journal of Medicine* 357 (11): 1121–35. https://doi.org/10.1056/NEJMra071667.

Yellon, Robert L, and Derek M Yellon. 2018. “Cardioprotection at the Bedside: An Exploration of Conditioning Phenomena and Their Clinical Applications,” 5.

Yilmaz, Atilla, Barbara Dietel, Iwona Cicha, Katja Schubert, Roland Hausmann, Werner G. Daniel, Christoph D. Garlichs, and Christian Stumpf. 2010. “Emergence of Dendritic Cells in the Myocardium after Acute Myocardial Infarction – Implications for Inflammatory Myocardial Damage.” *International Journal of Biomedical Science : IJBS* 6 (1): 27–36.

Zgheib, Carlos, Fouad A. Zouein, Mazen Kurdi, and George W. Booz. 2012. "Differential STAT3 Signaling in the Heart." *JAK-STAT* 1 (2): 101–10. https://doi.org/10.4161/jkst.19776.

Zhao, Zhi-Qing, Joel S. Corvera, Michael E. Halkos, Faraz Kerendi, Ning-Ping Wang, Robert A. Guyton, and Jakob Vinten-Johansen. 2003. "Inhibition of Myocardial Injury by Ischemic Postconditioning during Reperfusion: Comparison with Ischemic Preconditioning." *American Journal of Physiology-Heart and Circulatory Physiology* 285 (2): H579–88. https://doi.org/10.1152/ajpheart.01064.2002.

Zhe-Wei, Shi, Ge Li-Sha, and Li Yue-Chun. 2018. "The Role of Necroptosis in Cardiovascular Disease." *Frontiers in Pharmacology* 9 (July). https://doi.org/10.3389/fphar.2018.00721.

Zhou, Pingzhu, and William T. Pu. 2016. "Recounting Cardiac Cellular Composition." *Circulation Research* 118 (3): 368–70. https://doi.org/10.1161/CIRCRESAHA.116.308139.

Zimmermann, Matthias, Lucian Beer, Robert Ullrich, Dominika Lukovic, Elisabeth Simader, Denise Traxler, Tanja Wagner, et al. 2017. "Analysis of Region Specific Gene Expression Patterns in the Heart and Systemic Responses after Experimental Myocardial Ischemia." *Oncotarget* 8 (37): 60809–25. https://doi.org/10.18632/oncotarget.17955.

Zouein, Fouad A., Mazen O. Kurdi, and George W. Booz. 2013. "Dancing Rhinos in Stilettos." In *JAK-STAT*. https://doi.org/10.4161/jkst.24352.

Zouggari, Yasmine, Hafid Ait-Oufella, Philippe Bonnin, Tabassome Simon, Andrew P Sage, Coralie Guérin, José Vilar, et al. 2013. "B Lymphocytes Trigger Monocyte Mobilization and Impair Heart Function after Acute Myocardial Infarction." *Nature Medicine* 19 (10): 1273–80. https://doi.org/10.1038/nm.3284.

Annex

Published Second-Author Article

In an attempt to study the cardioprotective roles of STAT3, which are linked to the regulation of the mitochondrial activity during IR and IPoC, we first questioned its mitochondrial translocation and localization. Surprisingly, we were unable to detect STAT3 in pure mitochondrial fractions of adult cardiomyocytes. In addition, no involvement for STAT3 in the mitochondrial activity was observed. Thereafter, the aspect of this aim has shifted toward studying the pattern of localization of STAT3 in adult cardiac myocytes under various conditions. The detailed work and results, in the context of mitochondrial STAT3, are presented in our following published paper.

Contents lists available at ScienceDirect

Journal of Molecular and Cellular Cardiology

journal homepage: www.elsevier.com

Critical appraisal of STAT3 pattern in adult cardiomyocytes

Zeina Harhous [a, b, c], Sally Badawi [a, b, c], Noelle Gallo Bona [a, b], Bruno Pillot [a, b], Lionel Augeul [a, b], Melanie Paillard [a, b], George W. Booz [d], Emmanuelle Canet-Soulas [a, b], Michel Ovize [a, b], Mazen Kurdi [c, **], Gabriel Bidaux [a, b, *]

[a] Univ-Lyon, CarMeN Laboratory, INSERM 1060, INRA 1397, University Claude Bernard Lyon1, INSA Lyon, Oullins, France
[b] IHU OPeRa, Groupement Hospitalier EST, Bâtiment B13, 59 boulevard Pinel, F-69500 Bron, France
[c] Lebanese University, Faculty of Sciences, Doctoral School of Sciences and Techlogy, Laboratory of Experimental and Clinical Pharmacology, Hadat, Lebanon
[d] Department of Pharmacology and Toxicology, School of Medicine, The University of Mississippi Medical Center, Jackson, MS, USA

ARTICLE INFO

Keywords:
Mitochondria
Cardiomyocytes
Ischemia-reperfusion
T-tubules
Subcellular distribution
Mitochondria associated membranes

ABSTRACT

The signal transducer and activator of transcription 3, STAT3, transfers cellular signals from the plasma membrane to the nucleus, acting as a signaling molecule and a transcription factor. Reports proposed an additional non-canonical role of STAT3 that could regulate the activity of complexes I and II of the electron transport chain and the opening of the mitochondrial permeability transition pore (PTP) after ischemia-reperfusion in various cell types. The native expression of STAT3 in heart mitochondria, together with a direct versus an indirect transcriptional role in mitochondrial functions, have been recently questioned.

The objective of the present study was to investigate the cellular distribution of STAT3 in mouse adult cardiomyocytes under basal and stress conditions, along with assessing its presence and activity in cardiac mitochondria using structural and functional approaches. The analysis of the spatial distribution of STAT3 signal in the cardiomyocytes interestingly showed that it is transversely distributed along the T-tubules and in the nucleus. This distribution was neither affected by hypoxia nor by hypoxia/re-oxygenation conditions. Focusing on the mitochondrial STAT3 localization, our results suggest that serine-phosphorylated STAT3 (PS727-STAT3) and total STAT3 are detected in crude but not in pure mitochondria of mouse adult cardiomyocytes, under basal and ischemia-reperfusion conditions. The inhibition of STAT3, with a pre-validated non-toxic Stattic dose, had no significant effects on mitochondrial respiration, but a weak effect on the calcium retention capacity. Overall, our results exclusively reveal a unique cellular distribution of STAT3 in mouse adult cardiomyocytes, along the T-tubules and in nucleus, under different conditions. They also challenge the expression and activity of STAT3 in mitochondria of these cells under basal conditions and following ischemia-reperfusion. In addition, our results underline technical methods, complemental to cell fractionation, to evaluate STAT3 roles during hypoxia-reoxygenation and at the interface between nucleus and endoplasmic reticulum.

Critical Appraisal of Mitochondrial STAT3 in Adult Cardiomyocytes

Zeina Harhous1,2,3, Sally Badawi1,2,3, Noelle Gallo Bona2, Bruno Pillot2, Lionel Augeul2, Melanie Paillard2, George W Booz4, Emmanuelle Canet-Soulas1, Michel Ovize2, Mazen Kurdi3*, Gabriel Bidaux1,2*,

1 Univ-Lyon, CarMeN Laboratory, INSERM 1060, INRA 1397, University Claude Bernard Lyon1, INSA Lyon, Oullins, France.

2IHU OPeRa, Groupement Hospitalier EST, Bâtiment B13, 59 boulevard Pinel, F-69500 Bron, France

3Lebanese University, Faculty of Sciences, Doctoral School of Sciences and Technology, Laboratory of Experimental and Clinical Pharmacology, Hadat, Lebanon.

4Department of Pharmacology and Toxicology, School of Medicine, The University of Mississippi Medical Center, Jackson, MS USA

Running title: Mitochondrial STAT3

*To whom correspondences should be addressed:

Dr Gabriel Bidaux: CarMeN Laboratory, IHU Opera, INSERM U1060, Groupement Hospitalier EST, Bâtiment B13, 59 boulevard Pinel, F-69500 Bron, France. Tel: +33 (0) 478-777-047. Fax: +33 (0) 478-777-175. gabriel.bidaux@univ-lyon1.fr.

Dr Mazen Kurdi: Laboratory of Experimental and Clinical Pharmacology, Lebanese University, Faculty of Sciences, Hadat, Lebanon. Tel:+961 (3) 303 688. E-mail: mkurdi@ul.edu.lb

Keywords: mitochondria, cardiomyocytes, ischemia-reperfusion, t-tubules, subcellular distribution, mitochondria associated membranes

ABSTRACT

The signal transducer and activator of transcription 3, STAT3, transfers cellular signals from the plasma membrane to the nucleus, acting as a signalling molecule and a transcription factor. Reports proposed an additional non-canonical role of STAT3 that could regulate the activity of complexes I and II of the electron transport chain and the opening of the mitochondrial permeability transition pore (PTP) after ischemia-reperfusion in various cell types. The native expression of STAT3 in heart mitochondria, together with a direct versus an indirect transcriptional role in mitochondria functions, have been recently questioned.

The objective of the present study was to assess the presence and activity of STAT3 in heart mitochondria using structural and functional approaches. Our results suggest that serine-phosphorylated STAT3 (PS727-STAT3) and total STAT3 are detected in crude but not in pure mitochondria of mouse adult cardiomyocytes, under basal and ischemia-reperfusion conditions. Interestingly, the analysis of the spatial distribution of STAT3 signal in mouse cardiomyocytes showed that it is transversely distributed in the cardiac cells along the T-tubules and in nucleus as well. The inhibition of STAT3, with a pre-validated non-toxic Stattic dose, had no significant effects on mitochondrial respiration, but a weak effect on the calcium retention capacity. Overall, our results challenge the expression and activity of STAT3 in mouse adult cardiomyocytes mitochondria under basal conditions and following ischemia-reperfusion, and they underline technical methods, complemental to cell fractionation, to evaluate its roles during hypoxia-reoxygenation and at the interface between nucleus and endoplasmic reticulum.

1. INTRODUCTION

The signal transducer and activator of transcription 3 (STAT3) is a member of the STAT family of proteins. It transfers information from the plasma membrane to the nucleus, acting as a signaling molecule and a transcription factor [1]. It is activated by growth factors, cytokines, inflammation, stress conditions and oncogenic kinases [2]. The activation of STAT3 occurs through phosphorylation of its tyrosine 705 (Y705) residue. PY705-STAT3 molecules form dimers which translocate to the nucleus, bind to certain targeted DNA sequences and regulate expression of various genes [3]. STAT3 is also phosphorylated at its serine 727 (S727) residue. Phosphorylation of S727 has been described to be required and self-sufficient for STAT3 transcriptional activity [4]–[6]. Alternatively, a non-canonical role of STAT3 has been reported in the mitochondria [3], [7]. Mitochondria are major players in ischemia-reperfusion-induced cell death, including through opening of the mitochondrial permeability transition pore [8]–[10]. STAT3 has been suggested to enhance the activity of the electron transport chain, to increase ATP production and to decrease ROS generation by interacting with mitochondria complexes I and II [7], [11]. Recent reports using pharmacological or genetic modulation of STAT3 activity and expression in adult cardiomyocytes and various cell lines propose that mitochondrial STAT3 could contribute to protection against ischemia-reperfusion injury by ischemic conditioning [7], [12]–[15] . Alternatively, several attempts and approaches to detect STAT3 in the mitochondria have been unsuccessful, and the specificity of its pharmacological inhibitor, Stattic, raises questions.

Therefore, the aim of the present study was to examine the expression and activity of STAT3 in mitochondria of mouse adult cardiomyocytes under different conditions. Using several independent methods, we could confirm neither total nor phosphorylated STAT3 expression in cardiac mouse mitochondria under both baseline and ischemia-reperfusion conditions. Moreover, we were unable to confirm that STAT3 inhibition, by a non-toxic concentration of Stattic, could impair mitochondrial respiration. We finally discuss how STAT3 might, however, play a role in ischemia-reperfusion injury and possible important methodological drawbacks in this field of research.

2. MATERIALS AND METHODS

2.1 Animals

The present study was performed following the approval by the local institutional animal research committee (N°DR2018-35v2). It conforms to the NIH Guide on the Use of Laboratory Animals (NIH Publication No. 85-23, revised 1996). C57bl/6J male mice aged between 8-12 weeks were obtained from Charles River Laboratories.

2.2 In vivo Myocardial Ischemia-Reperfusion Injury

As previously described [16], mice received a sub-cutaneous injection of the anesthetics mix (buprenorphine 0.075mg/kg + medetomidine 0.3mg/kg) and the analgesics mix (lidocaine 2mg/kg + Alfaxan 80mg/kg). They were then placed on a blanket at 37°C until fully asleep. ECG and heart rate were monitored using EGC electrodes, and an oximeter was used for SpO2 monitoring. A tracheotomy was performed and mice were mechanically ventilated. The hearts was exposed via a left thoracotomy, and myocardial infarction was induced by placing an 8-0 suture around the left anterior descending (LAD) artery. Following 45 min ischemia, the infarcted area was reperfused for 15 min through the loosening of the suture. The area at risk were identified by the absence of blue staining and was collected for pure mitochondrial isolation prior to western blot analysis.

2.3 Cell Culture

The rat derived H9C2 cell line of cardiomyoblasts and mouse embryonic fibroblasts (MEFs), wild type (WT) and STAT3 knockout (KO), were cultured in Dulbecco's Modified Eagle's Medium (DMEM) (41965-039 Gibco), supplemented with 10% Fetal Bovine Serum and 100 U/ml penicillin/streptomycin under a humidified incubator aerated with 5% CO2 at 37°C. WT and KO MEFs were generated by Valeria Poli (University of Torino, Torino, Italy).

2.4 Mitochondrial Isolation

To optimize the yield of intact mitochondria, all procedures were carried out on ice, with the centrifugations performed at 4°C. Crude mitochondria were used for the assessment of mitochondrial functions, while pure mitochondria were used for the qualitative detection of STAT3 under various conditions.

2.4.1 Crude Mitochondrial isolation

As previously described [17], after euthanizing the mice by cervical dislocation, the hearts were extracted while still beating and immediately placed in cold buffer A [70mM sucrose, 210 mM mannitol, 1 mM EDTA and 50 mM Tris HCl (pH 7.4)]. Atria were then removed, and ventricular tissues thoroughly minced with scissors. A Potter-Elvehjem (glass-glass) tissue grinder was used for homogenization. The homogenates were centrifuged at 1,300g for 3 min and the supernatants then collected and centrifuged at 10,000g for 10 min. The mitochondrial pellets were suspended in isolation buffer B (same as buffer A except for EDTA 0.1 mM). The suspensions were centrifuged at 10,000g for 10 min and homogenized in 100µL of buffer B. Protein contents were assessed using Bradford reagent with bovine serum albumin as standard.

2.4.2 Pure Mitochondrial isolation

As previously described [18], after euthanizing the mice by cervical dislocation, the hearts were extracted and immediately placed in Isolation Buffer, IB1, (225 mM mannitol, 75 mM sucrose,

0.5% BSA, 0.5 mM EGTA and 30 mM Tris HCl pH7.4). Atria were then removed, and the tissues finely minced with scissors. The pieces were then homogenized by applying 10-20 strokes in a glass-teflon tissue grinder. The homogenates were centrifuged at 740g for 5 min, and the supernatants were then taken and similarly centrifuged. The new supernatants were collected and centrifuged at 9,000g for 10 min at 4°C. The pellets were gently resuspended in a Stop Buffer, SB, (225 mM mannitol, 75 mM sucrose, 30 mM Tris-HCl pH7.4) and centrifuged at 10,000g for 10 min. The pellets of crude mitochondria were resuspended in Mitochondria Resuspending Buffer, MRB, (250 mM mannitol, 5 mM HEPES (pH7.4) and 0.5 mM EGTA). For obtaining pure mitochondria, suspensions of crude mitochondrial fractions were layered on top of Percoll medium (225 mM mannitol, 25 mM HEPES, 1 mM EGTA and 30% Percoll (vol/vol) in 14 ml thin-wall ultracentrifuge tubes. MRB was finally layered on top of the mitochondrial suspensions to fill up the tubes. The latter were centrifuged at 95,000g for 30 min. Purified mitochondria, localized at the bottom of the tube as a dense band, were collected and washed twice by centrifugation at 6,300g for 10 min.

2.5 Mitochondrial Oxidative Phosphorylation

Oxidative phosphorylation of 350 µg crude mitochondria was measured at 25°C using a Clark-type electrode (Oroboros oxygraph, Austria) in 2 mL of respiration buffer (pH 7.4) [100 mM KCl, 50 mM MOPS, 1 mM EGTA, 5 mM KH2PO4 and 1 mg/mL fatty acid-free BSA], as previously described [19]. Glutamate/Malate/Pyruvate (5 mM each), succinate (5 mM) and TMPD-ascorbate (0.125-1.25 mM respectively) were used as substrates for complexes I, II, and IV respectively. Rotenone (1 µM) and Antimicyn A (12.5 µM) were respectively added as specific inhibitors of complexes I and III. The maximal oxygen uptake after uncoupling of respiratory chain with FCCP (2.8µM) was also determined. The ADP (200µM)-stimulated respiration was measured. The oxygen consumption of the complexes is expressed in nmol O2/min/mg of proteins.

2.6 Mitochondrial Calcium Retention Capacity (CRC)

The calcium retention capacity of 250 µg of crude mitochondrial proteins was determined in 2 mL of incubation buffer C (150 mM sucrose, 50 mM KCl, 2 mM KH2PO4, 20 mM tris/HCl) at 25°C using 5 mM (Glutamate/Malate/Succinate), with ADP-stimulated respiration in the presence of MgCl2 (1.2 mM), as previously described [17]. The extra-mitochondrial Ca2+ concentration was estimated with a spectrofluorometer using 1 µM of the calcium sensitive probe calcium green 5N (Life technology) (excitation wavelength: 500nm; emission: 530nm). Mitochondria were gently stirred, and 40 nmol CaCl2 pulses were applied every 2 min until a rapid calcium release occurred indicating PTP opening. CRCs were expressed in nmoles of Ca2+/mg of proteins.

2.7 Pharmacologic inhibition of STAT3

A dose-effect assessment of the STAT3 inhibitor, Stattic (sigma-S7946), was tested on isolated mouse cardiomyocytes as follows: cells were treated for 1 or 2 hours, at 37°C, with either Stattic (10-100µM) or DMSO vehicle. Crude mitochondria were incubated with 50 µM Stattic, a concentration which induced a significant decrease in Y705-STAT3 phosphorylation, or with DMSO vehicle for 1 hour at 4°C. The mitochondrial calcium retention capacities and oxygen consumption were consequently measured.

2.8 Western blotting

Proteins were extracted from cells and mitochondria (pure and crude) using complete RIPA lysis buffer with anti-proteases (Sigma; P8340) and anti-phosphatases (Sigma; p5726). The collected proteins were then quantified, and SDS-PAGE Western blotting was performed. Membranes were cut in strips in order to detect several proteins (STAT3 and markers of compartments) at the same time. Reblotting was performed in order to assess the detection of the different forms of STAT3 and different markers of the same size. Membrane strips were blocked for 1 hour with 5% bovine serum albumin (BSA)-PBS. Immunoblotting was performed by incubating the membranes, overnight at 4°C, with primary antibodies: Rabbit anti-PY705-STAT3 (dil: 1/1,000; Cell Signaling; 9145), rabbit anti-total STAT3 (dil: 1/1,000; Cell Signaling; 4904), mouse anti-PS727-STAT3 (dil: 1/1,000; Santa Cruz; sc-136193) batch 1 (May 2016) and batch 2 (March 2018), mouse anti-GRIM19 (1/200; Santa Cruz; sc- 514111), mouse anti-TOM20 (dil: 1/200; Santa Cruz; sc- 17764), mouse anti-tubulin (dil: 1/2,000; Santa Cruz; sc-5286), rabbit anti-GAPDH (dil: 1/500; Santa Cruz; sc-25778), mouse anti-cytochrome C (dil: 1/500; Santa Cruz; sc-13156) or anti-NDUFB6 (dil: 1/1,000; Abcam; ms108) prepared in 5% BSA-PBS. Corresponding horseradish-peroxidase conjugated anti-mouse and anti-rabbit secondary antibodies (dil: 1/10,000) were added and followed by 1h incubation at room temperature. Revelation was done using the reaction substrate ECL prime reagent (GE healthcare), and the acquisition was performed with Bio-Rad Molecular Imager Gel Doc XR+ (Bio-Rad). Image Lab software was used for quantification.

2.9 Hypoxia-Reoxygenation of cardiomyocytes

Cardiomyocytes were isolated from hearts of C57bl/6J mice using Langendorff system, as previously described [20]. They were deposited in 8-well plates and were subjected to 90 min hypoxia (0.5 % oxygen) in glucose-free medium (mM: 140 NaCl, 5 KCl, 1 MgCl2, 10 HEPES [pH 7.4], 10 CaCl2) in a hypoxic incubator (Eppendorf; galaxy 48R-CO48EN200259), followed by 1 h of reoxygenation (glucose-containing medium). Cells were then immuno-labeled and visualized by microscopy.

2.10 Immunofluorescence

Cardiomyocytes, plated in glass Labtech plates (PEZGS0816, Merck Millipore), were fixed for 15 min with 2% paraformaldehyde-PBS prior to 4 washes with PBS. They were then permeabilized

with 0.1% Triton-PBS for 10 min. Following 4 times PBS washes, the nonspecific binding was blocked using 5% BSA-PBS for 1h at room temperature (RT). The cells were then incubated for 1 h at room temperature with primary antibodies prepared in the blocking buffer. Following the primary antibody incubation, the wells were washed 4 times with PBS and corresponding secondary antibodies (Alexa Fluor 488 rabbit and/or Alexa Fluor 647 mouse - 1/2,000 - Jackson Immunoresearch) were applied for another 1h at room temperature in darkness. The nuclei were stained through a 10 min incubation with Bis-benzimide (5µg/mL). After washing 3 times with PBS, the cells were mounted with FluoromountTM Aqueous Mounting Medium (Sigma-F4680) and were gently covered by glass coverslips.

The primary antibodies were: mouse anti-ryanodine receptor (RyR) (Abcam; ab2827) (1/500), mouse anti-PS727-STAT3 (batch 1) (Santa Cruz; sc-136193), rabbit anti-PS727-STAT3 (Cell Signaling; 9134), rabbit anti-total STAT3 (Cell Signaling; 4904), mouse anti-total STAT3 (Santa Cruz; sc-8019), rabbit anti-TOM22 (Santa Cruz, sc-14896) and mouse anti-GRIM19 (Santa Cruz; sc- 514111) all diluted at 1/200.

2.11 Cloning of STAT3-eYFP

Mouse STAT3 coding sequence was amplified by PCR with High Fidelity Phusion DNA polymerase (Finnzymes; Thermo Fisher Scientific, Waltham, MA). After a 0.8% (w/vol) agarose-gel extraction of specific DNA bands (Wizard SV gel and PCR Clean-Up System; Promega, Madison, WI), PCR products and recipient vector pVLL-42-mEYFP [21] were digested with High Fidelity NheI and AgeI (New England Biolabs, Ipswich, MA) at 37°C overnight, cleaned-up on column prior to be ligated with T4 ligase (New England Biolabs) at 16°C overnight. Products were transformed in JM109 chemo-competent bacteria (New England Biolabs). Plasmid clones were extracted and sequenced before experiments.

2.12 Confocal Imaging

Confocal imaging was performed using a confocal microscope (Nikon Eclipse Ti, A1R confocal microscope) with a 40x oil immersion objective (N.A. 1.3), equipped with thermos-controlled chamber. The laser lines 405, 488, 514 and 633 nm were used for excitation. The emission wavelengths were acquired sequentially to prevent spectral overlapping. The depth of the focal plan was 0.5 µm, pixel size was chosen between 60 nm to 90 nm in order to respect the Shannon criterion and images were acquired by averaging 4 scanning-lines. Images were further processed with NIS software (Nikon) to adjust brightness and contrast and to calculate the spatial cross-correlation of the two fluorescent signals.

2.13 Statistics

All values are expressed as mean ± standard error of the mean (SEM) for n number of independent observations. Data were analyzed with GraphPad Prism 5.0 using one way ANOVA followed by Dunnett's multiple comparison test or using t-test. $P < 0.05$ was considered indicative of a significant difference.

3. RESULTS

3.1 STAT3 is detected in crude but not pure heart, liver and brain mitochondria

We focused on crude and pure mitochondrial protein extracts by western blotting. In crude cardiac mitochondrial fraction, phosphorylated (PY705 and PS727) and total STAT3 forms were detected, along with the mitochondrial proteins GRIM-19 and Tom20. However, the cytoplasmic protein tubulin was also strongly detected, which indicates fraction contamination with cytosolic proteins (Fig. 1A). Specificity of anti PS727-STAT3 for phosphate group was assessed by a serine phosphatase treatment that gradually removed the signal (Fig. S1). Since the crude mitochondrial fraction is not reliable for true assessment of exact STAT3 localization, we proceeded toward enriched mitochondrial investigation. Under baseline aerobic conditions, the western blot analysis of cytosolic and enriched, usually defined as "pure", mitochondrial fractions extracted from heart, liver, and brains (n=3) of C57bl6J mice showed that PS727-STAT3 and total STAT3 were exclusively expressed in the cytosolic fraction, along with the cytosolic proteins tubulin and GAPDH (Fig. 1B). On the pure mitochondrial level, the mitochondrial protein markers NDUFB6 (complex I subunit) and GRIM-19 were detected, ensuring the validity of this fraction.

We then aimed to determine if stress conditions, such as ischemia-reperfusion, might induce the mitochondrial translocation of STAT3. C57bl6J mice were subjected to 45 min of ischemia followed by 15 min of reperfusion (n=5). Samples were harvested from the area at risk, proteins were extracted and analyzed by western blotting. PS727-STAT3 and total STAT3 were checked along with the cytosolic proteins GAPDH and tubulin. The mitochondrial proteins NDUFB6 (complex I subunit), GRIM-19 andcytochrome C were also detected. A strong total STAT3 signal was detected in the cytosolic fraction and faint bands could be seen in pure mitochondrial fractions (Fig. 1C). However, faint bands could also be detected for the cytosolic freely diffusing GAPDH, while no signal could be found for the cytosolic and polymeric tubulin. Altogether, these results suggested that the faint total STAT3 and GAPDH signals most probably came from contamination of mitochondrial fractions by leakage of cytosolic proteins. Surprisingly, by means of a second batch of anti PS727-STAT3 (b2), we detected a strong band for PS727-STAT3 in the pure mitochondrial fractions exclusively, under both stress and control conditions (Fig. S2). Since the presence of PS727-STAT3 in control mitochondria contradicts what was previously observed in the three different organs experiment, and since PS727-STAT3 is part of the total STAT3 (i.e. total STAT3 must be detected where PS727-STAT3 is detected), we headed toward investigating the presence of such a band through validating the specificity of the antibodies used in these experiments. For this validation, STAT3-KO MEFs were used. The second batch of PS727-STAT3 antibody (PS727(b2)-STAT3) detected a dimer in control and a single band in KO cells. This showed that this batch was STAT3 unspecific. The first batch of PS727-STAT3 antibody (PS727-STAT3 b1), PY705-STAT3, and total STAT3 all detected a single band in control cells only (Fig.1 D). In all the following experiments, only the specific PS727(b1)-STAT3 antibody, which was also validated on serine phosphatase-treated protein extracts (Fig.S1), was used.

3.2 STAT3 is transversely distributed in cardiomyocytes according to the architecture of T-tubules

Following the detection of STAT3 by western blotting, we sought to study its localization and distribution pattern in cardiomyocytes (CMs) under various experimental conditions. Our results show that total STAT3 (t-STAT3) is arranged according to a transversal pattern similar to that of ryanodine receptors (RyRs), which lie within regularly spaced transverse striations corresponding to the positions of the T-tubules (Fig. 2A). In addition to the co-labeling of RyR and total STAT3 in CMs, we co-labeled total STAT3 and PS727-STAT3 with the mitochondrial proteins GRIM-19 and TOM22, respectively (Fig. 2 B and C). Our results suggest that STAT3 follows a pattern perpendicular to that of the mitochondrial proteins patterns, with the former being transversely dispersed in the cell, while the latter two are longitudinally dispersed following the normal cellular mitochondrial distribution pattern. The spatial cross-correlation of the fluorescent signals pattern was analyzed (Fig. 3A and 3D) and no cross-correlation could be found between STAT3 signal and mitochondrial signals.

We then studied if hypoxia-reoxygenation stress conditions could modulate the distribution of STAT3 and induce its mitochondrial translocation. CM underwent 90 minutes of hypoxia followed by 60 minutes of reoxygenation. Neither hypoxia (Fig. 3B) nor hypoxia-reoxygenation (Fig. 3C) induced a visible mitochondrial translocation of STAT3. Total STAT3 continued to follow a transversal distribution pattern in the cell and no cross-correlation patterns could be detected between STAT3 and GRIM19 (Fig 3 B and C). 3D images, collected following a Z-stacking, ensured the absence of co-localization of the two proteins (Fig. 3E) although STAT3 signal resided in structures close to mitochondria under such stress conditions. The specificity of antibodies used in the immuno-fluorescence experiments was also pre-validated on STAT3-EYFP-transfected cells (Fig. S3).

Finally, we assessed whether STAT3 overexpression could reveal the existence of a mitochondrial transportation mechanism. We thus overexpressed STAT3-EYFP and GRIM19 in H9C2 cardiomyoblasts, and we analyzed the localization of both proteins. A low intensity co-localization could be assumed as reported by the faint yellow color displayed by some of the mitochondria as depicted in the supplemental (Fig. S4). To validate this eye-viewed co-localization, we used the classical line-intensity profile analysis of STAT3 and GRIM19 signals. At the first glance, a strong over-lap between the two fluorescent signals could be observed at the level of four different mitochondria (four peaks). With a more careful analysis, we observed that, first, the peaks of fluorescence intensity of the 2 wavelengths were slightly shifted for profiles 2 and 3. Taken into account the diffraction limit of optical systems, this suggested that STAT3 signal could have been outside the mitochondria. Second, the 4th and 5th peaks of green fluorescence reporting STAT3 signal showed a similar shape and peak intensity, whereas the 4th peak co-localized with a mitochondria while the 5th was not. This could have been explained by a random co-localization between STAT3 hotspots and mitochondria. Since this line profile analysis does not report a 2D spatial co-localization, we performed the spatial cross-correlation of the fluorescent signals (Fig. S4B). Strikingly, clear and vivid donut-shaped cross-correlation patterns, around the mitochondria, were observed. This what reports that the highest cross-correlation of the two fluorescent signals

was found at the mitochondrial circumference rather than inside them. This presents a tipping point toward the probability that STAT3, even when over-expressed, might most-probably be located outside or around the mitochondrial rather than inside the mitochondria themselves.

The fact that we could not detect any clear STAT3 signal in mitochondria, whatever methods we used, does not guarantee that no STAT3 is expressed in mitochondria, but rather that its concentration is below the sensitivity of both Western-blot and immunofluorescence. Our results are in line with those of Phillips et al. who detected very small amount of STAT3 by mass-spectrometry in cardiac cells, at a concentration unlikely to be involved in a biological function in mitochondria[22].

3.3 The inhibition of STAT3 does not modify mitochondrial function

The mitochondrial oxygen consumption and calcium retention capacity were measured following pharmacological inhibition of STAT3 by Stattic. Boengler et al[11] originally demonstrated a strong inhibition of complex I and II activities following administration of 100 µM Stattic. Literature reports indicate that Stattic can be toxic as previously observed in cancer cells [23]. A dose-dependent assessment of this inhibitor (10-100 µM) showed that a 1 h treatment with 50 and 100 µM of Stattic significantly decreased PY705-STAT3 level (>50%), without any significant effect on PS727-STAT3 level (Fig.4 A and B). However, a 2 h Stattic treatment induced protein degradation at a 100µM dose (Fig. 4C). Subsequently, a dose of 50 µM Stattic, with a 1 h treatment, was used for further mitochondrial experiments.

The ADP-stimulated oxygen consumption of complexes I, II and IV was recorded following the incubation of crude mitochondria with DMSO (vehicle) or Stattic (50µM) for 1 h at 4°C (with agitation). Our results showed no significant effect for Stattic on complex activities under ADP-stimulated conditions (n=3) (Fig.4 D). The oxygen consumption of complexes I, II, and IV were 35.2 + 4.20, 25.2 + 3.41 and 80.63 + 12.3 nmole O2/min/mg protein, respectively, following DMSO treatment. These levels slightly and non-significantly shifted toward 34.2 + 5.24, 23.9 + 2.57 and 73.9 + 7 nmole O2/min/mg protein, respectively, following Stattic treatment (n=3).

Under the same treatment conditions, the calcium retention capacity (CRC) was measured in the presence of glutamate/malate and succinate as substrates for complexes I and II, respectively. ADP and MgCl2 were added for mimicking normal physiological conditions and ensuring optimal mitochondrial respiration. The results show that the CRC was, unexpectedly, increased from 666 + 68 nmole calcium/mg protein to 760 + 86 nmole calcium/mg protein (13%) in the presence of Stattic (n=3) (Fig.4 E).

4. DISCUSSION

In the present study, taking into account both sensitivity and specificity of the methods used, we could not detect significant levels of STAT3 proteins in mouse heart mitochondria under both baseline conditions and after prolonged ischemia-reperfusion. However, we report a novel prominent distribution of STAT3 along the architecture of T-tubules. We discuss the potential role of STAT3 in the regulation of mitochondrial permeability transition and more largely in cardioprotection

4.1 STAT3 in heart mitochondria

In the original study revealing the localization of STAT3 in heart mitochondria, Larner et al. [7]proposed that about 10% of STAT3 proteins were expressed within mouse heart mitochondria. In the same study, they reported a high concentration of PS727-STAT3 in heart mitochondria. Unfortunately, we could not exactly compare our experiments since the original antibodies which were used are no longer provided by the manufacturers and have been substituted with "more specific" ones as it is indicated on the manufacturer website (Santa Cruz). In the present study, we could not detect 10% of STAT3 being expressed in mitochondria whatever the anti-STAT3 antibody used (3 different validated antibodies). In a more recent study performed on mouse heart mitochondria as well, the authors also failed to detect PS727-STAT3 in mitochondria [12]. Rainer et al. showed that STAT3 was expressed in wild type heart mitochondria; however, a faint pair of bands was also detected in the mitochondria fraction of STAT3-KO [13]. Although a decrease in intensity can be seen, the fact that bands unrelated to STAT3 can be detected in extract of KO STAT3 cells question the specificity of the antibody. In our experiments with the unspecific S727(b2)-STAT3, we detected bands of low intensity of the expected size for STAT3 in STAT3 KO MEFs cells. This result was correlated with an opposite detection of signal in mitochondria vs. cytosolic fractions. Since we used 3 different antibodies validated against KO STAT3 extracts and showing a similar detection in cytosolic but not in mitochondrial fractions, we concluded the non-specificity of the antibody S727(b2)-STAT3. Our results indicate that one should avoid using antibodies that detect bands at the expected size of the candidate protein in its KO models. Following cell fractionation, one cannot guarantee the absolute purity of the fractions, hence only strong signals should be considered as acceptable. Noteworthy, the reference to "pure" mitochondrial fraction instead of enriched mitochondria fraction has maybe become misleading. This technical limitation strongly applies to proteins known to be expressed in ER or mitochondria associated membranes (MAMs), like STAT3 [24], since there is no guarantee that 100% of these membranes have been retrieved from the "pure" mitochondrial fraction. This might explain why we detected a strong STAT3 signal in crude mitochondrial extracts and virtually no or a non-consistent signal in pure mitochondria. This pattern is indeed the one often observed in several published studies.

The specificity of such detection is usually addressed by labeling compartment-specific proteins in order to show the clear cell compartment discrimination between the different fractions, taking

into account a comparable (long enough for weak signals) exposure time of the membrane for all protein markers, together with an appropriate choice of these markers. STAT3 is a soluble protein which is freely diffusing by Brownian motion in its media, whether it is cytoplasm, nucleoplasm or mitochondrial matrix. Authors historically used tubulin, a polymer anchored to membrane, as marker of cytosol; VDAC, a transmembrane protein, as marker of the outer mitochondrial membrane; and the sub-unit of the complex I, like GRIM19, as marker of the mitochondrial matrix. Although these markers are good to assess the contamination of fractions by membranes of other compartments, they are not suitable to assess contamination by protein diffusion that would occur when membranes are damaged. Since GRIM19 is a soluble protein, and because only a fraction of GRIM19 proteins is bound to the holoenzyme of complex I, we can consider it as a good marker for mitochondrial matrix. However, we claim here that tubulin is not the best marker to assess for contamination by cytosolic proteins, in such kind of experiments, and should be substituted by another proteins such as GAPDH. As shown in (Fig. 1C), tubulin was not detected in the mitochondrial fraction while GAPDH showed a weak band. Accordingly, although we indeed detected a weak STAT3 signal in the mitochondrial fraction, we could not conclude whether it was contamination or a specific localization.

While western blots do not conserve the original spatial information and assesses a cell population, immunofluorescence can be analyzed at the single cell level and provides information as to spatial localization by cross-correlation of signals labelling the proteins of interest and the compartments of interest. However, similar to western blotting, immunofluorescence relies on specificity and sensitivity of the antibodies. Using immunofluorescence we showed a good spatial cross-correlation between STAT3 signal and the ryanodine receptor localized in the junctional SR but no strong cross-correlation between STAT3 and mitochondria. Assuming that near 10% of STAT3 is expressed in mitochondria, we would have expected to detect a strong spatial cross-correlation between STAT3 and a marker of mitochondria.

We questioned the localization of STAT3 in the mitochondria of cell lines. An extensive literature supports the fact that STAT3 can be translocated to the mitochondria in different cell lines, particularly upon a strong expression in cytosol. According to the literature, experiments targeting STAT3 to the mitochondria by means of a mitochondria-localization site [12] or incubating mitochondria in the presence of a high concentration of STAT3 [14] induced a strong translocation of STAT3 into the mitochondria. An import mechanism of STAT3 to the mitochondria does exist, even though it likely requires either STAT3 overexpression or dysregulation, which could occur in cancer cells. In this study, we reported that the overexpression of STAT3-EYFP in H9C2 cardiomyoblasts-derived cell line was correlated with a significant level of fluorescence in the mitochondria, what supports the fact that a fraction of STAT3 may translocate into the mitochondria under specific conditions. However, our cross-correlation analysis also clearly demonstrated that the major STAT3 signal was actually observed all around the mitochondria not inside them. Given the dotted pattern of STAT3 signal, it is likely that a proportion of STAT3 proteins are bound to structures like membranes rather than freely diffusing in the cytosol. This suggests that a high proportion of STAT3 may be bound to ER membrane surroundings the mitochondria. This hypothesis is supported by a recent study [24] and could explain why a strong STAT3 signal is detected in the crude mitochondrial fraction which includes a large proportion of

ER membranes. It could also explain why a STAT3 contamination could be observed in "pure" mitochondrial fraction, since it is difficult to guarantee 100% removal of ER membranes.

Several studies reported that upon induction (including ischemia-reperfusion), STAT3 translocates from cytosol to nucleus or to mitochondria. On our side, we failed to detect STAT3 in mitochondria after ischemia-reperfusion, with both Western-blot and immunofluorescence, in both in vivo and in vitro models while, conversely, a strong signal was observed in cells nuclei.

Altogether, our results do not support a role for STAT3 in mouse cardiac mitochondria [12].

4.2 Specificity, sensitivity, and toxicity of Stattic

Stattic is a specific inhibitor of STAT3 [25] and has been used in numerous studies. We observed that in some studies [13], high concentration of Stattic (>100µM) were used regardless its IC50 for STAT3 phosphorylation (20 µM for 1hr incubation at 30°C) and for cell death induction (20 µM) [25]. Noteworthy, in the original article showing Stattic specificity, Stattic inhibited STAT1 at 40% with an IC50 of 10 µM at 30°C. In a recent study, authors confirmed that 10 µM Stattic inhibited both STAT1 and STAT3 phosphorylation activity [23]. In this latter study, a prolonged 20 µM Stattic treatment was found to be toxic and induced cell death. In our hands, a 100 µM Stattic treatment for 2 h induced STAT3 and tubulin degradation confirming that high Stattic concentration could trigger toxic effects non-related to its effect on STAT3 (Fig. 4C). We could not detect any inhibition of mitochondrial respiration when we treated isolated mitochondria with 50 µM for 1 h at 4°C (this temperature was used to preserve mitochondria during incubation). Rainer's group found a 50% decrease in complex I activity when incubating heart mitochondria with 200 µM Stattic for 1 h at 4°C [13]. Although the temperature of incubation is slowing down the reaction, Stattic can be considered as being in saturating condition since majority of cellular STAT3 is absent in crude mitochondrial fraction. Therefore, it is very unlikely that we could not observe an inhibitory effect of 50 µM Stattic if STAT3 is expressed in mitochondria and is regulating complex I activity. Conversely, the use of 200 µM Stattic could have induced: i) protein degradation and subsequent toxic effect down-regulating complex I activity, and ii) inhibition of STAT1 as it was detected in heart mitochondria [13]. Besides, it should be kept in mind that respiration and CRC experiments are usually carried on crude mitochondrial fractions, which incorporates a lot of STAT3 protein outside of the mitochondria. In case a direct effect on STAT3 inhibition would be observed, such as the small increase in CRC we observed, it should not be claimed that it is more likely related to an effect on STAT3 from the inside of mitochondria rather than from the outside of the mitochondria. In conclusion, both data of the literature and our results suggest a careful control of the non-specific effect of Stattic, particularly in experiments with cell fractions which may include no or low STAT3 levels.

4.3 The STAT3 KO phenotype

Previous reports suggest that mitochondrial respiration is down-regulated in cardiomyocytes of STAT3 KO mice and in STAT3 KO cell lines [7] [26]. Since STAT3 is primarily a transcription

factor and is known to regulate genes involved in metabolism and mitochondrial activity :[27], [28], one should not exclude a canonical genomic explanation to the down-regulation of respiration in heart mitochondria of STAT3 KO mice. In addition, sharing an apparent similar phenotype between in vivo cardiomyocytes and in vitro cell lines could not mandatorily be recapitulated by a common mechanism. Indeed, since we could not detect STAT3 in heart mitochondria but could see STAT3-EYFP around mitochondria of H9C2, it is unlikely that the effect of STAT3 on respiration would be caused by a common mechanism.

In conclusion, we could neither find a significant amount of STAT3 in mouse heart mitochondria, nor detect a direct involvement for it in the regulation of mitochondrial activities under physiologic conditions. In addition, we show a novel vivid distribution for STAT3 along T-tubules of cardiomyocytes. Although we agree that under certain conditions, such as STAT3 overexpression or MLS-tagged STAT3, STAT3 could be translocated to mitochondria, we speculate that this mechanism could mainly be relevant to cell lines already showing a strong expression of STAT3. Alternatively, our localization and functional experiments support the fact that STAT3 is localized around the mitochondria in a cardiomyoblasts cell line, and it may indeed support an indirect effect on their activity.

AUTHOR CONTRIBUTIONS

Conceived experiments: ZH, SB, MK, GB.

Performed experiments: ZH, SB, NGB, MP, BP, LA.

Wrote the manuscript: ZH, MO and GB.

Supervised the study: MK, GB.

Review the manuscript: MP, GWB, ECS, MO.

AKNOWLEGDMENTS

This study benefits from grants offered by INSERM, the Lebanese University, and The Cedar program of Campus France (#37303QA 2017-2018).

This work was supported by the IHU OPeRa (ANR-10-IBHU-004) within the program “Investissements d'Avenir” operated by the French National Research Agency (ANR).

Zeina Harhous was supported by the “Association de Specialisation et d’orientation Scientifique”.

Sally Badawi was supported by the Council for Scientific Research and Lebanese University fellowship (CNRS-L) program and the Eiffel scholarship program of excellence of Campus France.

We acknowledge the financial support from ITMO Cancer AVIESAN (Alliance Nationale pour les Sciences de la Vie et de la Santé, National Alliance for Life Sciences and Health) within the framework of the cancer plan for Orbitrap mass spectrometer founding.

We also thank Adeline Page for performing the mass spectrometry analysis (Protein Science Facility, SFR BioSciences CNRS UMS3444, Inserm US8, UCBL, ENS de Lyon, 50 Avenue Tony Garnier, 69007 Lyon, France).

REFERENCES

[1] K. Boengler, D. Hilfiker-Kleiner, H. Drexler, G. Heusch, et R. Schulz, « The myocardial JAK/STAT pathway: From protection to failure », *Pharmacol. Ther.*, vol. 120, nº 2, p. 172−185, Nov. 2008.

[2] X. Cheng, C. Peuckert, et S. Wölfl, « Essential role of mitochondrial Stat3 in p38MAPK mediated apoptosis under oxidative stress », *Sci. Rep.*, vol. 7, Nov. 2017.

[3] L. M. LaFave et R. L. Levine, « JAK2 the future: therapeutic strategies for JAK-dependent malignancies », *Trends Pharmacol. Sci.*, vol. 33, nº 11, p. 574−582, Nov. 2012.

[4] I. Hazan-Halevy *et al.*, « STAT3 is constitutively phosphorylated on serine 727 residues, binds DNA, and activates transcription in CLL cells », *Blood*, vol. 115, nº 14, p. 2852−2863, Apr. 2010.

[5] N. Sato *et al.*, « Physical and functional interactions between STAT3 and ZIP kinase », *Int. Immunol.*, vol. 17, nº 12, p. 1543−1552, Dec. 2005.

[6] Z. Wen, Z. Zhong, et J. E. Darnell, « Maximal activation of transcription by statl and stat3 requires both tyrosine and serine phosphorylation », *Cell*, vol. 82, nº 2, p. 241−250, July. 1995.

[7] J. Wegrzyn *et al.*, « Function of mitochondrial Stat3 in cellular respiration », *Science*, vol. 323, nº 5915, p. 793−797, Feb. 2009.

[8] L. Gomez *et al.*, « Inhibition of mitochondrial permeability transition improves functional recovery and reduces mortality following acute myocardial infarction in mice », *Am. J. Physiol.-Heart Circ. Physiol.*, vol. 293, nº 3, p. H1654−H1661, Sept. 2007.

[9] D. J. Hausenloy, H. L. Maddock, G. F. Baxter, et D. M. Yellon, « Inhibiting mitochondrial permeability transition pore opening: a new paradigm for myocardial preconditioning? », *Cardiovasc. Res.*, vol. 55, nº 3, p. 534−543, Aug. 2002.

[10] S. A. Javadov, S. Clarke, M. Das, E. J. Griffiths, K. H. H. Lim, et A. P. Halestrap, « Ischaemic preconditioning inhibits opening of mitochondrial permeability transition pores in the reperfused rat heart », *J. Physiol.*, vol. 549, nº Pt 2, p. 513−524, june 2003.

[11] K. Boengler, E. Ungefug, G. Heusch, et R. Schulz, « The STAT3 inhibitor stattic impairs cardiomyocyte mitochondrial function through increased reactive oxygen species

formation », *Curr. Pharm. Des.*, vol. 19, nº 39, p. 6890‑6895, 2013.

[12] K. Szczepanek *et al.*, « Cardioprotective function of mitochondrial-targeted and transcriptionally inactive STAT3 against ischemia and reperfusion injury », *Basic Res. Cardiol.*, vol. 110, nº 6, p. 53, Nov. 2015.

[13] K. Boengler, D. Hilfiker-Kleiner, G. Heusch, et R. Schulz, « Inhibition of permeability transition pore opening by mitochondrial STAT3 and its role in myocardial ischemia/reperfusion », *Basic Res. Cardiol.*, vol. 105, nº 6, p. 771‑785, Nov. 2010.

[14] P. Tammineni, C. Anugula, F. Mohammed, M. Anjaneyulu, A. C. Larner, et N. B. V. Sepuri, « The import of the transcription factor STAT3 into mitochondria depends on GRIM-19, a component of the electron transport chain », *J. Biol. Chem.*, vol. 288, nº 7, p. 4723‑4732, Feb. 2013.

[15] Q. Zhang *et al.*, « Mitochondrial localized Stat3 promotes breast cancer growth via phosphorylation of serine 727 », *J. Biol. Chem.*, vol. 288, nº 43, p. 31280‑31288, Oct. 2013.

[16] R. Harisseh *et al.*, « Unacylated ghrelin analog prevents myocardial reperfusion injury independently of permeability transition pore », *Basic Res. Cardiol.*, vol. 112, nº 1, p. 4, déc. 2016.

[17] A. Gharib *et al.*, « Opposite and tissue-specific effects of coenzyme Q2 on mPTP opening and ROS production between heart and liver mitochondria: Role of complex I », *J. Mol. Cell. Cardiol.*, vol. 52, nº 5, p. 1091‑1095, May 2012.

[18] M. R. Wieckowski, C. Giorgi, M. Lebiedzinska, J. Duszynski, et P. Pinton, « Isolation of mitochondria-associated membranes and mitochondria from animal tissues and cells », *Nat. Protoc.*, vol. 4, nº 11, p. 1582‑1590, Nov. 2009.

[19] D. De Paulis *et al.*, « Cyclosporine A at reperfusion fails to reduce infarct size in the in vivo rat heart », *Basic Res. Cardiol.*, vol. 108, nº 5, p. 379, Aug. 2013.

[20] T. D. O'Connell, M. C. Rodrigo, et P. C. Simpson, « Isolation and Culture of Adult Mouse Cardiac Myocytes », in *Cardiovascular Proteomics*, vol. 357, New Jersey: Humana Press, 2006, p. 271‑296.

[21] G. Bidaux *et al.*, « FRET Image Correlation Spectroscopy Reveals RNAPII-Independent P-TEFb Recruitment on Chromatin », *Biophys. J.*, vol. 114, nº 3, p. 522‑533, Feb. 2018.

[22] D. Phillips *et al.*, « Stoichiometry of STAT3 and mitochondrial proteins: Implications for the regulation of oxidative phosphorylation by protein-protein interactions », *J. Biol. Chem.*, vol. 285, nº 31, p. 23532−23536, July 2010.

[23] I. Sanseverino, C. Purificato, M. C. Gauzzi, et S. Gessani, « Revisiting the specificity of small molecule inhibitors: the example of stattic in dendritic cells », *Chem. Biol.*, vol. 19, nº 10, p. 1213−1214; author reply 1215-1216, Oct. 2012.

[24] L. Avalle *et al.*, « STAT3 localizes to the ER, acting as a gatekeeper for ER-mitochondrion Ca2+ fluxes and apoptotic responses », *Cell Death Differ.*, July. 2018.

[25] J. Schust, B. Sperl, A. Hollis, T. U. Mayer, et T. Berg, « Stattic: a small-molecule inhibitor of STAT3 activation and dimerization », *Chem. Biol.*, vol. 13, nº 11, p. 1235−1242, Nov. 2006.

[26] R. Yang *et al.*, « Mitochondrial Ca2+ and membrane potential, an alternative pathway for Interleukin 6 to regulate CD4 cell effector function », *eLife*, vol. 4, May 2015.

[27] V. Poli et A. Camporeale, « STAT3-Mediated Metabolic Reprograming in Cellular Transformation and Implications for Drug Resistance », *Front. Oncol.*, vol. 5, June 2015.

[28] M. Demaria, A. Camporeale, et V. Poli, « STAT3 and metabolism: How many ways to use a single molecule?: STAT3 and Metabolism », *Int. J. Cancer*, vol. 135, nº 9, p. 1997−2003, Nov. 2014.

FIGURES

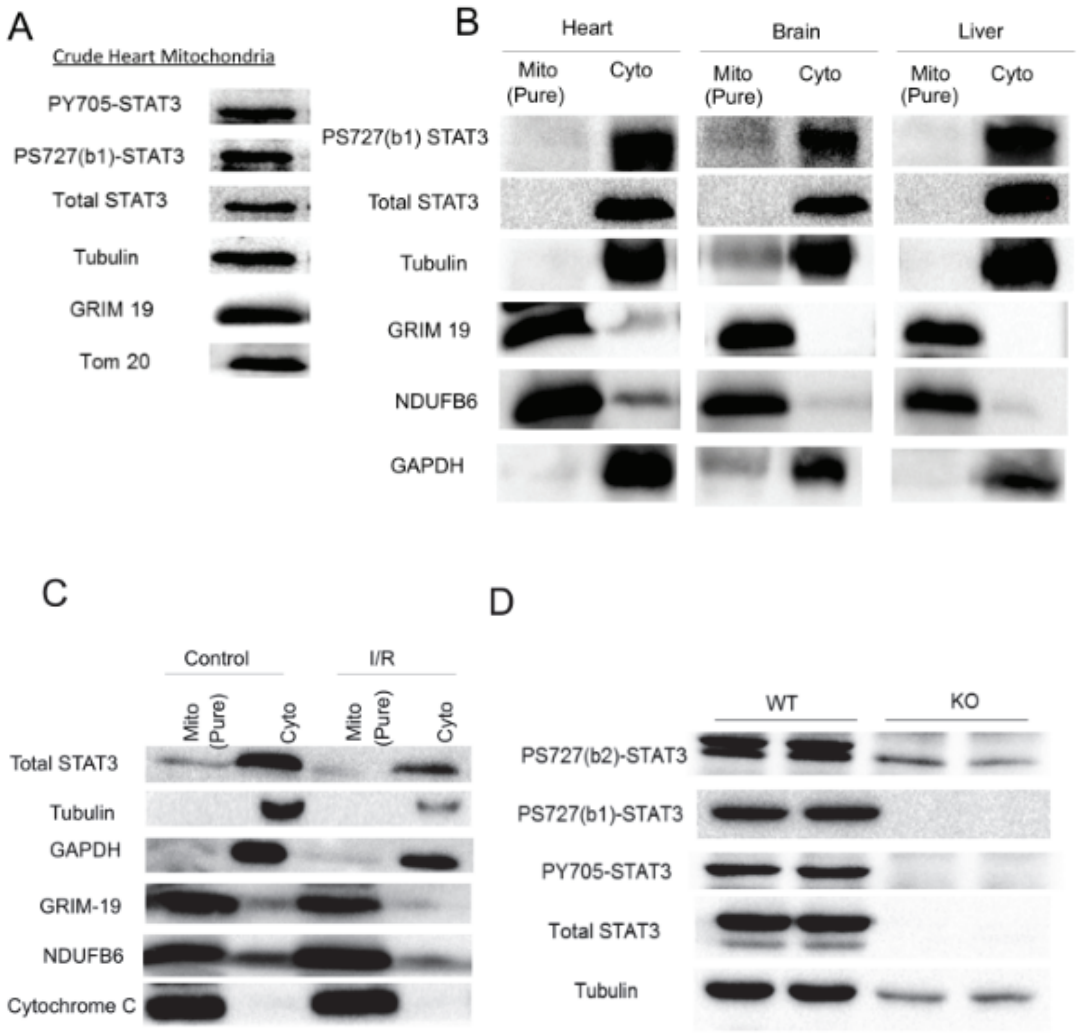

Figure 1. Cytosolic and mitochondrial fractions show the absence of STAT3 in pure mitochondria of different organs.

Western blots showing the detection of Y705- and S727-phosphorylated and total STAT3 forms; the cytosolic proteins tubulin and GAPDH; and the mitochondrial proteins Tom20, GRIM19, cytochrome C and NDUFB6 (complex I subunit) in (A) protein extract of crude mitochondria fraction (40µg) (n=3), (B) pure mitochondrial and cytosolic extracts from hearts, brains, and livers of control C57bl/6J mice (90 µg of protein extract per well) (n=3), (C) pure mitochondrial extracts from the area-at-risk of mouse heart subjected to 45 minutes of ischemia followed by 15 minutes of reperfusion (30 µg of protein extract per well) (n=5), (D) verification of the specificity of several STAT3 antibodies in 40 µg of total protein extract of wild type (wt) and STAT3-KO MEFs: PS727-STAT3 (batches one and two: b1 and b2), PY705-STAT3 and total STAT3 (n=3).

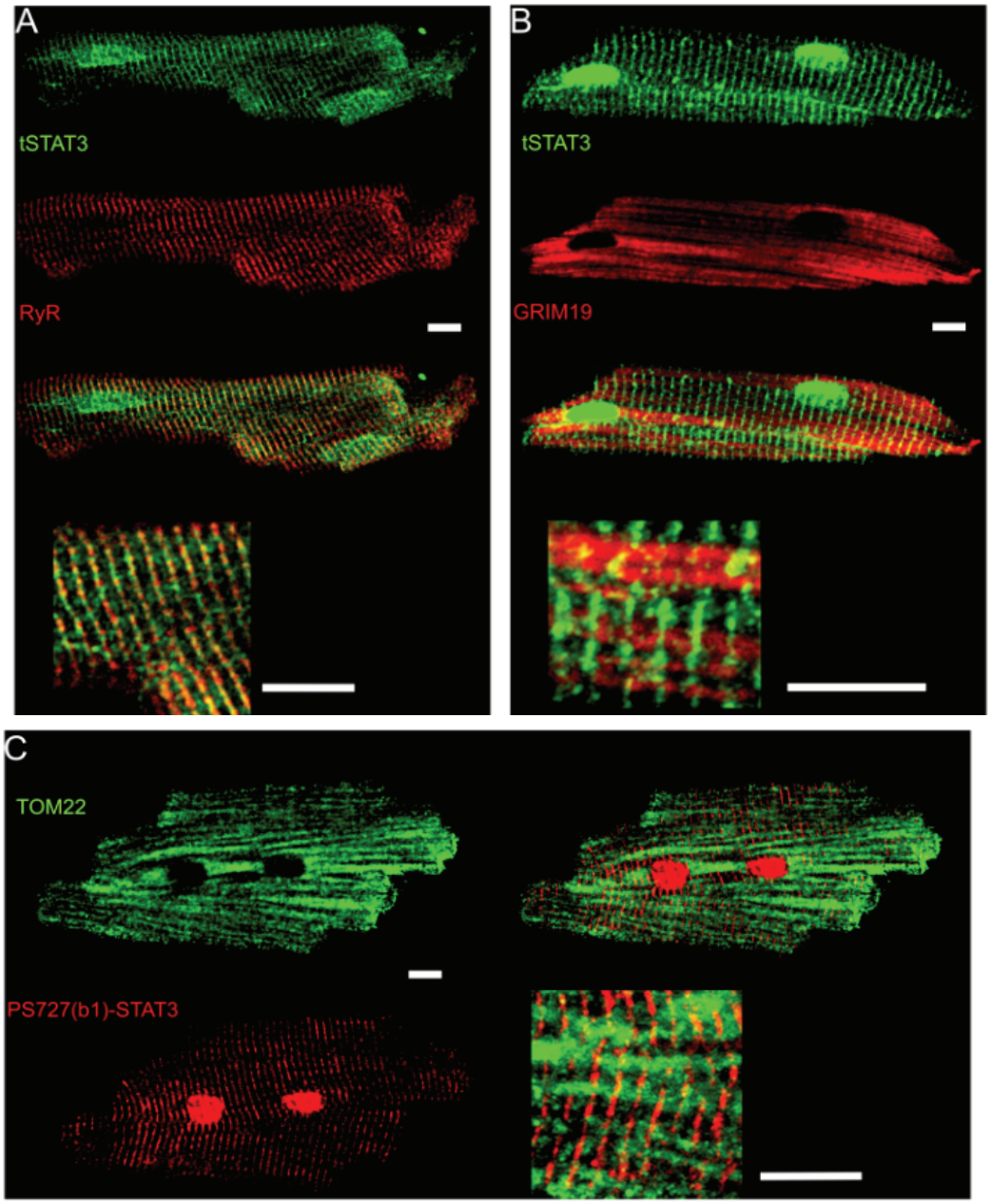

Figure 2. STAT3 is distributed in nucleus and along t-tubules of cardiomyocytes.

Confocal images of mouse isolated cardiomyocytes immuno-labelled with antibodies against (A) a marker of junctional sarcoplasmic reticulum, the ryanodine receptor type II (RyR2) in red and total STAT3 (green), (B) a mitochondrial marker, GRIM-19 (Red), and total STAT3 (Green) or the mitochondrial marker Tom20 (green) and (C) PS727(b1)-STAT3 (Red). Depth of the focal plane: 1 µm. Three independent experiments were carried out on different mouse hearts. Scale bars: 10 µm.

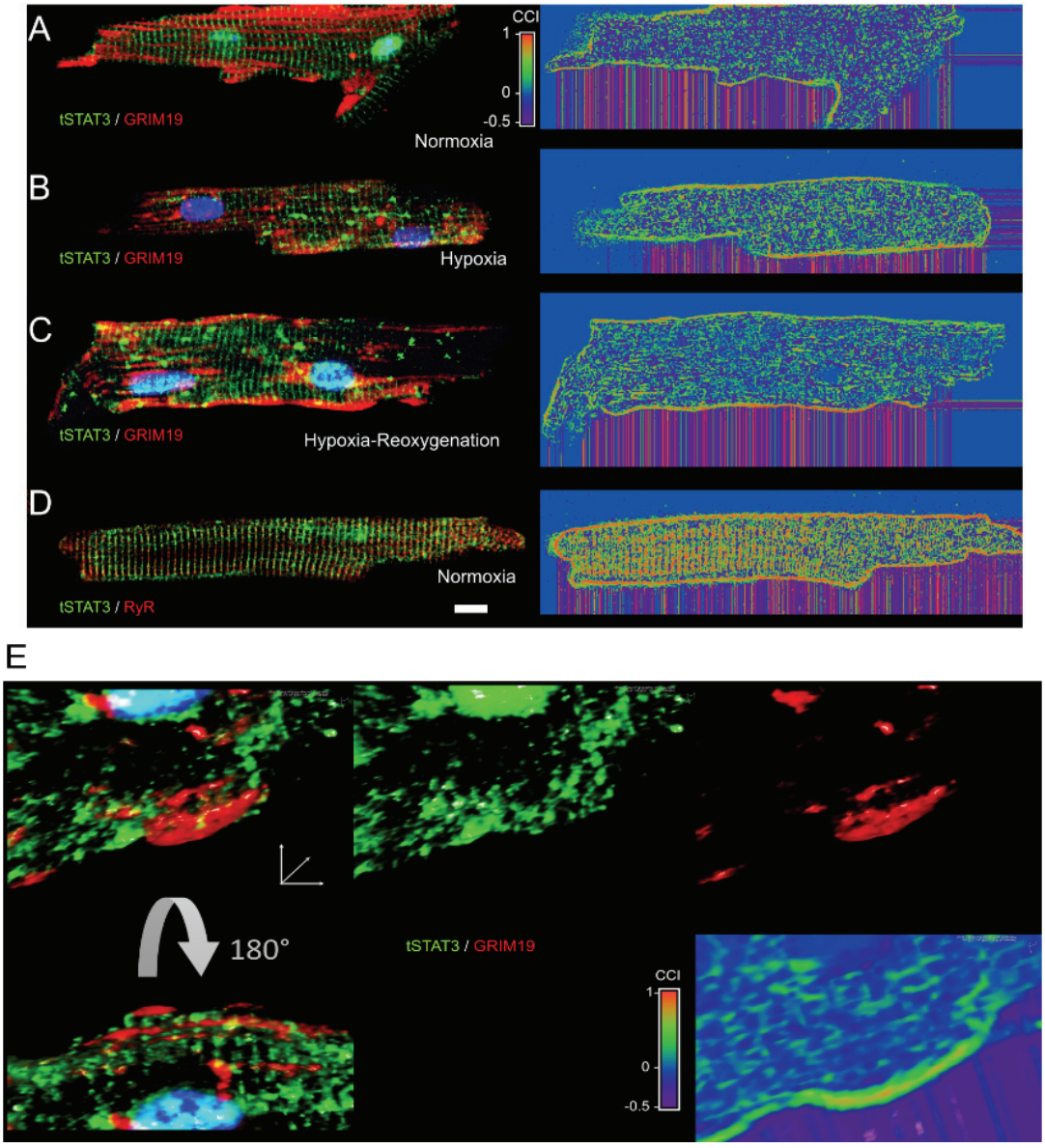

Figure 3. Hypoxia and hypoxia-reoxygenation do not induce the mitochondrial translocation of STAT3 in mouse-isolated cardiomyocytes.

Confocal images showing the merging of fluorescence image of total STAT3 (green) and GRIM-19 (red) in mouse isolated cardiomyocytes incubated under (A) normoxia, (B) hypoxia for 90 min or (C) hypoxia as in (B) followed by reoxygenation for 1 h (HR). Right images are quantifying the spatial cross-correlation intensity (CCI) of the 2 fluorescent signals. (D) The confocal image and co-localization pattern of total STAT3 (green) and RyR2 (red) in cardiomyocytes under normoxia conditions. (E) A 3D reconstructed projection showing the localization pattern of total STAT3 (green) and GRIM-19 (Red) in cardiomyocytes subjected to HR. Top row of image is showing the 3D rendering from above for merged fluorescence (left), STAT3 fluorescence alone (middle) and

GRIM-19 fluorescence alone (right). Bottom row showing the 3D rendering from below (left) and the 3D spatial cross-correlation image. Three independent experiments were carried out on different mouse hearts. Scale bar: 10 µm.

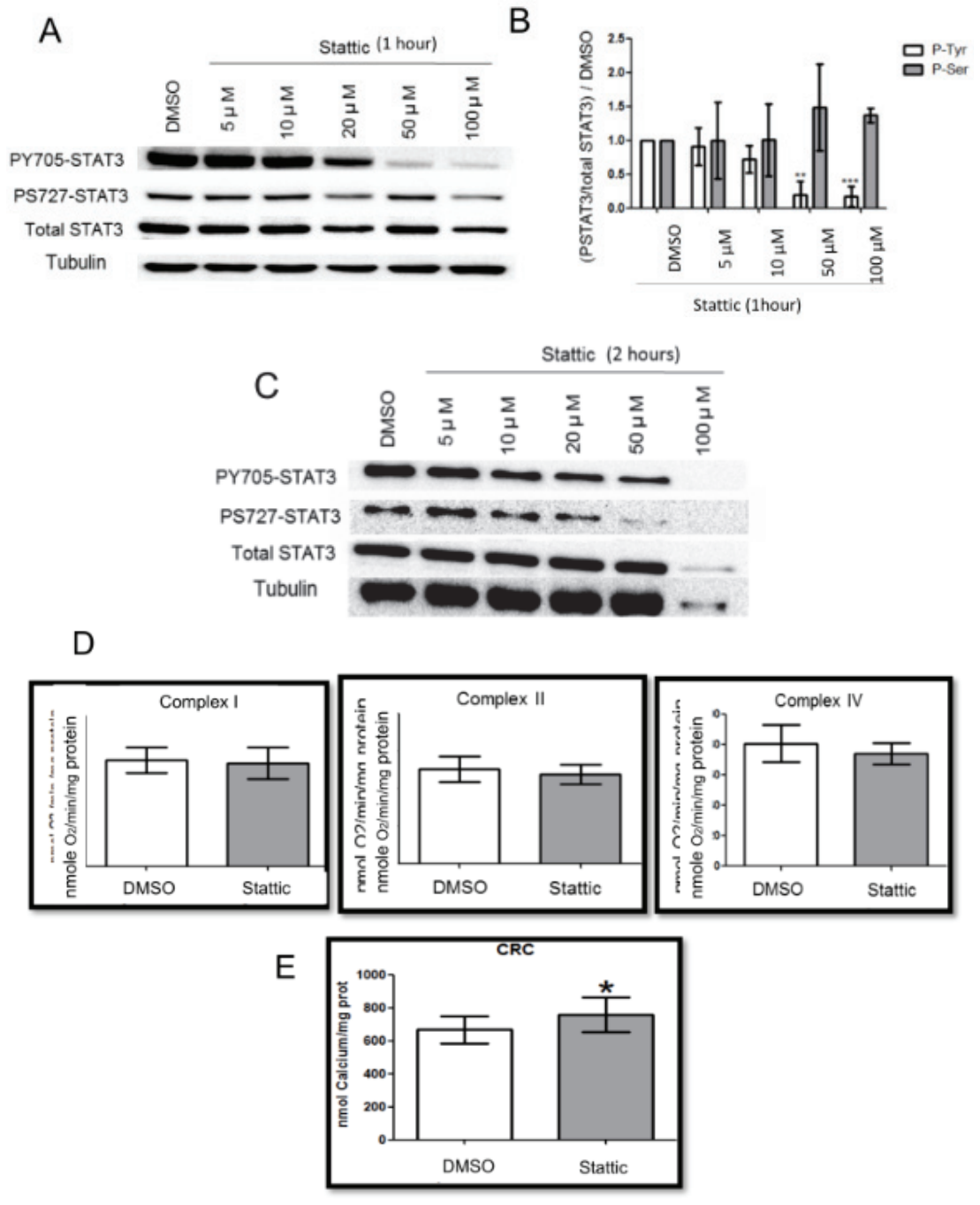

Figure 4: Pharmacological inhibition of STAT3 by Stattic has no effect on ADP-stimulated mitochondrial oxygen consumption but slightly increases calcium retention capacity.

Western-blots showing the dose-effect of a one hour- or (C) two hours- treatment with the STAT3 inhibitor, Stattic, on the phosphorylation of STAT3 in mouse isolated adult cardiomyocytes. (B) Phosphorylation of Y705 and S727 residues of STAT3 was quantified and divided by the amount of total STAT3 protein. STAT3 ratios for one hour Stattic-treated cells were normalized by DMSO treated condition. (D) Oxygen consumption rate by complexes I, II and IV (state 3) measured in isolated mitochondria of mouse cardiomyocytes, incubated with either DMSO or 50 µM Stattic for 1 h at 4°C. (E) Calcium retention capacity measurement for mitochondria treated with DMSO or 50 µM Stattic for 1 h at 4°C. Three independent experiments were carried out on different mouse hearts.

Supplementary Data

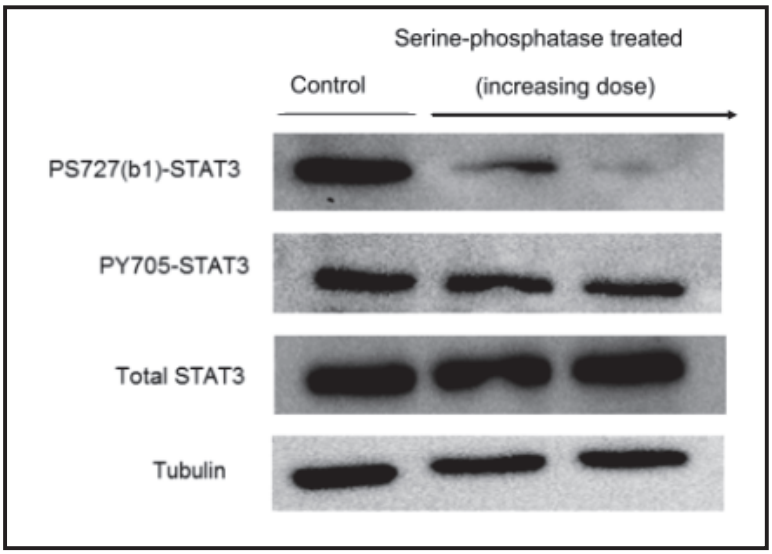

Figure S1: Specificity of the PS727(b1)-STAT3 antibody

Western blot analysis showing the effect of a serine-phosphatase treatment on the level of phosphorylation of Y705 and S727 STAT3. Tubulin reports the protein loads in each well. Three independent experiments were carried out on different mouse hearts.

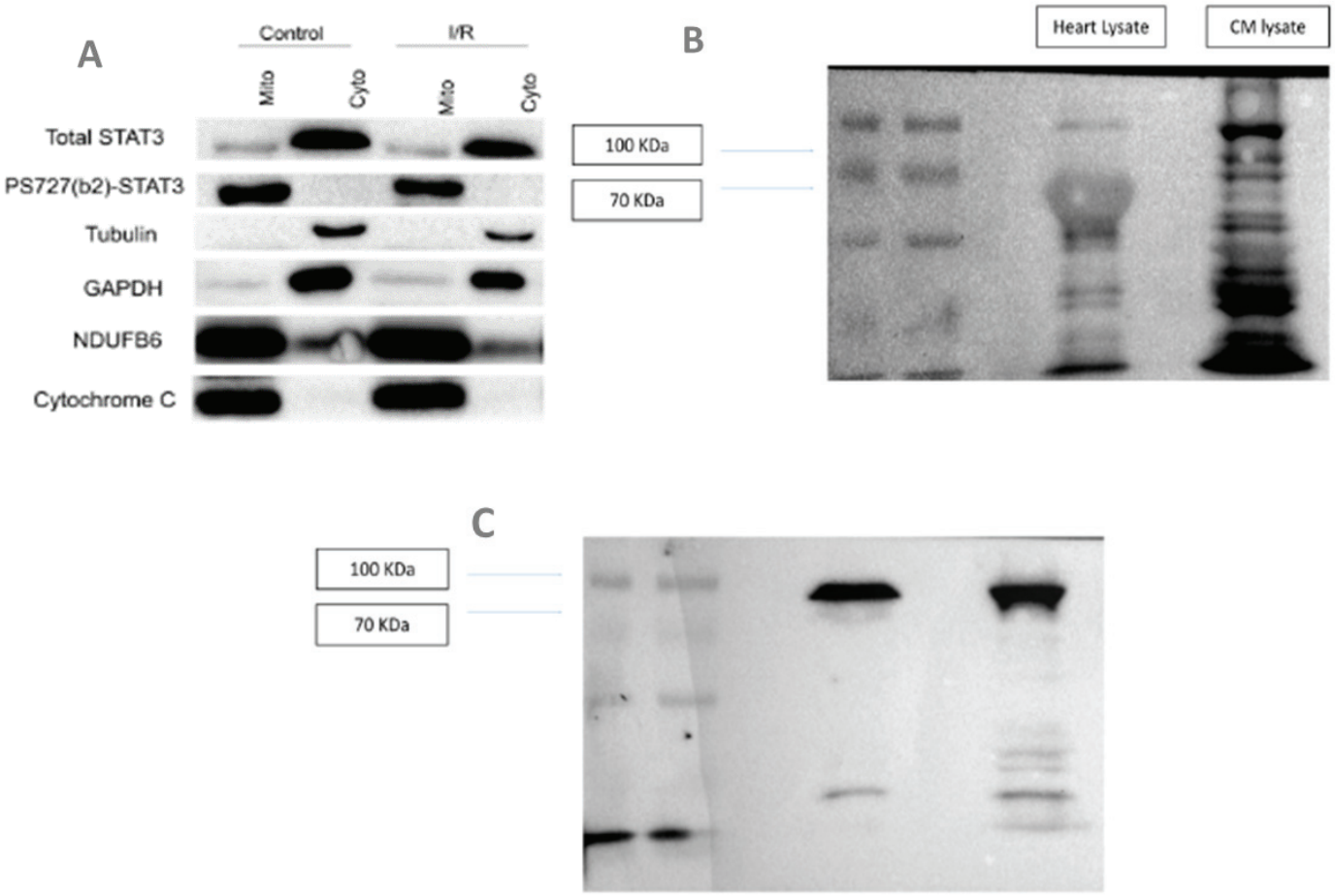

Figure S2: Lack of specificity of PS727(b2)-STAT3 antibody in mitochondrial and complete cardiac cell proteomic fractions

(A) Western blot analysis of PS727(b2)-STAT3, total STAT3, tubulin, GAPDH, Cytochrome C and GRIM-19 in pure mitochondrial extracts from the areas at risk of mice hearts subjected to 45 minutes of ischemia followed by 15 minutes of reperfusion or from control mice. Note that while PS727(b2)-STAT3 detects a band in the mitochondrial fraction, no total STAT3 can be detected, which is unfathomable. Six independent experiments were carried out on different mouse hearts.

(B) Western blot analysis of PS727(b2)-STAT3 in total cardiomyocyte proteomic sample.

(C) Western blot analysis of Total STAT3 in total cardiomyocyte proteomic sample

I. Specific and used Antibodies

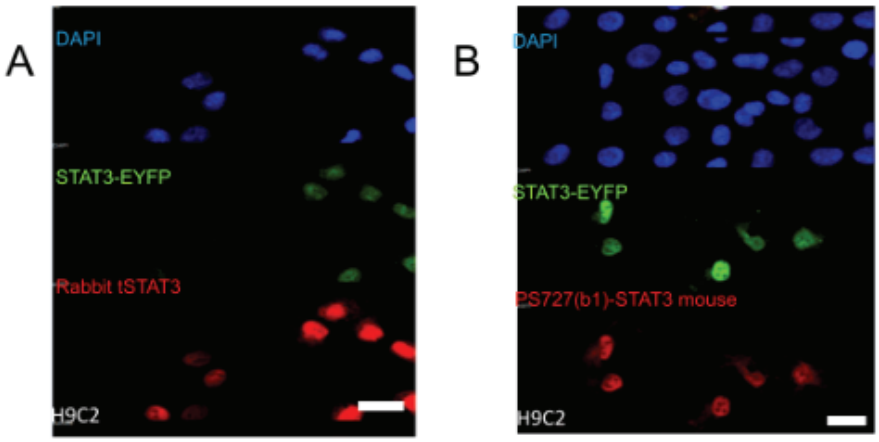

II. Non-specific Antibodies (unused)

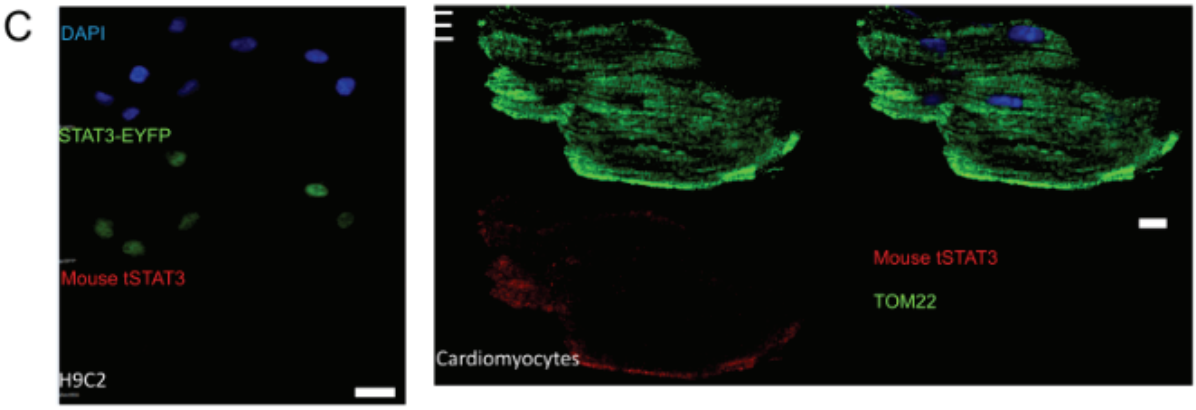

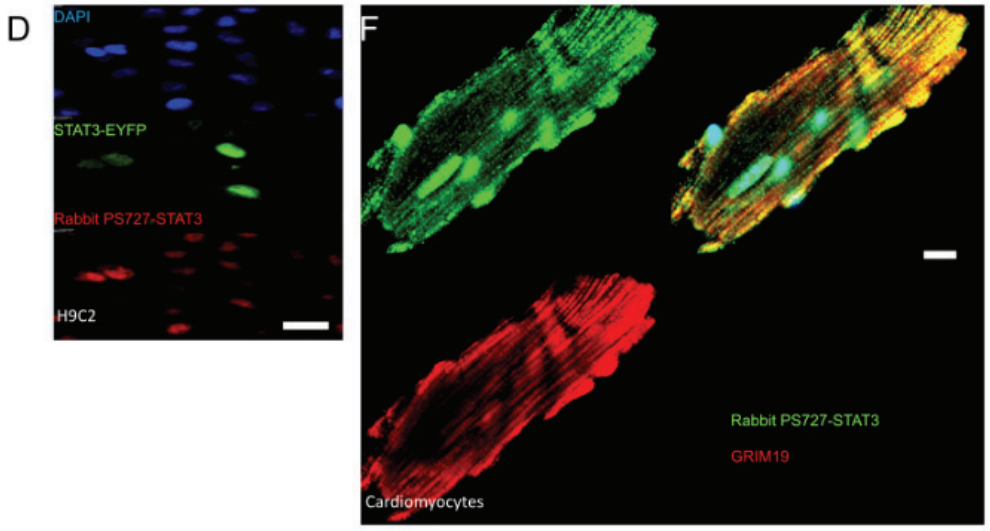

Figure S3: Specificity of the STAT3 antibodies in immunofluorescence experiments.

Confocal images of H9C2 cells transfected with STAT3-EYFP plasmids for 48h and then labeled with different antibodies:

I- Specific used antibodies (A) rabbit IgG anti-total STAT3 (tSTAT3), (B) mouse IgG anti- S727 phosphorylation of STAT3 (PS727(b1)-STAT3);

II- Non-specific unused antibodies (C) mouse IgG anti-total STAT3 (mouse tSTAT3) and (D) rabbit IgG anti- S727 phosphorylation of STAT3 (rabbit PS727-STAT3). (E) and (F), Immunofluorescence experiments on mouse isolated cardiomyocytes show the detection of TOM22 and GRIM19 proteins, respectively, in mitochondria and concomitantly to the non-specific fluorescent signal given by mouse IgG anti-total STAT3 (mouse tSTAT3) and rabbit IgG anti- S727 phosphorylation of STAT3 (rabbit PS727-STAT3), respectively. Three independent experiments were carried out on different mouse hearts.

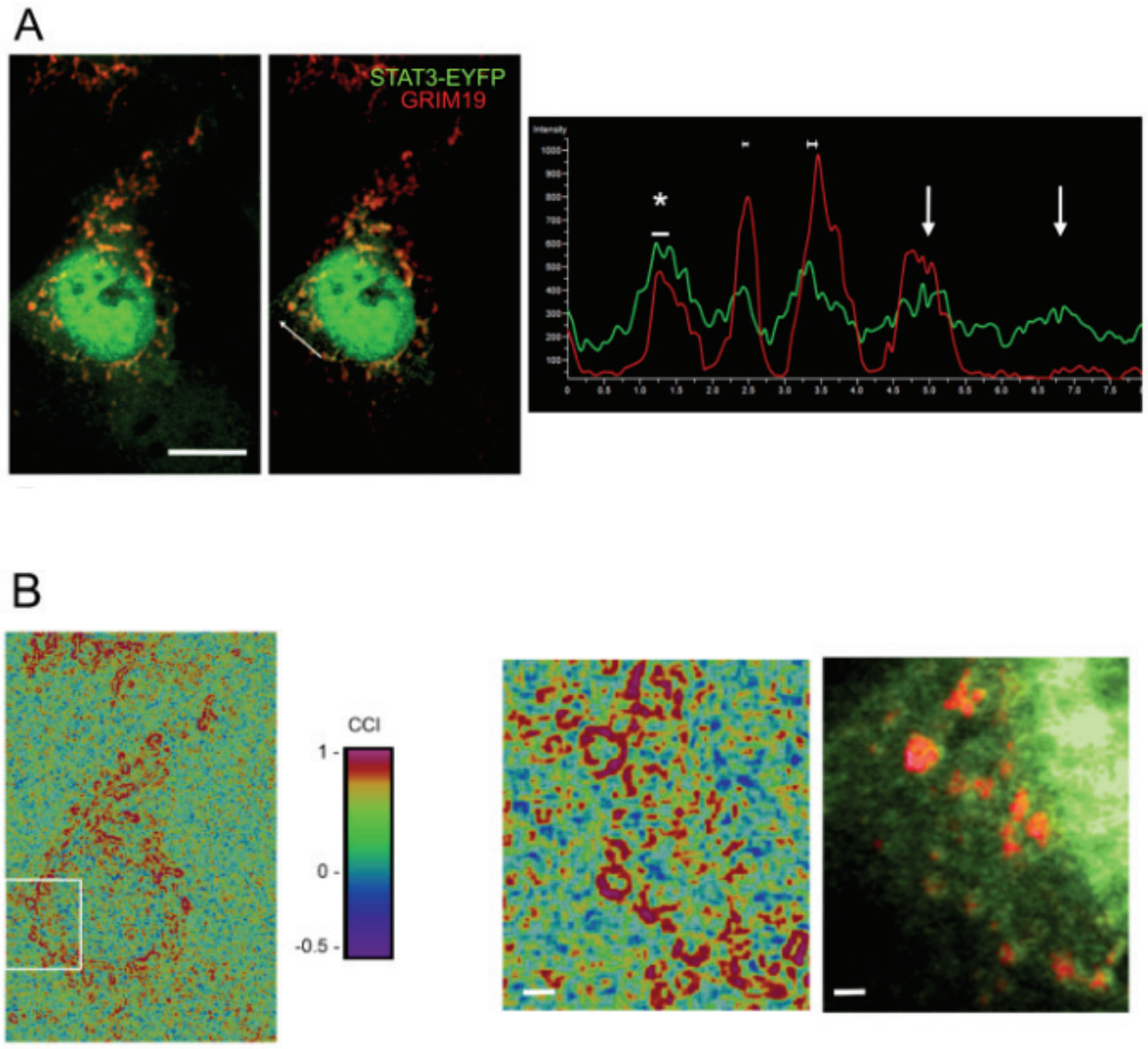

Figure S4: STAT3 and GRIM19 co-localize at the mitochondrial circumference in H9C2 cardiomyoblasts.

(A) Confocal images of H9C2 cardiomyoblasts co-transfected with STAT3-EYFP (green signal) and mCherry GRIM19 (red signal) plasmids for 48h (left panel), along with the line intensity profiler (middle right panel) and plot showing intensity profiles of both signals in four different randomly chosen mitochondria (right panel). Scale bar 10µm

(B) Map of the spatial cross-correlation intensity (CCI) of the two fluorescent signals (left panel) and a representation of the correlation pattern of distribution (red pattern) in a randomly chosen zoomed-in area (right panel), showing a donut-shaped co-localization pattern around mitochondria rather than inside them. Scale bar 1µm.